Chalcogen and Halogen Bonding Host Systems for Anion and Ion-Pair Recognition

Andrew Docker

Christ Church, University of Oxford



A thesis submitted for the degree of Doctor of Philosophy

Inorganic Chemistry Laboratory

University of Oxford

Trinity Term 2021

Abstract

Chalcogen and Halogen Bonding Host Systems for Anion and Ion-Pair Recognition

Andrew Docker, Christ Church, University of Oxford

Abstract of thesis submitted for the degree of D.Phil., Trinity Term 2021

This thesis describes the synthesis of acyclic and macrocyclic incorporating sigma-hole interactions including halogen and chalcogen bonding for anion and ion-pair recognition.

Chapter 1 introduces the general aspects in the field of supramolecular host-guest chemistry with particular emphasis on themes relevant to the topic of this DPhil research project, specifically anion and ion-pair recognition followed by a review of non-covalent interactions.

Chapter 2 describes the preparation of a series of chalcogen, halogen and hydrogen bonding acyclic anion receptors wherein structural and electronic factors that influence anion recognition potency and selectivity of σ-hole interactions are explored through anion binding studies and linear free energy relationship analysis.

Chapter 3 presents the synthesis of two chalcogen bonding heteroditopic receptor systems followed by extensive characterisation of their anion and ion-pair recognition properties. The most potent system is capable of selective KCl recognition, facilitating its solid-liquid, liquid-liquid extraction and liquid membrane transport.

Chapter 4 details the synthesis of a series of tetraphenylethene derivatives functionalised with highly potent electron-deficient perfluoroaryl iodo-triazole halogen bond donors. A suite of techniques reveal that the tetra-substituted halogen bonding receptor forms luminescent nanoscale aggregates, the formation of which is driven by XB-mediated anion coordination. Furthermore, the doubly substituted geometric isomers act as unprecedented photoswitchable XB donor anion receptors, where the composition of the photostationary state can be modulated by the presence of a coordinating halide anion.

Chapter 5 presents a series of novel heteroditopic halogen bonding receptor functionalised silica based materials, which are investigated for the cooperative binding and extraction of sodium halide ion-pair species from aqueous solution.

Acknowledgements

Firstly, I would like to express my sincere gratitude to Professor Paul Beer, his supervision, guidance and support over the years have been invaluable. If I may be so bold as to condense Paul's research wisdom into three maxims they would be as follows: i) 'You must keep up with the literature' ii) 'Clarity and brevity in scientific writing is of utmost importance' iii) 'Consistency, persistency and creativity are required for research'. His patience and unfailing kindness have been, and will continue to be, a source of inspiration.

From my start in the lab I was remarkably fortunate in that I was taught by Dr. Thanthapatra Bunchuay and Dr. Timothy Barendt, I am forever indebted to their generosity in selflessly sharing their time. I have also been privileged to share the lab with past Beer Group members, listed somewhat chronologically; Drs Sean Robinson, (almost Dr.) Thomas Mole, Hena Baga, Sam Sutton, Xiaoxiong Li. It has also been my pleasure to work with and share the friendship of an equally talented group of people including: Richard Tse, Robert Hein, Laura Bickerton, Aidan Kerckhoffs, Jane Liew, Krzysztof Bąk, Heike Kuhn, Charles Guthrie, Michael Ahrens, Caspar Whitehead, Omar Tsang, Christian Gately, Andrew Taylor and Zongyao Zhang.

Special thanks are also due to Professor Jason Davis whether marking 'largely incorrect or badly answered' tutorial work and encouraging me to 'consider my trajectory' at Oxford as an undergraduate or giving invaluable life advice as a college advisor. I must also credit my other former tutors at Christ Church; Professors Dirk Aarts and Sam Thompson and Dr Martin Grossel who inspired me to continue with chemistry.

And finally, my most heartfelt thanks to my brother and my parents, whose endless support, encouragement, and sacrifice would not be adequately described by any words.

List of Publications

T. Bunchuay, **A. Docker**, N. G. White, P. D. Beer. A new halogen bonding 1,2-iodo-triazolium-triazole benzene motif for anion recognition.
Polyhedron **2021**, DOI: 10.1016/j.poly.2021.115482.

A. Docker, J. G. Stevens, P. D. Beer. Halogen Bonding Heteroditopic Materials for Cooperative Sodium Iodide Binding and Extraction.
Chem. – Eur. J. **2021**, DOI: 10.1002/chem.202102952.

G. Turner, **A. Docker**, P. D. Beer. Anion recognition by halogen bonding and hydrogen bonding bis(triazole)-imidazolium [2]rotaxanes.
G. Turner, A. Docker, P. D. Beer, Dalton Trans. ***2021****, 50, 12800–12805.*

A. Docker, C. H. Guthrie, H. Kuhn, P. D. Beer. Modulating Chalcogen Bonding and Halogen Bonding Sigma-Hole Donor Atom Potency and Selectivity for Halide Anion Recognition.
Angew. Chem. Int. Ed. ***2021****, 60, 21973–21978*.

A. Docker, X. Shang, D. Yuan, H. Kuhn, Z. Zhang, J. J. Davis, P. D. Beer, M. J. Langton. Halogen Bonding Tetraphenylethene Anion Receptors: Anion-Induced Emissive Aggregates and Photoswitchable Recognition.
Angew. Chem. Int. Ed. **2021**, 60, 19442–19450.

L. E. Bickerton, **A. Docker (co-first author)**, A. J. Sterling, H. Kuhn, F. Duarte, P. D. Beer, M. J. Langton. Highly Active Halogen Bonding and Chalcogen Bonding Chloride Transporters with Non-Protonophoric Activity.
Chem. – Eur. J. **2021**, 27, 11738–11745.

S. C. Patrick, R. Hein, **A. Docker**, P. D. Beer, J. J. Davis. Solvent Effects in Halogen and Hydrogen Bonding Mediated Electrochemical Anion Sensing in Aqueous Solution and at Interfaces.
Chem. – Eur. J. **2021**, 27, 10201–10209.

Y. C. Tse, **A. Docker**, Z. Zhang, P. D. Beer. Lithium halide ion-pair recognition with halogen bonding and chalcogen bonding heteroditopic macrocycles.
Chem. Commun., **2021**, 57, 4950 – 4953.

A. Docker, T. Bunchuay, M. Ahrens, A. J. Martinez-Martinez, P. D. Beer. Chalcogen Bonding Ion-Pair Cryptand Host Discrimination of Potassium Halide Salts.
Chem. Eur. J. **2021**, 27, 7837 – 7841.

A. Docker, P.D. Beer. Halogen Bonding in Solution: Recognition with Macrocycles and Interlocked Systems.
Book Chapter, Wiley Publishers, **2020**, DOI:10.1002/9783527825738.ch3.

A. J. McConnell, **A. Docker**, P. D. Beer. From Heteroditopic to Multitopic Receptors for Ion-Pair Recognition: Advances in Receptor Design and Applications.
ChemPlusChem **2020**, 85, 1824 – 1841.

Ruengsuk, K. Khamphaijun, P. Pananusorn, **A. Docker**, J. Tantirungrotechai, M. Sukwattanasinitt, D. J. Harding, T. Bunchuay. Pertosylated pillar[5]arene: self-template assisted synthesis and supramolecular polymer formation.
Chem.Commun. **2020** , 56, 8739–8742.

T. Bunchuay, **A. Docker (co-first author)**, U. Eiamprasert, P. Surawatanawong, A. Brown, and P. D. Beer. Chalcogen Bond Mediated Enhancement of Cooperative Ion-Pair Recognition*,*
Angew.Chem. Int. Ed. **2020**, 59, 12007–12012.

E. A. K. Spearing-Ewyn, N. A. Beattie, A. L. Colebatch, A. J. Martinez-Martinez, **A. Docker**, T. M. Boyd, G. Baillie, R. Reed, S. A. Macgregor, A. S. Weller. The role of neutral Rh(PONOP)H, free NMe_2H, boronium and ammonium salts in the dehydrocoupling of dimethylamine-borane using the cationic pincer $[Rh(PONOP)(\eta^2\text{-}H_2)]^+$ catalyst.
Dalton Trans. **2019**, *48*, 14724–14736.

T. Bunchuay, **A. Docker**, A. J. Martinez-Martinez, P. D. Beer. A Potent Halogen-Bonding Donor Motif for Anion Recognition and Anion Template Mechanical Bond Synthesis.
Angew.Chem. Int.Ed. **2019**, 58,13823 –13827.

T. A. Barendt, **A. Docker**, I. Marques, V. Félix, P. D. Beer. Selective Nitrate Recognition by a Halogen-Bonding Four-Station [3]Rotaxane Molecular Shuttle*.*
Angew. Chem. Int. Ed. **2016**, *55*, 11069–11076.

Abbreviations

δ	chemical shift
λ	wavelength
μ	micro, dipole moment
v	frequency
°	degree
°C	degrees Celsius
Å	Ångstrom
A	acceptor
A^-	anion
abs	absorption
aq.	aqueous
Ar	aromatic
Arg	arginine
Asp	aspartate
ATP	adenosine triphosphate
a.u.	arbitrary units
bipy	2,2'-bipyridine
Boc	di-*tert*-butyl dicarbonate
BODIPY	Boron-dipyrromethene
br	broad
Bu	butyl
cat.	catalytic
conc.	concentrated
COSY	homonuclear correlation spectroscopy
CPS.	counts per second
CuAAC	copper(I)-catalysed azide–alkyne cycloaddition
D	donor
d	doublet
dd	doublet of doublets
DIPEA	*N*,*N*-di-*iso*-propylethylamine
DMF	*N*,*N*-dimethylformamide
DMSO	dimethyl sulfoxide
DNA	deoxyribonucleic acid
e.g.	*exempli gratia*
eq., equiv.	equivalent
ESI	electrospray ionisation
Et	ethyl
g	gram
G	Gibbs free energy
HB	hydrogen bonding

HOMO	highest occupied molecular orbital
hr.	hour
HSQC	heteronuclear single quantum coherence
Hz	hertz
I	intensity
int.	internal
i.e.	*id est*
J	Joule
J	coupling constant
k	kilo
K	Kelvin
K_{Ass}	association constant
L	litre
LUMO	lowest occupied molecular orbital
M	molar
M	mega, molecular ion
m	milli, multiplet,
m	*meta*
m/z	mass-to-charge ratio
Me	methyl
Mes	1,3,5-trimethylbenzene
MIM	mechanically interlocked molecule
min	minute
MLCT	metal-to-ligand charge transfer
mol	mole
MS	mass spectrometry
Ms, mesyl	methanesulfonyl chloride
n	nano
NMR	nuclear magnetic resonance
OAc	acetate
o/n	overnight
p	*para*
PET	photoinduced electron transfer
pH	$-\log_{10}[H^+]$
Ph	phenyl
pK_a	$-\log_{10}K_a$
ppm	parts per million
Pr	propyl
Py	pyridinium
q	quartet
quin.	quintet
R	chemical substituent
RCM	ring closing metathesis

ROESY	rotating-frame nuclear Overhauser effect correlation spectroscopy
rt	room temperature
s	second, singlet
sat.	saturated
sept.	septet
St	stopper
t	triplet
t, tert	tertiary
TBA	tetrabutyl ammonium
TBDMSCl	tert-butyldimethylsilyl chloride
TBTA	tris[(1-benzyl-1*H*-1,2,3-triazol-4-yl)methyl]amine
TLC	thin layer chromatography
Ts, tosyl	*para*-toluenesulfuonyl chloride
UV	ultra-violet
V	volt
vis.	visible
vs.	*versus*
VT	variable temperature
v/v %	volume/volume percent
wt.	weight
X	halogen atom
XB	halogen bonding

Contents

Abstract iii
Acknowledgements iv
List of Publications v
Chapter 1 Introduction 1
1.1 Supramolecular Chemistry: Origins and Principles 2
1.2 Non-covalent interactions: The tools of supramolecular chemistry 4
1.2.1 Electrostatic interactions 4
1.2.2 Hydrogen bonding (HB) 4
1.2.3 Ion-π interactions 4
1.2.4 van der Waals interactions 5
1.2.5 Hydrophobic and solvophobic effects 6
1.3 Biotic Recognition of charged species 7
1.4 The design of synthetic anion receptors 9
1.4.1 The motivation and challenges of anion recognition 9
1.4.2 Properties of anions 9
1.4.3 General strategies for anion receptor design 11
1.5 Sigma-hole interactions 13
1.5.1 Historical context 13
1.5.2 Sigma-hole interactions in anion recognition 15
1.6 Ion-pair recognition 26
1.6.1 Binding mode and cooperativity 26
1.6.2 Binding motifs 29
1.6.3 Pseudorotaxane and interlocked ion-pair receptor topologies 33
1.7 Project outlines 36
1.8 References 37
Chapter 2 Modulating Chalcogen Bonding and Halogen Bonding Sigma-hole Donor Atom Potency and Selectivity for Halide Anion Recognition 42
2.1 Introduction 43
2.2 Chapter Aims 46
2.3 Acylic chalcogen, halogen and hydrogen bonding 3,5-bis-triazole pyridine anion receptors 47
2.3.1 Design of the ChB, XB and HB anion receptors 47
2.3.2 Synthesis of the ChB, XB and HB anion receptors 47
2.3.3 Aryl Azide Precursor Synthesis 47
2.3.4 Dimethyl and Diaryl Ditelluride Synthesis 48
2.3.5 CuAAC synthesis of the ChB, XB and HB receptors 50
2.3.6 Anion Binding Studies of 1·ChB, 1·XB and 1·HB receptor series 56

2.3.7 Anion Binding Studies of 2·ChB receptor series 58
2.3.8 Anion Binding Studies of 3·ChB receptor series 60
2.4 Conclusions 63
2.5 References 64
Chapter 3 Highly Cooperative Chalcogen Bonding Heteroditopic Receptors for KCl Selective Recognition 65
3.1 Introduction 66
3.2 Chapter aims 67
3.3 ChB heteroditopic receptor synthesis 68
3.3.1 The synthesis of 3,5-bis-alkyne nitrobenzene precursors 68
3.3.2 Benzo-15-crown-5 ditelluride synthesis 69
3.3.3 CuAAC synthesis of the ChB receptors 70
3.4 Anion and ion-pair recognition studies 72
3.5 Solid-liquid extraction studies 76
3.6 Solid state structure determination 80
3.7 Liquid-liquid extraction studies 82
3.8 Liquid membrane transport studies 83
3.9 Conclusions 84
3.10 References 85
Chapter 4 Halogen Bonding Tetraphenylethene Anion Receptors 87
4.1 Introduction 88
4.2 Chapter Aims 91
4.3 Halogen Bonding Tetraphenylethylene (TPE) Anion Receptors 91
4.3.1 Synthesis of bromo- and alkyne- TPE precursors 91
4.3.2 Synthesis of mono-, bi-dentate and tetra-dentate TPE precursors 92
4.3.3 Preliminary anion binding studies 93
4.3.4 Solid-State Structure Determination 98
4.3.5 Anion coordination induced aggregation and anion sensing 101
4.3.6 Photoswitchable Anion Receptor studies 105
4.4 Conclusions 109
4.5 References 110
Chapter 5 Halogen Bonding Heteroditopic Materials for Cooperative Ion-Pair Binding and Extraction 112
5.1 Introduction 113
5.2 Chapter Aims 115
5.3 Halogen Bonding Heteroditopic Materials for Cooperative Ion-Pair Binding and Extraction 116

5.3.1 Design and synthesis of XB and HB heteroditopic receptor functionalised silica materials 116
5.3.2 Preliminary Extraction Studies 120
5.4 Conclusions 122
5.5 References 123
Chapter 6 Conclusions 125
Chapter 7 Experimental and Synthetic Procedures 128
7.1 General considerations 129
7.1.1 Chemicals and solvents 129
7.1.2 Instrumentations 129
7.2 ^{1}H-NMR titration protocols 129
7.2.1 Anion binding in organic and aqueous-organic mixture 129
7.3 Synthetic Procedures and Characterisation for Compounds in Chapter 2 129
7.4 Synthetic Procedures and Characterisation for Compounds in Chapter 3 142
7.5 Synthetic Procedures and Characterisation for Compounds in Chapter 4 148
7.6 Synthetic Procedures and Characterisation for Compounds in Chapter 5 156
7.7 Crystal structure determination 167
7.7.1 Structures for Chapter 2 167
7.7.2 Structures for Chapter 3 168
7.7.3 Structures for Chapter 4 172

Chapter 1 Introduction

1.1 Supramolecular Chemistry: Origins and Principles

Supramolecular Chemistry is defined as “the chemistry of the intermolecular bond, covering the structures and functions of the entities formed by association of two or more chemical species”.[1] By virtue of non-covalent interactions, chemical species can associate to form more complex, supramolecular entities. The library of non-covalent interactions used to assemble such entities include electrostatics, dispersion forces, aromatic donor-acceptor interactions (for example π-π stacking), hydrogen bonding (HB), halogen bonding (XB) and hydrophobic or solvaphobic effects. Whilst in isolation these interactions are typically weaker than covalent bonds, the concerted and considered employment of these non-covalent interactions can elicit remarkably stable molecular assemblies. Generally, supramolecular chemistry may be further classified into two categories: Host-guest recognition and Self-assembly (Figure 1.1). The former maybe considered an extension to coordination chemistry, in which a ligand architecture is capable of recognition, or binding, of another chemical entity through typically reversible non-covalent interactions. The latter concerns the ability of discrete molecular components to organise themselves into a defined structure, in which the agency behind this emergence of order is the formation of multiple, and frequently cooperative, non-covalent interactions.

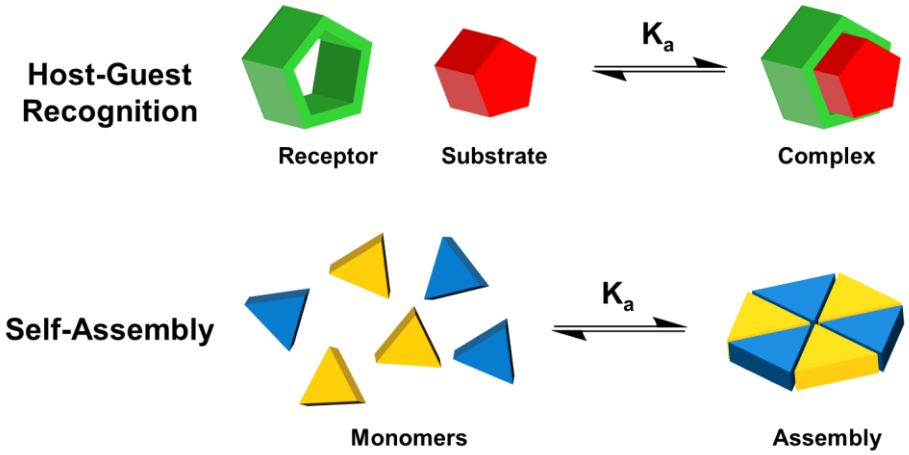


Figure 1.1 Cartoon representation of host-guest recognition (top) and self-assembly (bottom).

Generally, regarded as the inception of supramolecular chemistry, Pedersen’s seminal work in 1967 reported a family of variously substituted and sized cyclic polyethers and their coordination complexes with a range of alkali and alkaline earth metal ions.[2] Coined ‘crown ethers’, the serendipitous discovery heralded a milestone of achievement as previously no synthetic ligand was known to form stable complexes with alkali metals. Reports by Lehn[3] and Cram[4] in subsequent years would follow producing increasingly elaborate molecular

architectures for alkali metal cation complexation including cryptands and spherands (Figure 1.2).

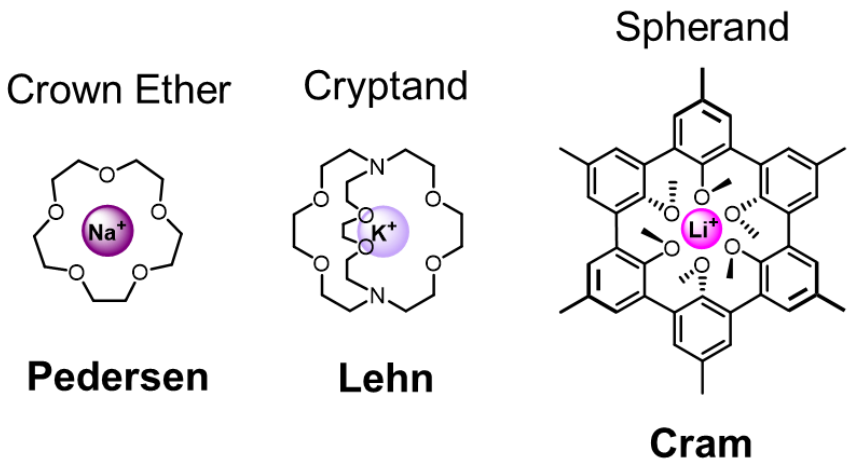


Figure 1.2 Chemical structures of Pedersen's crown ether, Lehn's cryptand and Cram's spherand.

Cram later formalised two central concepts of 'host-guest' chemistry[5]: *complementarity* and *preorganization*:

Complementarity: *"to complex, hosts must have binding sites which can simultaneously contact and attract the binding sites of the guests without generating internal strains or strong nonbonded repulsions."*

Preorganisation: "*the more highly hosts and guests are organised for binding and low solvation prior to their complexation, the more stable will be their complexes."*

While contemporary supramolecular chemistry has delineated specific types of complementarity and preorganisation, these maxims provide a succinct statement of the guiding principles at the crux of supramolecular host-guest chemistry. Indeed, in recognition of their contributions the 1987 Nobel prize was jointly awarded to Pedersen, Lehn and Cram 'for their development and use molecules with structure-specific interactions of high selectivity'.

However, further concepts relevant to the field of self-assembly have also emerged. In light of their observations on thermodynamically controlled multicomponent macrocyclisation reactions, Sanders and co-workers observed that certain building blocks are capable of self-sorting despite the constituent building blocks possessing no intrinsic preorganisation favouring the formation toward a given structure.[6] Termed *predisposition* Sanders defined it as follows:

Predisposition: *"a strong conformational or structural preference expressed by the building block once incorporated into a larger structure."*

1.2 Non-covalent interactions: The tools of supramolecular chemistry

The objective of supramolecular host-guest chemistry is to design molecules that are capable of strong and selective recognition of a given species using a variety of concerted non-covalent interactions. The following sections summarises the principal interactions and effects that are typically employed in synthetic receptors for the recognition of cationic and anionic species.

1.2.1 Electrostatic interactions

Arguably the most fundamental, these are attractive Coulombic interactions between oppositely charged species (Figure 1.3a). Intuitively, the employment of electrostatic interactions in synthetic receptor design is most common for the recognition of charged species, however the absence of directionality compromises the utility of ion-ion interactions for the purposes of selective recognition. However, the exploitation of ion-dipole interactions, albeit somewhat weaker than ion-ion counterparts, are more common by virtue of their directional dependence. In solution phase, the strength of these interactions are highly subject to the dielectric constant (ε) of the medium, for example the electrostatic interaction energy between two ions is anticipated to be attenuated by a factor 16 moving from a non-polar solvent like chloroform (ε = 4.81) to a highly polar solvent such as water (ε = 78.1).

1.2.2 Hydrogen bonding (HB)

Pervasive in both biotic and synthetic receptor systems, HB is described as the attractive interaction between a hydrogen atom which when bonded to an electronegative element exhibits a partial positive charge which is capable of interacting with a Lewis base (Figure 1.3b). In contrast to single covalent bonds, which typically exhibit strengths which vary by a factor of 4 (120-500 $kJmol^{-1}$), HB strengths, although in general of smaller magnitude, exhibit a wider range of interaction strengths (8-160 $kJmol^{-1}$). A commonly observed characteristic of stronger HB interactions is the tendency towards a linear interaction geometry between the HB donor and Lewis base, while weaker HB interactions typically possess a wider angular range.[7] The facile accessibility of potent multidentate HB donor motifs and their high degree of directionality has made them a veritable workhorse of molecular assembly and recognition.[8] Extensively studied in the solid-state, solution phase and computationally, a vast quantity of data concerning strength and geometrical preferences has been collated, for which it is generally considered an electrostatic rationale satisfactorily describes the situation in most cases.[9]

1.2.3 Ion-π interactions

Aromatic π-systems can also provide appropriate areas of electron density/deficiency to attractively interact with charged species (Figure 1.3c). In this context, carefully selected arrangements of electron-rich aromatic units provide potent recognition environments for cationic species, termed cation-π interactions. These are perhaps most well documented in

biotic systems in which the recognition of quaternary ammonium species is primarily achieved by paneled binding sites comprising of tyrosine and tryptophan residues.[10–13] Metal cations are also known to participate in similar cation-π interactions, with the group 1 alkali metal cations and silver(I) cations featuring most heavily.[14] Indeed, the potential of this interaction as an exploitable non-covalent force in supramolecular host design is exemplified by calculations which suggest that interaction energies between K^+ and the aromatic π-system benzene, ca. 80 $kJmol^{-1}$, surpasses that of a $K^+\cdots OH_2$, ca. 75 $kJmol^{-1}$, in the gas phase.[12] The association of anions to electron deficient aromatic systems known as anion-π interactions was first conceived *in silico*.[15–18] Exploiting electron deficient aromatic units such as triazine or highly perfluorinated aryl groups, has facilitated the recognition of a wide range of anionic species.[19–21]

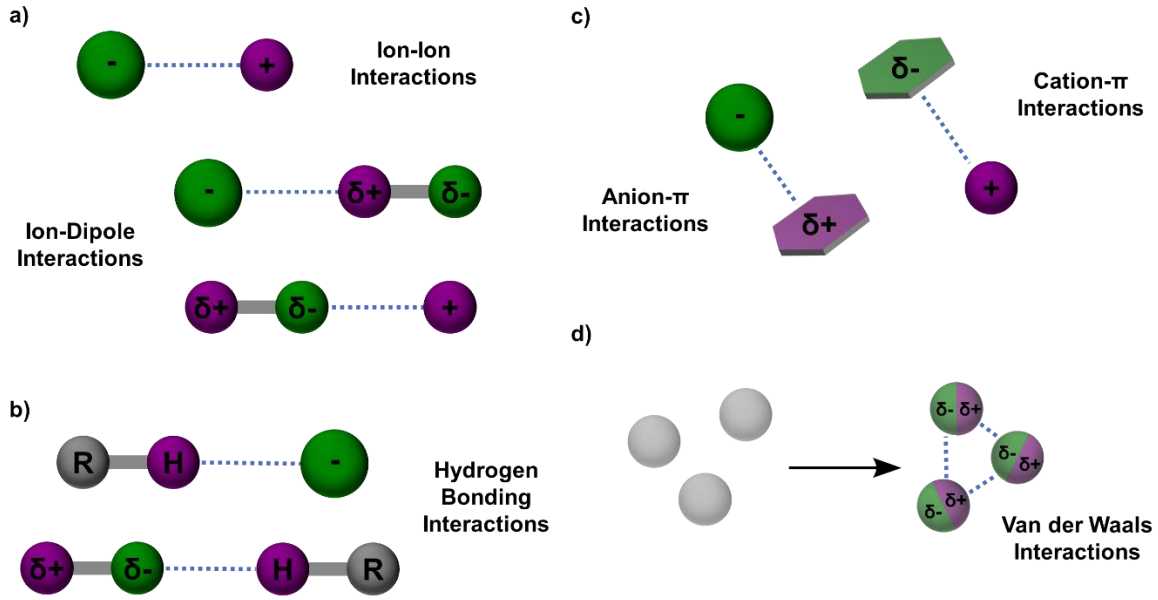


Figure 1.3 Cartoon representation of the selected non-covalent interactions a) Electrostatic b) Hydrogen bonding c) ion-π d) van der Waals.

1.2.4 van der Waals interactions

Also referred to as dispersion forces and often the weakest non-covalent interaction (typically < 5 $kJmol^{-1}$), this attractive interaction occurs as a result of a molecule or atom possessing a temporary dipole which is capable of polarising the electron density of another chemical entity generating a transient attractive electrostatic attraction (Figure 1.3d). Although this interaction is typically overlooked in the context of rational receptor design due to non-specificity and its non-directional nature, van der Waals interactions can contribute a considerable energetic component in the overall thermodynamic stability of associative processes. This is especially true for heavy elements, which by virtue of their greater polarisability tend to exhibit the strongest van der Waals interactions. For example, low-coordinate Au(I) compounds are known to associate into dimers or oligomers via attractive 'aurophilic interactions'.[22] This

cohesive interaction between 'closed-shell' d^{10} metal centres is estimated to be in the range of 5-25 kJ mol^{-1} and is believed to originate from unusually strong van der Waals interactions.[23]

1.2.5 Hydrophobic and solvophobic effects

The solvent medium in which host-guest association takes place is of paramount importance. Key interactions such as solute-solvent and solvent-solvent can be profound, particularly for polar protic media such as methanol and water. The strength of these solvent-solvent interactions in polar protic solvent media causes non-polar compounds to aggregate, which has been exploited in the recognition of 'solvaphobic' cationic, anionic and neutral species. Whilst the origins of these 'recognition events' is not driven by host-guest directed non-covalent interactions *per se,* the means by which they operate are *via* the previously mentioned interactions. Since these effects are generally most pronounced in media in which interactions between solvent molecules is greatest. It is unsurprising that these solvophobic effects operating in water, termed 'hydrophobic', are capable of eliciting dramatic recognition events. The 'classical' hydrophobic effect is entropically driven, due to the release of water molecules from highly ordered solvation shells surrounding the host and guest.[24,25] The 'non-classical' hydrophobic effect is characterised by an enthalpic contribution arising from 'high energy' water molecules being released into the bulk forming strong HB interactions. [26–28] Typically, host molecules capable of binding cations or anions in this fashion are macrocyclic and possess deep hydrophobic cavities which favour the complexation of large charge-diffuse, poorly hydrated species. Currently underdeveloped, the exploitation of these effects for the purposes of charged species recognition has proved promising. For example Brotin and co-workers have reported water soluble cryptophanes (Figure 1.4),[29] which are capable of binding Cs^+ with remarkable high affinity $\log K_a = 6.8$. Nau has reported the strong binding of dodecaborate ($B_{12}H_{12}^{2-}$) with γ-cyclodextrin $\log K_a = 3.3$.[30]

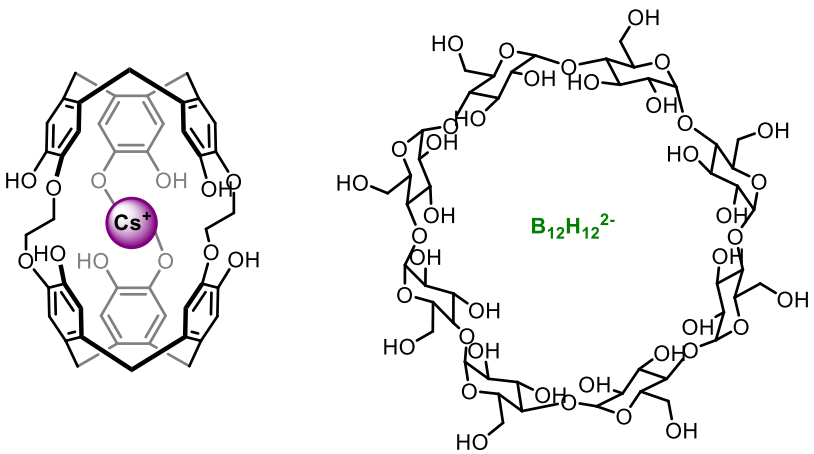


Figure 1.4 a) Caesium cation binding cryptophane b) γ-cyclodextrin encapsulation of a $B_{12}H_{12}^{2-}$.

1.3 Biotic Recognition of charged species

The precise regulation of charged species in biological systems underpins many of the processes required for life, consequently nature has developed a plethora of strategies for their recognition, translocation, and transformation. Biotic systems possess highly elaborate binding sites capable of exploiting subtle differences between guest species through multiple complementary concerted interactions. The origin of such substrate specificity is the electronic and topological complementarity of the binding site to the guest, tailoring the recognition site through functional group specific interactions. Typically non-covalent in character, the diverse range of interactions exploited is often, but not limited to, a highly sophisticated combination of those previously mentioned. Whilst synthetic chemists can only aspire to the complexity achieved in biotic systems, inspiration can be taken in terms of host-design.

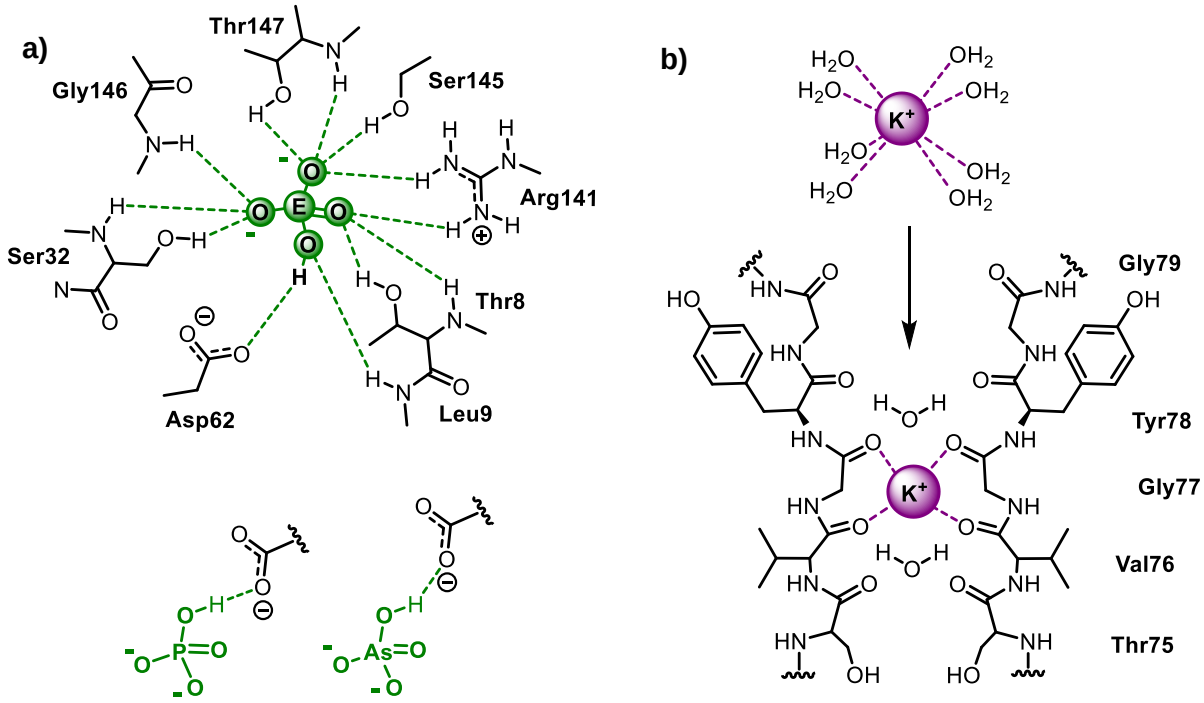


Figure 1.5 a) Phosphate binding protein sequestering HEO_4^{2-} (E=P, As) through twelve HB interactions and close-up view of the short hydrogen bond between the bound phosphate or arsenate oxoanion and the carboxylate of Asp62. b) Truncated structure of the potassium channel KscA.

For example, phosphate (PO_4^{3-}) constitutes a building block requisite for the construction of DNA and RNA, whereas its heavier group 15 congener, arsenate (AsO_4^{3-}) is highly toxic. However, their remarkably similar physiochemical properties including shape, basicity, hydration enthalpies and redox behaviour, means effective discrimination between these species is challenging. Elias and Tawfik have demonstrated that a species of bacteria is capable of selectively extracting and processing phosphate to maintain growth in the presence of markedly higher arsenate concentrations.[31] The ability of the bacterium to survive

in such inhospitable conditions originates from highly specialised phosphate binding proteins (PBPs). X-ray crystallographic analysis of HPO_4^{2-} and $HAsO_4^{2-}$ bound PBP structures demonstrate that both anions, in their dibasic form, are bound in very similar fashions, in which a series of N-H and O-H hydrogen bond donor containing residues encapsulate the oxoanions forming in total 12 hydrogen bonds (Figure 1.5a). However, close inspection reveals a significant peturbation of the HB array encapsulating arsenate when compared to phosphate, notably the short contact (ca. 2.50 Å) between the pendant carboxylate of Asp62 and the hydroxyl group of the oxoanions. In the case of phosphate, the O-H···O bond angle is close to linearity at 176 °, while for arsenate it is a considerably distorted 127 °. The origin of the structural differences results from a longer As-O bond relative to P-O. Although PO_4^{3-} and AsO_4^{3-} differ in radii by only 4%, the strict requirement for interaction distances endowed by the well-defined topology of the PBP binding site magnifies this minor structural difference to elicit an enormous change in affinity.

Often overlooked in the recognition of charged species is the crucial role solvation effects play in determining the critical functions of the host and guest.[32,33] This is demonstrated by the ion transport proteins which to some degree dehydrate a charged guest to facilitate translocation to or from various aqueous environments separated and compartmentalised by non-polar lipid membranes.[34] The KscA protein, one of the potassium channels responsible for controlling electric potentials across cell membranes, is capable of enabling near diffusion-limit K^+ transport whilst exhibiting a 10^4-fold selectivity for potassium ions over sodium ions.[35–38] Insight into the mechanism of this remarkable feat of selectivity is obtained by inspection of the pore 'filter'. Comprised from four peptide subunits, high resolution crystal structure analysis of the potassium loaded extracellular entryway reveals the presence of a hydrated K^+ ion possessing a square antiprismatic hydration shell which itself is complexed with a precisely ordered array of HB interactions from proximal threonine residues. The pore entrance is decorated with Gly79 carbonyl oxygen atoms pointing directly into the extracellular environment as to encourage the requisite dehydration of the incoming potassium cation. Once translocated to the filter system, the encapsulated K^+ exhibits 8 contacts with amide carbonyls of coordination distances in the range of 2.70 to 3.08 Å, and a mean value of 2.85 Å in an arrangement resembling the structure of its hydration shell in bulk solution (Figure 1.5b). The highly specific match between cavity size, preferred coordination number and geometry of K^+ is thought to be a major contribution to the remarkable selectivity, as a smaller Na^+ cation would be incapable of optimally interacting with eight oxygen donors and is thereby unable to fully compensate the energetic cost of desolvation.[39]

1.4 The design of synthetic anion receptors

1.4.1 The motivation and challenges of anion recognition

Anions play innumerable roles in biological, industrial, and environmental spheres. Indeed, the majority of biological processes are intimately implicated with anionic species including: DNA, responsible for the storage of genetic information; adenosine triphosphate (ATP), a repository and relay-mechanism of chemical energy driving cellular function and the activation of enzymes by anionic co-factors. Anthropogenic sources of nitrates and phosphates from excessive fertiliser use in arable farming has led to eutrophication of waterways resulting in harmful algae blooms, while combustion of fossil fuels contributes to the highly toxic arsenate and selenate entering the biosphere. Hence considerable efforts have been directed towards the design and synthesis of artificial receptors capable of anion binding, sequestration, and sensing, especially in aqueous or physiologically relevant media.

1.4.2 Properties of anions

Size and shape

Anions typically possess larger radii than their isoelectronic cations and as a consequence exhibit significantly weakened electrostatic interactions with potential host systems. Even simple inorganic anions adopt a broad range of geometries (Figure X) including spherical (halides), linear (thiocyanate, azide), bent (nitrite), trigonal planar (nitrate, carbonate), square planar (tetrachloroaurate), tetrahedral (sulphate, phosphate, perrhenate), octahedral (hexafluorophosphate) and icosahedral (dodecaborate). Furthermore biological anions such as nucleotides have more complex structures in the form of polyanions such as double helical DNA.

pH dependence

Many anions exist under multiple protonation equilibria and can be subject to significant speciation such that the identity of species may only exist within a narrow range of pH. Furthermore, certain classes of anion receptor, for example polyammonium host systems are pH dependent. Consequently, anion recognition by these systems can only occur within a limited pH window (Figure 1.6). Indeed, aside from the overall pH of the medium, highly basic anions such as fluoride, cyanide and acetate may also deprotonate acidic sites on receptor species.

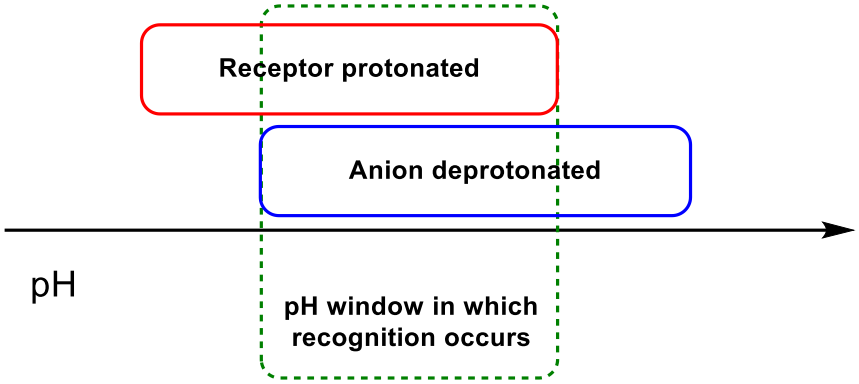


Figure 1.6 Schematic illustration of the pH window in which an anion may be recognised by a pH dependent receptor.

Solvation energy

As alluded to earlier, solvation often plays a critical role in the recognition of charged species. This is especially true for anions which are typically more strongly solvated than cations of similar radii. For example, the free energies of hydration (ΔG_{hyd}^{o}) for K^+ and F^-, are -295 kJ mol^{-1} and -465 kJ mol^{-1} respectively. A receptor capable of binding an anion must, partially at least, desolvate the anion prior to complexation and therefore overcome a considerable enthalpic penalty. As a consequence of this considerable enthalpic penalty the majority of anion receptors reported to date function in aprotic organic solvent media such as chloroform or acetone. High polarity protic solvents such as methanol or water are capable of effectively solvating anionic species through the formation of hydrogen bonding interactions, the extent of this solvation is reflected in the Hofmeister series of hydrophobicity (Figure 1.7). From left to right, as the charge density of the anion decreases weaker hydration results in increasing lipophilicity.

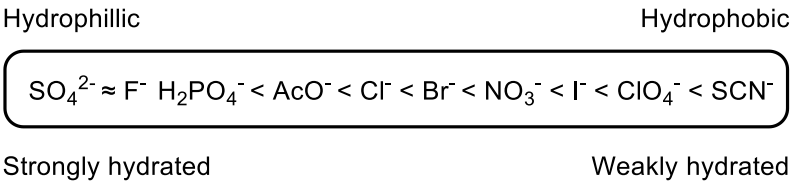


Figure 1.7 The Hofmeister series of anion hydrophobicity.

1.4.3 General strategies for anion receptor design

In 1968 Park and Simmons reported the first synthetic anion receptors, diazabicyclic compounds coined 'katapinates' (Figure 1.8a).[40] In acidic aqueous media, the protonated dicationic cryptand-like receptors were shown to encapsulate halides with modest stability (K_a (Cl^-) = 4 M^{-1} and K_a(Br^-) = 1 M^{-1} by a combination of favourable electrostatics and hydrogen bonding (HB) interactions. Subsequent decades would witness an extension of this strategy with Lehn's polyammonium macrocycles[41] and Schmidtchen's pH-independent macrotricyclic quaternary ammonium salts[42] (Figure 1.8b and 1.8c), However, it was quickly acknowledged that whilst eliciting high affinities these highly-charged systems typically exhibited relatively poor discrimination between negatively charged species. Recent years have focused on developing low charge or neutral receptors typically featuring NH hydrogen bond donor motifs based on amide, urea and pyrrole such as those reported by Crabtree (Figure 1.8d),[43,44] Fabbrizzi,[45,45] and Sessler (Figure 1.8e).[46,47]

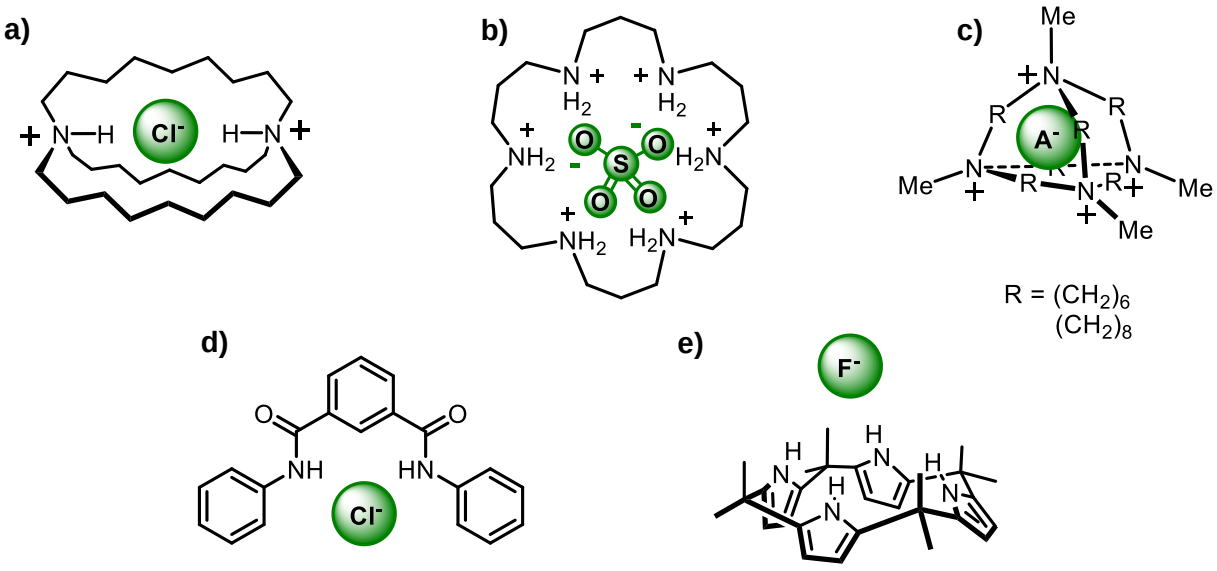


Figure 1.8 a) Park and Simmons' marcobicyclic ammonium receptor. b) Lehn polyammonium sulphate binding macrocycle. c) Schmidtchen's quaternary ammonium cages. d) Crabtree's isophthalimide receptor. e) Sessler's fluoride binding calix[4]pyrrole.

However, recent pioneering investigations by Flood and others have demonstrated that CH groups integrated into inductively electron-withdrawing host structural frameworks such as cyanostilbene and 1,2,3-triazole heterocycles (Figure 1.9a), constitute a valuable addition to the repertoire of HB donors. A seminal report in 2013 by Flood detailed the synthesis of a pentagonal macrocycle comprised of cyanostilbene repeat units forming a rigid electropositive cavity (Figure 1.9b), capable of complexing anions normally considered non-coordinating such as hexafluorophosphate in a 2:1 host-guest stoichiometry with remarkable overall stabilities $\beta \approx 10^{12}$ M^{-2} in MeOH:CH_2Cl_2 4:6 (v/v) solvent mixtures.[48] A subsequent report by the same group demonstrated that even higher numbers of C-H HB donors can be

exploited in the anion binding cavities (Figure 1.9c). Comprised of alternating triazole and carbazole units, the shape persistent macrocycle bound larger anions such PF_6^- ClO_4^- and SbF_6^- in a similar 2:1 stoichiometric sandwich complex-like fashion.[49]

In a very recent example Flood has continued to challenge conventional wisdom regarding the potency of C-H HB donors with a neutral macrobicyclic cage (Figure 1.9d) capable of chloride binding with attomolar (10^{17} M^{-1}) affinity in CD_2Cl_2 solution.[50] The cryptand-like cage molecule selectively removes NaCl from aqueous solution.

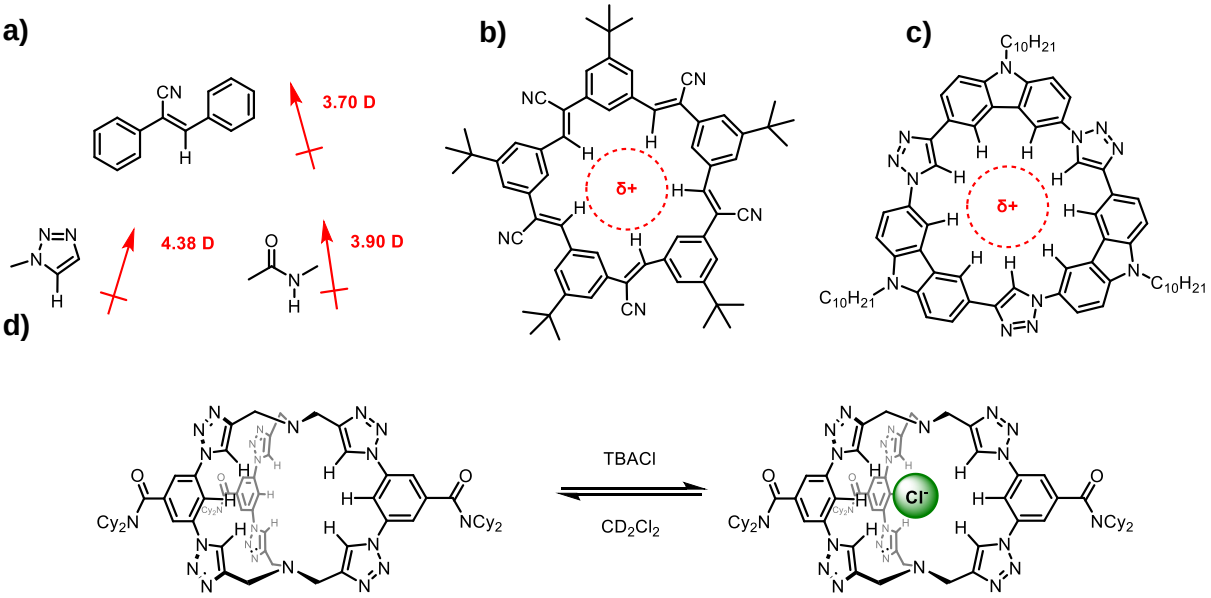


Figure 1.9 a) Representation of dipole moments of cyanostilbene, 1*H*-1,2,3-Triazole and *N*-methylacetamide. Flood's a) 'cyanostar' and c) 'tricarb' macrocycles d) chloride selective cryptand.

1.5 Sigma-hole interactions

In the last decade, a new class of supramolecular interactions have emerged and begun to be exploited in anion host-guest recognition applications in particular. Coined sigma-hole interactions, this group of non-covalent interactions can be broadly defined as the attractive interaction between an electrophilic region of a main-group element and a nucleophilic Lewis base. The following summarises a brief chronology of their discovery, discussion of their fundamental properties and highlights recent seminal anion recognition examples.

1.5.1 Historical context

In 1954, Hassel et al. reported the X-ray crystallographic analysis of a yellow solid 'adduct' formed by the mixing of bromine and 1,4-dioxane.[51] The structure featured chains of alternating dioxane and Br_2 molecules directed by linear O···Br-Br···O arrangements (Figure 1.10a). Of particular note were the O···Br distances which were considerably shorter than the sum of the van der Waals radii. The authors attributed these observations to 'very strong interactions' between neighbouring bromine and oxygen atoms. Analogous studies with various halogen species e.g. ICl and CHI_3 and Lewis bases such as pyridine, hexamethylenetetramine and dithiane revealed this interaction type was commonplace (Figure 1.10b and 1.10c).[52,53] Indeed, structural analysis in later decades demonstrated analogous interactions between heavier p-block elements and neutral and anionic species were ubiquitous, constituting a pervasive structural feature in main-group chemistry.

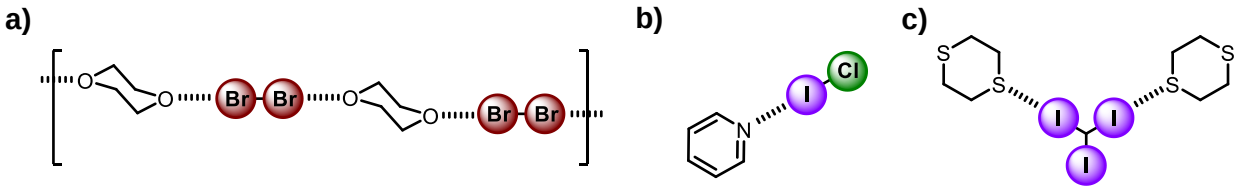


Figure 1.10 a) Linear O-Br-Br-O linkages in the solid-state structure of bromine 1,4 dioxane b) linear N---I-Cl arrangements observed in the crystal structure of pyridine-iodo monochloride; c) neighbouring I---S-C interactions present in the crystal structure of dithiane-iodoform.

Surprisingly, it is only in the last decade or so that quantitative investigations have been undertaken to elucidate the origin and nature of sigma-hole interactions. Reports by Clark[54] and Frontera[55] have shown computationally that when group 14-17 atoms are covalently linked to electron-withdrawing groups the electron density of the main group atom is anisotropically perturbed (Figure 1.11). The electron-deficient regions of these atoms are known as the sigma (σ)-holes and the corresponding respective type of bonding with Lewis bases is named according to the main group-element that functions as an electron acceptor, i.e. halogen, chalcogen, pnictogen and tetrel bonding (XB, ChB, PnB and TrB, respectively). Crucially, these studies provide a rationale for the long-known characteristics of these interactions, for example the strict angular requirement of donor-acceptor geometries is a direct consequence of the highly localised nature of the σ-hole. Furthermore, the observation that the most potent σ-hole interactions are typically observed with the heaviest p-block is also consistent with models reliant on atom polarisability.

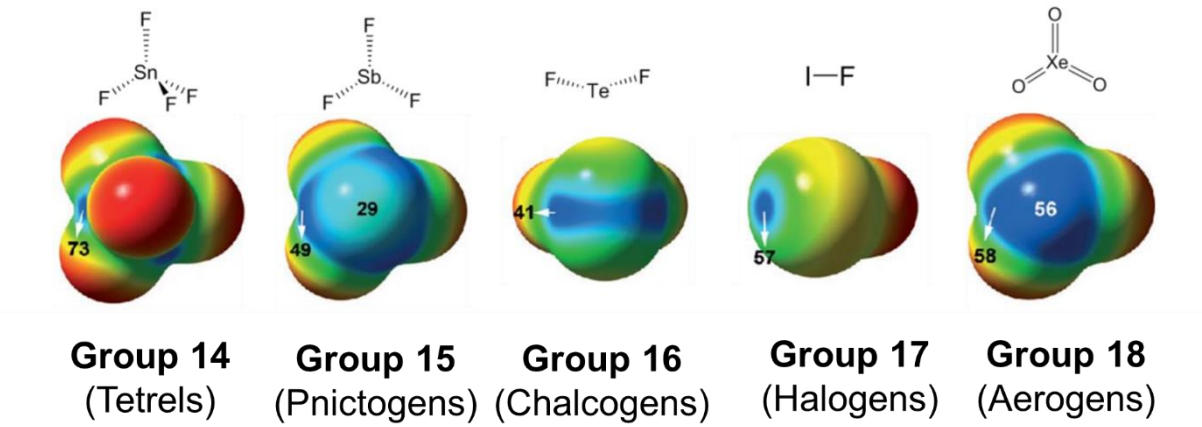


Figure 1.11 Molecular Electrostatic Potential (MEP) surfaces of several σ-hole donor molecules. Blue regions denote the electron-deficient σ-holes whilst red regions represent high electron density. Some of the MEP energy values in kcal mol^{-1} are displayed.

1.5.2 Sigma-hole interactions in anion recognition

Whilst σ-hole interactions have been widely acknowledged as valuable directing elements in the construction of crystalline materials for quite sometime,[56,57] their application in solution phase anion receptor design is a recent development.[58–61] The following details a survey of synthetic receptor systems grouped by σ-hole bonding interaction type.

Halogen bonding (XB) anion receptors

The most exploited XB donor motifs for anion recognition almost invariably possess a heavy halogen atom covalently linked to an electron withdrawing organic residue. In no small part due to their extensive use in crystal engineering and synthetic accessibility, perfluorinated aromatic motifs were some of the first XB donors to appear in host design. A seminal report by Resnati[62] et al. in 2005 described a tripodal receptor comprised of a tris(polyoxyethylene)amine unit and three pendant 4-iodotetrafluorophenyl groups (Figure 1.12a); ^{1}H NMR complexation experiments in $CDCl_3$ solution confirmed the receptor capable of binding a NaI ion-pair with a considerably higher affinity than its perfluorinated analogue. X-ray structural analysis of the sodium iodide receptor complex revealed the concomitant binding of a NaI ion-pair, through a cryptand-like sequestration of Na^+ by the amino-polyether section and I^- binding through the formation of short C-I$\cdots$I$^-$ contacts. Reports by Taylor et al. were to follow six years later towards the goal of generating multidentate XB donor arrays,[63] where it was demonstrated that multiple concerted XB$\cdots$Cl$^-$ interactions can be exploited as the sole driving force for chloride binding in acetone-d_6 solution (Figure 1.12b).

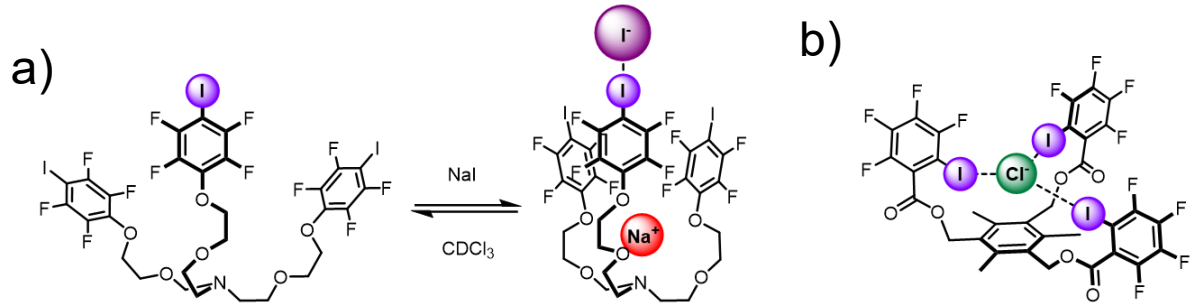


Figure 1.12 a) Resnati's tripodal iodoperfluoroarene XB receptor capable of binding NaI. b) Taylor's tripodal chloride binding iodoperfluoroarene receptor.

The surge in interest for XB-mediated recognition has stimulated further development of neutral and cationic XB donor motifs of varying potency and synthetic modularity. Mostcommonly encountered motifs include: halotriazole/halotriazolium, haloimidazolium and halopyridinium (Figure 1.13).

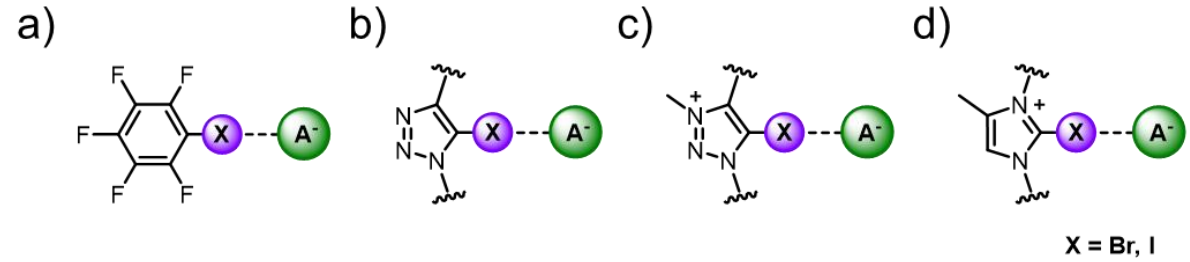


Figure 1.13 a) Haloperfluoroarene, b) halotriazole, c) halotriazolium and d) haloimidazolium XB donor motifs; X = halogen atom, typically Br and I.

Examples include Schubert and co-workers reporting a series of acyclic halotriazole and halotriazolium-based XB receptors capable of effective anion recognition in highly competitive media.[64] Anion binding studies in DMSO-d_6 revealed larger halide affinities for more charge-dense halides, as well as a general preference for the binding of more basic oxoanions. As anticipated, the dicationic triazolium receptor exhibited stronger binding of chloride in comparison to the neutral bis-iodotriazole analogue (K_a = 1,200 M^{-1} and K_a = 51 M^{-1}, respectively) (Figure 1.14), highlighting the potency of charge-assisted XB.

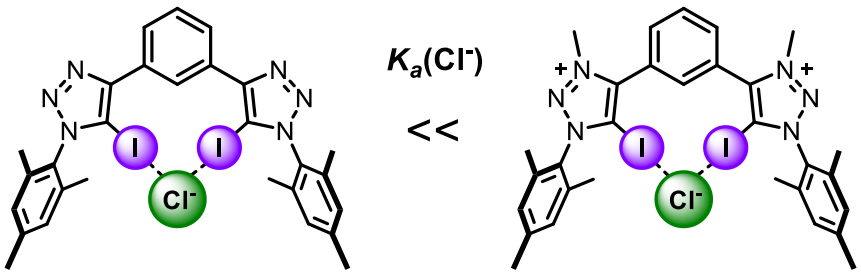


Figure 1.14 Schubert's iodotriazolium and iodotriazole acyclic receptors.

As alluded to previously, one of the most crucial considerations in the design of synthetic receptor systems is *preorganisation*. Specifically, the ability to construct a host which undergoes minimal conformational change upon guest complexation increases the thermodynamic stability through enthalpic and entropic effects. In this vein, recent years have witnessed the employment of a diverse range of strategies to confer preorganisation on XB-systems as a means of increasing receptor anion binding potency. For instance, Huber's bis-iodo-benzimidazolium receptor (Figure 1.15a) maintains a convergent XB donor conformation due to the restricted C-N bond rotation imposed by the ortho-substituted trifluoromethyl group.[65] Conformationally locking XB donor orientation has also been achieved in a neutral bimetallic rhenium(I) bis-iodotriazole pyrimidine system in which chelation of a Re(I) centre by Lewis basic nitrogens of the triazole and pyrimidine unit also enforces receptor rigidity (Figure

1.15b).[66] This ambivalent character of the iodo-triazole group has been exploited as a preorganisational tool via non-covalent means by Schubert et al.,[67] wherein a bis-iodotriazole carbazole cleft-type receptor exhibited enhanced halide anion affinity in THF solution when the central carbazole unit was functionalised with phenol groups which facilitated intramolecular O-H···N hydrogen bond formation, thereby restricting rotational freedom (Figure 1.15c). Molina's report of a bis-iodotriazolium containing receptor appended with pyrene termini achieved conformational preorganisation by exploiting π-π stacking between the pendant aromatic residues as means of favouring bidentate complexation of $HP_2O_7^{3-}$ (Figure 1.15d).[68] Whilst our current understanding of XB ascribes the Lewis acidic behaviour of XB donors to an anisotropically depleted electron density at a localised region of the halogen atom, an implicit corollary to the anisotropic electron distribution, is the preservation of electron dense regions. Conceivably, this property imparts XB donors with amphoteric character, wherein the constituent halogen can function as an electrophile or nucleophile. In a notable study, Berryman reported a series of 1,3-bis(4-ethynylpyridinium) receptors,[69] in which extensive solution phase, crystallographic and computational studies demonstrated that installation of a central aniline unit serves to non-covalently preorganise the halo-pyridinium XB donors through intramolecular N-H···I formation (Figure 1.15e). Remarkably, it was also demonstrated that the formation of the HB interactions to the iodine atom increased the potency of XB interactions formed in solution by a novel non-covalent polarisation enhancement.

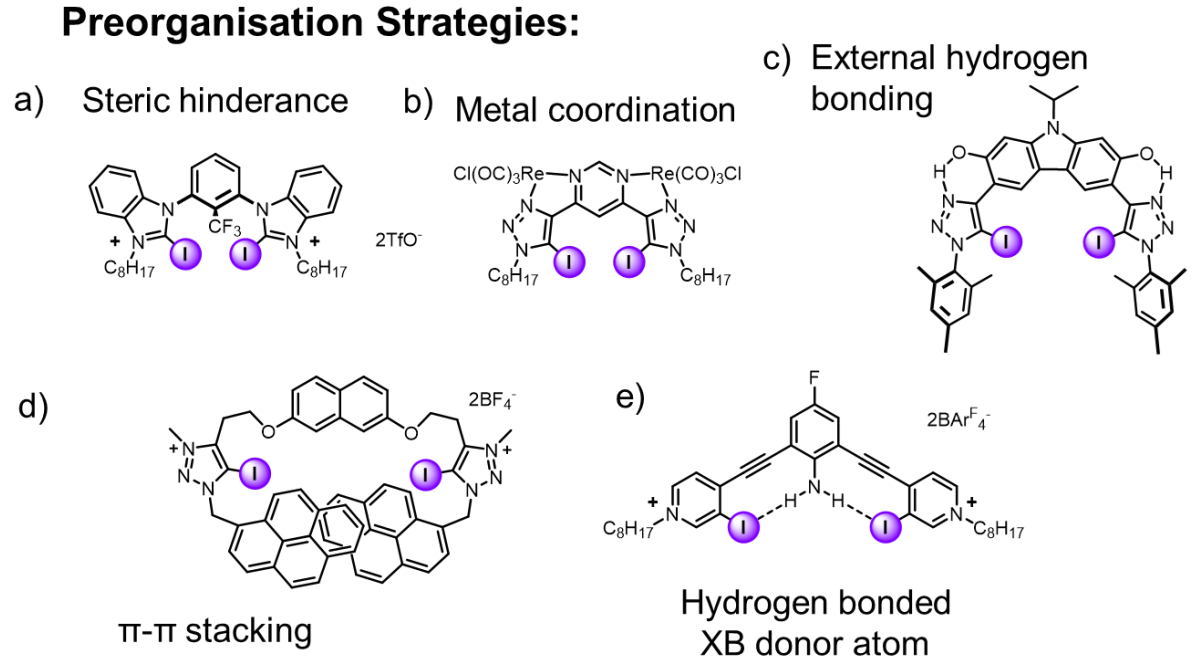


Figure 1.15 Summarised strategies of preorganisation in XB anion receptor motifs.

Macrocyclic systems offer synthetically accessible, highly preorganised architectures which have featured heavily in supramolecular host-guest chemistry. It is therefore of little surprise that XB macrocyclic systems were explored as anion recognition motifs. In 2011 and 2012 Beer *et al.* integrated 2-bromo- and 2-iodo- haloimidazolium motifs into a series of macrocyclic haloimidazoliophane receptors (Figure 1.16a and 1.16b).[70,71] The meta-xylyl spacer XB receptor, (Figure 1.16a), was capable of halide binding in competitive CD_3OD: D_2O (1:1 v/v) solvent mixtures, ^1H NMR titration studies revealed considerable bromide selectivity over both chloride ($K_a(Br^-)/ K_a(Cl^-) > 80$) and iodide ($K_a(Br^-)/ K_a(I^-) > 4$). Notably the HB proto-imidazolium analogue, exhibited considerably diminished anion affinity. Solid state characterization of the meta-xylyl-spacer receptor bromide complex confirmed a cooperative bidentate XB-bromide binding mode, suggesting this conformation is the optimal geometry for Br^-. Capitalising on the high anion affinity exhibited by the dicationic cyclophane system, the same group extended this work by integrating fluorescent naphthyl groups (Figure 1.16b). The resultant XB receptors functioned as highly sensitive chemosensors, wherein halide sensing was achieved by monitoring the anion-induced perturbations of naphthyl fluorescence emission spectra. Quantitative fluorescence titration experiments demonstrated the bromo- and iodoimidazolium XB receptors were capable of strong binding (log $K_a > 4$) bromide and iodide in the same CD_3OD: D_2O (1:1 v/v) competitive aqueous solvent medium. Conceivably a consequence of the considerable steric demands of the larger halogen atoms, higher denticity XB donor arrays are rare. However, Kubik *et al.* have reported a cyclic pseudo-peptide (Figure 1.16c),[72] the anion recognition behavior of tridentate XB donor was investigated by quantitative ^1H NMR titration and ITC experiments, showing impressive halide association constants of log K_a = 3.28, 2.85 and 2.15 for Cl^-, Br^- and I^- respectively in [D_6]-DMSO/H_2O (97.5:2.5 v/v) solvent mixtures.

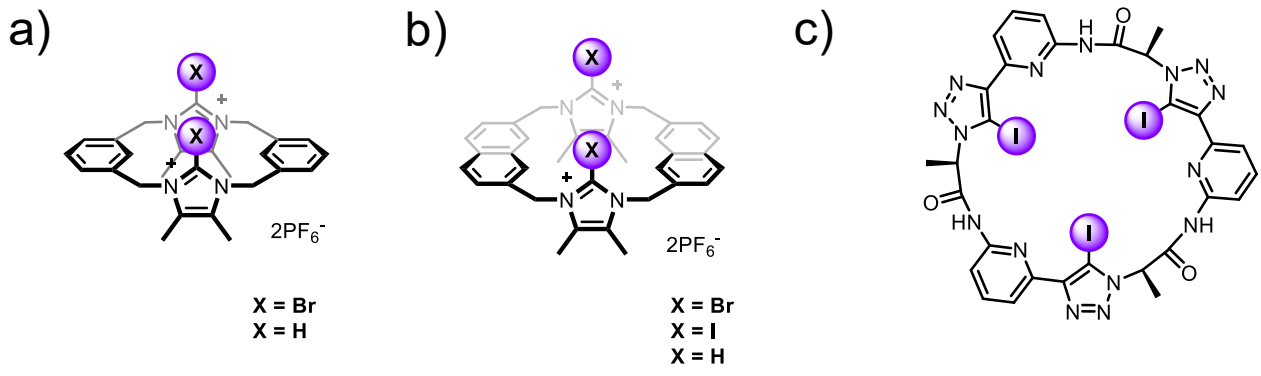


Figure 1.16 Beer's haloimidazoliophane receptors a) and b). c) Kubik's tridentate cyclopeptide receptor.

Biotic anion receptors mitigate the challenges of anion recognition in water *via* highly preorganised convergent arrays of HB donors and acceptors buried deep beneath the protein surface, effectively shielding the binding site from competitive water solvation. One of the most significant challenges in supramolecular chemistry is to replicate the affinity and selectivity towards guest recognition demonstrated by nature. Interlocked hosts, to some extent, provide analogues to the aforementioned biological systems where the mechanical bond serves to create a three-dimensional cavity capable of encapsulating a target species. In 2014 Beer *et al.* reported a bidentate XB 3,5-bis-(iodotriazole)-pyridinium motif functionalised with permethylated β-cyclodextrin termini (Figure 1.17).[73] Investigation of the anion recognition properties of the XB [2]rotaxane by ^{1}H NMR titration experiments revealed the host was capable of halide recognition in water with a significant selectivity for the heavier halides, $K_a(I^-)$/ $K_a(Cl^-)$ = 40 and $K_a(I^-)$/ $K_a(Br^-)$ = 8.

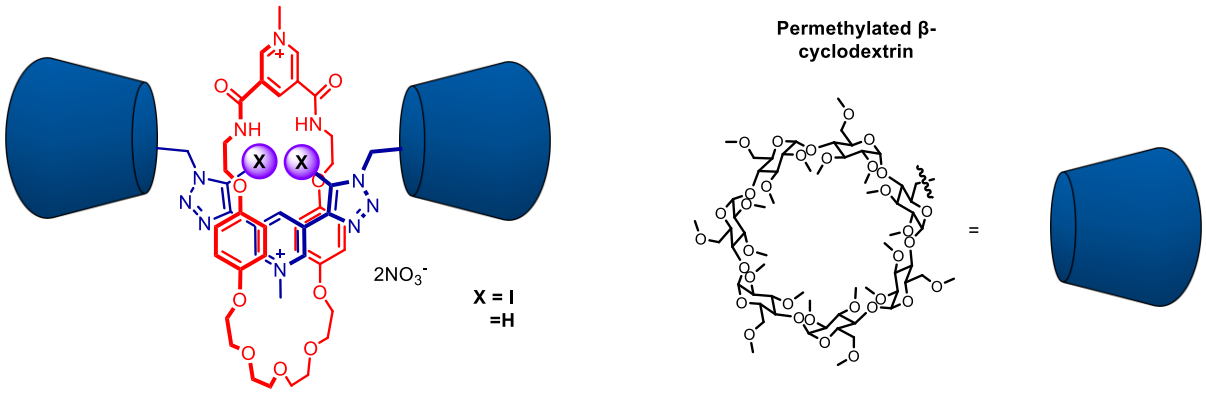


Figure 1.17 Beer's water soluble XB [2]rotaxane.

Importantly, the proto-triazole HB [2]rotaxane analogue possessed considerably inferior, anion association constants for all anions investigated. Particularly striking is the XB rotaxane exhibiting a more than two orders of magnitude increase in binding strength for iodide ($K_a(I^-)$ = 2,200 M^{-1}) in comparison to the HB rotaxane analogue ($K_a(I^-)$ = 20 M^{-1}). The thermodynamic parameters of iodide complexation for both XB and HB [2]rotaxanes were also investigated *via* van't Hoff analysis, wherein iodide halide association of XB [2]rotaxane was determined to be enthalpically driven, attributed to the formation of strong XB-anion interactions, while the HB counterpart demonstrated only a favourable entropic contribution. Crucially, the thermodynamic signatures of the binding events serve as an important piece of evidence in the ascribed role of XB driven anion recognition, as opposed to 'classical' hydrophobic effects.

Through extensive experimental and computational investigation, more recent times have sought to delineate the relative contributions of electrostatics, dispersion forces and charge transfer character of σ-hole interactions. It is widely acknowledged that electrostatics are a major component of XB-anion interactions, however, aspects of covalent character can

also contribute to σ-hole interactions. For example Beer et al., recently reported a series of iodotriazolium and bis-iodotriazole pyridinium receptors, in which single crystal X-ray structure analysis of their chloride salts revealed the halide to exhibit mono- and bidentate XB-anion contacts respectively (Figure 1.18).[74] X-ray absorption spectroscopy (XAS) measurements on these systems showed an intense pre-edge feature in the respective Cl K-edge spectra, which is indicative of formal donation of electron density from the halide to the XB donor iodine atom i.e. covalent character. Remarkably, quantitative analysis of the XAS absorption feature suggested 6% and 11% donation of the Cl_{3p} electron density in the mono- and bidentate receptors respectively, comparable to covalent contributions exhibited by divalent transition metal chloride complexes ($[MCl_4]^{2-}$ M= Cu, Ni, Co, Fe).

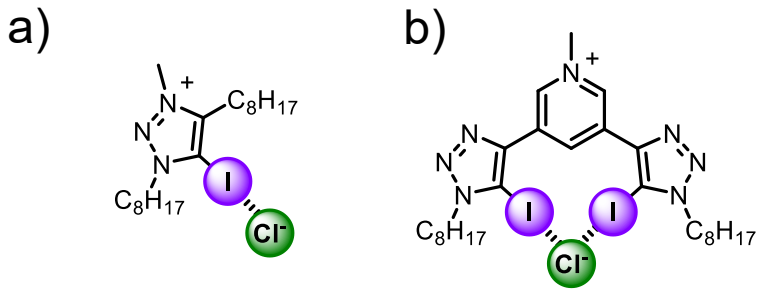


Figure 1.18 Beer's acyclic a) XB iodotriazolium and b) bis-iodotriazole pyridinium receptors displaying strong XB-anion interactions.

The observed strength of XB-Lewis base interactions typically increase in the order; I > Br > Cl, which is rationalized by the increasing polarisability of the halogen atom influencing the magnitude of the σ-hole. Consequently, XB donors employed in supramolecular architectures are principally iodine or bromine containing motifs. However, a rare example of a chlorine containing XB donor was evidenced by Martinez et. al., in which a charge assisted P-Cl bond of chloroazaphosphatrane unit was investigated as an XB donor motif.[75] ^{1}H NMR titration experiments in CD_3CN solutions revealed the cationic receptor was capable of binding, albeit modestly ($K_a \approx 50$ M^{-1}), a range of anions including the halides, acetate and cyanide in CD_3CN (Figure 1.19).

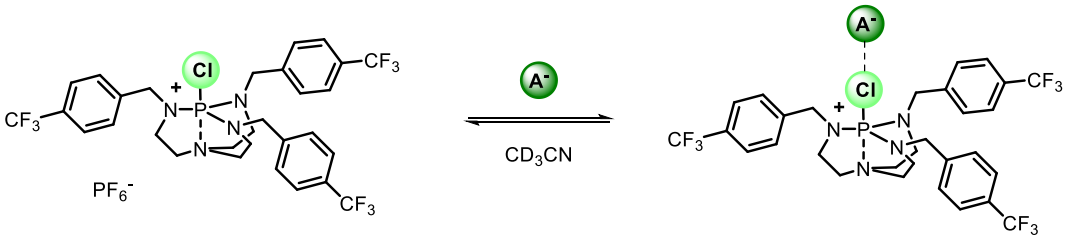


Figure 1.19 Martinez's chloroazaphosphatrane XB anion receptor.

Hypervalent iodine compounds demonstrate rich structural variation and in concert with the heightened Lewis acidity anticipated from an increase oxidation state make them attractive candidates for exploration as novel potent XB donor motifs. Whilst the electrophilicity

of I(V) and I(III) derivatives, e.g. Dess-Martin's periodinane and Koser's reagent is well documented in the context of organic synthesis,[76] their high reactivity typically prohibits any practical use in supramolecular systems. One strategy to overcome the relative instability of I(III) systems is the integration of the iodine atom into kinetically stabilising cyclic systems, reducing the propensity of the halogen compound to undergo reductive elimination or C-I bond insertion decomposition pathways.

Very recently, seminal studies by Huber[77] have reported the first application of I(III) diaryliodonium salts as novel XB donors capable of halide recognition. It is notable that despite their simplicity these monodentate systems exhibited remarkable bromide affinities log(K_a(Br^-) > 6, as determined by ITC experiments, in acetonitrile solution, surpassing that of even a dicationic bidentate iodine(I) reference system (Figure 1.20).

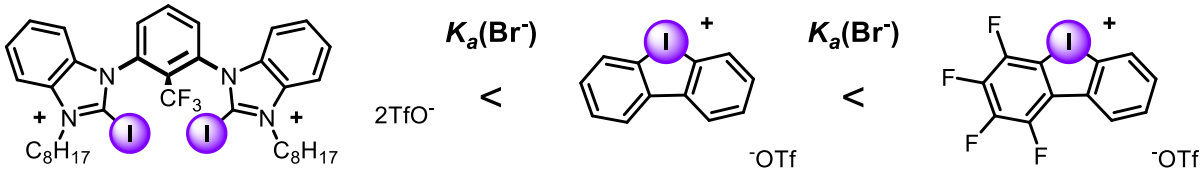


Figure 1.20 Huber's I(III) diaryl iodonium receptors ordered by bromide affinity relative to a benchmark bidentate I(I) system.

Chalcogen bonding (ChB) anion receptors

ChB is a non-covalent interaction in which an electron-deficient chalcogen atom serves as a Lewis acid. Akin to XB, the heavier and more polarisable chalcogen atoms selenium and tellurium form the strongest ChB donors, having comparable interaction strengths with Lewis bases to that of HB. However, the application of solution phase ChB for the purposes of anion recognition has notably lagged behind that of XB particularly for Te-containing donor molecules. A contributing factor to the paucity of potent ChB receptor systems is the inherent weakness of the C-Te bond (bond strength approximately 200 kJ mol^{-1}) which often results in air and moisture sensitivity. As a consequence, the lighter chalcogens, Se in particular have been more widely employed in anion recognition and catalysis applications. The first Te ChB anion receptor was reported as recently as 2010 by Gabbai and Zhao.[78] A bidentate boron-tellurium based receptor (Figure 1.21a) displayed enhanced fluoride affinity in methanol (K_a = 750 M^{-1}) relative to a sulfur-analogue, attributed to the formation of a potent ChB Te-halide anion interaction. Subsequent reports by Gabbai have demonstrated that simple methyl diaryl telluronium ChB donors (Figure 1.21b) can function as potent anionophores for transmembrane chloride transport and more potent bidentate receptor systems (Figure 1.21c) are capable of functioning as halide abstraction agents for electrophilic catalysis applications via metal-chloride bond activation.

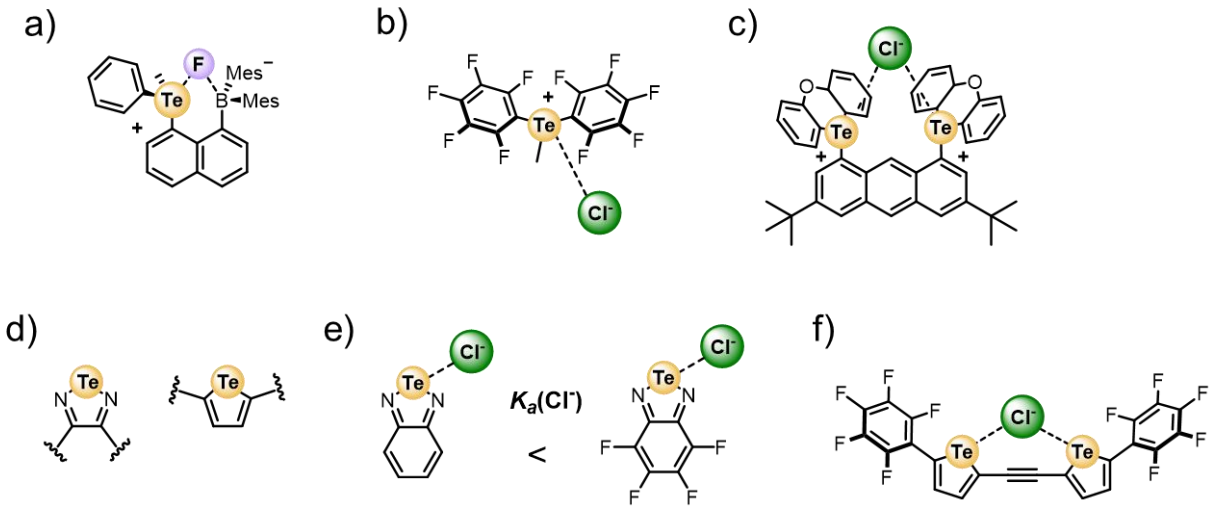


Figure 1.21 Gabbai's telluronium based ChB anion receptor systems a), b) and c). d) tellurium chalcogenadiazoles and chalcogenophenes motifs. Taylor's e) telluriumdiazole and f) tellurophene based receptors.

Endocyclic ChB donors, namely chalcogenadiazoles and chalcogenophenes (Figure 1.21d), have accounted for a large portion of ChB receptor systems reported to recognise anions. For example, Taylor described a series of synthetically versatile benzotelluradiazoles, with different aryl substitution patterns,[79] capable of chloride selective ChB-mediated anion recognition (Figure 1.21e). A Linear free energy relationship (LFER) between chloride affinity binding (ChB donor ability) and the calculated electrostatic potential at the tellurium centre was demonstrated. In particular, an impressive micromolar chloride affinity was observed for the most electron-deficient tetrafluoro-substituted receptor in THF-d_8 (K_a = 13,000 M^{-1}). In addition, Taylor developed electron-deficient bidentate tellurophene derivatives which display strong chloride affinity and selectivity in organic solvent media (Figure 1.21f).[80] The bidentate perfluoroaryl-functionalised receptor displayed an order of magnitude enhancement in chloride affinity relative to a monodentate receptor analogue.

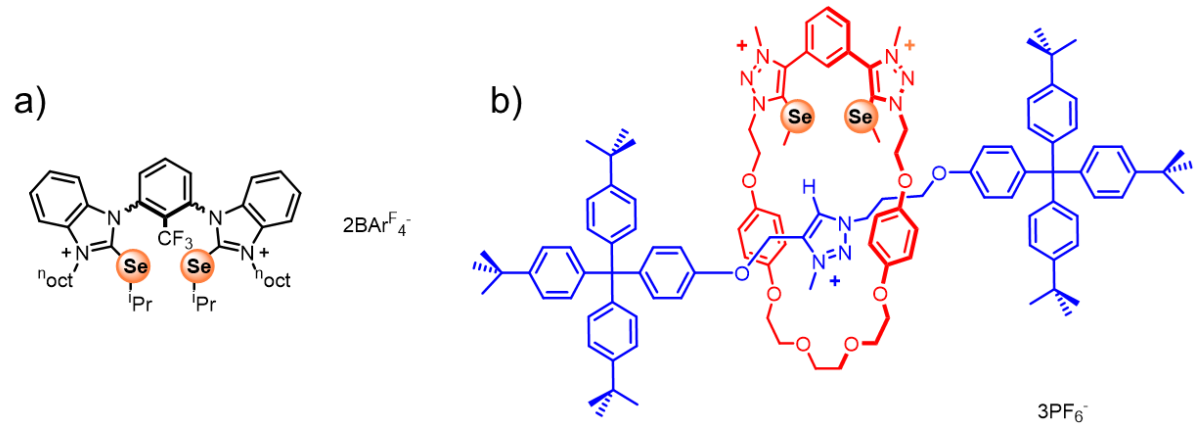


Figure 1.22 a) Huber's selenoimidazolium based receptor b) Beer's bis-seleno triazolium [2]rotaxane.

More recently, divalent exocyclic ChB donors specifically Se/Te-imidazolium and triazolium - have emerged as highly effective moieties for ChB-mediated anion recognition. For example, in 2017, Huber and co-workers reported the first application of selenium-based ChB donors as organic catalysts. The bidentate cationic receptor (Figure 1.22a), consisting of a bis(benzimidazolium)-based backbone, was demonstrated to catalyse the solvolysis of benzhydryl bromide in wet acetonitrile by serving as a Lewis acid. Furthermore, Beer has incorporated methylchalcogeno appendages to 1,2,3- triazolium motifs in interlocked host architectures. In 2017, a selenotriazolium [2]rotaxane exhibited charge-assisted ChB-mediated anion recognition in aqueous solvent mixtures (Figure 1.22b).

Pnictogen (PnB) and Tetrel (TrB) bonding anion receptors

The strength of PnB and TrB interactions can be of a similar magnitude or even exceed those of their ChB and XB counterparts. In 2017 Christianson and Gabbai reported a chlorinated stibanindole derivative (Figure 1.23a),[81] which underwent significant ^{1}H NMR spectroscopic perturbations and changes in optical absorbance behaviour upon the addition of Cl^- as its TBA salt. Chloride affinity measurements determined an impressive $K_a(Cl^-)$ = 9.5 x 10^4 M^{-1} in acetonitrile solution. The role of the electronegative chlorine substitutent increasing the Lewis acidity of the Sb(III) centre is evidenced by no measurable chloride affinity exhibited by its phenyl appended analogue (Figure 1.23b).

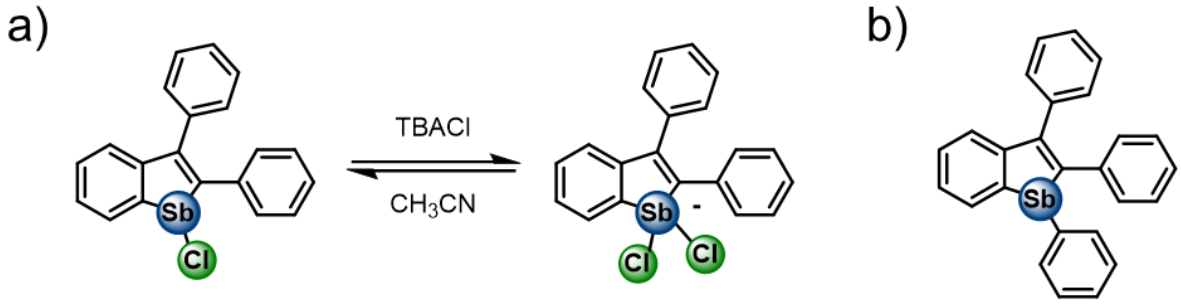


Figure 1.23 Gabbai's a) chloro-substituted and b) phenyl-substituted stibanindole.

In 2018, Matile et al. demonstrated the first application of PnB in catalysis,[82] in which a PnB catalyst capable of activating simple halide (chloride) abstraction reactions is described. These simple organic transformations are known to be accelerated by various Lewis acid catalysts, via stabilisation of the transition state in the rate-limiting step, in which chloride is eliminated. The neutral PnB stibine (Figure 1.24a, Pn = Sb) containing three pentafluorophenyl substituents was found to exhibit the highest catalytic activity in comparison to ChB (Figure 1.24b) and XB catalysts (Figure 1.24c).

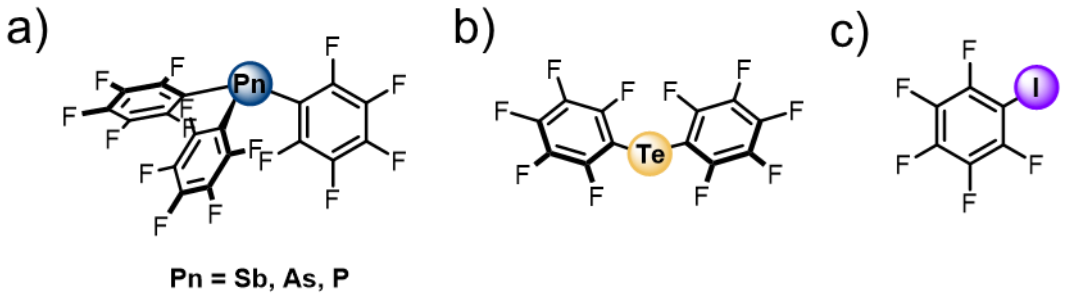


Figure 1.24 Matile's a) triarylantimony(III) PnB b) diaryltellurium(II) ChB and c) aryliodine(I) XB donor systems.

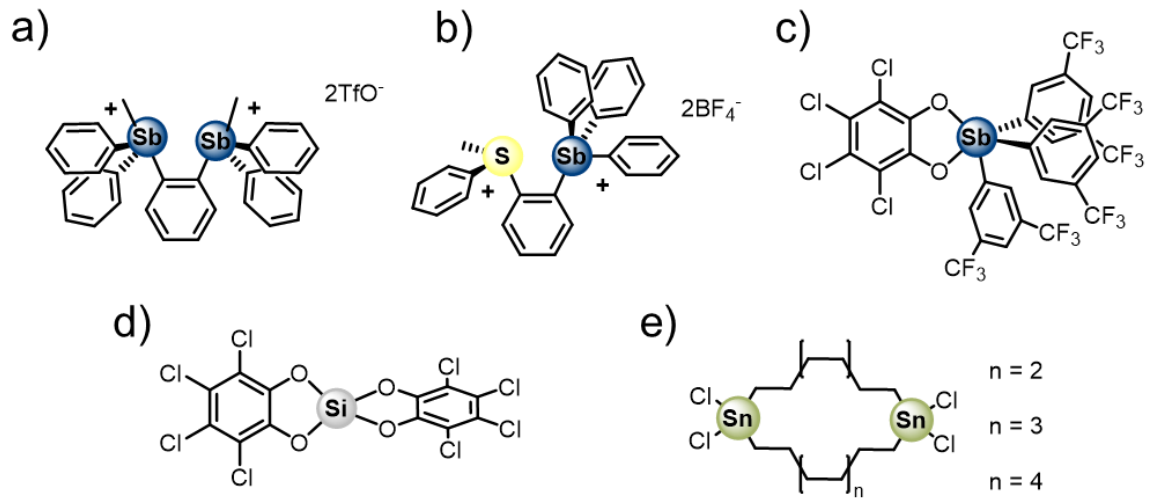


Figure 1.25 a) and b) Gabbai's stibonium Sb(III) PnB receptors. c) Gabbai's Sb(V) neutral PnB receptor. d) Neutral Si(IV) 'super acid'. e) Newcomb's dinuclear Sn(IV) macrocycles.

Gabbai et al. have arguably made the largest strides to the expanding the scope of pnictogen bonding motifs. Notable contributions include an ortho-substituted bidentate distibonium dicationic system (Figure 1.25a),[83] which through X-ray structural analysis revealed bidentate coordination of a triflate counteranion with short Sb(III)···O contacts distinctly shorter than the sum of their van der Waals radii; 81% and 85%. Also exploiting an ortho-phenyl backbone, integration of mixed PnB-ChB donor motifs was achieved in 2020 (Figure 1.25b), wherein a tetraphenyl substituted stibonium and a methyl phenyl sulfonium unit was capable of remarkably strong chloride (K_a >10^6 M^{-1}) complexation in MeCN.[84] Gabbai has also explored Sb(V) systems (Figure 1.25c),[85] demonstrating through anion binding studies, organocatalyst investigations and computational modelling that increasing the oxidation state of the Sb atom leads to a lowering of the σ^* orbital energy and enhanced Lewis acid character.

The lighter elements feature heavily in TrB based receptors. Indeed, the strategy of increasing Lewis acidic character by appendage of electron-withdrawing substituents, in this case perchlorocatecholates, to a Si(IV) centre has realised one of the first neutral silicon(IV) 'super acids', as defined by fluoride ion affinities which exceed that of SbF_5 (Figure 1.25d).[86] As early as 1987, Newcomb et. al. demonstrated organotin macrocyclic hosts capable of binding chloride via Sn···Cl^- TrB interactions (Figure 1.25e).[87] ^{119}Sn NMR titrations provided evidence for both 1:1 and 1:2 host:anion complexes, with modest chloride affinities typically of the order of 10^2 M^{-1} in CD_3CN/C_6D_6 solutions.

1.6 Ion-pair recognition

Heteroditopic ion-pair receptors, possessing binding sites for both cations and anions, have been constructed to overcome the energetic cost associated with inherent electrostatic interactions between the charged species. Importantly such receptors can confer prodigious advantages in both affinity and selectivity relative to monotopic recognition.

The following surveys the various ion-pair binding modes for heteroditopic receptors before discussing the role of cooperativity in ion-pair recognition.

1.6.1 Binding mode and cooperativity

The relationship of co-bound ions in a heteroditopic receptor, or *binding mode*, constitutes a useful categorisation tool of ion-pair host structures (Figure 1.26). In general, receptor types can be conveniently divided into *contact ion-pair,* where the ions are considered to be in direct contact with each other, and *separated ion-pair* receptors, in which either the cation and anion binding sites are sufficiently disposed as to prevent mutual ion-contact (Figure 1.26b) or the bound ion-pair exhibits interaction with another chemical entity, typically solvent (Figure 1.26c).

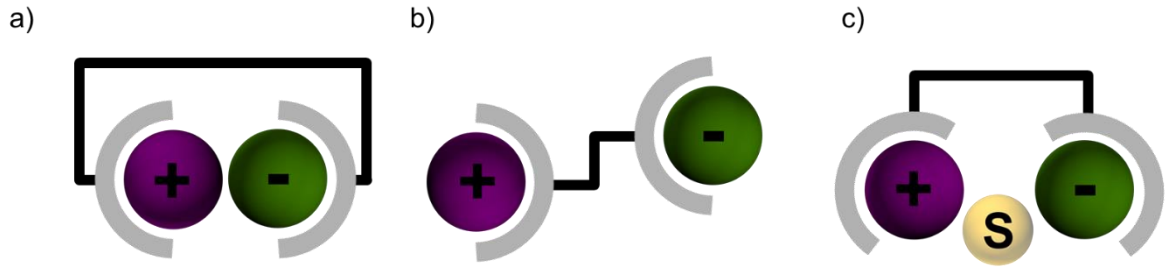


Figure 1.26 Cartoon representation ion-pair receptor types a) contact b) host separated c) solvent separated.

Heteroditopic receptor systems frequently exhibit modulated binding behaviour relative to their monotopic receptor counterparts. The source of this difference may be traced to the mutual influence co-bound species exert over each other, termed *cooperativity*. When the binding of an ion enhances or inhibits counterion association, the cooperativity may be referred to as positive or negative, respectively. In rare instances where the binding events exert no measurable effect on each other the recognition is referred to as non-cooperative. The relationship between the respective cation (K_C), anion (K_A), ion-pair (K_{IP}) binding affinities, exogeneous ion-pairing (K_{IP*}) and cooperative behaviour is summarised in Figure 1.27.

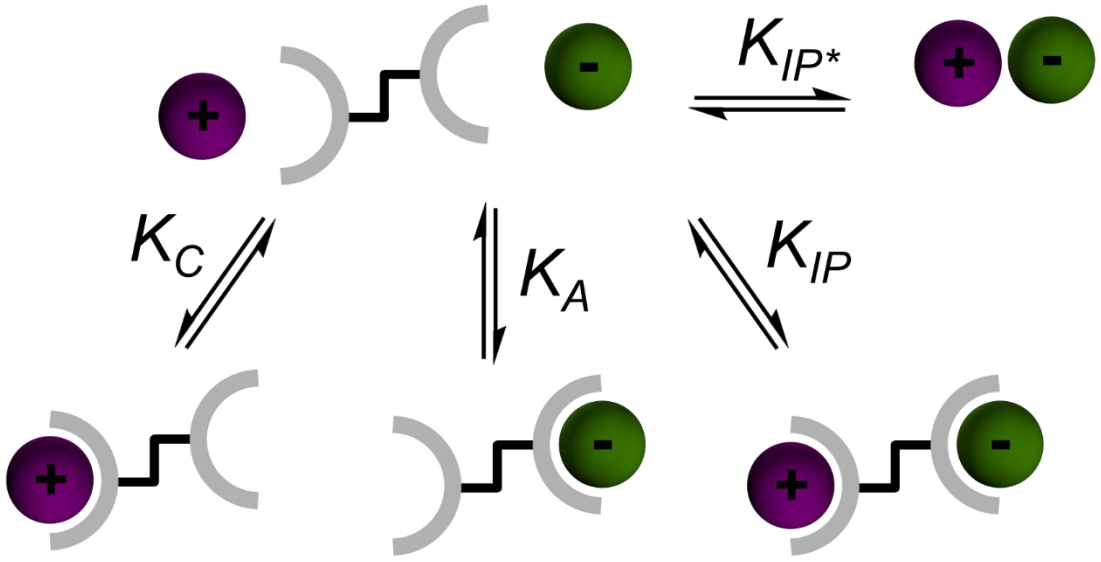


Figure 1.27 Simplified diagram showing the major equilibria in an ion-pair binding system, and the different modes of cooperativity.

Importantly, it is the exploitation of positive cooperativity in heteroditopic receptor design that has been the main stimulus for research in the area. The mechanisms of cooperativity are typically proximal favourable electrostatic interactions between complexed ions and/or allosteric conformational changes induced by a binding event.[88–90]

Determining the relative contributions of these cooperative mechanisms is somewhat complicated by the multiple equilibria involved in the overall ion-pair recognition process (Figure 1.27).[91] Cooperativity factors, the ratio of a receptor's affinity for a given ion, in the presence and absence of a counterion, are a quantitative means of assessing a heteroditopic receptor's ability to function as an ion-pair receptor. For example, Martinez's heteroditopic hemicryptophane[92] (Figure 1.28a) was found to bind Br^-, added as its TBA salt, with an association constant of $1.05\times10^3\ M^{-1}$ in $CDCl_3$. However, in the presence of tetramethylammonium picrate the K_a (Br^-) value increased to $13.5\times10^3\ M^{-1}$, indicating the presence of NMe_4^+ enhances bromide binding with a cooperativity factor of 13, presumably via proximal favourable electrostatic interactions.

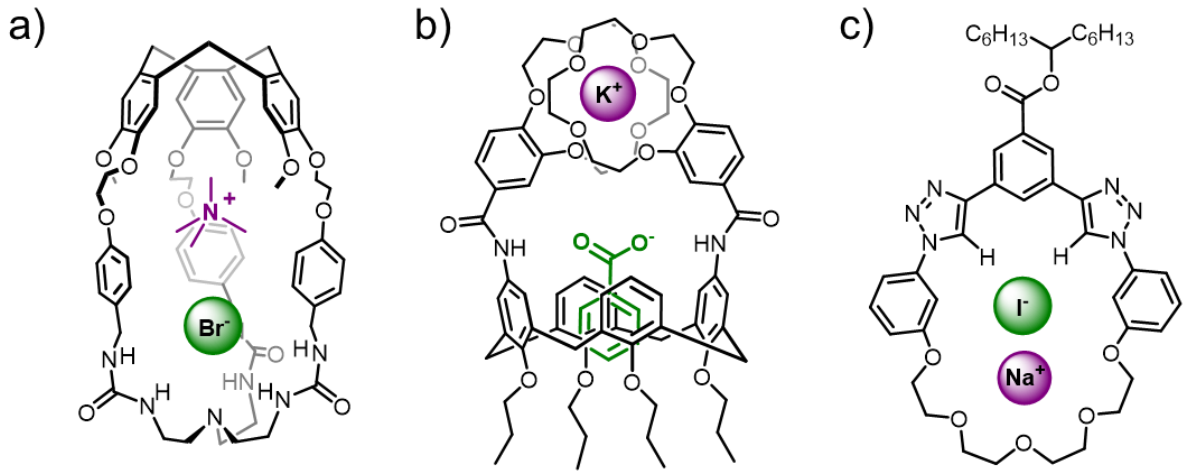


Figure 1.28 a) Martinez's hemicryptophane receptor b) Beer's bis-B15C5 calix[4]arene receptor c) Flood's aryl-bis proto-triazole macrocycle.

The effect of cation size on preorganisation was illustrated by Beer and co-worker in their report of a calix[4]arene receptor functionalised with upper-rim bis(benzo-15-crown-5 ether) amide substituents (Figure 1.28b). The receptor exhibited a 10-fold enhancement in benzoate affinity in the presence of K^+ in CD_3CN:DMSO-d_6 1:1 (v/v). This enhancement was attributed to the formation of a 1:1 intramolecular potassium – bis(benzo-15-crown-5 ether) sandwich complex, which favoured the convergent orientation of the amide HB donors. In contrast the smaller Na^+ cation was incapable of forming a similar sandwich complex and hence exhibited no such benzoate binding enhancement.

In 2015 Flood reported an ion-pair binding polyether-strapped bis-prototriazole macrocyclic system (Figure 1.28c).[93] From extensive cation, anion and ion-pair affinity

measurements, supplemented by computational studies, the authors were able to ascribe thermodynamic parameters to cooperativity and deconvolute contributions from electrostatic and allosteric effects. The multiequilibrium model employed facilitated the quantification of experimental cooperativity ΔG_{α}, where the associated free energy ΔG_{α} is defined as the overall binding $\Delta G_{overall}$ minus the anion and cation binding free energies ΔG_{anion} and ΔG_{cation} respectively: $\Delta G_{\alpha} = \Delta G_{overall} - \Delta G_{anion} - \Delta G_{cation}$. ΔG_{α} was determined to be – 18 kJmol^{-1} and -15 kJmol^{-1} for NaI and $NaClO_4$ respectively in CD_2Cl_2/CD_3CN 4:1 (v/v).

1.6.2 Binding motifs

The means by which anion complexation is achieved in heteroditopic receptor design has been overwhelmingly dominated by hydrogen bonding in combination with crown-ether recognition sites for co-bound alkali metal cation recognition. Indeed, a vast library of receptor types now exist containing relatively simple urea, thiourea and squaramide N-H donor motifs, with recent times exploiting non-traditional C-H HB donors (Figure 1.29).[94–96] The following section will primarily focus on contemporaneous approaches to heteroditopic receptor design, firstly discussing the exploitation of unusual non-covalent interactions in macrocyclic receptor systems and subsequently the use of complex heteroditopic host molecular topologies.

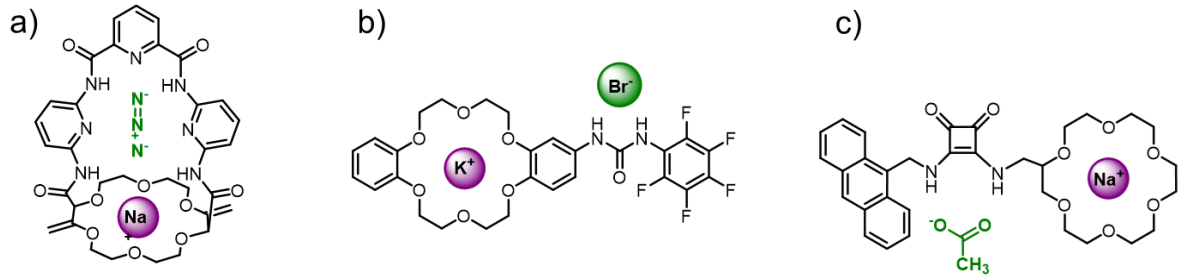


Figure 1.29 Selected heteroditopic ion-pair receptor systems by a) Lacour[95] b) Ghosh[94] c) Frontera.[96]

As mentioned previously, the emergence of σ-hole interactions in the field of anion recognition is in no small part due to the enhanced affinity and unique selectivity profiles exhibited by these systems. However, despite an early report by Resnati and Metrangolo demonstrating the potential of XB mediated ion-pair recognition, it was over a decade later before another example appeared. Schubert's 2017 report[97] described an iodo-triazole motif integrated into a triethylene glycol containing macrocycle (Figure 1.30). Conceptually, the receptor aimed to exploit the basic triazole nitrogen atoms as an ancillary donor to generate a six-coordinate Na^+ binding environment and to favour exotopic anion binding by the XB donor. Solution phase ^{1}H NMR titration experiments determined the crown-ether like system was capable of binding a sodium cation in 1:1 host-guest stoichiometry $K_a(Na^+)$ = 434 M^{-1} in CD_2Cl_2/CD_3CN (3 : 1) mixtures. Practical reasons necessitated the use of ^{13}C NMR titrations for the anion affinity determination in which it was revealed the receptor possessed modest iodide affinity $K_a(I^-)$ = 4.7 M^{-1}. However, upon complexation with $NaBPh_4$ this was dramatically

improved, $K_a(I^-)$ =135 M^{-1}. This observed cooperativity was rationalized on the basis of favourable electrostatic interactions and improved XB donor potency by cation induced C-I bond polarisation. Interestingly, its proto-triazole HB analogue not only exhibited diminished sodium cation affinity, $K_a(Na^+)$ = 126 M^{-1}, but also no measurable iodide binding. ^1H-^1H ROESY NMR and X-ray crystallographic analysis revealed the source of this contrasting behaviour was the formation of an intramolecular HB interaction between the triazole C-H donor and the polyether oxygens.

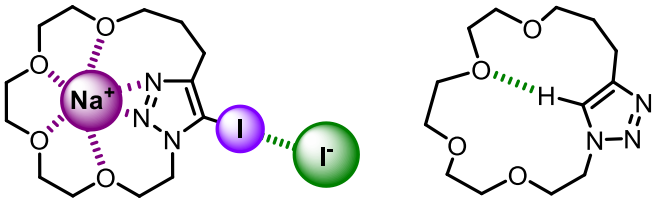


Figure 1.30 Schubert's XB and HB triazole crown-ether like receptors.

The interaction between electron deficient aromatic systems and anions is arguably the least exploited non-covalent interaction in either anion or ion-pair receptor design. Wang reported[98] a macrocylic system composed of two chlorotriazine units strapped with a pentaethylene glycol chain (Figure 1.31). Calcium cation complexation by the receptor's oligoethoxyethylene group facilitated bromide and iodide binding in a 1:2 host-guest stoichiometry with association constants of 477 M^{-2} and 5508 M^{-2}, respectively in CD_3CN solution. The role of anion-π interactions in the ion-pair recognition behaviour of the receptor system was determined to be crucial as comparison with its diethylamino substituted triazine exhibited no measurable anion affinity.

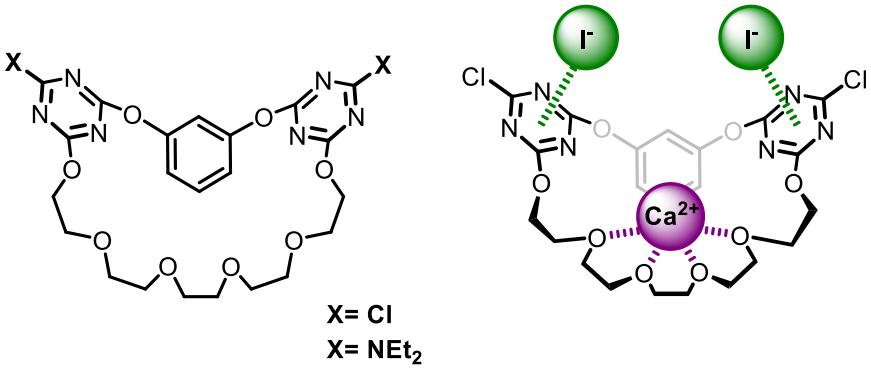


Figure 1.31 Wang's chlorotriazine based ion-pair receptor.

The cationic counterpart to anion-π interactions in biological systems has been acknowledged as a contributing factor in protein structure and enzymatic function. Inspired by these observations, synthetic receptor design has exploited cyclic arrays of electron rich aromatics to bind a range of ammonium, pyridinium and metal cations. Sessler for example has exploited the interior cone-like conformation of a *meso*-octamethylcalix[4]pyrrole receptor as a binding site for caesium cations. Metal cation complexation preorganises the pyrrole units towards convergent N-H···Cl^- HB formation, thereby facilitating cooperative CsCl binding in nitrobenzene solution (Figure 1.32a).[99] In a similar approach, Akazome has exploited a novel cyclic tripeptide-like host for the neurotransmitter acetylcholine chloride (ACh·Cl).[100] Quantitative ^{1}H NMR titration experiments reveal that the receptor is capable of binding ACh·Cl with considerable affinity K_a = 1640 M^{-1} in $CDCl_3$ (Figure 1.32b). However, the use of a chloride source with a larger countercation; tetrabutylammonium (TBA), in which the potential for cation-π interactions is considerably diminished, demonstrated a much lower affinity of K_a = 252 M^{-1}. X-ray crystallographic studies and ^{1}H-^{1}H NOESY experiments reveal Cl^- binding is accompanied by a ring-flip process in which the amide HB donors arrange to concertedly interact with the halide on one side of macrocycle. This results in a cavity of amino-phenol based panels facilitating the binding of the -NMe_3^+ group of acetylcholine via multiple cation-π interactions cooperatively stabilising the ion-pair complex.

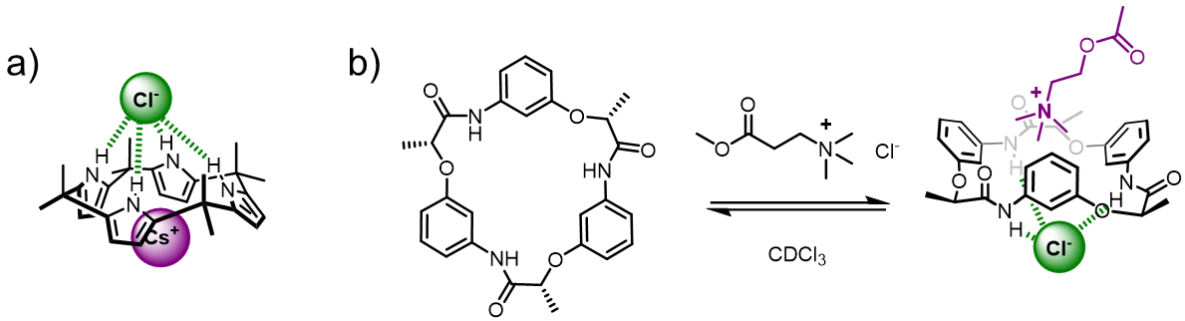


Figure 1.32 a) Sessler's calix[4]pyrrole caesium halide receptor b) Akazome's acetylcholine chloride receptor.

First reported in 2008,[101] pillar[*n*]arenes are a series of macrocycles consisting of *n* dialkoxybenzene panels (typically *n* = 5, 6) linked by methylene units. As a consequence of their rigid structure and electron rich interior, pillar[*n*]arenes, and pillar[*5*]arenes in particular, have been shown to form interpenetrated complexes with a wide range of electron poor neutral and cationic organic molecules. However, their application in heteroditopic receptor design is somewhat more limited. An elegant example by Huang et al. has capitalised on the alkyl functionalised rim as unconventional HB donors for the recognition of AgOTf ion-pairs (Figure 1.33a). Specifically the 2019 report details how a perethylated pillar[*5*]arene was capable of encapsulating a dimer of silver trifluoroacetate (AgOTf).[102] Solid state structural analysis demonstrated that the complexation event is driven by the formation of multiple bifurcated $Ag^{+}\cdots\pi$ interactions in concert with C-H···O and C-H···F contacts with the trifluoroacetate counteranion. Importantly, it was also shown that the unique nature of $Ag^{+}\cdots\pi$ was a significant determinant in complex stability as the receptor exhibited no affinity for $Cu(OTf)_2$, NaOTf or KOTf.

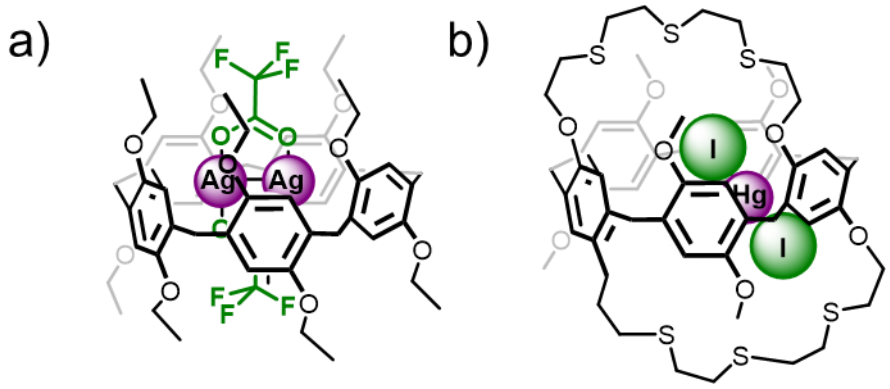


Figure 1.33 Pillar[5]arene based ion-pair receptors a) Huang's silver triflate receptor and b) Lee's HgI_2 receptor.

In a similar vein, Lee has recently reported the selective encapsulation of HgI_2 ion-triplet by a trithiane strapped pillar[5]arene (Figure 1.33b).[103] The endotopic complexation mode is driven by a mercury(II) pentagonal planar arrangement of $Hg^{2+}\cdots\pi$ contacts, with the electron rich interior supplemented by multiple C-H···I interactions.

1.6.3 Pseudorotaxane and interlocked ion-pair receptor topologies

Mechanically interlocked molecules (MIMs) consist of molecular components that are linked to one another not *via* a covalent bond, but rather as a result of their entanglement in space. The two most common MIMs include rotaxanes and catenanes; the former consisting of a dumbbell shaped axle component encircled by a macrocyclic molecule, in which the dissociation of the components is inhibited by the sterically encumbering termini of the axle (Figure 1.34a). A catenane consists of macrocyclic components joined in the same fashion as the links in a chain (Figure 1.34b).

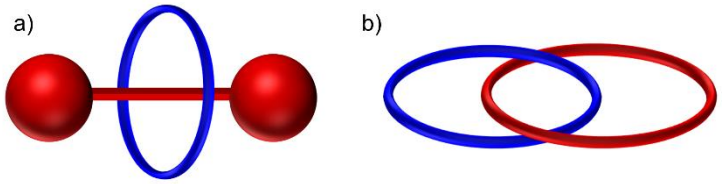


Figure 1.34 Cartoon representation of a) [2]rotaxane and b) [2]catenane.

From the viewpoint of anion or cation binding, MIMs provide access to unique coordination environments, in which arrays of donor atoms are topologically constrained in three dimensional cavities. Indeed, the use of MIMs in the recognition of charged species has already proven to be a powerful approach to construct highly potent and selective receptor systems.[104,105] However, presumably as a result of synthetic challenges, interlocked structures capable of ion-pair recognition are remarkably rare. The first report of this kind was in 2014,[106] in which a neutral [2]rotaxane was used to bind 'axle separated' alkali metal halide ion-pair species (Figure 1.35). Specifically, the ion-pair binding behaviour relied upon an alkali metal cation induced pirouetting of the calix[4]diquinone containing macrocycle and pyridine N-oxide functionalised axle to bind either a lithium, sodium or potassium metal cation, to preorganise the amide hydrogen bond donor components for anion binding. Quantitative ^{1}H NMR titration experiments revealed sodium cations generated the largest enhancements in halide affinities relative to lithium and potassium; in particular complexation with Na^{+} demonstrated a pronounced 15-fold enhancement for chloride in $CDCl_3/CD_3OD$ (4:1) solvent mixtures.

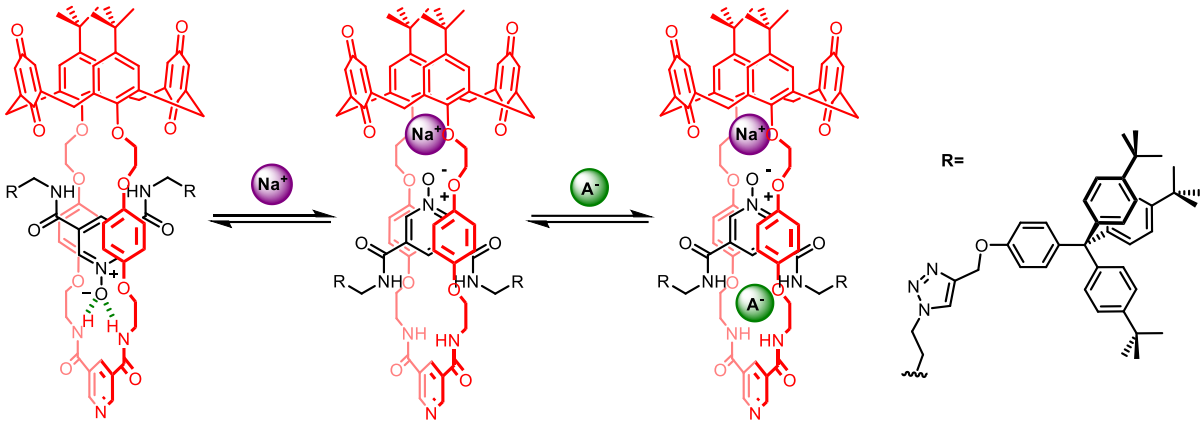


Figure 1.35 Beer's calix[4]diquinone based [2]rotaxane exhibiting Na^+ induced pirouetting behaviour.

Ballester has also explored calix[4]pyrrole-based interlocked topologies for the binding of ion-pairs, exploiting cation-π interactions between tetraalkylammonium cations and anions of various geometries, including chloride, isocyanate and nitrate (Figure 1.36).[107] Isothermal titration calorimetry (ITC) experiments revealed the cylindrically shaped cavity of the bis-calix[4]pyrrole macrocycle component favoured binding of TBANCO over $TBANO_3$ and TBACl with association constants of 7.9×10^5 M^{-1}, 4×10^4 M^{-1} and 5×10^4 M^{-1}, respectively in $CDCl_3$. Importantly, the nature of the quaternary ammonium was also shown to dramatically influence the ion-pair affinities, in which similar experiments with methyltrioctylammonium chloride (MTOCl), an organic cation capable of interacting with the calix[4]pyrrole cone interior, was bound with an affinity of 1.58×10^7 M^{-1}, over a 300-fold enhancement relative to TBACl.

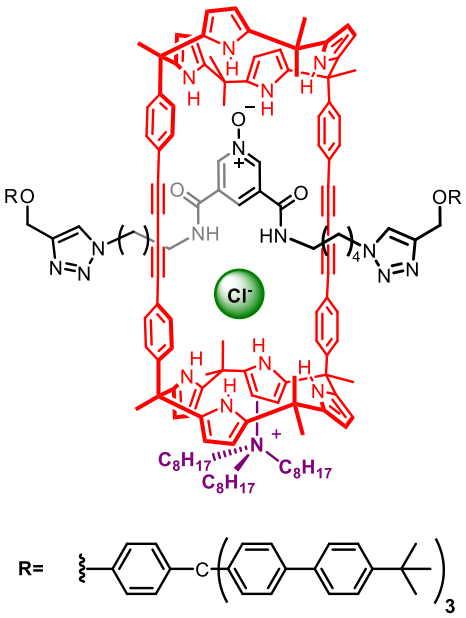


Figure 1.36 Ballester's [2]rotaxane for the recognition of quaternary ammonium salts.

A particularly attractive feature of interlocked host structures is the ability to dramatically alter anion or cation environments by subtle control of the co-conformations between mechanically interlocked components, thereby dramatically switching ion-pair recognition capabilities. This form of conformational control was demonstrated by Goldup's [2]rotaxane (Figure 1.37),[108] in which intercomponent HB formation between the Lewis basic nitrogen atoms of a bipyridine containing macrocycle component and a urea-containing axle component, confirmed by ^{1}H NMR and X-ray crystal structure, serves to conformationally lock the structure. However, upon protonation of the bipyridine motif the macrocycle shuttles to the triazole station of the axle. Crucially, this shuttling behaviour facilitates the urea motif to engage as a potent HB donor and exhibits considerable anion affinities in $CDCl_3/CD_3CN$ (1:1) solvent mixtures; $K_a(Cl^-) > 10^4\ M^{-1}$, $K_a(Br^-) = 4.7\times10^3\ M^{-1}$ and $K_a(HSO_4^-) = 2.3\times10^3\ M^{-1}$. In contrast, the absence of the pH stimulus the rotaxane possesses no appreciable anion affinity.

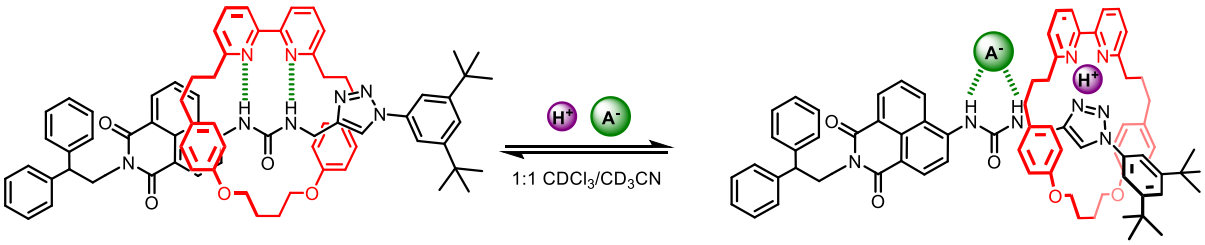


Figure 1.37 Goldup's allosterically regulated [2]rotaxane ion-pair receptor.

1.7 Project outlines

The main objective of the various research projects discussed in this thesis is to develop novel sigma-hole donor host molecules for anion and ion-pair recognition.

Chapter two discusses structural and electronic factors that influence anion recognition potency and selectivity properties of σ-hole interactions. Specifically through the synthesis, anion binding studies and linear free energy relationship analysis of a library of structurally homologous ChB, XB and HB acyclic receptor systems.

Chapter three focuses on the construction of highly cooperative ChB heteroditopic receptor systems for alkali metal cation-halide anion ion-pair recognition. Extensive multinuclear NMR, UV-Vis spectroscopy and X-ray structural characterization investigations are followed by solid-liquid and liquid-liquid alkali metal halide extraction and preliminary membrane transport and organocatalysis studies.

Chapter four details the synthesis and anion binding properties of mono-, bi- and tetra-functionalised XB tetraphenylethylene(TPE) receptor systems. In particular, bidentate XB TPE derivatives are also investigated for photoswitchable anion recognition.

Chapter five details the synthesis of novel heteroditopic XB receptor functionalised silica based materials. Solid-liquid extraction studies, quantified by ICP-MS analysis, are undertaken to investigate alkali metal salt extraction properties from aqueous media.

1.8 References

[1] J.-M. Lehn, *Angew. Chem. Int. Ed. Engl.* **1988**, *27*, 89–112.

[2] C. J. Pedersen, *J. Am. Chem. Soc.* **1967**, *89*, 2495–2496.

[3] B. Dietrich, J. M. Lehn, J. P. Sauvage, *Tetrahedron Lett.* **1969**, *10*, 2889–2892.

[4] K. N. Trueblood, C. B. Knobler, E. Maverick, R. C. Helgeson, S. B. Brown, D. J. Cram, *J. Am. Chem. Soc.* **1981**, *103*, 5594–5596.

[5] D. J. Cram, J. M. Cram, *Science* **1974**.

[6] S. J. Rowan, D. G. Hamilton, P. A. Brady, J. K. M. Sanders, *J. Am. Chem. Soc.* **1997**, *119*, 2578–2579.

[7] T. Steiner, G. R. Desiraju, *Chem. Commun.* **1998**, 891–892.

[8] Y. Aoyama, in *Supramol. Chem.* (Eds.: V. Balzani, L. De Cola), Springer Netherlands, Dordrecht, **1992**, pp. 17–30.

[9] G.-M. E. Bertrand, in *Adv. Mol. Cell Biol.* (Eds.: E.E. Bittar, N.M. Allewell, C. Woodward), Elsevier, **1997**, pp. 109–132.

[10] D. A. Dougherty, *J. Nutr.* **2007**, *137*, 1504S-1508S.

[11] J. P. Gallivan, D. A. Dougherty, *Proc. Natl. Acad. Sci.* **1999**, *96*, 9459–9464.

[12] J. C. Ma, D. A. Dougherty, *Chem. Rev.* **1997**, *97*, 1303–1324.

[13] E. A. Meyer, R. K. Castellano, F. Diederich, *Angew. Chem. Int. Ed.* **2003**, *42*, 1210–1250.

[14] C. R. Forbes, S. K. Sinha, H. K. Ganguly, S. Bai, G. P. A. Yap, S. Patel, N. J. Zondlo, *J. Am. Chem. Soc.* **2017**, *139*, 1842–1855.

[15] H.-J. Schneider, F. Werner, T. Blatter, *J. Phys. Org. Chem.* **1993**, *6*, 590–594.

[16] I. Alkorta, I. Rozas, J. Elguero, *J. Am. Chem. Soc.* **2002**, *124*, 8593–8598.

[17] D. Quiñonero, C. Garau, C. Rotger, A. Frontera, P. Ballester, A. Costa, P. M. Deyà, *Angew. Chem. Int. Ed.* **2002**, *41*, 3389–3392.

[18] M. Mascal, A. Armstrong, M. D. Bartberger, *J. Am. Chem. Soc.* **2002**, *124*, 6274–6276.

[19] B. L. Schottel, H. T. Chifotides, K. R. Dunbar, *Chem. Soc. Rev.* **2008**, *37*, 68–83.

[20] D.-X. Wang, M.-X. Wang, *J. Am. Chem. Soc.* **2013**, *135*, 892–897.

[21] M. Giese, M. Albrecht, K. Rissanen, *Chem. Rev.* **2015**, *115*, 8867–8895.

[22] H. Schmidbaur, *Gold Bull.* **2000**, *33*, 3–10.

[23] P. Pyykkö, *Chem. Rev.* **1997**, *97*, 597–636.

[24] M. S. Cubberley, B. L. Iverson, *J. Am. Chem. Soc.* **2001**, *123*, 7560–7563.

[25] N. T. Southall, K. A. Dill, A. D. J. Haymet, *J. Phys. Chem. B* **2002**, *106*, 521–533.

[26] F. Biedermann, W. M. Nau, H.-J. Schneider, *Angew. Chem. Int. Ed.* **2014**, *53*, 11158–11171.

[27] K. I. Assaf, W. M. Nau, *Angew. Chem. Int. Ed.* **2018**, *57*, 13968–13981.

[28] E. E. Meyer, K. J. Rosenberg, J. Israelachvili, *Proc. Natl. Acad. Sci.* **2006**, *103*, 15739–15746.

[29] T. Brotin, R. Montserret, A. Bouchet, D. Cavagnat, M. Linares, T. Buffeteau, *J. Org. Chem.* **2012**, *77*, 1198–1201.

[30] K. I. Assaf, M. S. Ural, F. Pan, T. Georgiev, S. Simova, K. Rissanen, D. Gabel, W. M. Nau, *Angew. Chem.* **2015**, *127*, 6956–6960.

[31] M. Elias, A. Wellner, K. Goldin-Azulay, E. Chabriere, J. A. Vorholt, T. J. Erb, D. S. Tawfik, *Nature* **2012**, *491*, 134–137.

[32] M. Rekharsky, Y. Inoue, in *Supramol. Chem.*, American Cancer Society, **2012**.

[33] K. Kanagaraj, M. Alagesan, Y. Inoue, C. Yang, in *Compr. Supramol. Chem. II* (Ed.: J.L. Atwood), Elsevier, Oxford, **2017**, pp. 11–60.

[34] E. Gouaux, R. MacKinnon, *Science* **2005**.

[35] C. Lim, T. Dudev, in *Alkali Met. Ions Their Role Life* (Eds.: A. Sigel, H. Sigel, R.K.O. Sigel), Springer International Publishing, Cham, **2016**, pp. 325–347.

[36] R. MacKinnon, *Angew. Chem. Int. Ed.* **2004**, *43*, 4265–4277.

[37] S. Y. Noskov, S. Bernèche, B. Roux, *Nature* **2004**, *431*, 830–834.

[38] M. S. P. Sansom, I. H. Shrivastava, J. N. Bright, J. Tate, C. E. Capener, P. C. Biggin, *Biochim. Biophys. Acta BBA - Biomembr.* **2002**, *1565*, 294–307.

[39] S. Bernèche, in *Encycl. Biophys.* (Ed.: G.C.K. Roberts), Springer, Berlin, Heidelberg, **2013**, pp. 1926–1933.

[40] C. H. Park, H. E. Simmons, *J. Am. Chem. Soc.* **1968**, *90*, 2431–2432.

[41] B. Dietrich, M. W. Hosseini, J. M. Lehn, R. B. Sessions, *J. Am. Chem. Soc.* **1981**, *103*, 1282–1283.

[42] F. P. Schmidtchen, *Angew. Chem. Int. Ed. Engl.* **1977**, *16*, 720–721.

[43] K. Kavallieratos, S. R. de Gala, D. J. Austin, R. H. Crabtree, *J. Am. Chem. Soc.* **1997**, *119*, 2325–2326.

[44] K. Kavallieratos, C. M. Bertao, R. H. Crabtree, *J. Org. Chem.* **1999**, *64*, 1675–1683.

[45] M. Boiocchi, L. Del Boca, D. E. Gómez, L. Fabbrizzi, M. Licchelli, E. Monzani, *J. Am. Chem. Soc.* **2004**, *126*, 16507–16514.

[46] P. A. Gale, J. L. Sessler, V. Král, V. Lynch, *J. Am. Chem. Soc.* **1996**, *118*, 5140–5141.

[47] I. Saha, J. T. Lee, C.-H. Lee, *Eur. J. Org. Chem.* **2015**, *2015*, 3859–3885.

[48] S. Lee, C.-H. Chen, A. H. Flood, *Nat. Chem.* **2013**, *5*, 704–710.

[49] S. Lee, B. E. Hirsch, Y. Liu, J. R. Dobscha, D. W. Burke, S. L. Tait, A. H. Flood, *Chem. – Eur. J.* **2016**, *22*, 560–569.

[50] Y. Liu, W. Zhao, C.-H. Chen, A. H. Flood, *Science* **2019**, *365*, 159–161.

[51] O. Hassel, J. Hvoslef, E. H. Vihovde, N. A. Sörensen, *Acta Chem. Scand.* **1954**, *8*, 873–873.

[52] O. Hassel, Chr. Rømming, J. G. Ormerod, E. Stenhagen, B. Thorell, *Acta Chem. Scand.* **1956**, *10*, 696–698.

[53] T. Bjorvatten, O. Hassel, O. Buchardt, G. E. Olsen, C. Pedersen, J. Toft, *Acta Chem. Scand.* **1961**, *15*, 1429–1436.

[54] T. Clark, M. Hennemann, J. S. Murray, P. Politzer, *J. Mol. Model.* **2007**, *13*, 291–296.

[55] A. Bauzá, A. Frontera, *Angew. Chem. Int. Ed.* **2015**, *54*, 7340–7343.

[56] P. Metrangolo, G. Resnati, T. Pilati, S. Biella, in *Halog. Bond. Fundam. Appl.* (Eds.: P. Metrangolo, G. Resnati), Springer, Berlin, Heidelberg, **2008**, pp. 105–136.

[57] M. Saccone, L. Catalano, *J. Phys. Chem. B* **2019**, *123*, 9281–9290.

[58] A. Brown, P. D. Beer, *Chem. Commun.* **2016**, *52*, 8645–8658.

[59] A. Docker, P. D. Beer, in *Halog. Bond. Solut.*, John Wiley & Sons, Ltd, **2021**, pp. 83–120.

[60] J. Y. C. Lim, P. D. Beer, *Chem* **2018**, *4*, 731–783.

[61] M. S. Taylor, *Coord. Chem. Rev.* **2020**, *413*, 213270.

[62] A. Mele, P. Metrangolo, H. Neukirch, T. Pilati, G. Resnati, *J. Am. Chem. Soc.* **2005**, *127*, 14972–14973.

[63] M. G. Sarwar, B. Dragisic, S. Sagoo, M. S. Taylor, *Angew. Chem. Int. Ed.* **2010**, *49*, 1674–1677.

[64] R. Tepper, B. Schulze, M. Jäger, C. Friebe, D. H. Scharf, H. Görls, U. S. Schubert, *J. Org. Chem.* **2015**, *80*, 3139–3150.

[65] S. H. Jungbauer, S. M. Huber, *J. Am. Chem. Soc.* **2015**, *137*, 12110–12120.

[66] T. K. Mole, W. E. Arter, I. Marques, V. Félix, P. D. Beer, *J. Organomet. Chem.* **2015**, *792*, 206–210.

[67] R. Tepper, B. Schulze, H. Görls, P. Bellstedt, M. Jäger, U. S. Schubert, *Org. Lett.* **2015**, *17*, 5740–5743.

[68] F. Zapata, A. Caballero, P. Molina, I. Alkorta, J. Elguero, *J. Org. Chem.* **2014**, *79*, 6959–6969.

[69] A. M. S. Riel, D. A. Decato, J. Sun, C. J. Massena, M. J. Jessop, O. B. Berryman, *Chem. Sci.* **2018**, *9*, 5828–5836.

[70] F. Zapata, A. Caballero, N. G. White, T. D. W. Claridge, P. J. Costa, V. Félix, P. D. Beer, *J. Am. Chem. Soc.* **2012**, *134*, 11533–11541.

[71] A. Caballero, N. G. White, P. D. Beer, *Angew. Chem. Int. Ed.* **2011**, *50*, 1845–1848.

[72] D. Mungalpara, S. Stegmüller, S. Kubik, *Chem. Commun.* **2017**, *53*, 5095–5098.

[73] M. J. Langton, S. W. Robinson, I. Marques, V. Félix, P. D. Beer, *Nat. Chem.* **2014**, *6*, 1039–1043.

[74] S. W. Robinson, C. L. Mustoe, N. G. White, A. Brown, A. L. Thompson, P. Kennepohl, P. D. Beer, *J. Am. Chem. Soc.* **2015**, *137*, 499–507.

[75] C. Li, A.-D. Manick, J. Yang, D. Givaudan, B. Biletskyi, S. Michaud-Chevalier, J.-P. Dutasta, D. Hérault, X. Bugaut, B. Chatelet, A. Martinez, *Inorg. Chem.* **2021**, *60*, 11964–11973.

[76] D.-Q. Dong, S.-H. Hao, Z.-L. Wang, C. Chen, *Org. Biomol. Chem.* **2014**, *12*, 4278–4289.

[77] D. L. Reinhard, F. Heinen, J. Stoesser, E. Engelage, S. M. Huber, *Helv. Chim. Acta* **2021**, *104*, e2000221.

[78] H. Zhao, F. P. Gabbaï, *Nat. Chem.* **2010**, *2*, 984–990.

[79] G. E. Garrett, G. L. Gibson, R. N. Straus, D. S. Seferos, M. S. Taylor, *J. Am. Chem. Soc.* **2015**, *137*, 4126–4133.

[80] G. E. Garrett, E. I. Carrera, D. S. Seferos, M. S. Taylor, *Chem. Commun.* **2016**, *52*, 9881–9884.

[81] A. M. Christianson, F. P. Gabbaï, *Organometallics* **2017**, *36*, 3013–3015.

[82] S. Benz, A. I. Poblador-Bahamonde, N. Low-Ders, S. Matile, *Angew. Chem. Int. Ed.* **2018**, *57*, 5408–5412.

[83] M. Hirai, J. Cho, F. P. Gabbaï, *Chem. – Eur. J.* **2016**, *22*, 6537–6541.

[84] G. Park, F. P. Gabbaï, *Chem. Sci.* **2020**, *11*, 10107–10112.

[85] M. Yang, D. Tofan, C.-H. Chen, K. M. Jack, F. P. Gabbaï, *Angew. Chem. Int. Ed.* **2018**, *57*, 13868–13872.

[86] R. Maskey, M. Schädler, C. Legler, L. Greb, *Angew. Chem. Int. Ed.* **2018**, *57*, 1717–1720.

[87] Martin. Newcomb, A. M. Madonik, M. T. Blanda, J. Kevin. Judice, *Organometallics* **1987**, *6*, 145–150.

[88] A. J. McConnell, P. D. Beer, *Angew. Chem. Int. Ed.* **2012**, *51*, 5052–5061.

[89] Q. He, G. I. Vargas-Zúñiga, S. H. Kim, S. K. Kim, J. L. Sessler, *Chem. Rev.* **2019**, *119*, 9753–9835.

[90] S. K. Kim, J. L. Sessler, *Chem. Soc. Rev.* **2010**, *39*, 3784–3809.

[91] S. Roelens, A. Vacca, O. Francesconi, C. Venturi, *Chem. – Eur. J.* **2009**, *15*, 8296–8302.

[92] M. Delecluse, C. Colomban, D. Moraleda, I. de Riggi, F. Duprat, S. Michaud-Chevallier, J.-P. Dutasta, V. Robert, B. Chatelet, A. Martinez, *Chem. – Eur. J.* **2019**, *25*, 3337–3342.

[93] B. Qiao, A. Sengupta, Y. Liu, K. P. McDonald, M. Pink, J. R. Anderson, K. Raghavachari, A. H. Flood, *J. Am. Chem. Soc.* **2015**, *137*, 9746–9757.

[94] B. Akhuli, P. Ghosh, *Chem. Commun.* **2015**, *51*, 16514–16517.

[95] S. K. Ray, A. Homberg, M. Vishe, C. Besnard, J. Lacour, *Chem. – Eur. J.* **2018**, *24*, 2944–2951.

[96] A. Frontera, M. Orell, C. Garau, D. Quiñonero, E. Molins, I. Mata, J. Morey, *Org. Lett.* **2005**, *7*, 1437–1440.

[97] R. Tepper, B. Schulze, P. Bellstedt, J. Heidler, H. Görls, M. Jäger, U. S. Schubert, *Chem. Commun.* **2017**, *53*, 2260–2263.

[98] J. Luo, Y.-F. Ao, C. Malm, J. Hunger, Q.-Q. Wang, D.-X. Wang, *Dalton Trans.* **2018**, *47*, 7883–7887.

[99] M. P. Wintergerst, T. G. Levitskaia, B. A. Moyer, J. L. Sessler, L. H. Delmau, *J. Am. Chem. Soc.* **2008**, *130*, 4129–4139.

[100] M. Akazome, N. Hamada, K. Takagi, D. Yagyu, S. Matsumoto, *Tetrahedron Lett.* **2014**, *55*, 2226–2229.

[101] T. Ogoshi, S. Kanai, S. Fujinami, T. Yamagishi, Y. Nakamoto, *J. Am. Chem. Soc.* **2008**, *130*, 5022–5023.

[102] B. Hua, L. Shao, Z. Zhang, J. Liu, F. Huang, *J. Am. Chem. Soc.* **2019**, *141*, 15008–15012.

[103] M. Shin, S. Seo, I.-H. Park, E. Lee, Y. Habata, S. S. Lee, *Chem. Commun.* **2020**, *56*, 10135–10138.

[104] M. J. Langton, P. D. Beer, *Acc. Chem. Res.* **2014**, *47*, 1935–1949.

[105] K. M. Bąk, K. Porfyrakis, J. J. Davis, P. D. Beer, *Mater. Chem. Front.* **2020**, *4*, 1052–1073.

[106] R. C. Knighton, P. D. Beer, *Chem. Commun.* **2014**, *50*, 1540–1542.

[107] J. R. Romero, G. Aragay, P. Ballester, *Chem. Sci.* **2016**, *8*, 491–498.

[108] M. Denis, L. Qin, P. Turner, K. A. Jolliffe, S. M. Goldup, *Angew. Chem. Int. Ed.* **2018**, *57*, 5315–5319.

Chapter 2 Modulating Chalcogen Bonding and Halogen Bonding Sigma-hole Donor Atom Potency and Selectivity for Halide Anion Recognition

2.1 Introduction

The ubiquity of hydrogen bonding in biological and synthetic receptor systems has prompted extensive crystallographic, solution-phase and computational studies which have generated a wealth of information concerning the nature, strength, and geometrical preferences of HB interactions. In contrast however, the bulk of existing data of σ-hole···Lewis base interactions is confined to the solid state. Notwithstanding this scarcity the information provided by these studies has helped empirically establish several defining characteristics of these interaction types. For example, inspection of the interatomic distance between the Lewis base and σ-hole donor atom is usually interpreted as a measure of interaction potency, decreasing distance correlating with increased strength, wherein the distance is commonly expressed as a percentage shorter than the sum of the van der Waals radii (%vdW). In particular, it has been demonstrated that increasing the electron-withdrawing ability of a covalently appended substituent has the effect of typically shortening observed σ-hole···Lewis base distances. For example, measurements of nearest interatomic contacts between an I(III) centre of a diaryl iodonium species and its BF_4^- counteranion reveals that substitution of a phenyl group with an electron deficient pentafluorophenyl (PFP) group is accompanied by a significant shortening of closest I···F distance (Figure 2.1a).[1,2] Reports by Gabbai have also demonstrated this effect for methyl diaryl telluronium species (Figure 2.1b), wherein substitution of mesityl group for a PFP group similarly results in a shortening of the major Te···F contact between the Te(IV) centre and a fluorine atom of the tetrafluoroborate counteranion.[3]

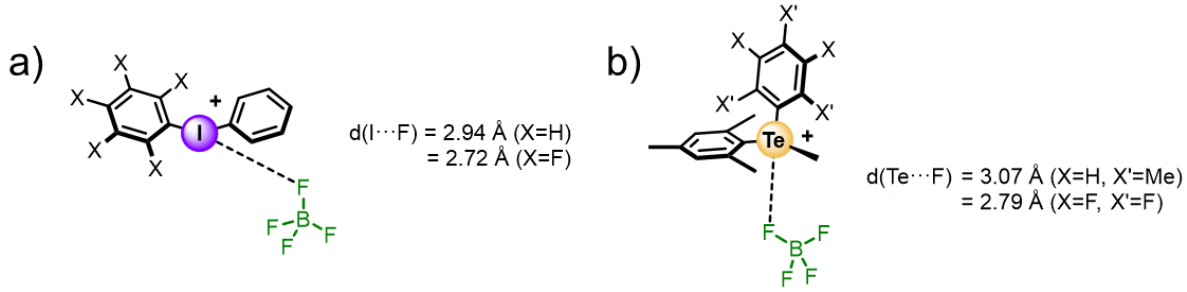


Figure 2.1 a) Short I-F contacts observed in the crystal structure of perfluoroaryl-functionalised diphenyliodonium tetrafluoborate; b) Short Te-F contacts observed in the crystal structure of perfluoroaryl-functionalised methyldiaryltelluronium tetrafluoborate.

While this characteristic of increased σ-hole···anion interaction potency with increasing electron-withdrawing capability has been established in the solid state, evidence of how these electronic factors translate into solution phase anion binding capabilities is rare. In 2017, Matile demonstrated for a series of ChB benzodiselenazoles that chloride affinity in THF solution[4] progressively increased by oxidation of the sulfur containing group from sulfide to sulfoxide to sulfone (Figure 2.2a). Similar effects have also been observed with charge-assisted XB anion receptors, wherein integration of perfluoraryl spacer units in 3,5-bis-iodo-triazole pyridinium receptors exhibit a three-fold enhancement in $K_a(Cl^-)$ relative to a non-fluorinated analogues in DMSO-d_6 solution (Figure 2.2b).[5]

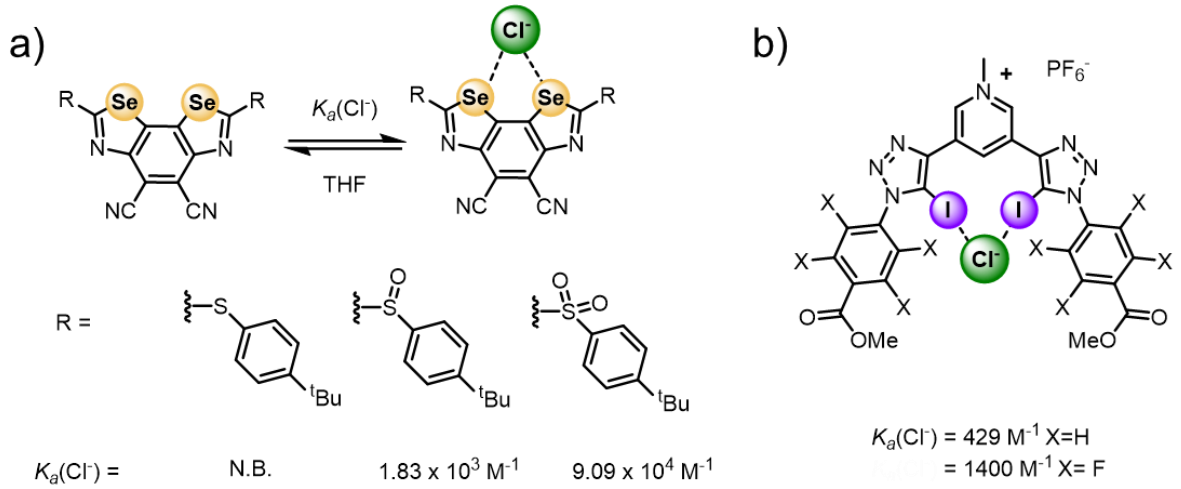


Figure 2.2 a) Chloride association constants (K_a, in THF) of Matile's sulfur appended benzodiselenazole receptors (NB = No binding); b) Chloride association constants (K_a, in DMSO-d_6) of Beer's acyclic bis-iodotriazole pyridinium receptors.

However, for the considered exploitation of σ-hole donors in anion receptor design, it is desirable to be able to relate anion binding potency with a set of chemically meaningful parameters such as molecular electrostatic surface potential or LUMO energies of the σ-hole donor. To this end linear free energy relationships (LFERs) have emerged as powerful tools in aiding quantitative analysis of electronic substitution effects on solution phase HB-anion interactions.[6,7] For example, Johnson et al. used LFERs to elucidate how the electronic properties of the central aryl unit influence C-H···anion HB interactions in a series of bis-ethynyl-spaced urea receptors (Figure 2.3a). ^{1}H NMR titration experiments determined affinities for a wide range of anions including; Cl^-, Br HS^- and HSe^-.[8] It was shown that for all anions investigated a general increase in K_a values was observed with increasingly electron withdrawing substituents. Supported by computational modelling studies, the authors attributed this to an increasing polarisation of the C-H bond and therefore increasing HB donor potency. LFER plots using the Hammett equation (Figure 2.3b) which relates log(K_a) values and aryl substituent constants (σ), determined the corresponding ρ (gradient) values - a measure of the substituent effect relative to the benchmark deprotonation of benzoic acid in

water.[9] Comparing the ρ values for each anion determined that hydrosulfide affinity was ca. 2.5 times more sensitive to electronic aryl C-H HB donor polarisation effects than chloride, bromide and hydroselenide, presenting a highly novel approach to engineering selectivity in a HB-mediated anion receptor system (Figure 2.3c).

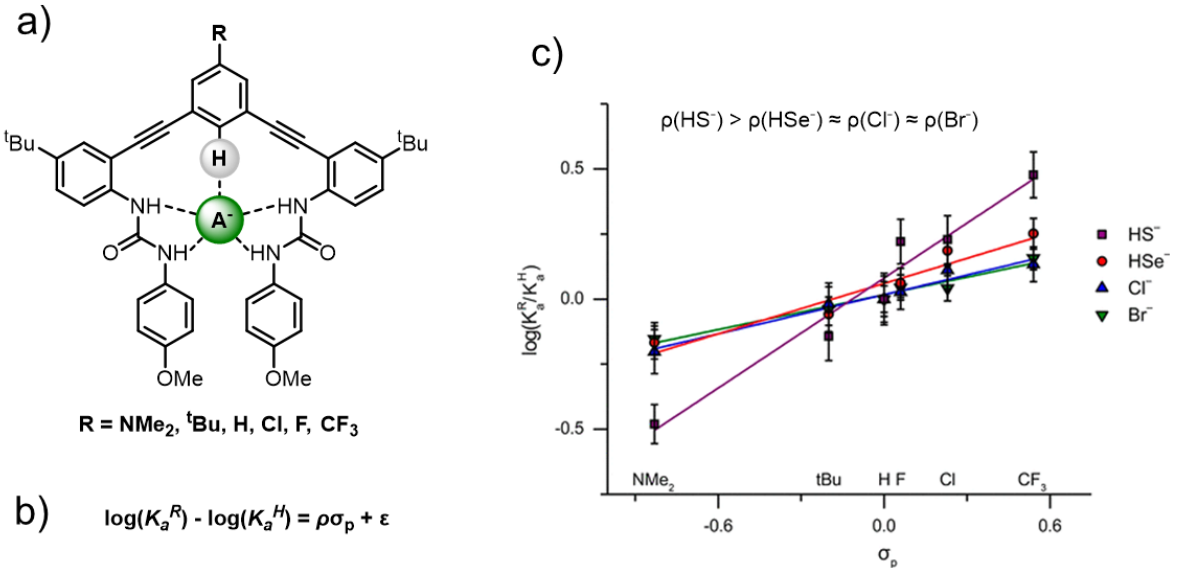


Figure 2.3 a) Johnson's series of aryl bis-ethynyl-spaced urea receptors appended with electron-donating or withdrawing groups b) Modified Hammett equation used to fit Ka values that includes an origin offset value (ε) c) Generated Hammett plots between the receptors and different anion guests.

2.2 Chapter Aims

With the aim of delineating the electronic and structural factors that govern the potency and selectivity of ChB, XB and HB donors in anion recognition behaviour, this chapter's objectives are to:

- Establish the role that electronic polarisation effects play in augmenting the anion recognition properties of a series of acyclic triazole-containing ChB, XB and HB receptor systems.
- Investigate and quantify how the integration of electron-withdrawing or electron-donating substituents affect the anion binding potency and selectivity of ChB receptor systems.

To this end, this chapter investigates a series of structurally analogous neutral receptors incorporating XB, ChB or HB donor atoms into a bidentate 3,5-bis-triazole pyridine motif. Their anion binding properties are studied by extensive ^{1}H NMR anion titration experiments. Moreover, systematic variation of the electron-withdrawing/-donating properties of the aryl substituents attached to either the triazole unit (Figure 2.4a and 2.4b) or directly bonded to the tellurium-based ChB donor (Figure 2.4c) facilitates Hammett plot LFER analysis, which crucially correlates anion affinity and selectivity with the extent of electronic polarisation.

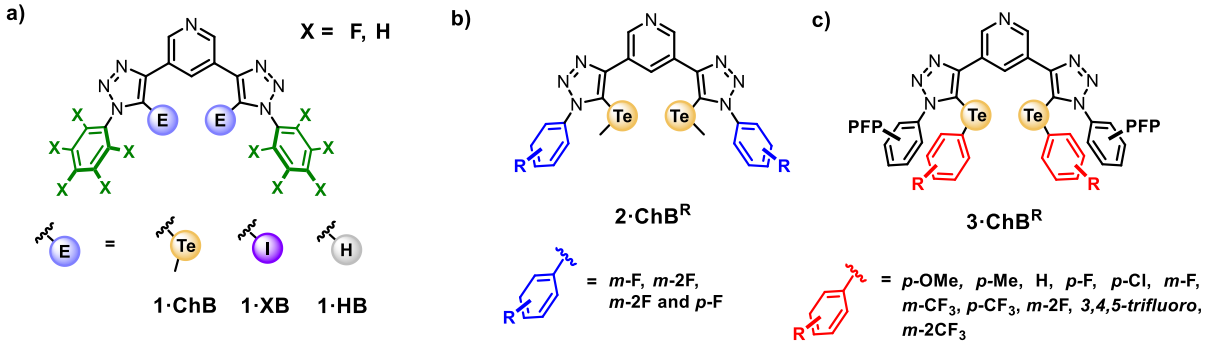


Figure 2.4 Receptor series a) **1·ChB**, **1·XB** and **1·HB** b) **2·ChB^{R}** c) **3·ChB^{R}**.

2.3 Acylic chalcogen, halogen and hydrogen bonding 3,5-bis-triazole pyridine anion receptors

2.3.1 Design of the ChB, XB and HB anion receptors

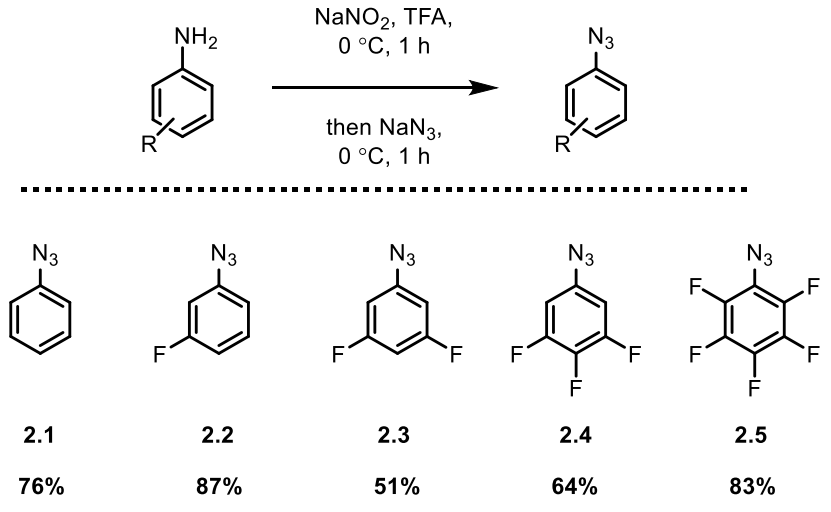
The first-generation receptors investigated, **1·ChB**, **1·XB** and **1·HB**, comprise of telluromethyl-, iodo- or proto-triazole units respectively, appended with phenyl (Ph) or highly electron deficient perfluorophenyl (PFP) groups (Figure 2.4a). Systematically varying the degree of the electron-withdrawing/-donating capabilities of either the triazole-bound aryl substituents in the **2·ChB** series(Figure 2.4b), or the Te-bound aryl substituents in the **3·ChB** series (Figure 2.4c) was anticipated to delineate the relative structural influence of electronic polarisation on anion binding properties.

2.3.2 Synthesis of the ChB, XB and HB anion receptors

The target hosts were constructed via copper(I)-catalysed azide-alkyne cycloaddition (CuAAC) 'click' methodology, exploiting the reaction's diverse functional group tolerability, regio-selectivity, and high yielding nature. The following section describes the syntheses of the target ChB, XB and HB receptors.

2.3.3 Aryl Azide Precursor Synthesis

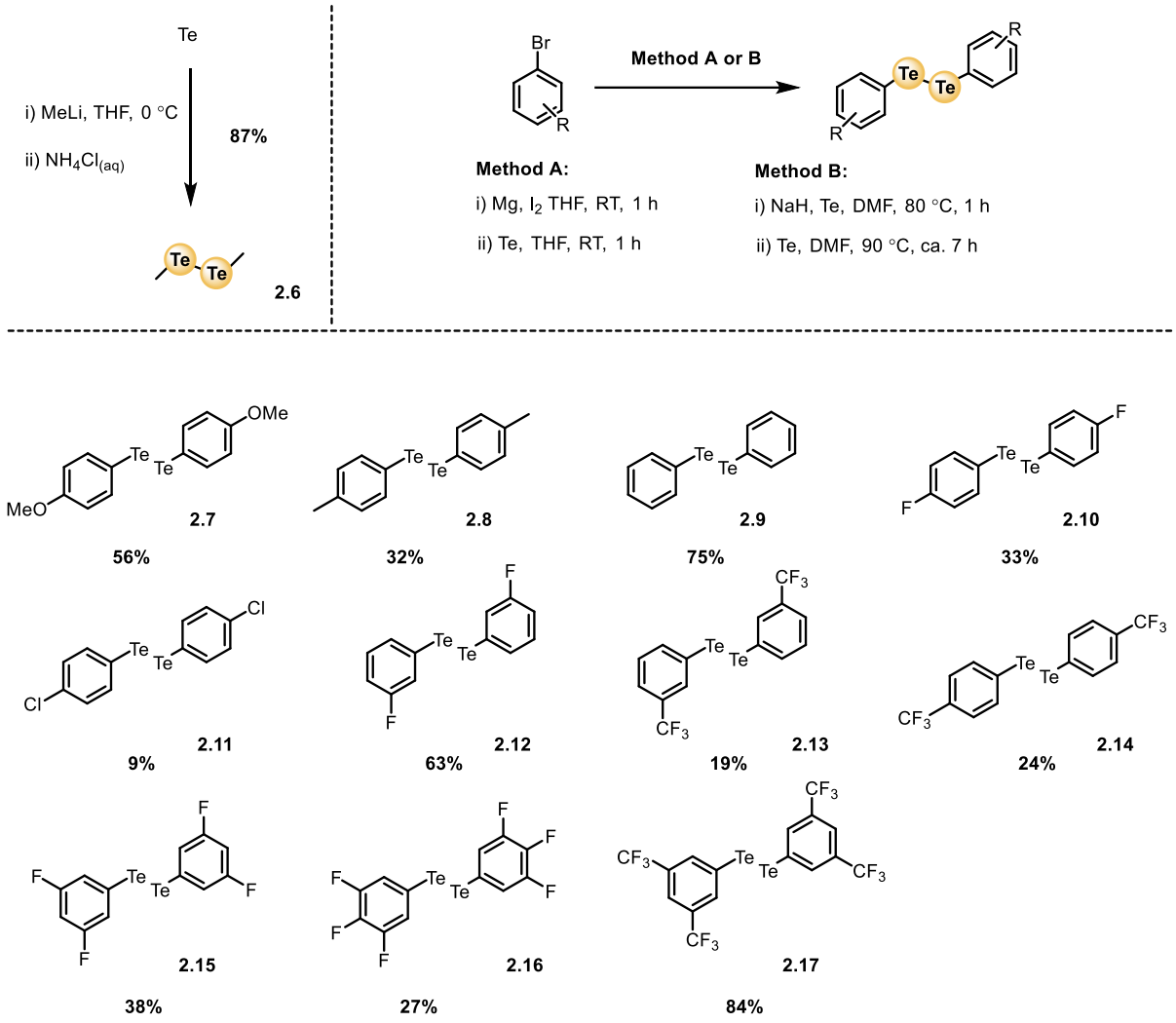
The appropriately functionalised aryl azides were synthesised according to a standard diazotisation procedure of the parent aniline with $NaNO_2$ in trifluoroacetic acid solution at 0 °C and subsequent treatment with NaN_3 to afford the range of phenyl, **2.1**, and fluorinated azides **2.2**-**2.5** in good yields without need for purification (Scheme 2.1).[10]



Scheme 2.1 Synthesis of aryl azide precursors.

2.3.4 Dimethyl and Diaryl Ditelluride Synthesis

The ditellurides required for the synthesis of the corresponding tellurium-functionalised alkynes were obtained by methods outlined in Scheme 2.2. Dimethyl ditelluride **2.6** was obtained by treatment of elemental tellurium with a MeLi solution in anhydrous THF to afford the MeTeLi intermediate. Careful quenching of the lithium telluride species with an aqueous ammonium chloride solution gave the tellurol MeTeH, whereupon exposure to the air immediately generated a dark brown solution. Aqueous work-up procedures followed by silica gel column chromatography (SGCC) afforded dimethyl ditelluride **2.6** in good yield 87% as an intensely coloured brown oil.[11] The diaryl ditellurides were synthesised by either one of two methods. In the majority of cases (Method A), ditelluride synthesis was achieved by addition of the commercially available aryl halide with freshly activated magnesium turnings in anhydrous THF for in situ Grignard formation of the corresponding aryl magnesium bromide. Subsequent addition of Te(0) powder, followed by quenching with aqueous NH_4Cl and aerial oxidation afforded the diaryl ditellurides as dark red or brown solids after chromatographic purification in variable yields 27-84%.[12,13] Interestingly, this method proved unsuccessful for the preparation of para-trifluoromethyl or para-chloro substituted diaryl ditellurides, necessitating an alternative procedure (Method B). The compound NaTeH, generated in situ from a dispersion 60% of NaH in mineral oil with tellurium in DMF at elevated temperature, was reacted with the aryl bromide at 90 °C until TLC analysis confirmed consumption of the starting material affording **2.14** and **2.11** in 24% and 9% yields respectively.[14]

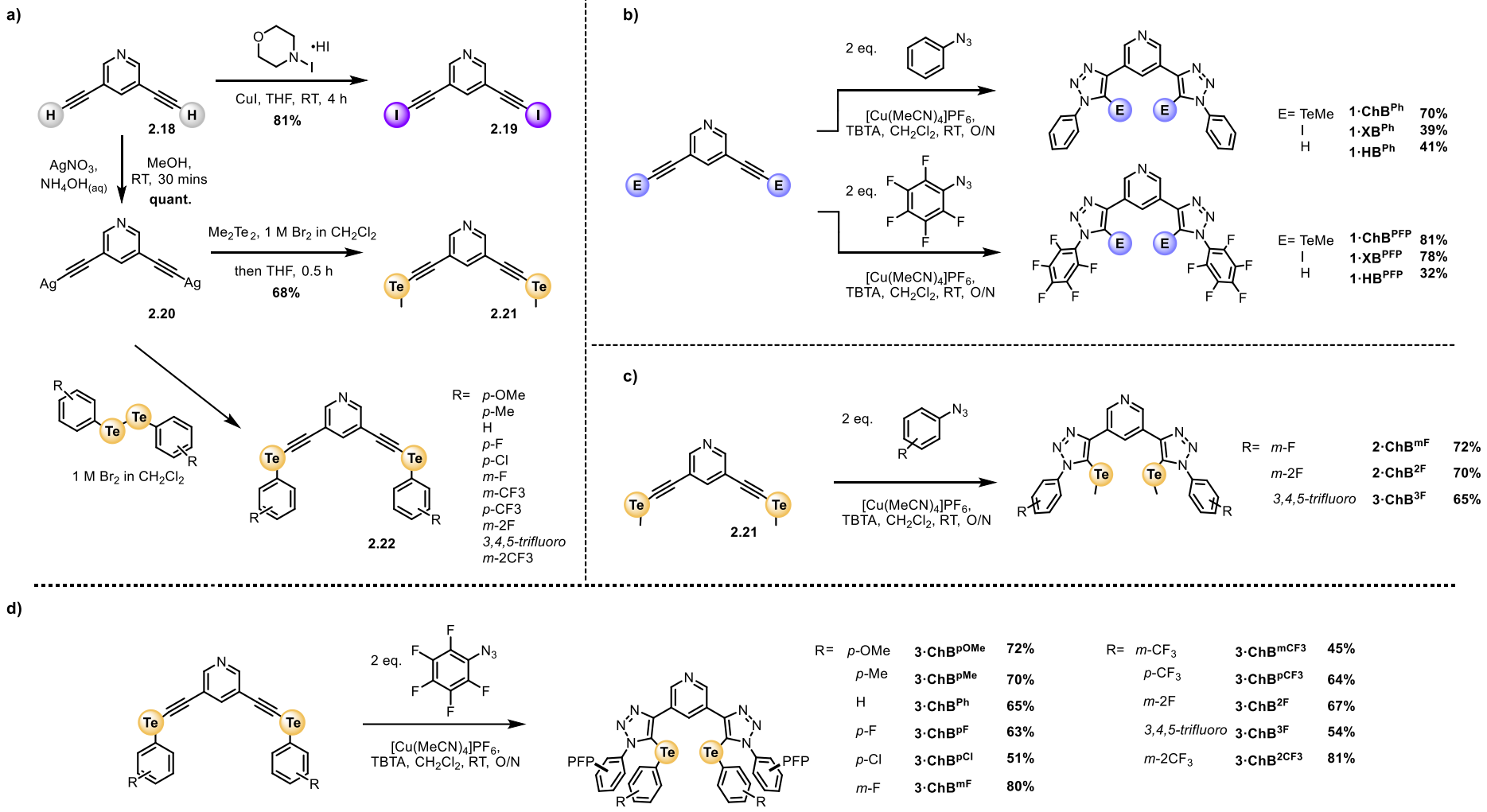


Scheme 2.2 Synthesis of ditelluride precursors.

2.3.5 CuAAC synthesis of the ChB, XB and HB receptors

The requisite iodo- and tellurium-functionalised alkyne precursors, **2.19** and **2.20** were synthesised according to Scheme 2.3a, from 3,5-diethynyl pyridine **2.18**. Treatment of the proto-alkyne **2.18** with *N*-iodomorpholine in the presence of catalytic CuI gave the requisite bis-iodine functionalised alkyne in **2.19** in 81% yield. Reaction of the parent bis-proto-alkyne **2.18** with freshly ground $AgNO_3$ with catalytic $NH_4OH_{(aq)}$ in a MeOH solution facilitated the isolation of bis-Ag(I)-acetylide **2.20**. In general, the synthesis of the appropriate bis-telluro alkynes was achieved by treatment of the appropriate dialkyl- or diaryl ditelluride with a 1 M Br_2 solution to generate the corresponding organotellurium(II) bromide, which was reacted immediately with an anhydrous THF suspension of the silver acetylide **2.20**, to afford the series of bis-telluro functionalised alkynes **2.21** and **2.22** after purification by rapid SGCC.

The target ChB, XB and HB based receptors were synthesised according to a general CuAAC procedure between the appropriately functionalised alkyne and aryl-azide with catalytic quantities of $[Cu(MeCN)_4PF_6]$ and the rate-accelerating ligand TBTA (Scheme 2.3). Once determined complete by TLC analysis, the reaction mixtures were subject to aqueous NH_4OH/EDTA work-up procedures and purification of the crude mixtures by SGCC gave the receptors as white stable solids in yields in the range of 41-81%. Whilst generally high yielding, the somewhat modest yields for **1·HB^{PFP}**, **1·HB^{Ph} and 1·HB^{PFP}** were attributed to the poor solubility of the receptors in almost all organic solvents (e.g., CH_2Cl_2, $CHCl_3$, MeOH). The 20 novel anion receptors were characterised by ^{1}H, ^{13}C NMR and high resolution ESI-MS.



Scheme 2.3 a) Synthesis of the requisite functionalised alkyne derivatives. CuAAC synthesis of the a) **1·ChB**, **1·XB** and **1·HB** series c) **2·ChB** series d) **3·ChB**.

Crystals of **1·XB^{PFP}**, **1·ChB^{PFP}**, **1·HB^{PFP}**, **3·ChB^{pCl}**, **3·ChB^{2F}** and **3·ChB^{3F}** suitable for X-ray structural analysis were grown from slow evaporation of chloroform solutions (Figure 2.4). The structures show the σ-hole donors participating in intermolecular N···I XB or N···Te ChB interactions respectively whilst the **1·HB^{PFP}** forms linear chains in the solid state directed by triazole C-H···N interactions and **1·HB^{PFP}**.

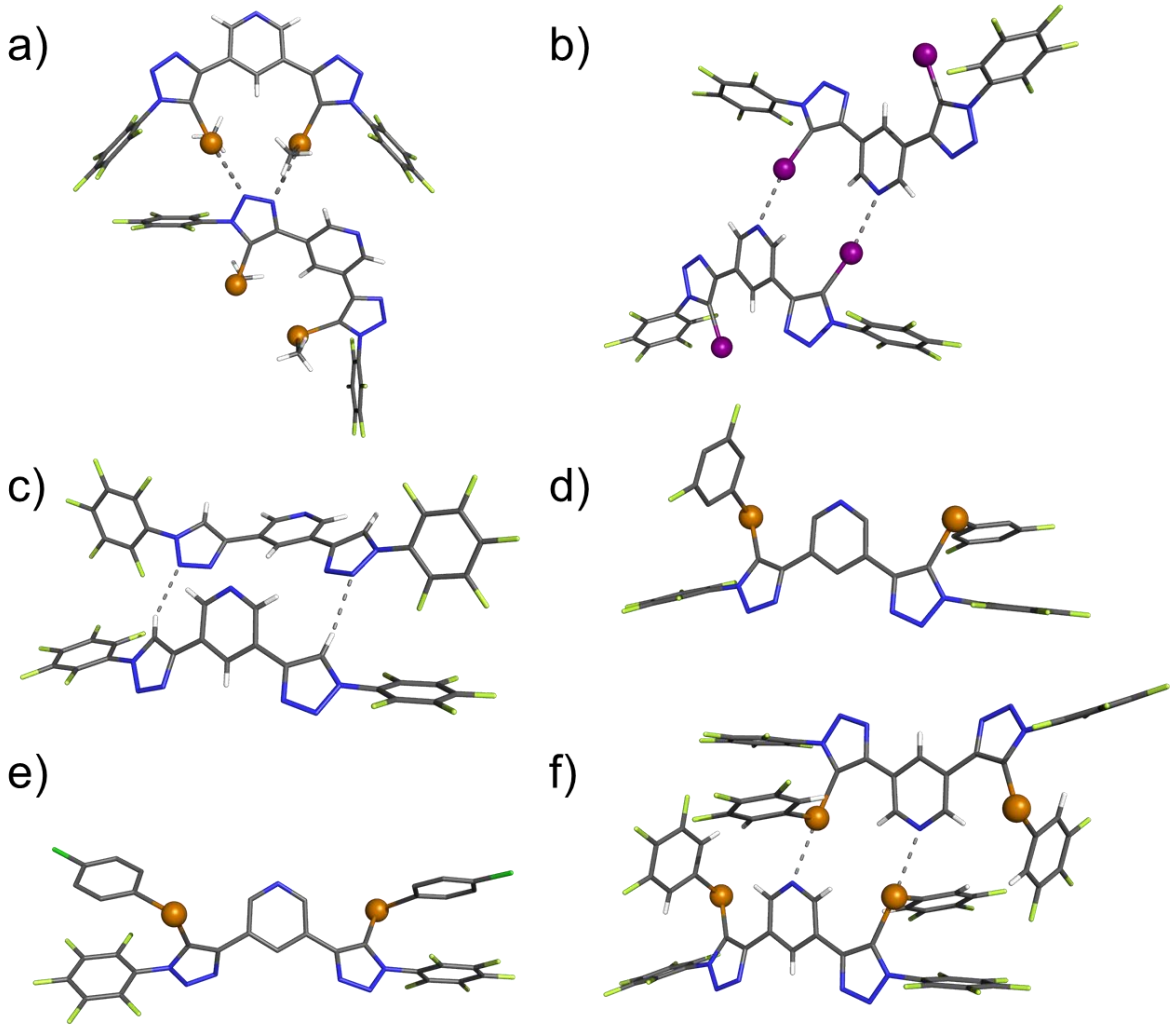


Figure 2.5 X-ray crystallographic structures of a) **1·ChB^{PFP}**, b) **1·XB^{PFP}** and c) **1·ChB^{PFP}** d) **3·ChB^{pCl}** e) **3·ChB^{2F}** f) **3·ChB^{3F}** showing the formation of ChB/XB/HB interactions in the solid state, represented by dashed lines. Grey = carbon, blue = nitrogen, white = hydrogen, green = fluorine, dark green = chlorine, orange = tellurium, purple = iodine.

Comparison of their ^{1}H NMR spectra highlights diagnostic key differences between the receptors, relating to the electronic nature of the heteroatom donor and appended aryl component. As a representative example, inspection of the ^{1}H NMR spectra of phenyl-appended receptors **1·XB^{Ph}**, **1·ChB^{Ph}** and **1·HB^{Ph}** in acetone-d_6 highlight the consequences of donor atom variation (Figure 2.6). As expected, a clear downfield shift can be observed for internal pyridyl proton b (triplet) as the donor atom increases in electronegativity (I > Te > H), rendering the proton more deshielded.

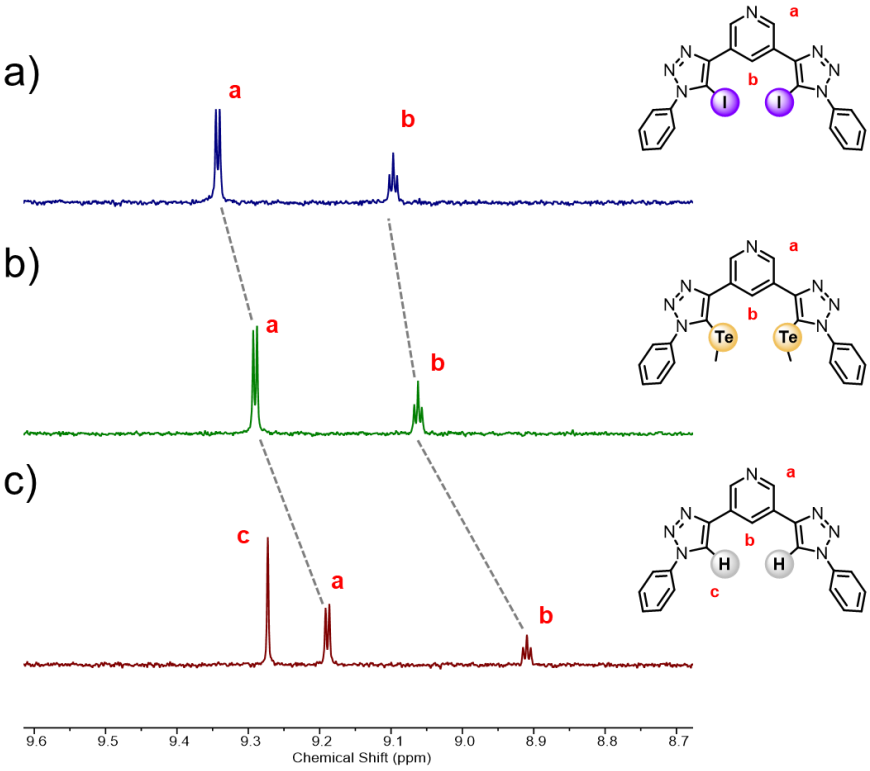


Figure 2.6 Stacked ^{1}H NMR spectra of a) **1·XB^{Ph}** , b) **1·ChB^{Ph}** and c) **1·HB^{Ph}** (acetone-d_6, 400 MHz, 298 K).

The effects of increasing polarisation in these systems - by modification of the pendant aryl substituents - can also be observed by inspection of the ^{1}H NMR spectra. Figure 2.7 shows the pyridine aromatic resonances a and b of **1·ChB^{PFP}** and b **1·ChB^{PFP}** which undergo significant downfield shifts upon changing the spacer substituent from phenyl to a more electron-withdrawing perfluorophenyl.

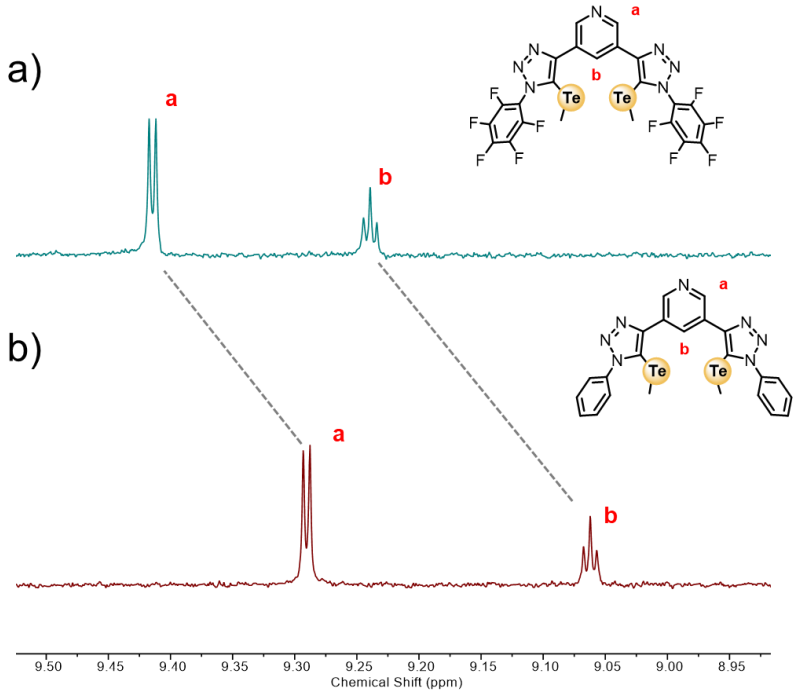


Figure 2.7 Stacked ^{1}H NMR spectra of a) **1·ChB^{PFP}** , b) **1·ChB^{Ph}** (acetone-d_6, 400 MHz, 298 K).

Representative spectroscopic data for the **3·ChB** series is shown in Figure 2.8, wherein inspection of the NMR spectroscopic characterisation data for the **3·ChB** receptor series also reveals well resolved ^{1}H signals, in the case of **3·ChB^{pCF3}** four signals in both the ^{1}H and ^{19}F NMR spectra (Figure 2.8b and 2.8c). This suggests any steric effects imposed by introducing two tellurium bound aryl groups is not sufficient to cause hindered rotation around the bis-triazole units. Characterisation by high resolution ESI-MS also revealed a complex diagnostic mass profile from eight tellurium isotopes (Figure 2.8d).

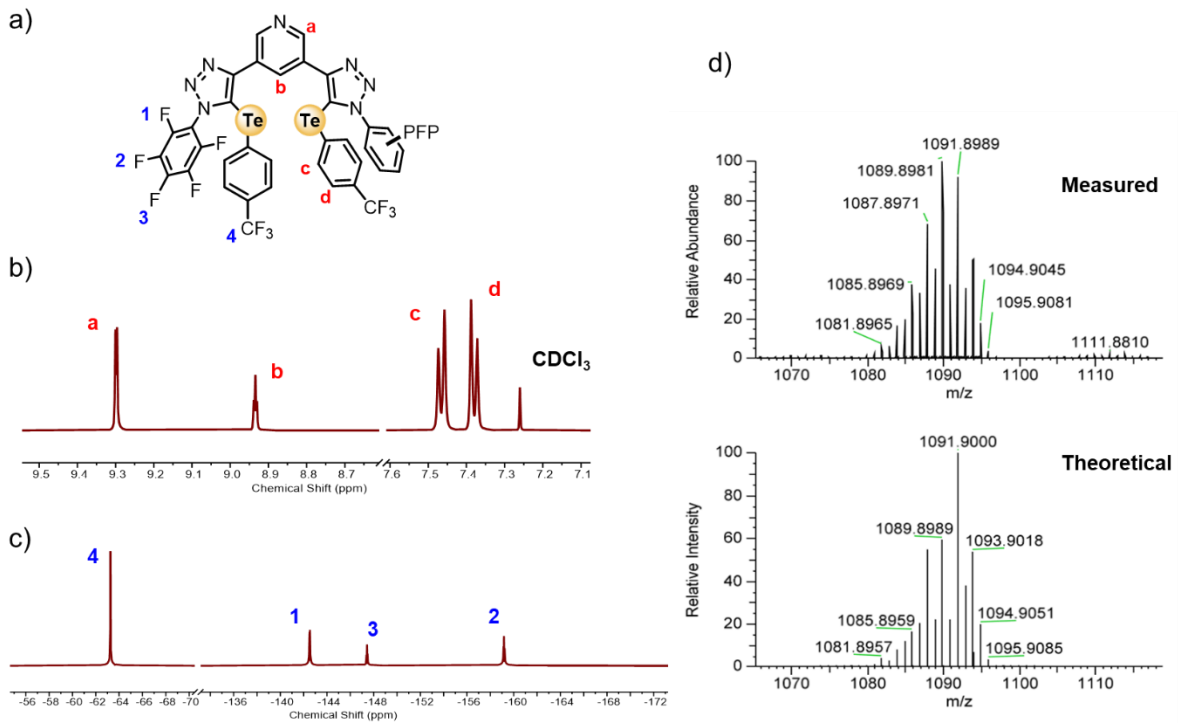


Figure 2.8 a) Chemical structure of **3·ChB^{pCF3}** b) Truncated ^{1}H NMR spectrum of **3·ChB^{pCF3}** ($CDCl_3$, 500 MHz, 298 K) c) Truncated ^{19}F NMR of **1·ChB^{Ph}** ($CDCl_3$, 470 MHz, 298 K) d) Theoretical (bottom) and measured (top) high resolution ESI spectrum.

2.3.6 Anion Binding Studies of 1·ChB, 1·XB and 1·HB receptor series

In order to assess the anion binding properties of the **1·ChB**, **1·XB** and **1·HB** receptor series, preliminary ^{1}H NMR spectroscopic anion titration experiments in acetone-d_6 were conducted. Aliquots of halides as their tetrabutylammonium (TBA) salts were titrated against solutions of the six receptors, with the most significant proton resonances perturbed being associated with the bis-triazole binding clefts (representative example in Figure 2.9a and 2.9b). Upon the addition of increasing anion equivalents the ChB, XB and HB receptors' external pyridyl signal underwent an upfield shift, whereas the internal pyridyl proton universally shifted downfield. In addition, for the **1·HB** and **1·ChB** receptors downfield perturbations were also observed in the chemical shift of the corresponding triazole C-H and tellurium methyl (TeMe) protons, providing further evidence for the participation of HB and ChB interactions in the binding process. Binding isotherms generated from monitoring the chemical shift perturbations of the respective receptor's internal pyridine proton b was analysed using Bindfit, which determined 1:1 stoichiometric halide anion association constants (Figure 2.9c), which are summarised in Table 2.1.

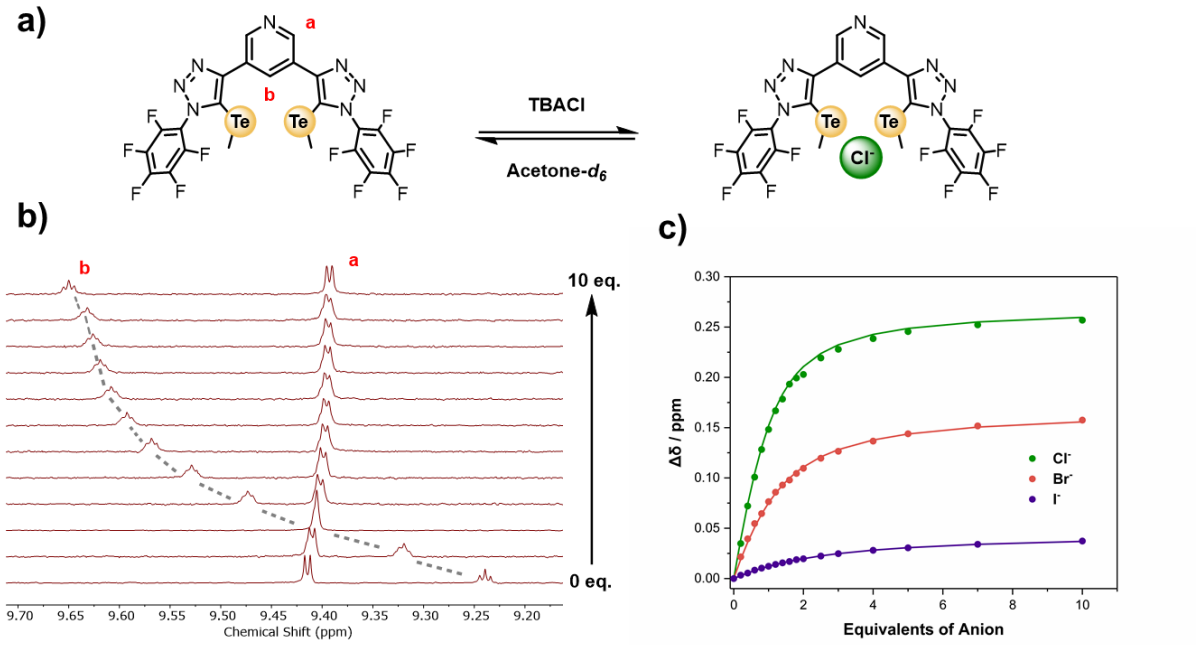


Figure 2.9 a) Chloride anion binding equilibria for **1·ChB^{PFP}**. b) Stacked ^{1}H NMR titration spectra for **1·ChB^{PFP}** with increasing equivalents of TBACl (acetone-d_6, 500 MHz, 298K). c) Anion Binding titration isotherm for **1·ChB^{PFP}** with chloride, bromide and iodide.

Table 2.1 Halide anion association constants and calculated binding enhancement factors for phenyl and pefluorophenyl appended ChB, XB and HB acyclic anion receptor systems.

Anion association constants K_a / M^{-1} [a]								
Anion[b]	Acetone-d_6						2.5 %-D_2O-acetone-d_6	
	1·ChB^{PFP}	**1·ChB^{Ph}**	**1·XB^{PFP}**	**1·XB^{Ph}**	**1·HB^{PFP}**	**1·HB^{Ph}**	**1·XB^{PFP}**	**1·XB^{Ph}**
Cl^-	18,600[c]	590	$>10^5$	15,800	386	394	2,920	416
Br^-	4,620	304	$>10^5$	7,800	116	191	4,600	1,060
I^-	1,230	234	24,600[c]	2,710	37	49	5,230	1,450

[a] Association constants determined by Bindfit analysis of internal pyridine proton signal, errors ± < 7% unless otherwise specified. [b] Anions added as their tetrabutylammonium salts. [c] Error < 13%.

The XB receptors display the greatest halide affinities, followed by the ChB hosts: XB > ChB > HB. Notably, the incorporation of perfluorophenyl substituents in receptors **1·XB^{PFP}** and **1·ChB^{PFP}** produces a dramatic enhancement in halide association constant magnitudes relative to their phenyl receptor analogues. Indeed, the remarkable halide anion affinities of perfluorophenyl-substituted **1·XB^{PFP}** ($>10^5$ M^{-1}) precluded accurate quantification of its halide association constants, necessitating the more competitive solvent mixture of 2.5% D_2O/acetone-d_6 (*v/v*) for their evaluation which resulted in a Hofmeister bias for anion afffinity; $I^- > Br^- > Cl^-$. The incorporation of spacer perfluorophenyl groups to the receptor produces a dramatic enhancement in its halide affinities relative to **1·XB^{Ph}**. Inspection of Table 2.1 also reveals a significant enhancement in halide affinity for **1·ChB^{PFP}** relative to **1·ChB^{Ph}**, illustrating the influence of the perfluorophenyl electron-withdrawing groups on the halide affinities of both XB and ChB sigma-hole type receptors.

In stark contrast, inspection of the anion association constants for the HB receptors **1·HB^{PFP}** and **1·HB^{Ph}**, demonstrate no such enhancement and apparently appear unaffected by the incorporation of electron-withdrawing perfluorophenyl groups. To enable quantitative evaluation of the relative augmentation of perfluorophenyl group incorporation in these receptor systems, halide anion binding enhancement factors ($\alpha = K_a^{PFP}/K_a^{Ph}$) were calculated. Importantly, surveying the determined binding enhancement factors (α), summarised in Table 2.2, demonstrates that for all halides the ChB receptor exhibits the largest α value relative to XB and HB analogues, as graphically illustrated in Figure 2.10. In particular, α values calculated for chloride reveal over a thirty-fold enhancement for ChB, whereas XB demonstrates an eight-fold enhancement. The pronounced increase of anion association constant magnitude by the perfluorophenyl substituent may be rationalised by the increased polarisability of the heavier ChB and XB donor atoms in the C-X bond (X = TeMe, I), relative to the proto-triazole HB donor.

The HB analogue's halide affinities appear surprisingly unperturbed upon incorporation of the highly electron-withdrawing aryl substituents (α ≈ 1), suggesting an apparent insensitivity of the HB donors to electronic substitution. Whilst initially surprising, considering HB donor acidity normally correlates with anion binding potency, the observations are most likely attributable to subtle solvation effects and competitive HB formation between the acidic triazole C-H donors and acetone solvent molecules, which is anticipated to be a more pronounced effect in the perfluorinated receptor.

Table 2.2 Calculated binding enhancement factors for **1·ChB**, **1·XB** and **1·HB** receptor series.

	Binding enhancement factors α = (K_a^{PFP}/ K_a^{Ph})		
Anion[a]	**1·ChB**	**1·XB**	**1·HB**
Cl^-	32 ± 4.00	7.0 ± 0.20	0.86 ± 0.06
Br^-	15 ± 0.50	4.4 ± 0.50	0.76 ± 0.033
I^-	5.2 ± 0.40	3.6 ± 0.32	0.86 ± 0.05

[a] Anions added as their tetrabutylammonium salts.

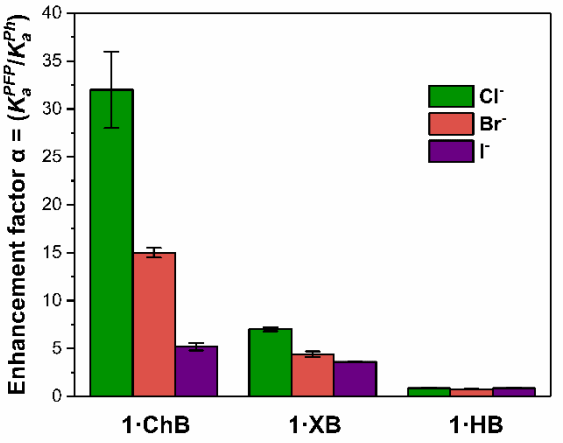


Figure 2.10 Plot showing the halide anion enhancement factors for the **1·ChB**, **1·XB** and **1·HB** receptor series.

2.3.7 Anion Binding Studies of 2·ChB receptor series

The halide anion affinities of the **2·ChB** receptor series were determined via ^{1}H NMR spectroscopic titration experiments. As expected, increasing the extent of fluorine substitution on the triazole linked aryl substituent results in a concomitant increase in halide association constant (Table 2.3). Furthermore, the additive nature of Hammett substituent constants (σ) facilitated the construction of LFER plots (Figure 2.11) in which the effect of the increasing electron withdrawing ability of aryl substituents on halide association constant values is quantified, as represented by the ρ value, which serves as a measure of the sensitivity of the ChB-anion interaction to the changing electronic properties of an aryl substituent. Summarised in Table 2.3, the ρ > 0 value for all halides indicates that anion binding potency increases as the sum of the electron withdrawing substituent constants (Σσ) increases. The sensitivity of this through-bond inductive polarisation appears to most pronounced for the lighter halides, Cl^- and Br^- with ρ = 0.91 and 0.81 respectively. Analogous plots constructed with K_a values for iodide, revealed a much less pronounced correlation with Σσ, possibly due to steric effects implicated in binding the larger halide.

Table 2.3 Halide anion association constants and the summed Hammett constants of the **2·ChB** receptor series.

	Anion association constants K_a / M^{-1} [a] for **1·ChB^{Ph}** and **2·ChB^{R}** series			
Anion[b]	**1·ChB^{Ph}**	**mF**	**2F**	**3F**
Cl^-	590	987[e]	2070	2950[e]
Br^-	304	592	966	145
I^-	234	217	547	497
Σσ[c]	0.00	0.337	0.674	0.736

[a] Association constants determined by Bindfit analysis of internal pyridine proton signal, conducted in acetone-d_6, errors ± < 7%. [b] Anions added as their tetrabutylammonium salts. [c] Sum of Hammett constants.

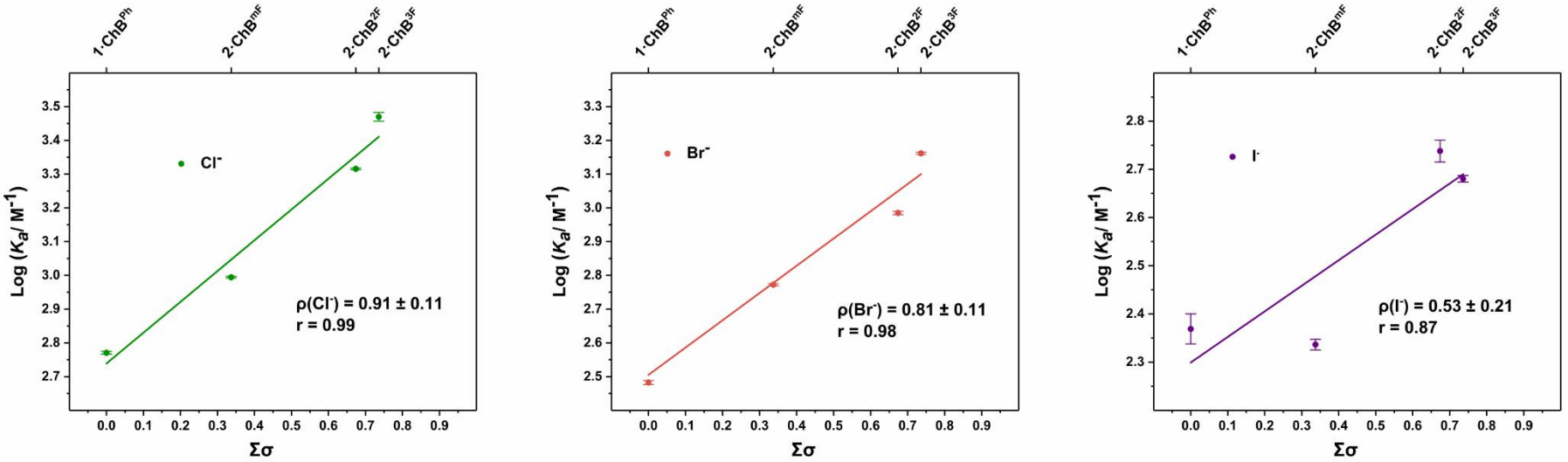


Figure 2.11 Hammett plot for the **2·ChB^{R}** receptor series.

2.3.8 Anion Binding Studies of 3·ChB receptor series

To firstly assess the effect of replacing the tellurium methyl group with a more sterically demanding aromatic substituent, preliminary ^{1}H NMR spectroscopic titration experiments in acetone-d_6 were performed on the **3·ChB** series, which, in general, revealed significant perturbations observed in the receptors' aryl and pyridyl proton resonances. The largest chemical shift perturbations were seen with the more electron-deficient aryl substituent systems, a representative example is shown in Figure 2.12.

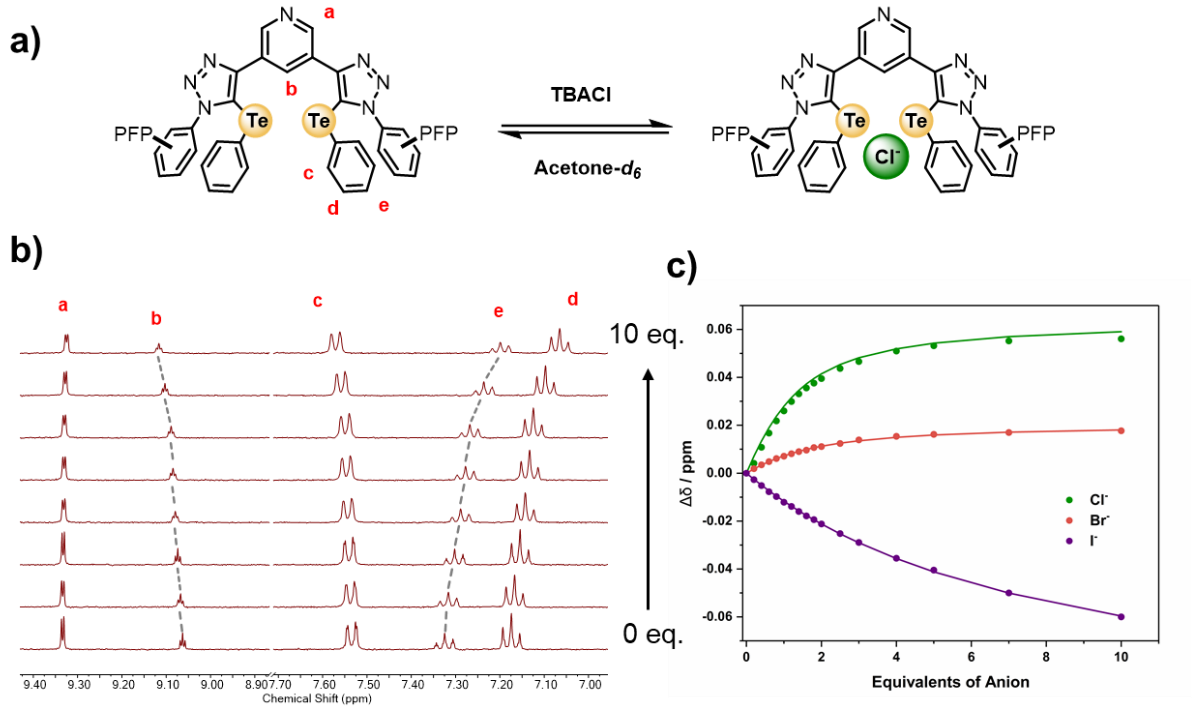


Figure 2.12 Figure 3. a) Chloride anion binding equilibria for **3·ChB^{Ph}**. b) Stacked ^{1}H NMR titration spectra for **3·ChB^{Ph}** with increasing equivalents of TBACl (acetone-d_6, 500 MHz, 298K). c) Anion Binding titration isotherm for **3·ChB^{Ph}** with chloride, bromide and iodide.

Analysis of the anion binding isotherms using the Bindfit programme determined 1:1 stoichiometric association constants (Figure 2.12c) summarised in Table 2.4 Interestingly, comparison of the anion binding properties of **3·ChB^{Ph}** relative to methyl functionalised analogue, **1·ChB^{Ph}**, demonstrates the replacement of the tellurium bound methyl group with a phenyl group significantly attenuates halide affinity, which is most likely attributable to steric effects. The halide K_a values of the ChB receptors follows the trend $Cl^- > Br^- > I^-$, which correlates with anion basicity influenced affinities. Upon traversing Table 2.4 from left to right, a significant increase in the association constant magnitudes are observed as the electron-withdrawing ability of the aryl substituents increase. Furthermore, the para-methyl and para-methoxy receptors **3·ChB^{pMe}** and **3·ChB^{pMeO}** displayed no measurable chemical shift perturbation upon the addition of 10 equivalents of iodide and only modest chloride and bromide affinity, whereas the remarkable halide affinity ($K_a > 10^5$ M^{-1}) of highly electron-

deficient receptors, such as **3·ChB^{3F}** and **3·ChB^{3F}**, precluded accurate quantification of their chloride association constants. LFER plots of halide K_a values versus Hammett aryl substituent constants (σ) (Figure 2.13) reveal in all cases that receptor-halide binding affinity correlates well with the aryl substituent σ-parameters. Several trends can be observed from the LFER analysis. As expected from the relative association constant values, the positive gradients indicate that incorporation of more potent electron-withdrawing aryl substituents in the receptor design universally increases halide anion binding affinities. Importantly, the ρ values demonstrate the significant influence of electron-withdrawing and donating groups on ChB anion binding strength. Moreover, relative to the ρ values obtained by variation of the triazole-appended aryl substituent (ρ(Cl^-) = 0.91) in the **2·ChB^R** series, modulating the electronic donating/withdrawing nature of the tellurium directly appended aryl substituent (**3·ChB^R**) has a considerably larger influence on anion binding potency (ρ(Cl^-) = 2.20). This is concordant with a conventional understanding of the significant distance dependence of inductive effects. However, it is noteworthy that comparison of the most electron withdrawing and the most electron donating substituents, has the effect of increasing the chloride association constant value by 4 orders of magnitude. Perhaps most interestingly the determined trend of ρ(Cl^-) > ρ(Br^-) > ρ(I^-), means that increasing the electron withdrawing potency of the Te-bonded aryl group has a more pronounced effect on chloride affinities over iodide affinities for example, thereby increasing selectivity towards the lighter halide. The postulated polarisation-induced halide anion discrimination presents a unique opportunity for engineering selectivity in ChB anion receptors via modulation of the intrinsic non-covalent interactions.

Table 2.4 Halide anion association constants and the summed Hammett constants of the **3·ChB** receptor series.

Anion association constants K_a / M^{-1} for **3·ChB^R** series [a]											
Anion[b]	**pOMe**	**pMe**	**Ph[c]**	**pF**	**pCl**	**mF**	**mCF3**	**pCF3**	**2F[c]**	**3F[c]**	**2CF3**
Cl^-	450	1140	1,360	1,610	4,790	14,000[f]	>10^5[d]	>10^5[d]	>10^5[d]	>10^5[d]	>10^5[d]
Br^-	230	518	822	863	2,540	2,740	7,540	7,270	5,180	11,800[f]	19,900[f]
I^-	NB[e]	NB[e]	119	398	674	592	1450	1,620	1,040	1,750	3,980
Σσ[e]	-0.268	-0.170	0.00	0.062	0.227	0.337	0.430	0.540	0.674	0.736	0.860

[a] Association constants determined by Bindfit analysis of Te-aryl chemical shift perturbations unless otherwise specified, errors ≤ 10% unless otherwise specified, conducted in acetone-d_6. [b] Anions added as their tetrabutylammonium salts. [c] Determined by monitoring of internal pyridine proton signal. [d] Too large to be accurately quantified by ^{1}H NMR titration. [e] No binding. [f] Error ≤ 26%.

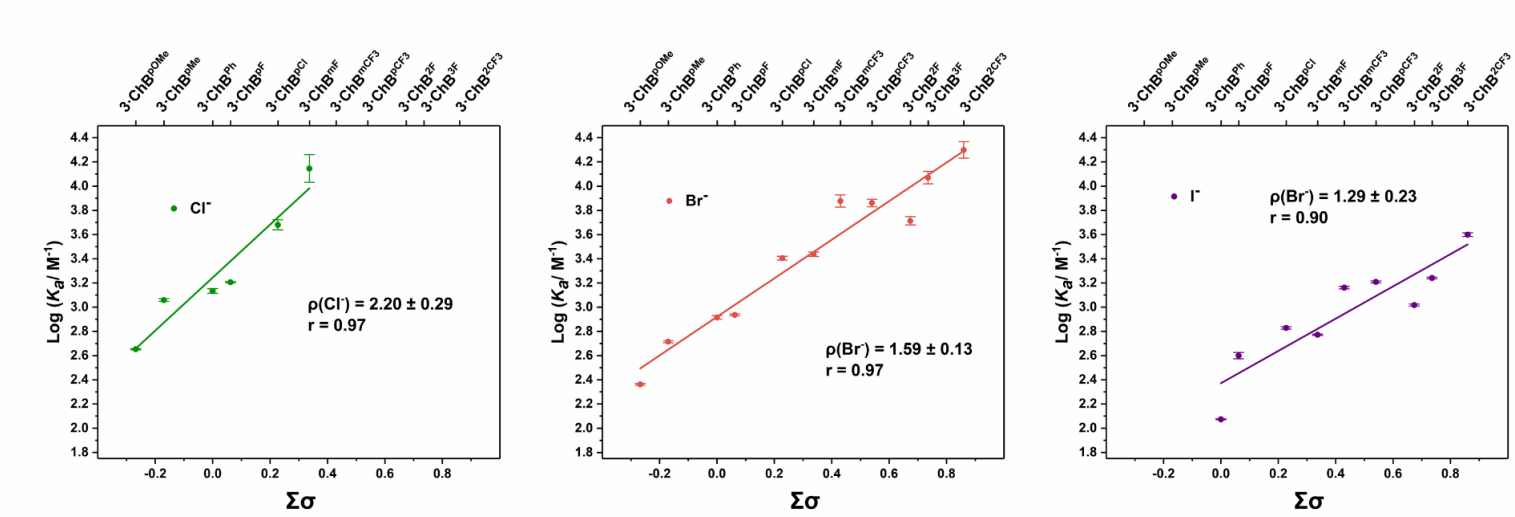


Figure 2.13 Hammett plot for the **3·ChB^R** receptor series.

2.4 Conclusions

In conclusion, a library of acyclic anion receptors containing chalcogen bond and halogen bond donors integrated into a neutral 3,5-bis-triazole pyridine scaffold appended with various phenyl and electron-withdrawing fluoroaryl substituents have been prepared for halide anion recognition investigations. With the first receptor series, **1·ChB**, **1·XB** and **1·HB**, the replacement of the triazole-phenyl substituents with perfluorinated analogues elicits dramatic halide anion affinity enhancements for the sigma-hole based, ChB and XB receptors, demonstrating an impressive 32-fold and 8-fold increase in chloride anion affinity respectively. Importantly, systematic variation of the electron-withdrawing potency of aryl-triazole and Te-bound-aryl groups facilitated the construction of Hammett plots, establishing linear free energy relationships between Σσ and determined anion K_a values. Determined ρ values of the **2·ChB^R** and **3·ChB^R** receptor series ($\rho(Cl^-)$ = 0.91 and 2.20 respectively), demonstrate that the tellurium ChB donor is highly sensitive to modulation of local electronic environments, which is most pronounced for those directly appended to the Te centre. In the case of **3·ChB^R** the observed trend $\rho(Cl^-) > \rho(Br^-) > \rho(I^-)$ translates to a remarkable enhancement of selectivity for the lighter halides as the electron-withdrawing ability of the Te-bonded aryl group increases. Most importantly, these results serve to highlight that through considered selection of electron-withdrawing aryl substituents covalently linked to the ChB donor atom, exquisite control over both anion binding potency and selectivity is achievable, providing an exciting opportunity for tuning non-covalent interactions in anion receptor design.

2.5 References

[1] Yu. T. Struchkov, T. L. Khotsyanova, *Bull. Acad. Sci. USSR Div. Chem. Sci.* **1960**, *9*, 771–779.

[2] F. Bailly, P. Barthen, H.-J. Frohn, M. Köckerling, *Z. Für Anorg. Allg. Chem.* **2000**, *626*, 2419–2427.

[3] B. Zhou, F. P. Gabbaï, *Chem. Sci.* **2020**, *11*, 7495–7500.

[4] S. Benz, J. Mareda, C. Besnard, N. Sakai, S. Matile, *Chem. Sci.* **2017**, *8*, 8164–8169.

[5] T. Bunchuay, A. Docker, A. J. Martinez-Martinez, P. D. Beer, *Angew. Chem. Int. Ed.* **2019**, *58*, 13823–13827.

[6] J. M. McGrath, M. D. Pluth, *J. Org. Chem.* **2014**, *79*, 11797–11801.

[7] B. W. Tresca, R. J. Hansen, C. V. Chau, B. P. Hay, L. N. Zakharov, M. M. Haley, D. W. Johnson, *J. Am. Chem. Soc.* **2015**, *137*, 14959–14967.

[8] H. A. Fargher, N. Lau, H. C. Richardson, P. H.-Y. Cheong, M. M. Haley, M. D. Pluth, D. W. Johnson, *J. Am. Chem. Soc.* **2020**, *142*, 8243–8251.

[9] L. P. Hammett, *J. Am. Chem. Soc.* **1937**, *59*, 96–103.

[10] L.-M. Jin, X. Xu, H. Lu, X. Cui, L. Wojtas, X. P. Zhang, *Angew. Chem. Int. Ed.* **2013**, *52*, 5309–5313.

[11] A. S. Dillon, B. L. Flynn, *Org. Lett.* **2020**, *22*, 2987–2990.

[12] F. V. Singh, H. A. Stefani, *Tetrahedron Lett.* **2010**, *51*, 863–867.

[13] D. Bornemann, C. R. Pitts, C. J. Ziegler, E. Pietrasiak, N. Trapp, S. Kueng, N. Santschi, A. Togni, *Angew. Chem. Int. Ed.* **2019**, *58*, 12604–12608.

[14] J. Liu, M. Qiu, X. Zhou, *Synth. Commun.* **1990**, *20*, 2759–2767.

Chapter 3 Highly Cooperative Chalcogen Bonding Heteroditopic Receptors for KCl Selective Recognition

3.1 Introduction

Despite the enormous progress that has been made in heteroditopic receptor design over the last few decades, the means by which anion binding is achieved in these host systems is overwhelmingly dominated by HB donor recognition sites. However, the recent emergence of anion recognition strategies employing sigma-hole based interactions such as XB and ChB has notably signified these non-covalent interactions to engender unique advantages associated with their use.[1–12] Indeed, rarer still is the incorporation of sigma-hole donors to serve as the anion recognition component in heteroditopic receptor systems.[13–17] A very recent report last year, 2020, by Beer *et al*. describes a direct comparison of unprecedented ChB ion-pair recognition with XB and HB using a series of structurally homologous heteroditopic receptors incorporating XB, ChB and HB donor groups covalently linked with benzo-15-crown-5 ether motifs (Figure 3.1). Extensive ^{1}H NMR titration experiments in 10 % d_6-DMSO/$CDCl_3$ solution with TBABr and TBAI, in the presence and absence of sodium cations determined $K_a(Na^+)/K_a$(None) cooperativity factors (α) for each receptor. All receptors demonstrated positive cooperativity (α>1), consistent with favourable electrostatic interactions. Most importantly, the XB and ChB analogues displayed remarkable 100- and 200-fold enhancements in halide affinity respectively, while only modest cooperativity factors were observed with the HB receptor. DFT calculations suggested the substantial α values for the ChB and XB receptors are attributable to a sodium cation-crown ether bound induced polarisation of the respective receptor's XB and ChB donor atoms, providing a unique mechanism of cooperativity.

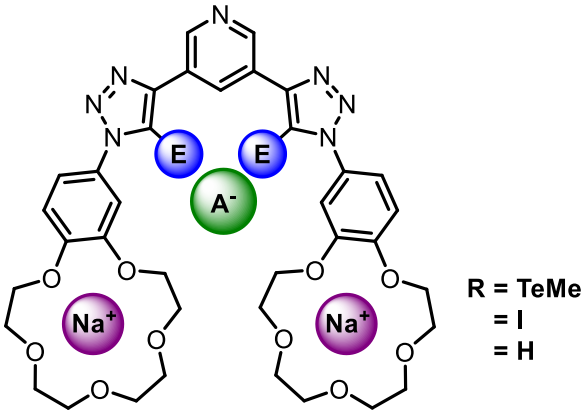


Figure 3.1 Beer's heteroditopic XB ion-pair receptor.

3.2 Chapter aims

Motivated by the results obtained in chapter 2, wherein the potency and selectivity of ChB donors could be effectively tuned by modulating the electron withdrawing properties of the aryl substituents directly appended to the tellurium centre, this chapter aims to exploit a non-covalent means of ChB donor polarisation facilitated by a cation binding event (Figure 3.2) to construct highly cooperative ChB ion-pair receptors. This chapter's objectives are to fulfil the following goals:

- Construct and investigate the ion-pair recognition properties of benzo-15-crown-5 appended acyclic bis-triazole ChB heteroditopic receptor systems

Through extensive ^{1}H NMR titration experiments, it is demonstrated that a co-bound potassium alkali metal cation is capable of polarising the ChB donor motif to facilitate the chloride anion selective recognition. Moreover, solid-liquid and liquid extraction experiments reveal the ChB heteroditopic receptor possesses considerable selectivity for the KCl ion-pair which is exploited for the purposes of facilitated KCl liquid membrane transport.

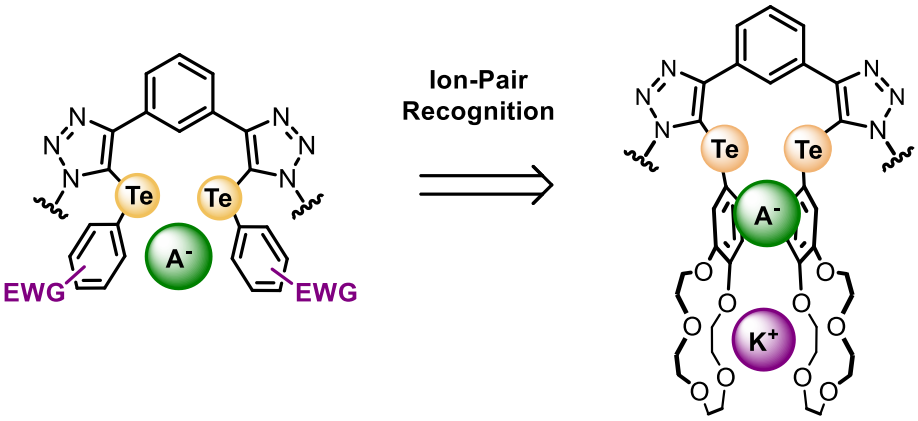


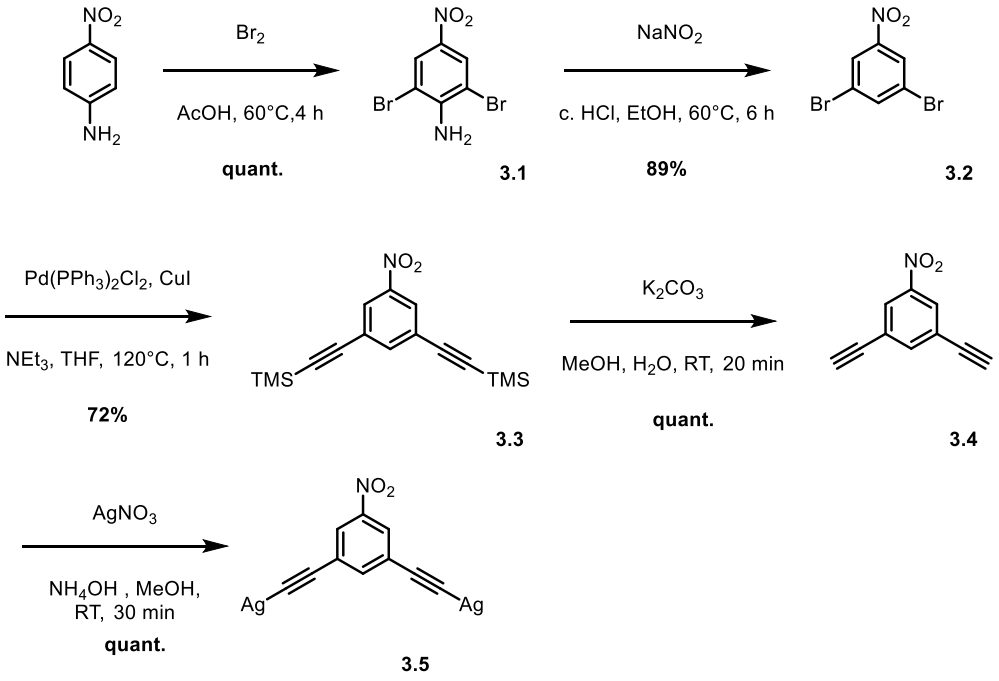
Figure 3.2 Receptor design strategy.

3.3 ChB heteroditopic receptor synthesis

The receptor design consists of a benzo-15-crown-5 appended bis-tellurotriazole motif integrated into an electron-withdrawing neutral nitrobenzene scaffold appended with various phenyl and electron-withdrawing perfluoroaryl substituents constructed via a CuAAC methodology.

3.3.1 The synthesis of 3,5-bis-alkyne nitrobenzene precursors

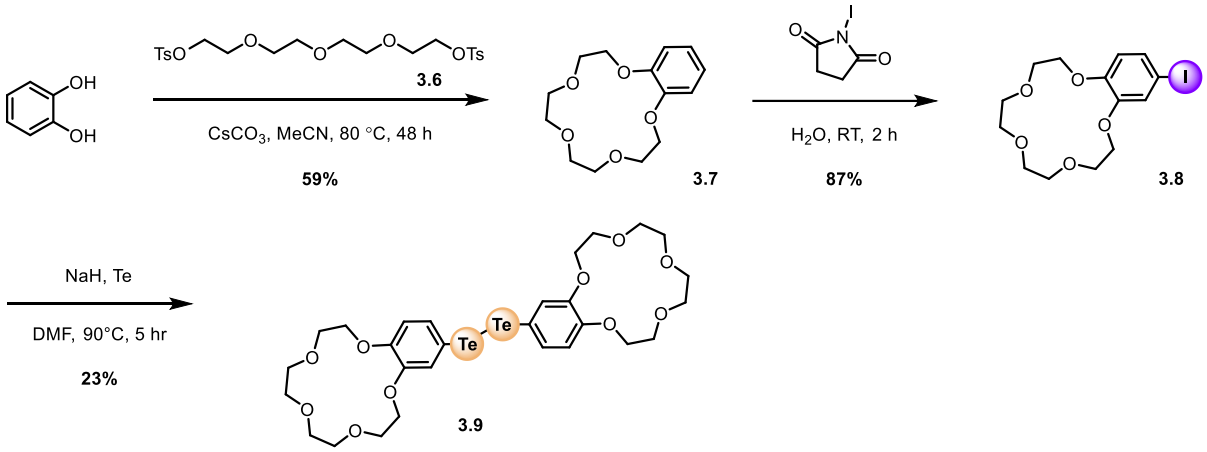
The synthesis of the requisite bis-alkyne nitrobenzene precursors is summarised in Scheme 3.1. Commercially available para-nitroaniline was subjected to a bromination reaction with elemental bromine in glacial acetic acid at elevated temperature for four hours to give **3.1** in quantitative yield requiring no further purification. The compound **3.1** was subjected to a diazotisation procedure with sodium nitrite in $HCl_{(aq)}$:EtOH mixtures, where prolonged heating of the formed diazonium salt liberated N_2 to afford **3.2** in 89% yield.[18] A Sonogashira reaction between dibromide **3.2** and TMS-acetylene under microwave irradiation afforded bis-TMS-protected alkyne **3.3** in good yield (72%) after chromatographic purification. K_2CO_3 mediated deprotection in MeOH:H_2O mixtures afforded the bis-proto-alkyne **3.4** in quantitative yield. Reaction of **3.4** with freshly ground $AgNO_3$ with catalytic $NH_4OH_{(aq)}$ in a MeOH solution facilitated the isolation of bis-Ag(I)-acetylide **3.5**.



Scheme 3.1 Synthesis of the 3,5-dinitro-benzene diethynyl precursors.

3.3.2 Benzo-15-crown-5 ditelluride synthesis

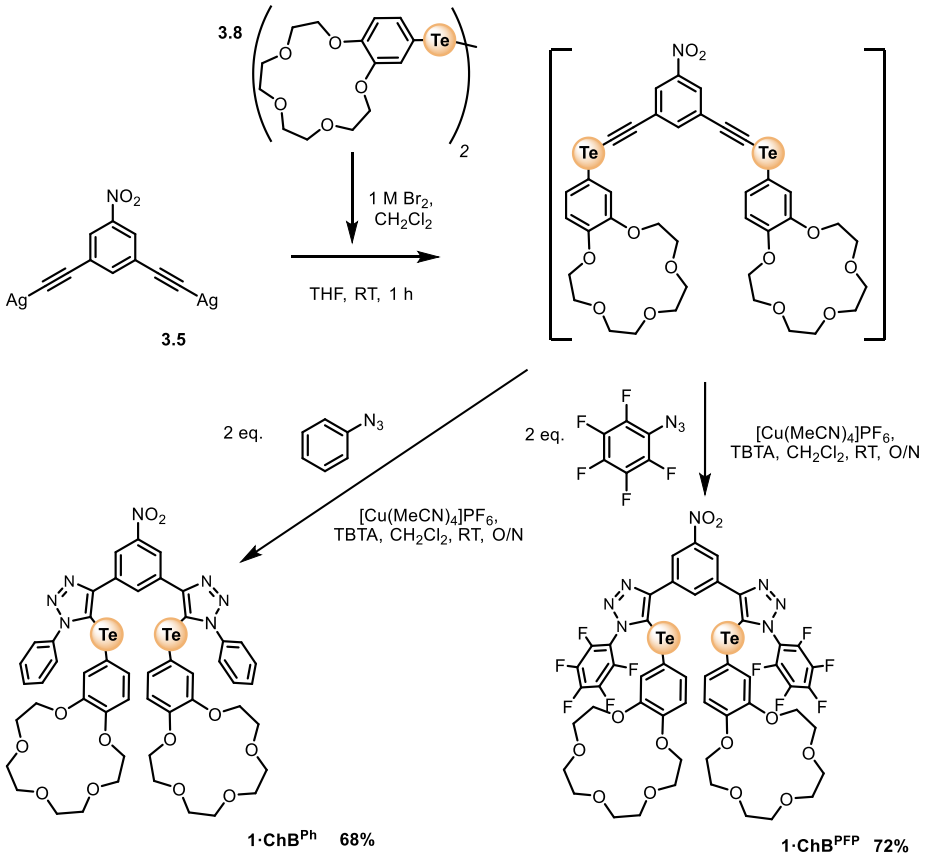
Benzo-15-crown-5 (B15C5) was synthesised according to a modified literature procedure (Scheme 3.2), via the slow addition of ditosylate, **3.6**, to a refluxing acetonitrile solution of catechol in the presence of caesium carbonate, which also acts as a template for macrocyclization. Following purification by recrystallisation from boiling hexanes, benzo-15-crown-5 **3.7** was isolated in 59% yield. B15C5 was subjected to an iodination reaction via treatment with *N*-iodosuccinimide in H_2O to give **3.8** in 87% yield. A nucleophilic substitution reaction between freshly generated NaTeH and iodo-arene **3.8**, followed by an aerial oxidation procedure afforded the requisite ditelluride **3.9** as a dark red solid after column chromatography in a yield of 23%.



Scheme 3.2 Synthesis of B15C5 ditelluride precursor.

3.3.3 CuAAC synthesis of the ChB receptors

The ChB heteroditopic receptors were synthesised according to a copper (I) catalysed alkyne-azide cycloaddition CuAAC methodology (Scheme 3.3). The synthesis of the bis-telluoro-B15C5 alkyne was achieved by careful treatment of the ditelluride with a 1 M Br_2 CH_2Cl_2 solution, forming the corresponding organotellurium bromide and reacted immediately with a THF suspension of bis-silver-acetylide **3.5**. The generated target bis-alkyne was used in a subsequent CuAAC reaction with two equivalents of the appropriate aryl azide in the presence of catalytic TBTA in anhydrous dichloromethane. Subsequent aqueous work-up procedures of the reaction mixtures and purification of the crude materials by column chromatography gave the novel heteroditopic receptors **1·ChB^{PFP}** and **1·ChB^{Ph}** in 72% and 68% yields respectively, characterised by ^{1}H, ^{13}C, ^{125}Te NMR and high resolution ESI-MS (Figure 3.3).



Scheme 3.3 CuAAC synthesis of **1·ChB^{PFP}** and **1·ChB^{Ph}**.

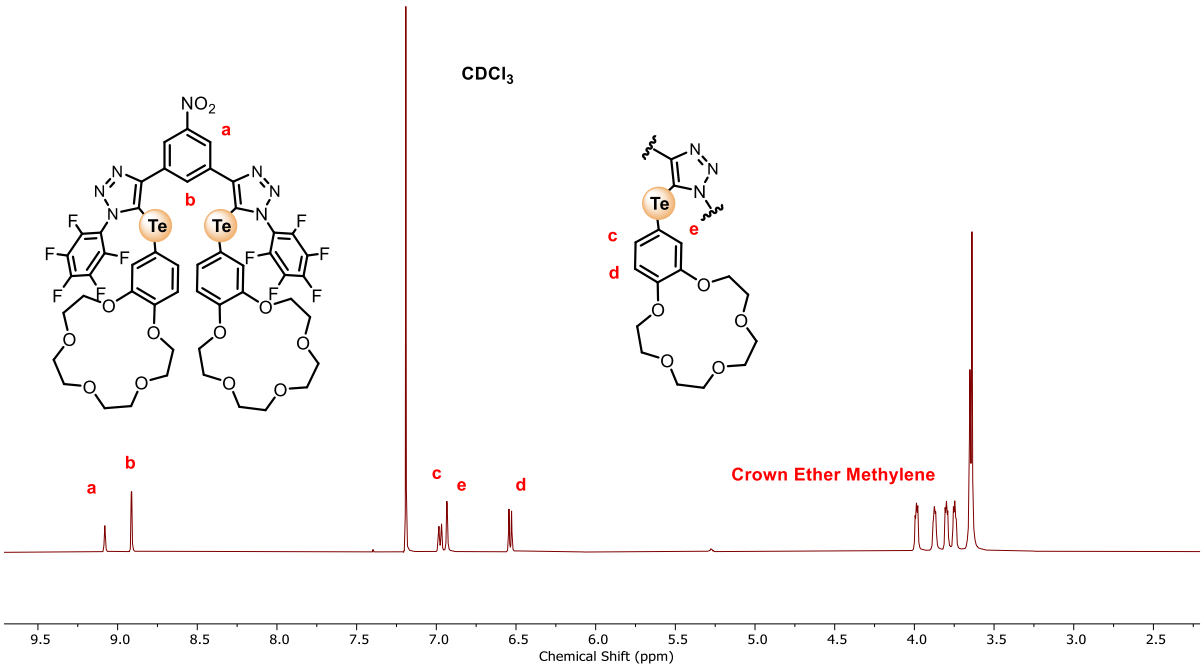


Figure 3.3 Chemical structure and ^{1}H NMR spectrum of **1·ChB^{PFP}** ($CDCl_3$, 500 MHz, 298 K).

3.4 Anion and ion-pair recognition studies

Initially, the potassium cation recognition properties of **1·ChB^{PFP}**, were investigated via ^{1}H NMR titration studies conducted by adding increasing equivalents of K^+ as the highly organic solvent soluble tetrakis 3,5-bis(trifluoromethyl)phenyl borate ($BAr^{F}_{4}^{-}$) salt to a 1:1 CD_3CN:$CDCl_3$ (v/v) solution of the receptor (Figure 3.4a and 3.4b). The addition of the potassium cation induced significant perturbations and broadening of the resonances associated with the crown ether methylene and aromatic regions. Indeed, broadening of signals c,d,e,f and h was so pronounced as to result in their disappearance until 1 equivalent of $KBAr^{F}_{4}$ had been administered, after which no further changes were observed, suggesting the formation of a highly stable 1:1 stoichiometric host:guest complex. Inspection of the ^{1}H NMR spectrum revealed several key features concerning the nature of the potassium complex, specifically the dramatic ca.1 and 0.5 ppm upfield shifts of CH_2 signals f and h of the polyether chain, indicating strong shielding effects from a proximal aromatic ring current, supporting the formation of an intramolecular co-facial K^+ bis-B15C5 sandwich complex.[19–21] Importantly, $KBAr^{F}_{4}$ titration experiments with **1·ChB^{Ph}** elicited similar spectroscopic changes indicating the formation of an analogous K^+-induced sandwich complex.

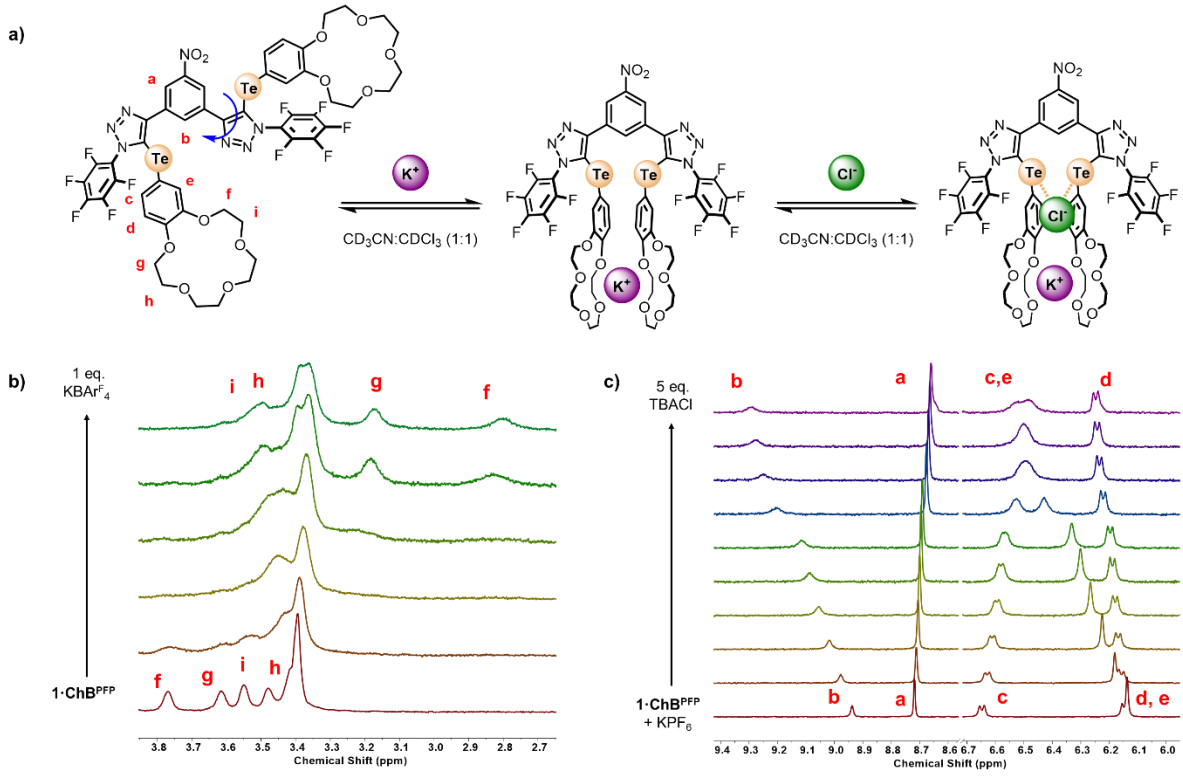


Figure 3.4 a) Potassium Chloride **1·ChB^{PFP}** binding equilibria. ^{1}H NMR titration experiments of b) $KBAr^{F}_{4}$ and **1·ChB^{PFP}** c) TBACl and **1·ChB^{PFP}** in the presence of one equivalent of KPF_6 (CD_3CN:$CDCl_3$ 1:1 (v/v), 500 MHz, 298 K).

The ion-pair binding capabilities of **1·ChB^{PFP}** and **1·ChB^{Ph}** were investigated by ^{1}H NMR anion titration experiments conducted in the presence of equimolar KPF_6 (Figure 3.4c). The addition of a variety of anions, added as their tetrabutylammonium salts, induced progressive downfield shifts of the internal aromatic signal b. Importantly, it was observed that the diagnostic features of the ^{1}H NMR spectrum associated with the K^+B15C5 sandwich complex, persisted upon anion addition, indicating concomitant ion-pair binding. Bindfit[22] analysis of the anion induced chemical shift perturbations (Figure 3.5) determined 1:1 stoichiometric host:guest association constants for the range of halide and oxoanions investigated (Table 3.1). Notably, anion titration experiments conducted in the absence of a K^+ source, elicited no chemical shift perturbations indicating a co-bound potassium cation is crucial in switching on the anion recognition capabilities of both receptors.

Table 3.1 Anion association constants for **1·ChB^{PFP}** and **1·ChB^{Ph}** anion receptor systems in CD_3CN:$CDCl_3$ 1:1 (v/v).

Anion	Anion association constant (K_a) in the presence of equimolar KPF_6 /M^{-1} [a]	
	1·ChB^{PFP}	**1·ChB^{Ph}**
Cl^-	1198	128
Br^-	1080	190
I^-	709	93
AcO^-	1020	-[d]
NO_3^-	276	-[d]
NO_2^-	458	-[d]
OCN^-	486	-[d]
ClO_4^-	-[c]	-[d]

[a] Determined from Bindfit analysis of the titration isotherm by monitoring of the chemical shift perturbation of internal aromatic signal b, error < 5%. [b] Anions added their tetrabutylammonium salts. [c] No binding. [d] Not performed.

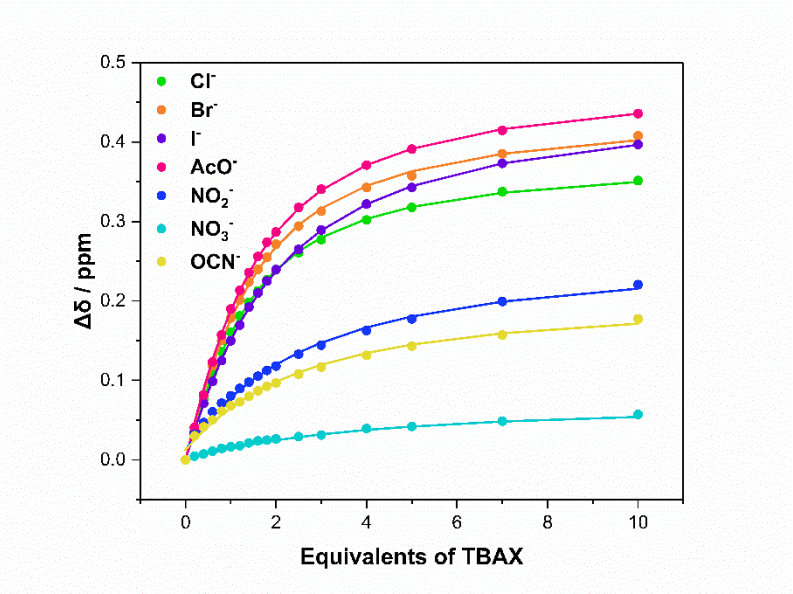


Figure 3.5 Anion binding isotherms for **1·ChB^{PFP}** where circles represent experimental data and solid lines represent fitted data.

For **1·ChB^{PFP}** inspection of Table 3.1 reveals strong halide and acetate binding, in particular chloride which is bound with an association constant (K_a) of 1,198 M^{-1}. The observed chloride selectivity, over anions such as acetate, is particularly impressive considering affinity trends in simple acyclic hydrogen bond donor anion receptor systems are typically dictated by inherent anion basicity.

In comparison to **1·ChB^{PFP}**, the halide association constant values for **1·ChB^{Ph}** are considerably diminished, by nearly an order of magnitude. Saliently, these results indicate that the major determinant in thermodynamic stability of the ion-pair complex is attributable to the formation of potent ChB-anion interactions and not a consequence of non-specific electrostatic interactions between the cationic K^+ receptor complex and the anion guest species.

Attention was subsequently directed towards investigating the role of the nature of the alkali metal cation in the formation of the sandwich complexation and its effects on the MX ion-pair recognition properties of the receptor. Inspection of the ^{1}H NMR spectra of **1·ChB^{PFP}** with equimolar potassium, rubidium or caesium perchlorate evidenced similar diagnostic chemical shift changes of the crown ether methylene region associated with the formation of the potassium cation induced sandwich complex (Figure 3.6). Whilst analogous complexation experiments conducted with $LiClO_4$ or $NaClO_4$ indicated very minor resonance perturbations and for the sodium complex a narrowing of crown-ether signals. These observations suggest that the larger alkali metal cations, K^+, Rb^+ and Cs^+, are all capable of forming an intramolecular sandwich complex between the pendant B15C5 units, while the smaller Li^+ and Na^+ cations are bound by a single B15C5 unit in fast exchange on the NMR timescale.

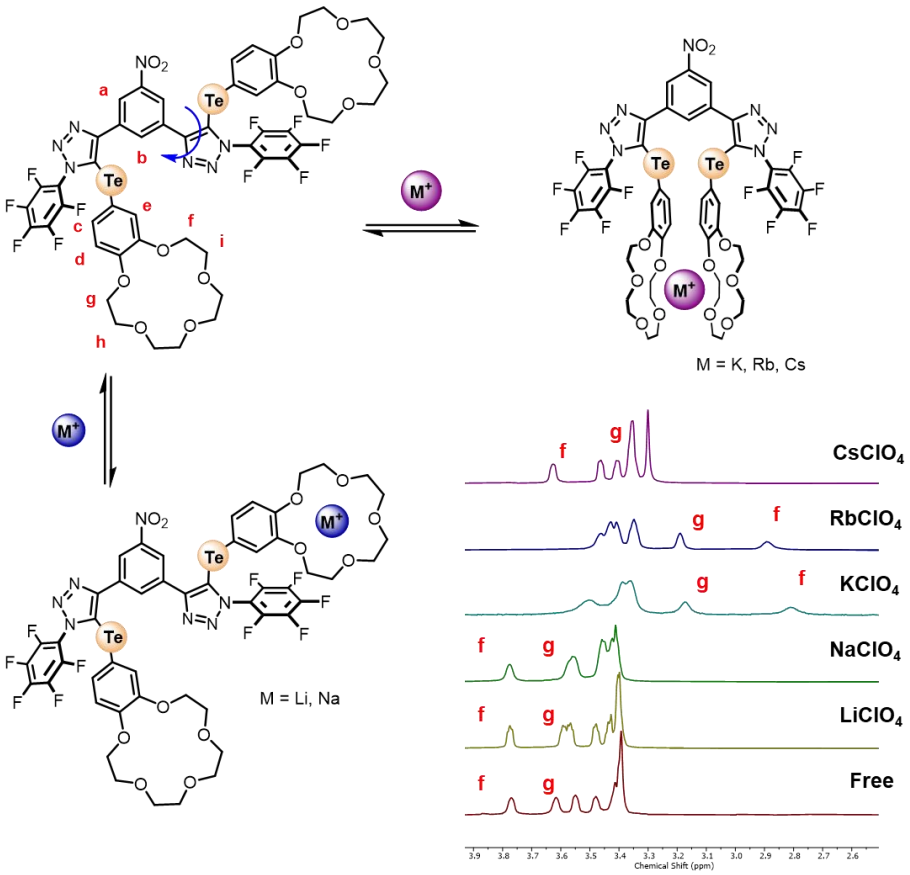


Figure 3.6 Alkali metal cation **1·ChB^{PFP}** binding equilibria. (Inset) ^{1}H NMR complexation experiments of **1·ChB^{PFP}** in the presence of one equivalent of $MClO_4$ (CD_3CN:$CDCl_3$ 1:1 (v/v), 500 MHz, 298 K).

When complexed with potassium, rubidium or caesium, increasing chloride equivalents induced similar significant downfield perturbations of the receptor's internal aromatic signal b. In contrast, in the presence of one equivalent of lithium or sodium perchlorate, no downfield shift of aromatic signal b was observed upon the addition of chloride. Furthermore, the minor crown-ether based perturbations observed, interpreted as a result of Li^+ or Na^+ complexation were lost upon the addition of one equivalent of chloride, indicating salt-recombination by direct electrostatic interactions between the chloride anion and either the lithium or sodium cation. Bindfit analysis[22] of the resultant binding isotherms revealed that the chloride affinity increases with decreasing group 1 metal cation radius, $K^+ > Rb^+ > Cs^+$ (Table 3.2).

Table 3.2 Chloride association constants for **1·ChB^{PFP}** in the presence of 1 eq. $MClO_4$ in $CD_3CN:CDCl_3$, 1:1, (v/v).

	Chloride association constant (K_a) of **1·ChB^{PFP}** in the presence of equimolar $MClO_4$ /M^{-1} [a]				
	$LiClO_4$	$NaClO_4$	$KClO_4$	$RbClO_4$	$CsClO_4$
Cl^-	-[c]	-[c]	1,100	742	605

3.5 Solid-liquid extraction studies

The potassium halide salt extraction properties of **1·ChB^{PFP}** were investigated under both solid-liquid extraction (SLE) and liquid-liquid extraction conditions. In a typical SLE experiment a colourless $CDCl_3$ solution of **1·ChB^{PFP}** was layered over microcrystalline samples of a potassium halide salt (Figure 3.7a), the mixture was stirred for 10 minutes and the ^{1}H NMR spectrum recorded. In the case of KCl, recording the ^{1}H NMR spectrum of the resultant yellow post-extraction solution revealed new sets of resonances in addition to those corresponding to the free receptor (Figure 3.7b). Control experiments reveal that the complexation of KCl is slow on the NMR timescale and the new signals correspond to that of the **1·ChB^{PFP}**·KCl complex. Notably, the internal aromatic signal, proximal to the ChB donor cleft, of the potassium chloride complex, b_{KCl}, exhbits a dramatic 0.6 ppm downfield shift relative to the same proton, b, of the free receptor. Integration of these respective signals enabled calculation of the KCl loading percentage, which was determined to be 47%.

In the case of SLE experiments performed with KBr and KI, only proton signals corresponding to the newly formed potassium halide complex were evidenced (Figure 3.7c), indicating near quantitative extraction (Table 3.2). Inspection of the internal aromatic signal of the free receptor and the respective KX (X= Cl, Br, I) complexes, reveals the chemical shift follows the trend; $b_{KCl} > b_{KBr} > b_{KI} > b$. Despite its low abundance, ^{125}Te nuclei are highly senstive to solution phase non-covalent interaction formation and provided a further opportunity to investigate **1·ChB^{PFP}** ion-pair binding behaviour.[23] Comparison of the pre- and post extraction ^{125}Te NMR spectra (Figure 3.7d), revealed, in a simlar fashion to ^{1}H NMR, the appearance of a new tellurium signal, shifted 45 ppm upfield relative to free **1·ChB^{PFP}**.

The improved extraction performance of **1·ChB^{PFP}** for KBr and KI relative to KCl, may be rationalised by the subtle interplay between the receptor's ion-pair affinity and the KX lattice enthalpy (ΔH_L) which reflects the thermodynamic penalty associated with salt dissolution. To confirm that the anion complexation process aids extraction performance, and thereby confirm the role of cooperative ion-pair binding in the extraction process, similar SLE experiments were undertaken with $KClO_4$. If the ability of **1·ChB^{PFP}** to extract potassium salts into a $CDCl_3$ phase was soley a function of the receptor's cation affinity, it is anticipated that the extraction efficiency would increase as the KX salt's ΔH_L value decreases. However, the determined extraction percentage of 35% for $KClO_4$, indicates that despite a ΔH_L value 100 kJ mol^{-1} smaller than that of KCl (Table 3.3), extraction efficiency is diminished by more than 10%. This mutual interdependece of the nature of the cation and anion on extraction behaviour motivated further SLE extraction experiments with a variety of alkali metal salts, summarised in Table 3.3. Importantly, the role of cooperativity is further evidenced by the quantitative extraction of RbI and CsI, while no extraction is observed for the corresponding perchlorate salts (Figure 3.8). Most notably, in comparison to the other group 1 metal chlorides, **1·ChB^{PFP}** exhibits

remarkable selectivity for KCl, demonstrating either no extraction as in the case of lithium, sodium, caesium or only 10% receptor loading for rubidium (Figure 3.9).

Futhermore, in order to further confirm the role of ChB-anion interactions in the solid-liquid extraction process, analogous experiments were conducted with **1·ChB^{Ph}** and potassium halides. Inspection of the post-extraction SLE ^{1}H NMR spectra for **1·ChB^{Ph}** demonstrates the receptor is capable of quantitative extraction of KBr and KI into $CDCl_3$. However, crucially no significant chemical shift perturbations were observed after a $CDCl_3$ solution was exposed to solid KCl, highlighting the importance of favourable ChB-anion interactions in extraction performance.

The observed colour change upon KCl extraction also stimulated UV-Vis studies of the extraction process (Figure 3.7e), in which it was shown through various control experiments that the naked-eye response is reliant on concomitant K^+ and Cl^- binding, while no measurable response was exhibited in the sole presence of either a potassium or chloride source with a non-coordinating counterion.

Table 3.3 Determined solid-liquid extraction values.

Salt	Solid Liquid Extraction (SLE) Percentages / %		Lattice Enthalpy ΔH_L / kJmol^{-1}
	1·ChB^{PFP}	**1·ChB^{Ph}**	
LiCl	-[c]	-[c]	-864
NaCl	-[c]	-[c]	-790
KCl	47	<5	-720
RbCl	10	-[c]	-695
CsCl	-[c]	-[c]	-670
KBr	>95	>95	-691
KI	>95	>95	-650
$KClO_4$	35	-[c]	-595
CsI	>95	-[c]	-613
$CsClO_4$	-[c]	-[c]	-550
RbI	>95	-[c]	-632
$RbClO_4$	-[c]	-[c]	-576
KNO_3	50	-[c]	-694

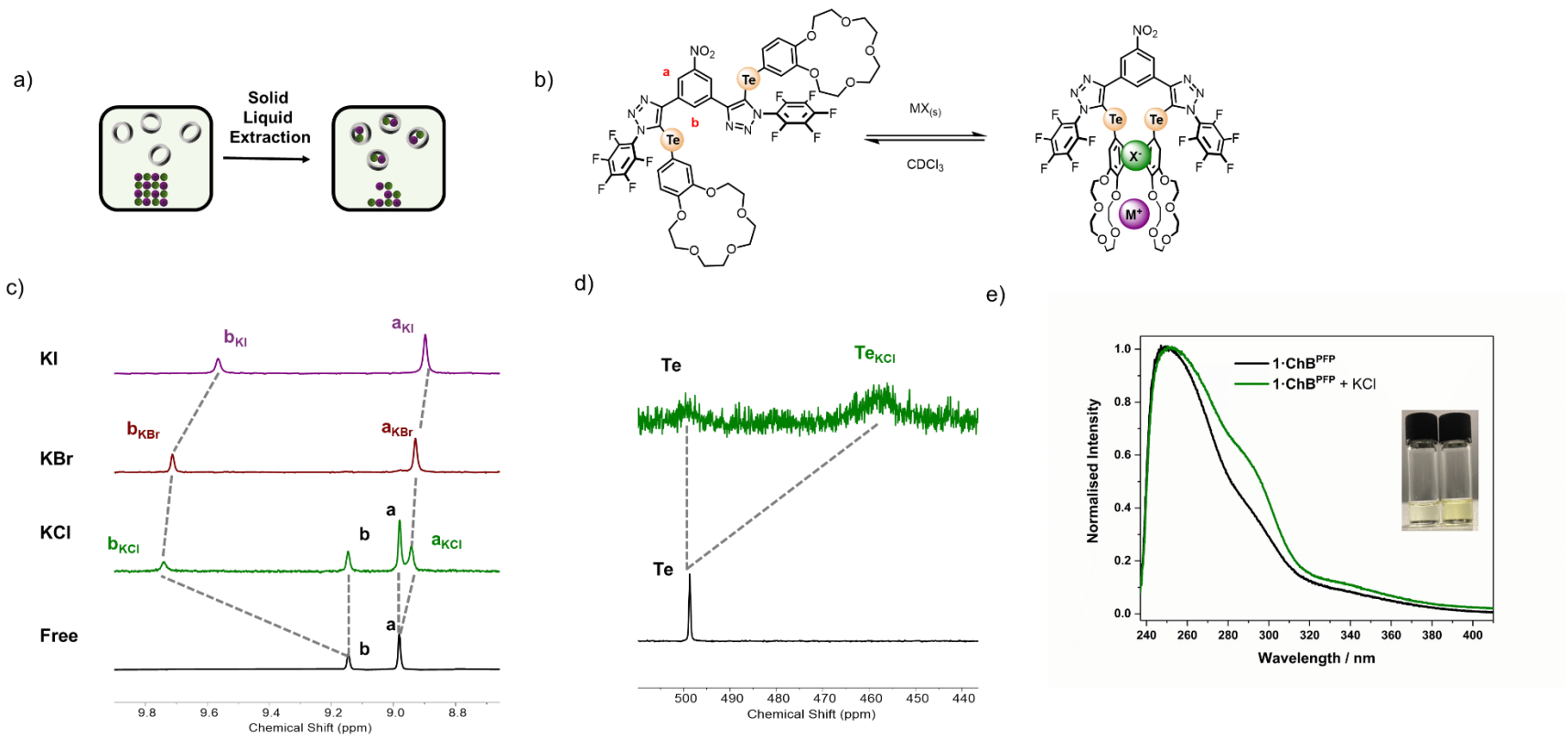


Figure 3.7 a) Cartoon representation of SLE b) postulated MX binding equilibrium of **1·ChB^{PFP}** c) Post extraction ^{1}H NMR spectra of **1·ChB^{PFP}** with KCl, KBr and KI ($CDCl_3$, 500 MHz, 298 K) d) Post extraction ^{125}Te NMR spectrum of **1·ChB^{PFP}** with KCl ($CDCl_3$ 126 MHz, 298 K) e) UV Vis spectrum of **1·ChB^{PFP}** and its KCl complex ($CDCl_3$, 10^{-3} M).

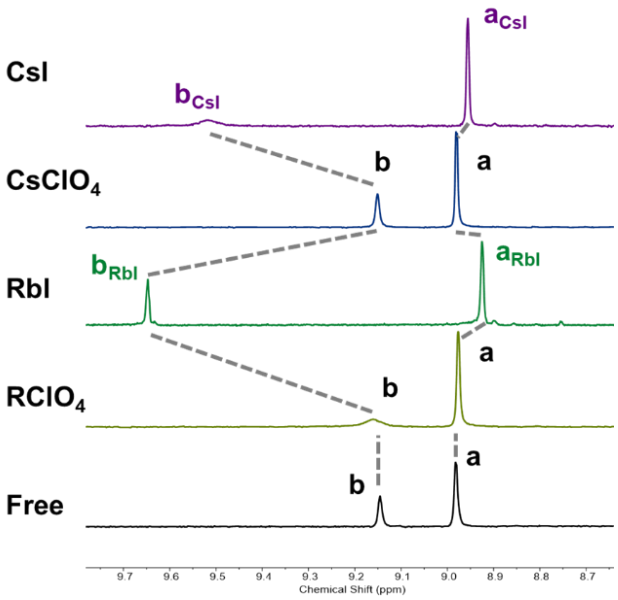


Figure 3.8 Truncated stacked post-extraction ^{1}H NMR spectra of **1·ChB^{PFP}** with rubidium and caesium iodides and perchlorates. ($CDCl_3$, 500 MHz, 298 K).

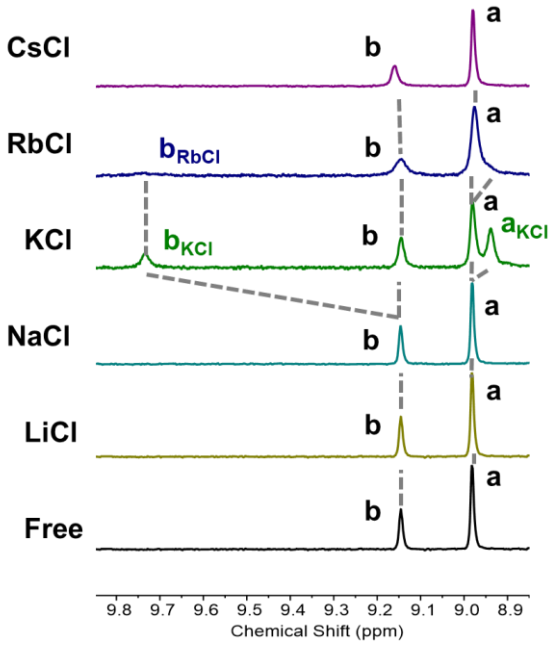


Figure 3.9 Truncated stacked post-extraction ^{1}H NMR spectra of **1·ChB^{PFP}** with alkali metal chlorides ($CDCl_3$, 500 MHz, 298 K).

3.6 Solid state structure determination

Further insight into the ion-pair binding behaviour of **1·ChB^{PFP}** was provided by solid state characterisation of the ion-pair receptor complexes. Crystals suitable for x-ray structural determination of the KCl, KBr, KI, RbI, CsI and NH_4Br complexes were obtained by slow diffusion of pentane into the respective SLE solutions. Concordant with ^{1}H NMR titration studies, potassium, rubidium and caesium cations are complexed via a co-facial B15C5 sandwich complex and the halide counteranions exhibit bifurcated chalcogen bond formation (Figure 3.10 and 3.11). Inspection of the summarised tellurium-halide interaction distances in Table 3.4 reveal short contacts, considerably shorter than the sum of their van der Waals radii.

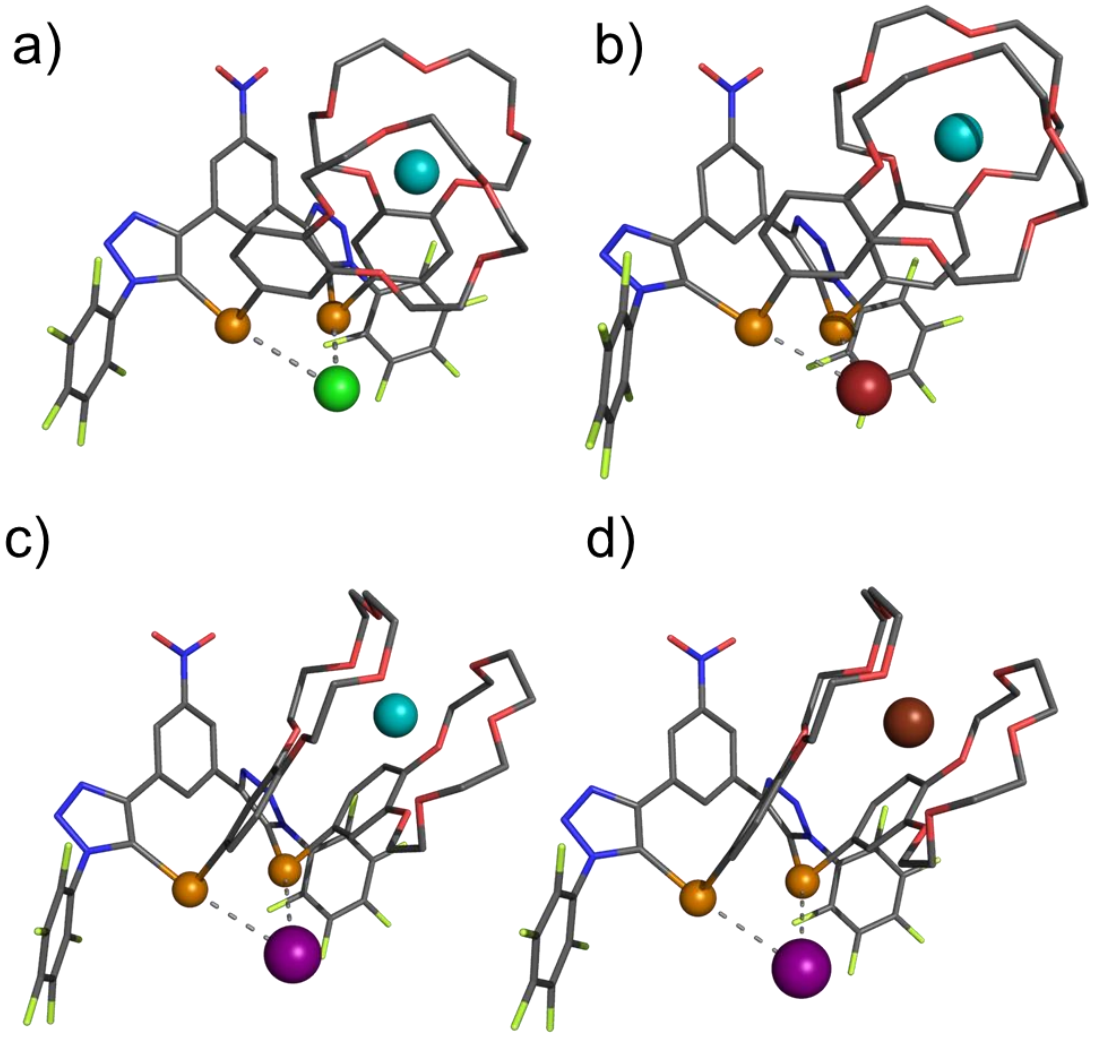


Figure 3.10 Solid state structures of the MX **1·ChB^{PFP}** complexes; a) KCl b) KBr c) KI d) RbI.

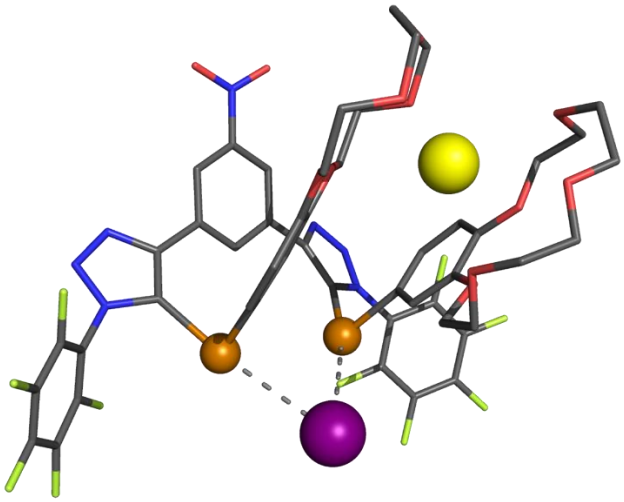


Figure 3.11 Solid state structure of the CsI **1·ChB^{PFP}** complex.

Table 3.4 Selected interaction distances obtained from crystal structure determination of **1·ChB^{PFP}** ion-pair complexes.

Salt	Interatomic distances (Te···X-/Å)	%vdW
KCl	3.099, 3.520	81, 92
KBr	3.245, 3.579	83, 92
KI	3.460, 3.889	86, 96
RbI	3.467, 3.873	86, 96
CsI	3.478, 3.904	86, 97

3.7 Liquid-liquid extraction studies

Efforts were also directed towards asessing the suitability of **1·ChB^{PFP}** of extracting KCl under LLE conditions (Figure 3.12a). A $CDCl_3$ (4.0 mM) solution of **1·ChB^{PFP}** was exposed to KCl in D_2O at concentrations in the range of 1 – 4 M. Similar to the SLE experiment, post-extraction spectra show two sets of readily distinguishable signals corresponding to free and KCl complexed receptor (Figure 3.12b), meaning relative LLE extraction percentages could be calculated by a similar method of ^{1}H NMR signal integration. The percentage of salt complexed receptor was determined to be 32%, 43%, 64% and 69% when exposed to 1 M, 2 M, 3 M and 4 M aqueous KCl solutions respectively (Figure 3.12c). Crucially, the selectivity for KCl over the other alkali metal chlorides is even more prounounced under LLE conditions as no extraction is evidenced by ^{1}H NMR for LiCl, NaCl, RbCl or CsCl.

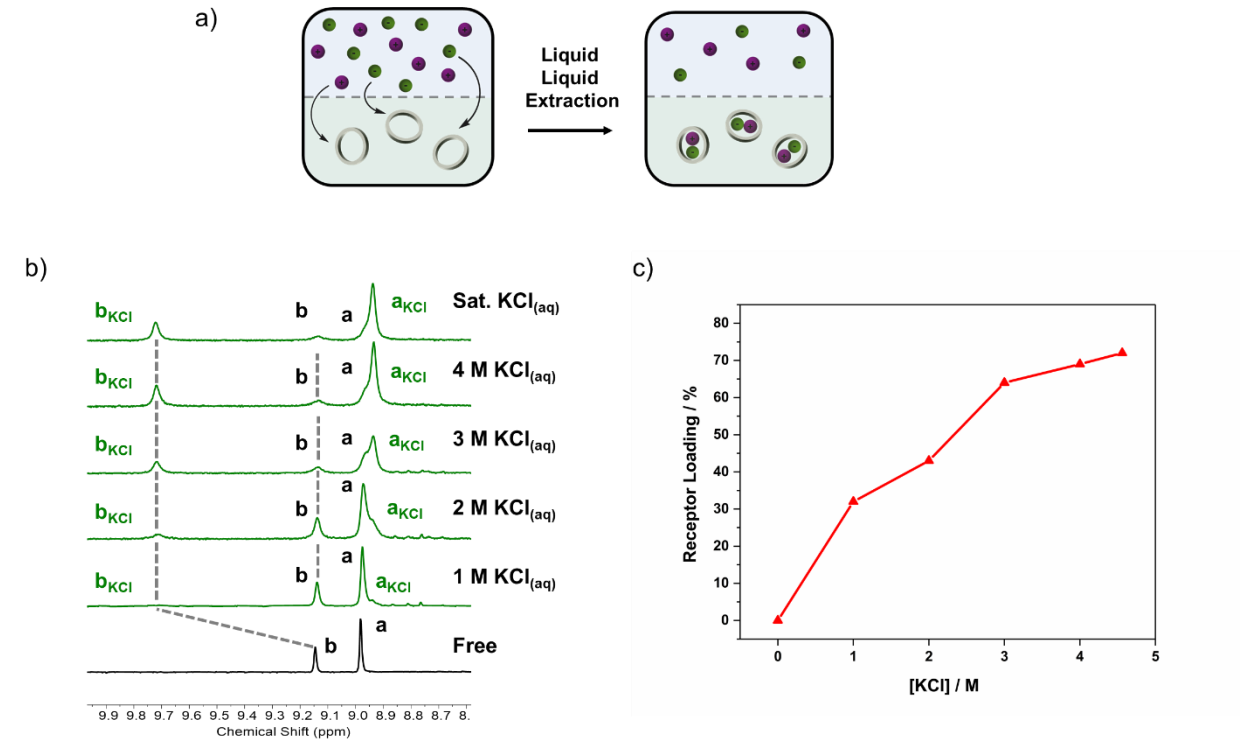


Figure 3.12 a) Cartoon representation of LLE extraction procedure. b) Stacked truncated post LLE ^{1}H NMR spectra conducted various KCl source phase concentrations ($CDCl_3$, 500 MHz, 298 K). c) Plot showing the effect of increasing KCl source phase concentration on receptor loading.

3.8 Liquid membrane transport studies

Motivated by the excellent KCl selectivity exhibited by **1·ChB^{PFP}**, preliminary liquid membrane U-tube transport experiments were undertaken. Specifically, a 4 M KCl aqueous source phase and a deionised water receiving phase are separated by a stirred 8 mM solution of **1·ChB^{PFP}** in $CHCl_3$ (Figure 3.13a and 3.13b). The chloride concentration in the receiving phase was monitored via an ion-selective electrode (Figure 3.13c), which revealed a steady increase over the course of 35 hours, after which time chloride concentration was determined to be ca. 0.7 M. Co-transport of potassium was confirmed by flame test analysis of the receiving phase. Crucially, the co-dependence of K^+ and Cl^- transport was demonstrated by using a NaCl source phase, where importantly after 35 hours no evidence of chloride was detected in the receiving phase.

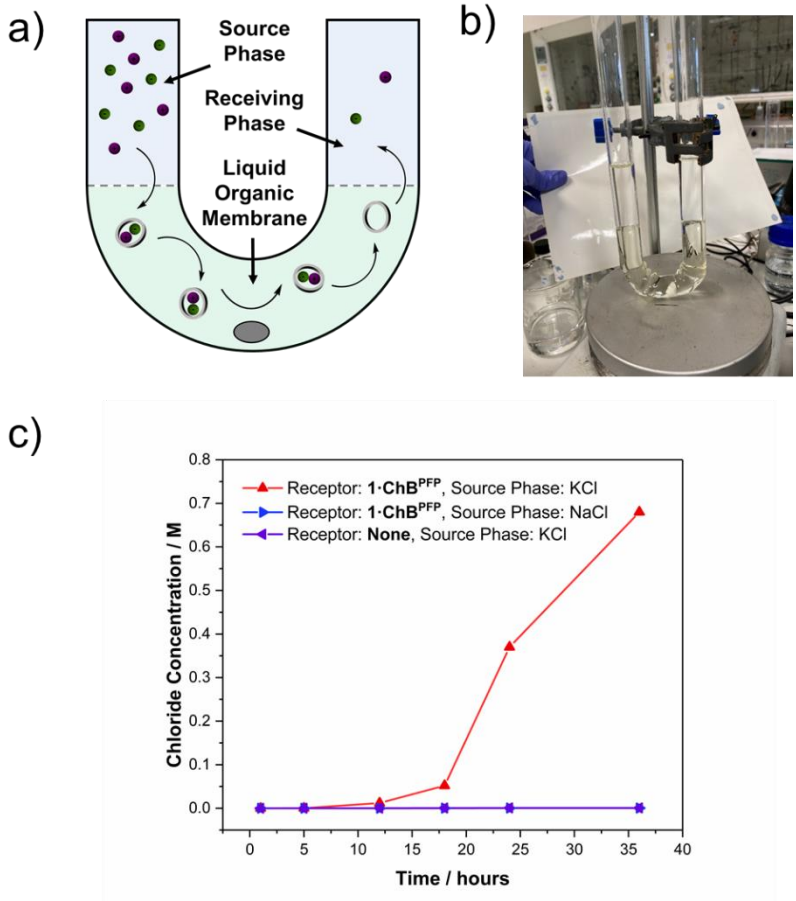


Figure 3.13 a) Cartoon representation of liquid membrane transport procedure. b) Photograph of experimental set-up c) Plot showing the changing receiver phase KCl concentration.

3.9 Conclusions

In conclusion, two ChB heteroditopic receptors containing tellurium chalcogen bond donors functionalised with B15C5 moieties integrated into a bis 3,5-bis-triazole nitrobenzene scaffold, appended with either phenyl, **1·ChB^{Ph}**, or electron-withdrawing perfluoroaryl, **1·ChB^{PFP}**, substituents have been synthesised and their alkali metal cation-halide anion ion-pair recognition properties investigated via extensive ^{1}H NMR titration studies. These reveal K^+, Rb^+ and Cs^+ are capable of forming an intramolecular co-facial M^+ bis-B15C5 sandwich complex, while the smaller Li^+ and Na^+ are bound by a single crown ether. Quantitative ion-pair titration experiments demonstrate that **1·ChB^{PFP}** exhibits selectivity KCl, in which it is postulated that the relatively smaller radius of the bis-B15C5 complexed potassium cation is reponsible for inducing the largest switch on in ChB donor potency for halide anion recognition, relative to the other larger sized alkali metal cations capable of forming the intramolecular bis-B15C5 sandwich complex.

The observed KCl selectivity of **1·ChB^{PFP}** stimulated investigations into using the receptor as a selective extractant material under solid-liquid and liquid-liquid extraction conditions, in which considerable selectivity over all other alkali metal chloride salts was observed. The receptor's ability to facilitate transmembrane KCl transport in liquid membrane studies is particularly notable in the context of developing synthetic ionophores which require high selectivity for KCl over NaCl for biomedical applications. More importantly, these results serve to highlight that through a non-covalent augmentation of the Te based ChB donors, **1·ChB^{PFP}** is capable of producing potent and highly selective cooperative heteroditopic ChB ion-pair receptors.

3.10 References

[1] A. Brown, P. D. Beer, *Chem. Commun.* **2016**, *52*, 8645–8658.

[2] A. Docker, P. D. Beer, in *Halog. Bond. Solut.*, John Wiley & Sons, Ltd, **2021**, pp. 83–120.

[3] J. Y. C. Lim, P. D. Beer, *Chem* **2018**, *4*, 731–783.

[4] T. Bunchuay, A. Docker, A. J. Martinez-Martinez, P. D. Beer, *Angew. Chem. Int. Ed.* **2019**, *58*, 13823–13827.

[5] A. Docker, X. Shang, D. Yuan, H. Kuhn, Z. Zhang, J. J. Davis, P. D. Beer, M. J. Langton, *Angew. Chem. Int. Ed.* **n.d.**, *n/a*, DOI 10.1002/anie.202107748.

[6] J. Y. C. Lim, M. J. Cunningham, J. J. Davis, P. D. Beer, *Chem. Commun.* **2015**, *51*, 14640–14643.

[7] M. J. Langton, S. W. Robinson, I. Marques, V. Félix, P. D. Beer, *Nat. Chem.* **2014**, *6*, 1039–1043.

[8] G. Berger, P. Frangville, F. Meyer, *Chem. Commun.* **2020**, *56*, 4970–4981.

[9] A. Borissov, I. Marques, J. Y. C. Lim, V. Félix, M. D. Smith, P. D. Beer, *J. Am. Chem. Soc.* **2019**, *141*, 4119–4129.

[10] L. E. Bickerton, A. Docker, A. J. Sterling, H. Kuhn, F. Duarte, P. D. Beer, M. J. Langton, *Chem. – Eur. J.* DOI 10.1002/chem.202101681.

[11] S. C. Patrick, R. Hein, A. Docker, P. D. Beer, J. J. Davis, *Chem. – Eur. J.* **2021**, *27*, 10201–10209.

[12] A. Docker, C. H. Guthrie, H. Kuhn, P. D. Beer, *Angew. Chem. Int. Ed.* **2021**, *60*, 21973–21978.

[13] A. Docker, T. Bunchuay, M. Ahrens, A. J. Martinez-Martinez, P. D. Beer, *Chem. – Eur. J.* **2021**, *27*, 7837–7841.

[14] Y. C. Tse, A. Docker, Z. Zhang, P. D. Beer, *Chem. Commun.* **2021**, *57*, 4950–4953.

[15] A. Mele, P. Metrangolo, H. Neukirch, T. Pilati, G. Resnati, *J. Am. Chem. Soc.* **2005**, *127*, 14972–14973.

[16] R. Tepper, B. Schulze, P. Bellstedt, J. Heidler, H. Görls, M. Jäger, U. S. Schubert, *Chem. Commun.* **2017**, *53*, 2260–2263.

[17] A. Brown, K. M. Mennie, O. Mason, N. G. White, P. D. Beer, *Dalton Trans.* **2017**, *46*, 13376–13385.

[18] S. J. Garden, JoséC. Torres, A. A. Ferreira, R. B. Silva, A. C. Pinto, *Tetrahedron Lett.* **1997**, *38*, 1501–1504.

[19] L. A. Lapkina, A. A. Sinelshchikova, K. P. Birin, V. E. Larchenko, M. S. Grigoriev, A. Yu. Tsivadze, Y. G. Gorbunova, *Inorg. Chem.* **2021**, *60*, 1948–1956.

[20] A. G. Martynov, M. A. Polovkova, G. S. Berezhnoy, A. A. Sinelshchikova, F. M. Dolgushin, K. P. Birin, G. A. Kirakosyan, Y. G. Gorbunova, A. Yu. Tsivadze, *Inorg. Chem.* **2020**, *59*, 9424–9433.

[21] S. P. Gromov, A. I. Vedernikov, N. A. Lobova, L. G. Kuz'mina, S. S. Basok, Y. A. Strelenko, M. V. Alfimov, J. A. K. Howard, *New J. Chem.* **2011**, *35*, 724–737.

[22] "BindFit v0.5 | Supramolecular," can be found under http://app.supramolecular.org/bindfit/.

[23] H. Zhao, F. P. Gabbaï, *Nat. Chem.* **2010**, *2*, 984–990.

Chapter 4 Halogen Bonding Tetraphenylethene Anion Receptors

4.1 Introduction

A common characteristic of organic luminescent materials is their concentration dependent photophysical properties. Traditional chromophores are typically extended planar aromatic systems, which are strongly emissive in dilute solutions, but exhibit a considerable attenuation in luminogenic properties with increasing concentration. This effect, referred to as aggregation-caused quenching (ACQ),[1–3] is generally attributable to excimer or exciplex formation which serves to favour non-radiative decay pathways of excited states.

This effect was considered an inherent property of fluorescent materials, however Tang's seminal report in 2001 detailed that the emissive properties of a pentaphenylsilole derivative could in effect be switched on by hydrophobically driven aggregation with increasing water fractions in THF:H_2O solvent mixtures (Figure 4.1a).[4] Extensive experimental and theoretical studies followed and revealed the origin of this unusual fluorescence behaviour upon aggregation was, in addition to other factors, attributable to a loss of intramolecular rotational freedom which normally provides non-radiative decay pathways of the excited state. Indeed, the discovery of this behaviour stimulated intense interest in the search for other aggregation-induced emission (AIE) molecules. Recent years have seen an ever-increasing library of AIE luminogenic (AIEgens) materials developed including annulenylidene, anthraquinodimethane and tetraphenylethylene derivatives[5] which upon aggregation exhibit restricted degrees of molecular freedom either rotational, vibrational or combinations of both (Figure 4.1b-d).

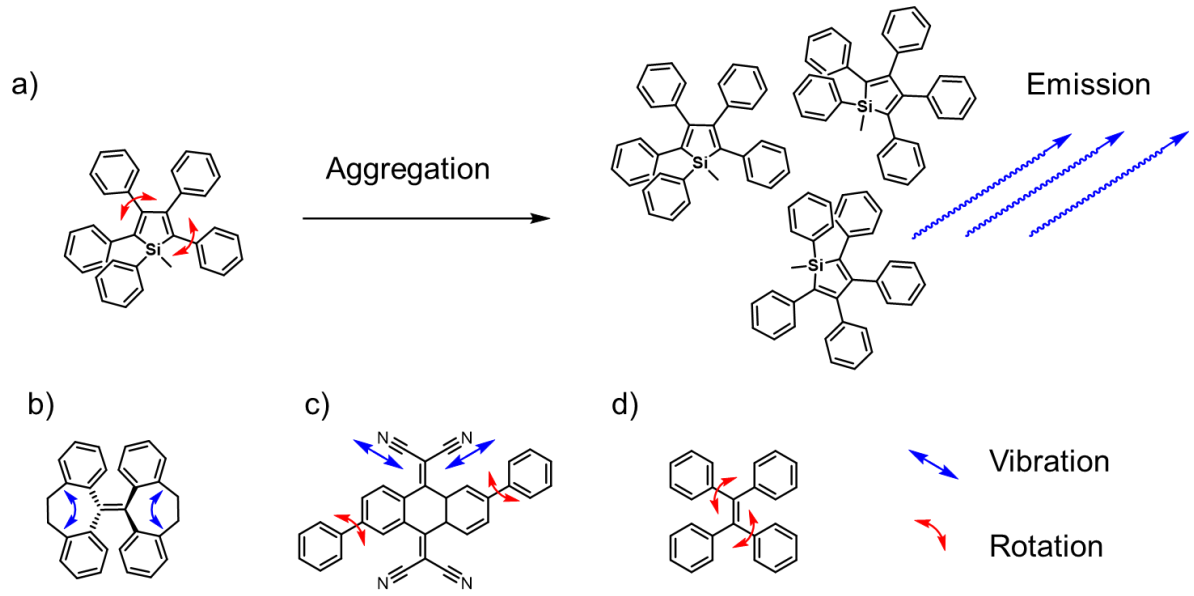


Figure 4.1 Archetypal AIEgens and their principal degrees of freedom restricted upon aggregation a) pentaphenylsilole b) tetrahydro-5,5'-bidibenzo[a,d][7]annulenylidene c) tetracyano-9,10-anthraquinodimethane d) tetraphenylethene.

In particular, tetraphenylethene (TPE) derivatives have come to the fore as synthetically accessible, modular, multivalent scaffolds for AIEgens in the construction of bio-imaging probes,[6,7] optoelectronic devices[8] and responsive materials.[9–12] TPE derivatives have also received significant interest in the development of chemical sensors which possess luminescent responsive behaviour in the presence of anions.[13–17] For example, a 2016 report exploited a triisopropylsilyl protected phenol group of a pyridinium TPE derivative which was capable of undergoing a F^- promoted desilylation reaction in aqueous media. The neutral product exhibited much poorer aqueous solubility relative to the charged starting material, inducing aggregation and therefore an enhancement of emission intensity (Figure 4.2a).[18] A later report by Li et al. similarly exploits changes in solubility of TPE derivatives in which a dipinacol borane substituted TPE system exhibited moderate aqueous solubility and was therefore highly emissive in aqueous organic H_2O:THF (99:1, v/v) solvent mixtures (Figure 4.2b).[19] However, upon treatment with hypochlorite the oxidative cleavage of the borane substituents to form the diquinoid TPE dramatically increased aqueous solubility and served to de-aggregate the TPE core units thereby functioning as a chemosdosimeter for ClO^-. However, the considered employment of TPE-derivatives within supramolecular host systems remains scarce,[20–23] with the overwhelming majority of reported examples reliant on irreversible chemical modification of the AIEgen core to sense the guest species.[24]

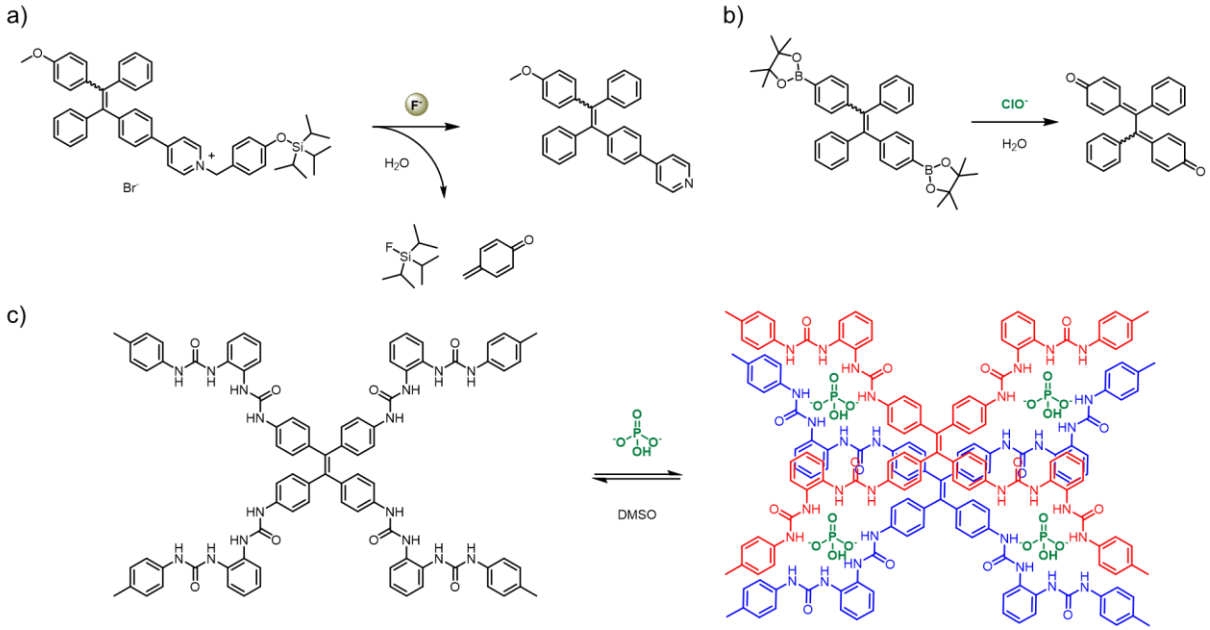


Figure 4.2 a) Zhang's fluoride responsive pyridinium TPE derivative b) Li's hypochlorite responsive dipinacolborane TPE chemodosimeter c) Wu's tetrapodal oligourea phosphate selective receptor.

In a rare example of genuine supramolecular anion-responsive TPE host systems, Wu et al. have reported an oligourea based receptor (Figure 4.2c).[20] The addition of hydrogen phosphate dianion induces the spontaneous assembly of a TPE dimer in which two urea functionalised arms are engaged in phosphate binding. Impressively, the oligourea complementarity for phosphate (PO_4^{3-} and HPO_4^{2-}), in terms of coordination number and geometry, translated into improved dimer structural integrity relative to other oxoanions e.g. CO_3^{2-} and therefore served as a phosphate selective fluorescent sensor.

An additional attractive feature of unsymmetrical doubly substituted TPE derivatives in particular, is their ability to undergo photoinitiated tautomerisation (Figure 4.3). The ability to control the interconversion of *Z*/*E* geometric isomers by light, is conceivably a highly desirable characteristic for anion host design wherein the distance between the substituents can dramatically affect factors such as chelate cooperativity. Whilst in principle behaving in a similar fashion to established photoswitches such as stilbenes or azo-benzenes, the application of disubstituted TPE derivatives for the purposes of stimuli-responsive guest recognition is without precedent. This may primarily be ascribed to the challenges in the stereoselective synthesis of TPE derivatives.[25]

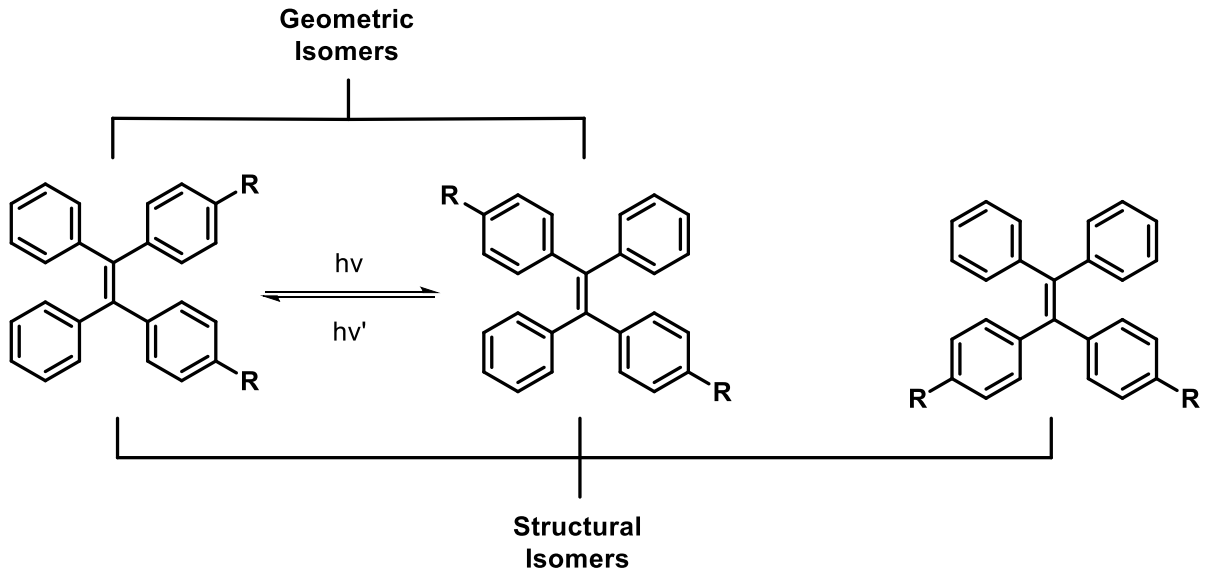


Figure 4.3 Structures and stereochemical relationship between disubstituted TPE derivatives.

4.2 Chapter Aims

This chapter's aims are to fulfil the following goals:

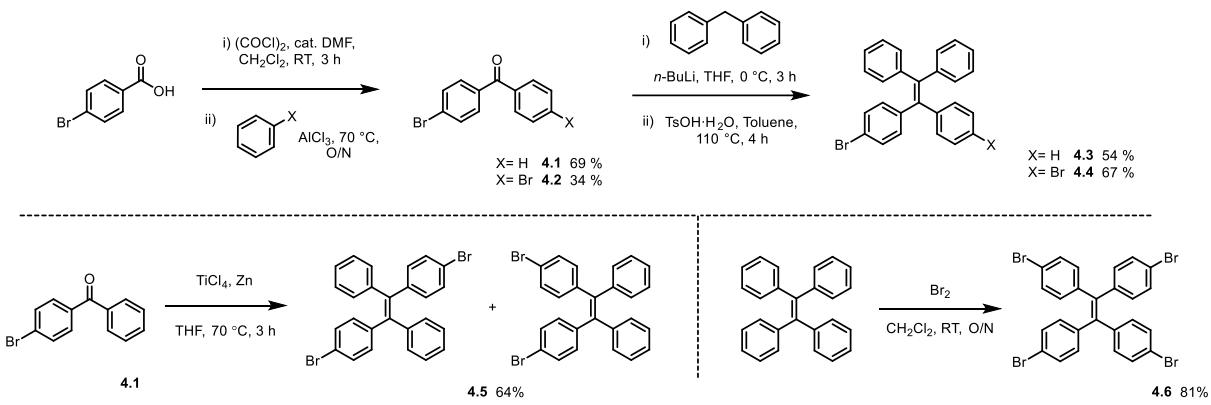
- Investigate the role of multivalency and relative stereochemical orientation of iodo-triazole XB donor motif incorporation on the anion recognition behaviour of a series of TPE derivatives.
- Construct unsymmetrically doubly substituted TPE derivatives for XB photoswitchable anion receptor investigation.

To this end, this chapter investigates a series of novel halogen bonding (XB) TPE-based anion receptors and demonstrates their anion recognition and sensing behaviour is dramatically dependent on the multiplicity and substitution pattern of the XB donor arm appended TPE core. Detailed study of the XB-TPE systems by fluorescence spectroscopy, dynamic light scattering measurements, transmission electron microscopy and X-ray structural analysis reveals the receptors are capable of forming chloride-anion assembled aggregates, concomitant with a dramatic enhancement in emission intensity. Furthermore, the first photo-switchable anion receptor that employs XB interactions for anion binding is demonstrated.

4.3 Halogen Bonding Tetraphenylethylene (TPE) Anion Receptors

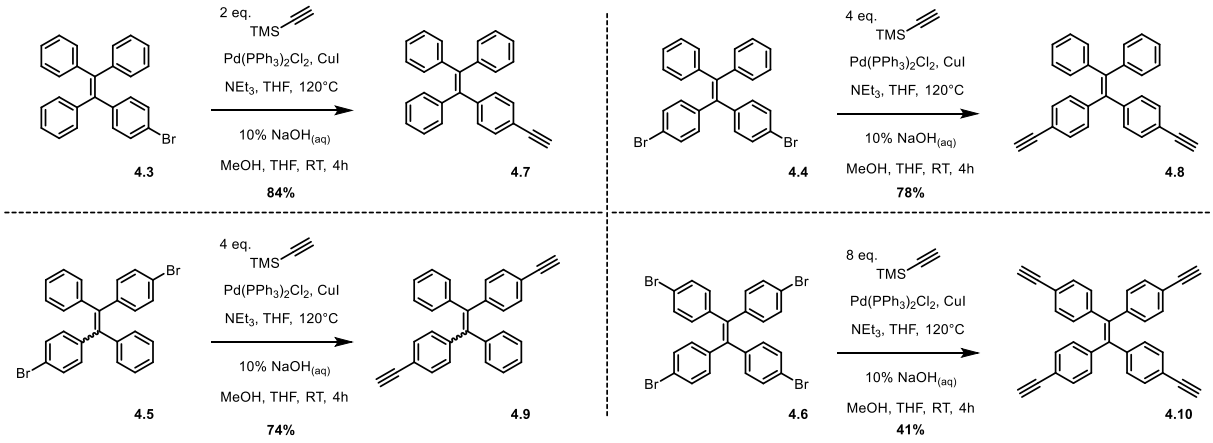
4.3.1 Synthesis of bromo- and alkyne- TPE precursors

The variously brominated TPE precursors were synthesised according to Scheme 4.1. The required diaryl ketones **4.1** and **4.2** were synthesised via a Friedel Crafts acylation reaction between the freshly generated acid chloride of 4-bromobenzoic acid and benzene or bromobenzene, in the presence of stoichiometric $AlCl_3$ to afford the mono-bromo and dibromo benzophenones **4.1** and **4.2** in 69% and 39% yields respectively.[26] The isolated ketones were treated with lithiated diphenylmethane in THF at 0 °C, which after quenching was subjected to a dehydration reaction to afford the parent mono-bromo and dibromo-TPE compounds **4.3** and **4.4** in yields of 54% and 67% respectively.[27] A McMurray coupling reaction conducted on dibromo-dibenzophenone **4.2** mediated by $TiCl_4$ and freshly activated Zn dust gave a mixture of the dibromo-TPE compounds **4.5** as an inseparable mixture of its geometric isomers.[28] Direct treatment of Br_2 with tetraphenylethylene in CH_2Cl_2 gave tetra-bromo TPE **4.6** in 81% yield after successive recrystallisations from hexane.[29]



Scheme 4.1 Synthesis of bromo-TPE derivatives.

The series of bromo-TPE derivatives were subjected to Sonogashira coupling reactions with TMS-protected acetylene and in the presence of $Pd(PPh_3)_2Cl_2$ and CuI, which after purification by column chromatography gave the corresponding protected TPE alkynes (Scheme 4.2).[30] TMS deprotection by $NaOH_{(aq)}$/MeOH/THF gave the series of proto-alkynes in yields in the range of 41-84%.

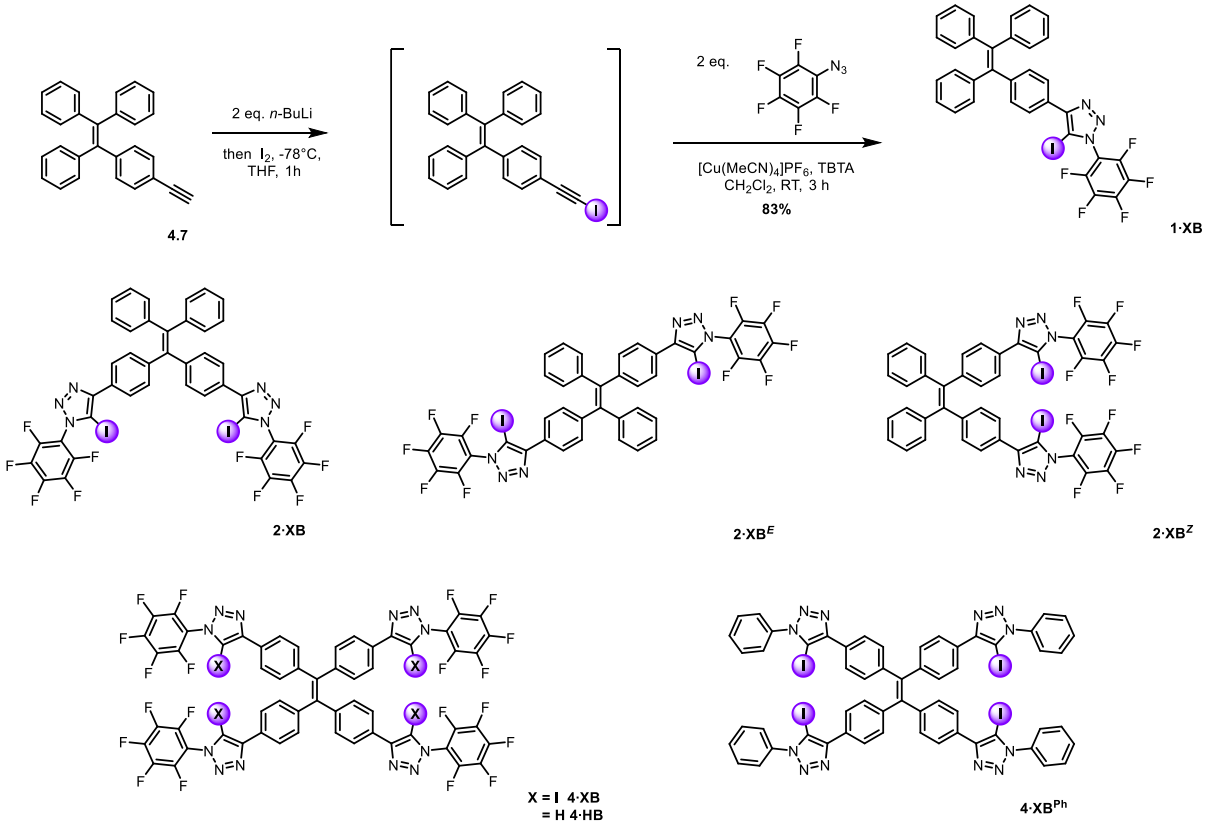


Scheme 4.2 Synthesis of alkyne functionalised TPE derivatives.

4.3.2 Synthesis of mono-, bi-dentate and tetra-dentate TPE precursors

Typically, the synthesis of the target receptors was accomplished by treatment of the proto-alkyne precursors with *n*-BuLi in anhydrous THF solution at −78°C, followed by reaction of the lithiated alkynes with iodine to afford the respective iodo-alkynes (Scheme 4.3). The target receptors were subsequently synthesized *via* a copper(I)-catalysed azide alkyne cycloaddition (CuAAC) reaction between the appropriate iodo-alkyne derivative and perfluorophenyl azide, in the presence of $Cu(MeCN)_4PF_6$ and the Cu(I) stabilising ligand tris(benzyltriazolylmethyl) amine (TBTA), which afforded **1·XB** and **2·XB** in yields of 83% and 57% respectively. In the case of **2·XB*E*** and **2·XB*Z***, a mixture of both isomers was obtained in a combined yield of 58%, because the parent bis-iodoalkyne was used as an inseparable mixture of the geometric isomers. Pleasingly, however, the introduction of the aryl-iodotriazole

motifs enabled resolution of the stereoisomers by silica gel column chromatography, facilitating the isolation of **2·XB^{E}** and **2·XB^{Z}** in 33% and 25% yields respectively. The synthesis of the tetra-substituted receptors **4·XB**, **4·XB^{Ph}** and **4·HB**, were prepared from the corresponding tetra-iodo/proto alkyne TPE derivatives using analogous procedures to those used for **1·XB**.



Scheme 4.3 Synthesis of the XB and HB TPE anion receptors.

4.3.3 Preliminary anion binding studies

With the series of mono- and di-functionalised TPE receptors in hand, their chloride anion recognition behaviour was investigated by ^{1}H NMR anion titration experiments. Aliquots of chloride, as the tetrabutylammonium salt, were added to solutions of the respective receptor in d_8-THF, monitoring the binding induced chemical shift perturbations. In the case of **1·XB**, **2·XB** and **2·XB^{E}**, chloride binding induced a downfield shift of the aryl signal directly adjacent to the iodo-triazole moiety, consistent with XB mediated anion complexation.

Analysis of the generated titration isotherm for **1·XB** using the Bindfit programme generated a 1:1 stoichiometric association constant, $K_{1:1}$(**1·XB**) = 2380 M^{-1}, which represents the chloride binding affinity to a single iodotriazole XB donor. Conceivably, incorporation of additional XB donors to the TPE receptor framework enables higher host-guest complex stoichiometries to be achieved, which in the case of **2·XB**, **2·XB^Z** and **2·XB^E** corresponds to a 1:2 host–anion stoichiometry. The geometeric arrangement of the two XB donors will intuitively influence anion complexation in one of the following ways: i) the XB donors are situated as to bind the anion convergently in a bidentate fashion (chelate cooperativity); ii) the XB donors act independently of one another i.e. are arranged such that the first binding event does not favour or disfavour the second binding event (no cooperativity) and iii) the binding of the first anion inhibits binding of the second (negative cooperativity). In the case of ii), the 1:1 and 1:2 host-guest binding constants, $K_{1:1}$ and $K_{1:2}$ respectively, are related by the expression $K_{1:1} = 4K_{1:2}$, accounting for statistical factors. Analysis of the chloride binding isotherms for the di-iodotriazole derivatives **2·XB**, **2·XB^Z** and **2·XB^E** (Figure 4.4c) revealed that the two XB donors in **2·XB** and **2·XB^E** bind chloride anions in a non-cooperative manner, with an interaction parameter $\alpha = 1$, where $\alpha = 4K_{1:2} / K_{1:1}$ (Table 4.1).

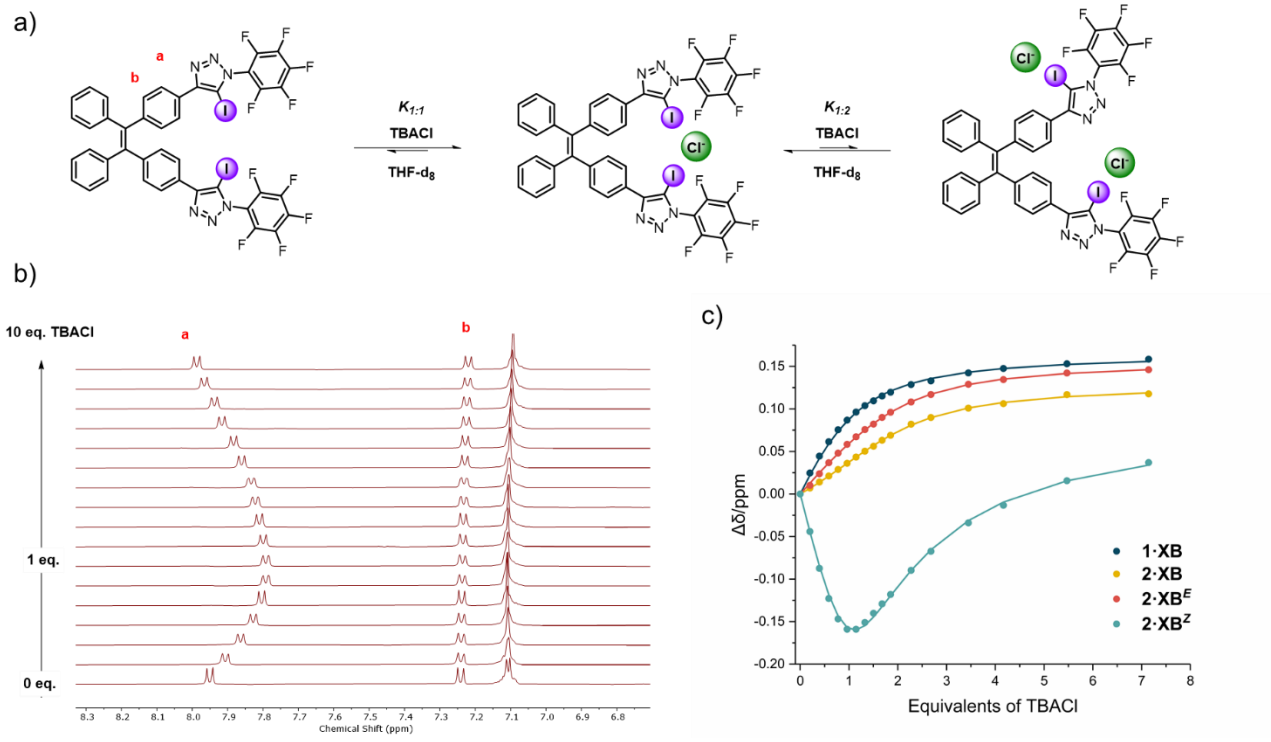


Figure 4.4 a) Postulated anion binding equilibrium for **2·XB^Z**. b) ^{1}H NMR TBACl titration of **2·XB^Z** (THF-d_8, 500 MHz, 298 K) c) Chloride binding isotherms for **1·XB, 2·XB**, **2·XB^E** and **2·XB^Z**, where circles represent experimental data and solid lines represent fitted data.

Table 4.1 Chloride association constants for mono- and di-substituted XB receptors in THF-d_8.

$K_a(Cl^-)$[a]/M^{-1}	**1·XB**[b]	**2·XB**[c,d]	**2·XB*E*** [c,d]	**2·XB*Z*** [c]
$K_{1:1}$	2380	5650[e]	4970	23,200
$K_{1:2}$	n/a	1410[e]	1240	960
α[e]	n/a	1	1	0.17

[a]Chloride added as its tetrabutylammonium salt, errors < 10%. [b] Fitted to a 1:1 binding isotherm. [c] Fitted to a 1:2 host-guest binding isotherm. [d] Binding model assumes $K_{1:1} = 4K_{2:1}$. [e]Interaction parameter $\alpha = 4K_{1:2} / K_{1:1}$, with $\alpha = 1$ indicating no cooperativity, and $\alpha < 1$ indicating negative cooperativity. [e] Perturbation of the equilibrium due to anion-induced aggregation effects not considered in the data fitting.

The Cl^- binding isotherm of **2·XB*Z*** exhibits a starkly contrasting profile, in which addition of up to 1 equivalent of chloride induced an upfield shift in proton *a* (Figure 4.4b), after which an inflection point is observed and subsequent addition of chloride resulted in a downfield shift. This behaviour is consistent with the initial formation of a 1:1 complex, and the formation of a considerably weaker 1:2 complex at higher concentrations of chloride. The reversed direction of chemical shift perturbation is interpreted as a consequence of conformational rearrangement upon transitioning from 1:1 to 1:2 stoichiometry, wherein the pendant XB donors motifs are disposed as to maximize their separation reducing electrostatic repulsion between the two anionic guests. (Figure 4.4a).

Analysis of the 1:1 stoichiometric binding constants for the three di-iodotriazole geometric isomers **2·XB**, **2·XB*E*** and **2·XB*Z*** provided evidence for the presence or absence of bidentate anion binding with chelate cooperativity for each isomer. The determined chloride affinity obtained for the reference mono-dentate compound **1·XB**, $K_{1:1}$(**1·XB**), quantifies the binding of the anion to a single iodotriazole binding site. The 1:1 binding constant for the di-iodotriazole derivatives **2·XB**, **2·XB*E*** and **2·XB*Z*** is given by $2K_{1:1}$(**1·XB**) in the absence of chelate cooperativity and when statistical factors associated with binding of one anion to a ditopic host are considered. Inspection of the values of $K_{1:1}$ for the di-iodotriazole derivatives reveals that, in the case of **2·XB** and **2·XB*E***, the two iodotriazole donors are too far apart to allow for chelation of the anion in a bidentate fashion: $K_{1:1}$(**2·XB**) and $K_{1:1}$(**2·XB*E***) ~ $2K_{1:1}$(**1·XB**). In contrast, in **2·XB^Z** the perfluoroaryl appended XB donors are considerably closer in space, facilitating chloride anion chelation, such that $K_{1:1}$(**2·XB^Z**) ~$10K_{1:1}$(**1·XB**). The considerably diminished $K_{1:2}$(**2·XB^Z**) value relative to $K_{1:2}$(**2·XB**) and $K_{1:2}$(**2·XB^E**) indicates a pronounced negative cooperativity in binding of the second Cl^- anion, reflected in the interaction parameter α = 0.17. Presumably this arises due to the combination of mutual anion-anion electrostatic repulsion and the requirement to break the bidentate XB-chloride interactions.

Subsequent ^{1}H NMR anion titration experiments of **2·XB^Z** with the heavier halides revealed that bromide and iodide produced similar binding isotherms (Figure 4.5) with somewhat attenuated association constants, consistent with anion basicity trends (Table 4.2).

Table 4.2 Halide association constants for **2·XB^Z** in THF-d_8.

K_a[a]/M^{-1}	**Cl$^-$** [b]	**Br$^-$** [b]	**I$^-$** [b]
$K_{1:1}$[e]	23,200	8080	1050
$K_{1:2}$	960	1330	40

[a] Anions added as their tetrabutylammonium salts, errors < 10%. [b] Fitted to a full 1:2 model.

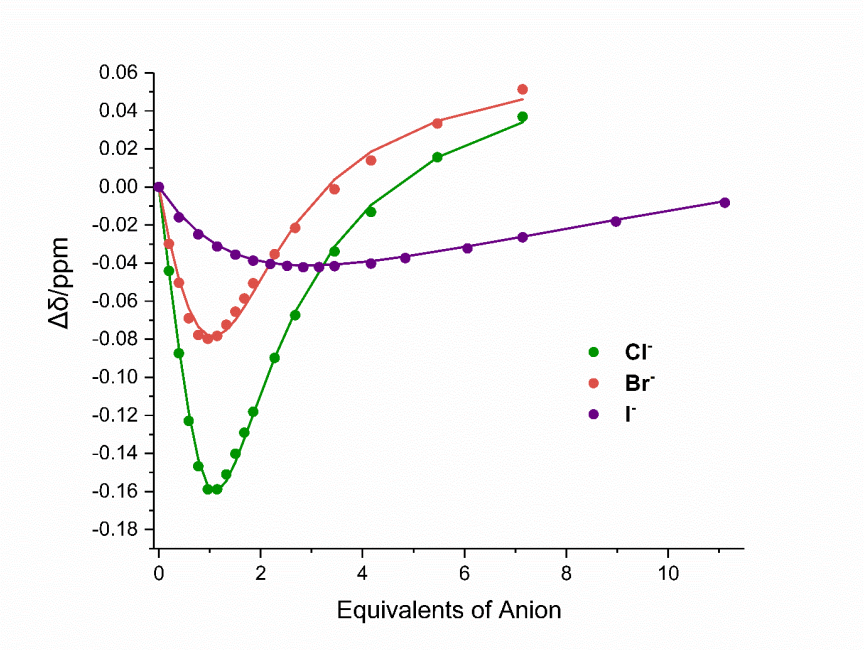


Figure 4.5 Halide binding isotherms for **2·XB^Z**, where circles represent experimental data and solid lines represent fitted data.

^{1}H NMR chloride titration experiments were conducted on **4·XB**, **4·XB^{Ph}** and **4·HB**, to elucidate the role and potency of XB interactions on the anion recognition process. Chloride binding titration experiments with **4·XB** revealed a chemical shift perturbation profile with an inflection point similar to that observed with **2·XB^Z**, in which up to two equivalents of TBACl induced an almost linear upfield perturbation of the aryl proton *a*, indicative of near quantitative formation of a 1:2 receptor:anion complex (Figure 4.6b). Addition of equivalents beyond two equivalents caused a progressive downfield shift, indicating the formation of higher receptor:anion stoichiometries presumably up to 1:4 (Figure 4.6a and 4.6b). The populations of the various receptor:anion complexes are expected to be weighted by association constants of the respective equilibria.

Similar chemical shift perturbations were observed for **4·XB^{Ph}**, while binding to the hydrogen bonding analogue **4·HB** was weak as reflected in the absence of any asymptotic or inflection behaviour (Figure 4.7). Furthermore, the preference for the lighter halides observed for **2·XB^{Z}** appears to also translate to **4·XB**, upon visual analysis of the bromide and iodide binding isotherms (Figure 4.6c).

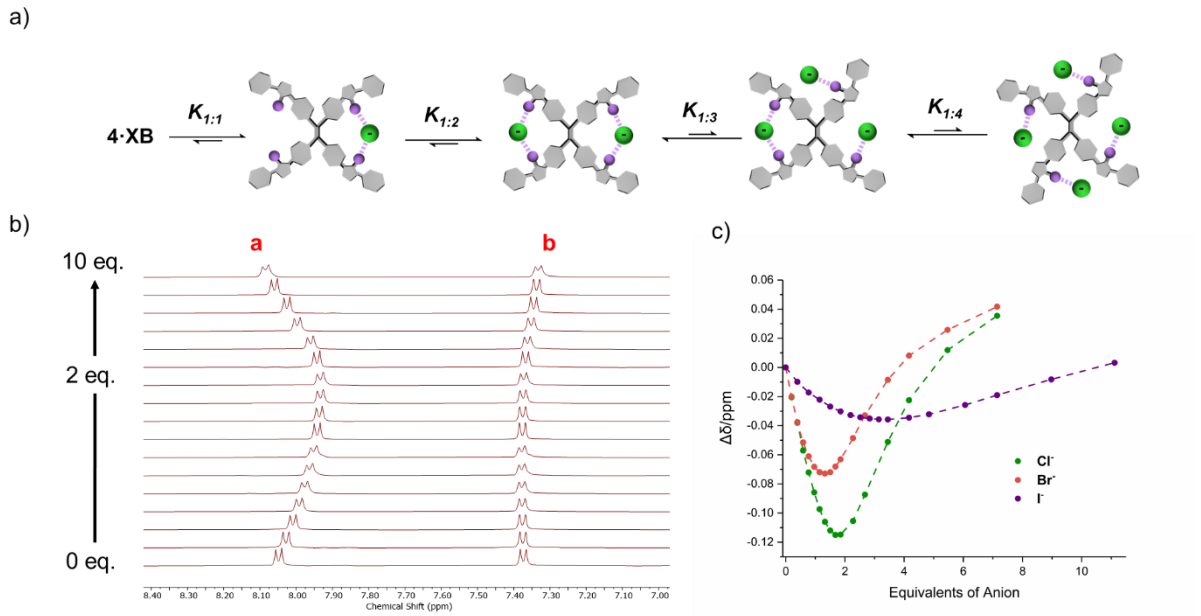


Figure 4.6 a) Postulated anion binding equilibrium for **4·XB.** b) ^{1}H NMR TBACl titration of **4·XB** (THF-d_8, 500 MHz, 298 K). c) Halide binding isotherms for **4·XB,** where circles represent experimental data and dashed lines are a visual aid.

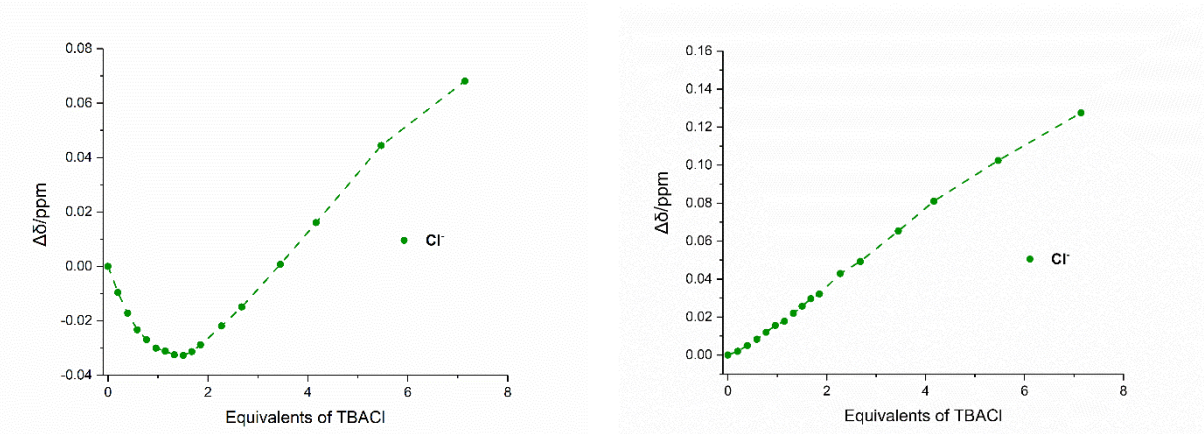


Figure 4.7 Binding Isotherm derived from ^{1}H NMR TBACl titrations of **4·HB** (left) and **4·XB^{Ph}** (right) where circles represent experimental data and dashed lines are a visual aid (THF-d_8).

4.3.4 Solid-State Structure Determination

Further insight into the anion binding mode of the halogen bonding TPE systems was obtained by solid-state characterisation of **4·XB** (Figure 4.8) and in the presence of a source of chloride anion (Figure 4.9 and 4.10).

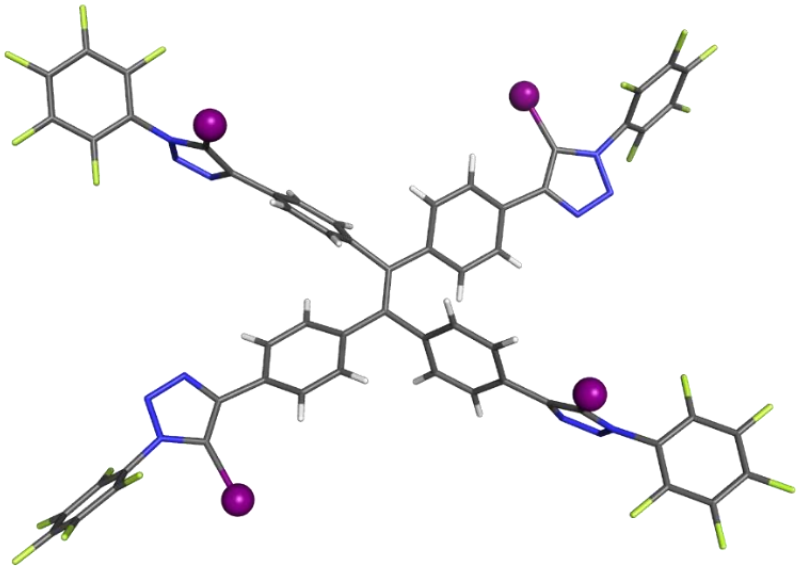


Figure 4.8 Solid state structure of the **4·XB**. Grey = carbon, blue = nitrogen, white hydrogen, light green = fluorine, iodine = purple, green = chloride, cyan = sodium.

It is noteworthy that attempts to crystallize **4·XB** with a non-coordinating organic countercation (e.g. tetraethylammonium, tetrabutylammonium or benzyltrimethylammonium) persistently yielded the NaCl complex of **4·XB** (Figure 4.9a). The propensity of **4·XB** to crystalize with adventitious sodium cation, presumably from glass containers or trace solvent contaminants is understandable by inspection of the solid-state structure in which the sodium cation is situated proximal to a chloride anion simultaneously exhibiting four C-I···Cl^- XB interactions with four distinct **4·XB** molecules (Figure 4.10a and b). Close examination of the structure reveals that the four-fold coordination of chloride, enforces close proximity of the TPE aromatic cores, as clearly visualised in the space filling representation (Figure 4.9c). To establish the relative roles of the Na^+ and Cl^- in the formation of these solid-state aggregates, efforts were also directed towards obtaining structural information in the presence of other halides. Crystals suitable for X-ray diffraction were obtained by the slow diffusion of pentane into a 9:1 $CHCl_3$:acetone (v/v) solution of **4·XB** in the presence of excess NaI. Single-crystal X-ray analysis revealed the NaI·**4·XB** complex displays a highly similar four-fold anion coordination mode via C-I···I^- XB interactions in an approximately square pyramidal geometry around iodide, however the sodium cation in this case resides in a vacancy between the central aromatic units of the tetraphenylethene core (Figure 4.10b). This is most likely due to reduced electrostatic interaction between the larger iodide anion and the sodium cation. The structural

resemblance of the sodium chloride and sodium iodide complexes reveals the crucial role of potent XB-anion interactions in the assembly of the aggregates. Encouraged by these findings, attention then turned to investigating whether these anion induced aggregates persist in the solution phase.

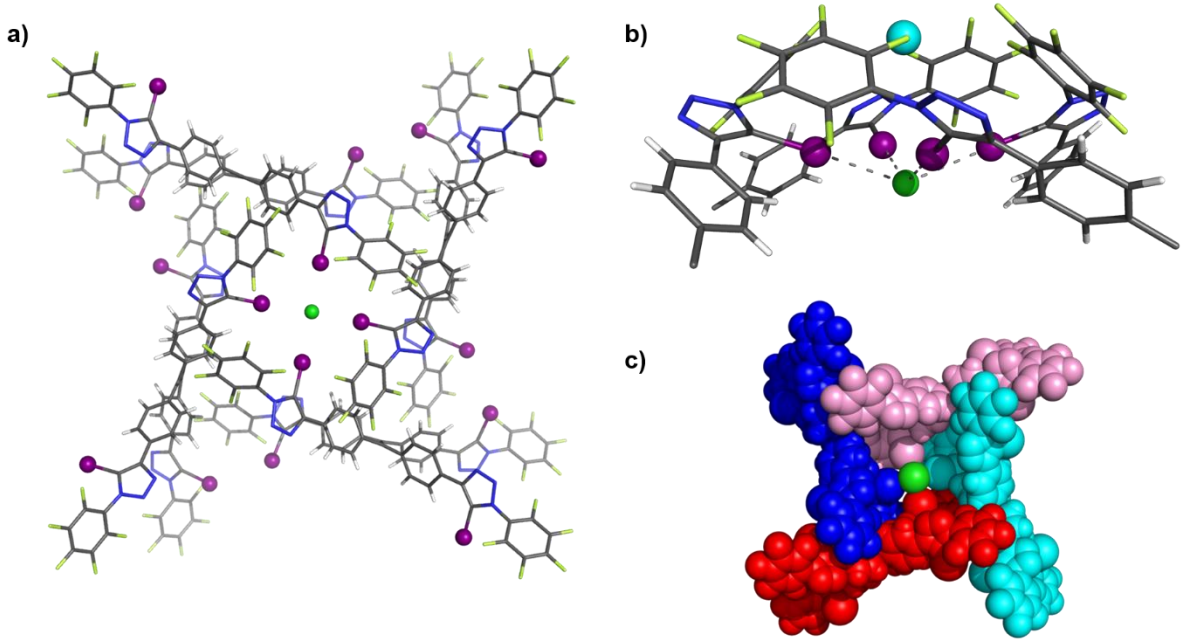


Figure 4.9 a) Solid state structure of the **4·XB**·NaCl, presented as a wire frame structure. b) Truncated view of chloride coordination in **4·XB**·NaCl. c) Space filling representation of **4·XB**·NaCl. Grey = carbon, blue = nitrogen, white = hydrogen, green = chlorine, light green = fluorine, purple = iodine, cyan = sodium.

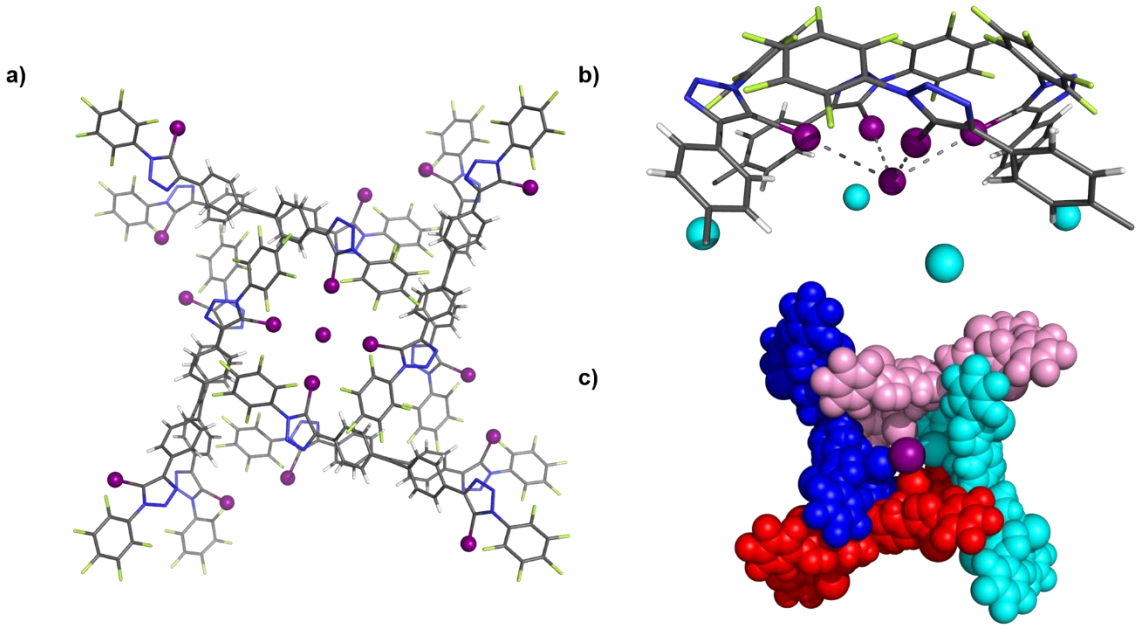


Figure 4.10 a) Solid state structure of the **4·XB**·NaI, presented as a wire frame structure. b) Truncated view of chloride coordination in **4·XB**·NaI. c) Space filling representation of **4·XB**·NaI. Grey = carbon, blue = nitrogen, white = hydrogen, light green = fluorine, purple = iodine, green = chloride, cyan = sodium.

4.3.5 Anion coordination induced aggregation and anion sensing

Consistent with the well-established emission behaviour of TPE derivatives, fluorescence measurements of **4·XB** in THF solution (10^{-5} M) revealed that it is weakly emissive (λ_{ex} = 350 nm). However, a dramatic increase in emission intensity is observed with an increasing water fraction (f_w), the most notable increase at f_w >60 %, indicative of the anticipated aggregation-induced emission behaviour of TPE derivative **4·XB** (Figure 4.11a, top). The formation of aggregates was confirmed by dynamic light scattering (DLS) measurements (Figure 4.11a, bottom), clearly showing the formation of species larger than 100 nm. Addition of increasing equivalents of chloride to a THF solution of **4·XB** led to an increase in fluorescence intensity (λ_{max} = 520 nm), with a three-fold increase observed after the addition of 10 equivalents (Figure 4.11b, top), accompanied by a considerable hypsochromic shift (~ 20 nm). Recent studies to elucidate the mechanism of AIE in TPE derivatives have demonstrated that hypsochromic or bathochromic shifts of λ_{max} are linked to the relative rotations of the four aryl units to the alkene core. An increase in planarity between the constituent phenyl rings leads to increasing π-conjugation and red-shifting of the emission, whilst adoption of a perpendicular conformation decreases π-conjugation and results in blue-shifted emission. Inspection of the solid state structures for **4·XB** and its NaCl complex readily rationalise the observed changes in the emission profile, whereby the intermolecular coordination of the halide by halogen bond interactions not only induces the formation of closely intertwined complexes, restricting possible rotational degrees of freedom, but also enforces a more perpendicular geometry of the core aromatic scaffold (See Figure 4.12 and Table 4.3). Addition of the non-coordinating anion hexafluorophosphate did not affect the emission spectrum, further demonstrating that XB-mediated coordination to chloride is required to mediate aggregation as opposed to changing solvent viscosity or changes in the medium's dielectric properties. Dynamic light scattering (DLS) measurements of freshly prepared THF solutions (10^{-5} M) of **4·XB** indicate that the free receptor is non-aggregated in the absence of chloride, but the addition of 1 equivalent of TBACl induces the formation of aggregates on the order of 100 nm in diameter (Figure 4.11, bottom). Further evidence for anion-induced aggregate formation of **4·XB** was provided by transmission electron microscopy (TEM) which, consistent with results from DLS, revealed that the addition of 1 eq. of TBACl to a 1 mM solution of **4·XB** in THF led to the formation of ~100 nm sized particles, while no such species were observed for the free receptor in the absence of chloride (Figure 4.13).

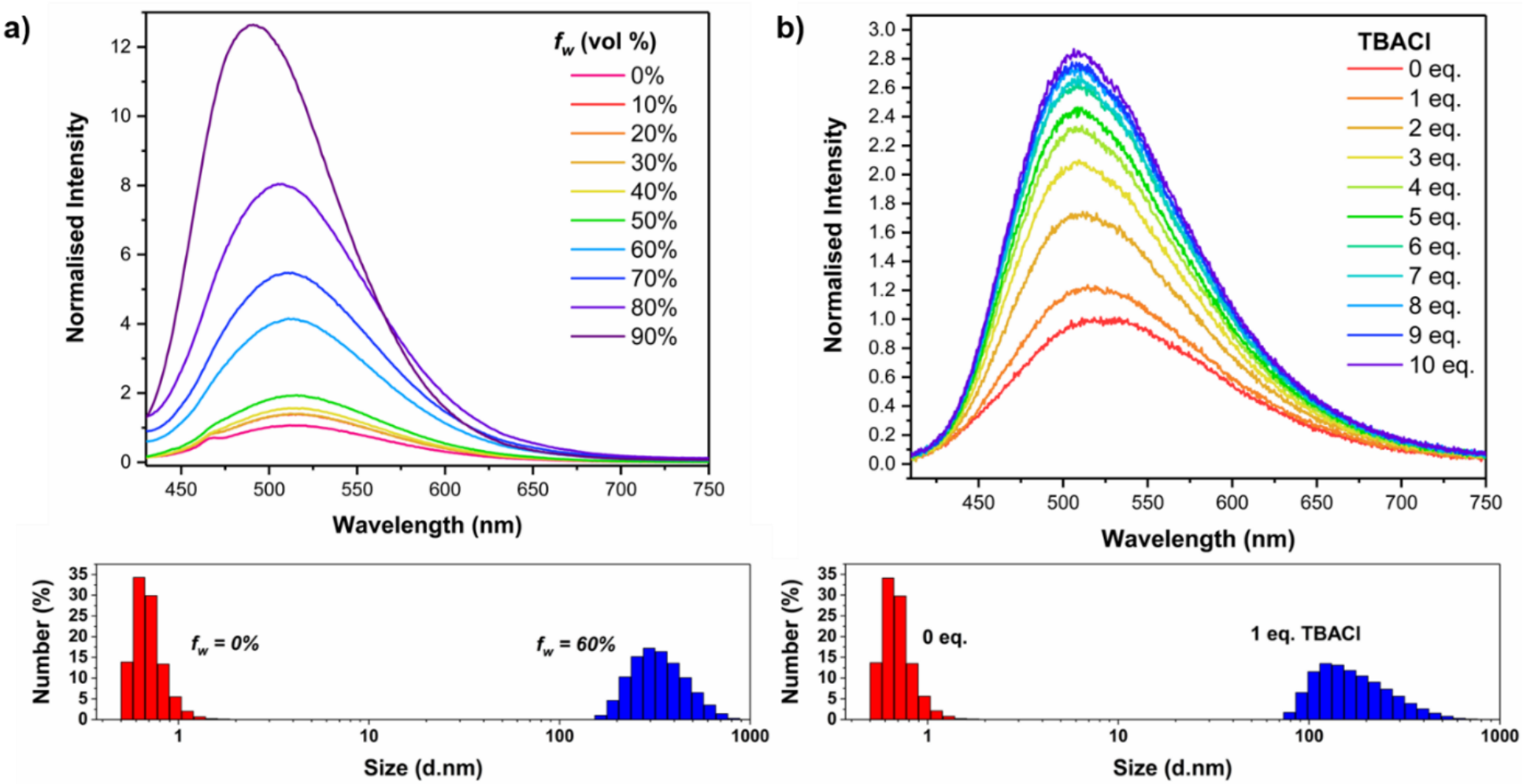


Figure 4.11 Fluorescence spectra (top) (THF, 10^{-5} M, λ_{ex} = 350 nm) and overlaid DLS measurements (bottom) of **4·XB** in the presence of (a) increasing water fraction (f_w) and (b) Increasing equivalents of TBACl.

Table 4.3 Summary of angles of distortion for **4·XB** and **4·XB**·NaCl, uncertainties indicated in parentheses.

	Distortion angle(s)/ ° [a]
4·XB	62.0 (0.2)
	27.1 (1.3)
4·XB·NaCl	56.2 (0.4)

[a]Errors indicated in parentheses.

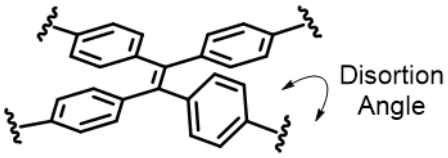


Figure 4.12 Truncated diagram of the TPE core of **4·XB** and indicated angle of the distortion.

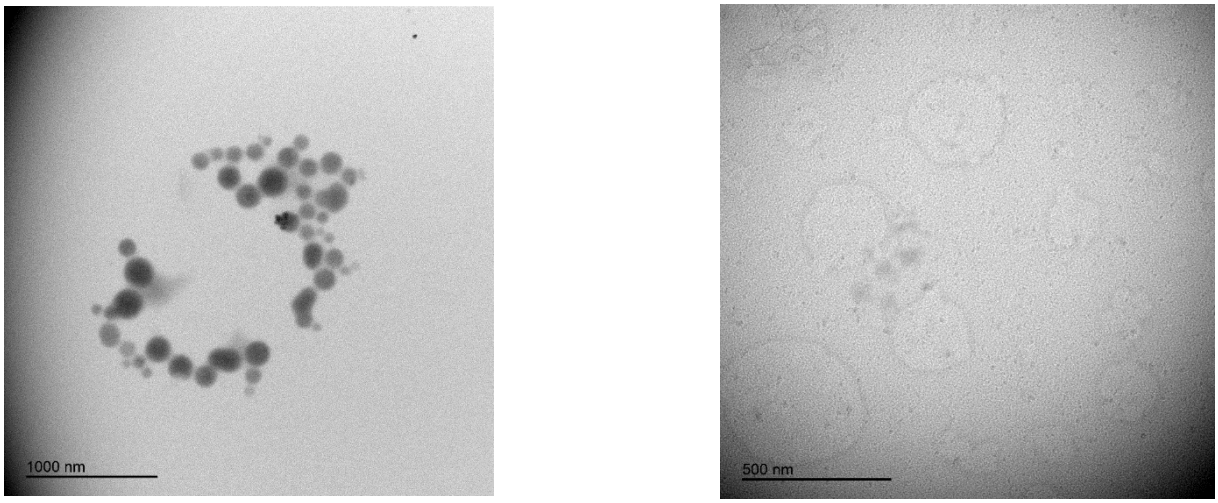


Figure 4.13 TEM image of **4·XB** in the presence of 1 eq. of TBACl added (left) and in the absence of TBACl (right) as a THF solution (10^{-3} M).

To further explore the role of spatial orientation and potency of the halogen bond donors in the formation of the anion-mediated aggregates, the relative fluorescence response for all receptors was recorded in the presence of 10 equivalents of TBACl, and the data summarised in Figure 4.14. The largest emission intensity increases are observed for **4·XB** and **2·XB**, and the formation of aggregates in the presence of 1 equivalent of TBACl in both cases was confirmed by DLS measurements. In contrast, **1·XB, 2·XB*Z*** and **2·XB*E*** exhibited only minor perturbations in fluorescence intensity upon the addition of 10 equivalents of TBACl and DLS analysis revealed no evidence for the formation of anion induced aggregates. Together, these results provide compelling evidence that the observed emission enhancement arises from XB-mediated chloride induced aggregation of **4·XB** molecules. The absence of anion-coordination induced aggregation for **2·XB*Z***, despite the receptor possessing the largest chloride affinity relative to all other mono- and di-substituted TPE derivatives, demonstrates that spatial orientation of the XB donors is crucial in the formation of the chloride induced XB aggregates. Under analogous conditions **4·XB^{Ph}** and the hydrogen bonding analogue **4·HB** also demonstrated no significant emission intensity change, providing further strong evidence for the requirement for multiple and potent XB-anion interactions to drive aggregate formation. Analogous experiments were also undertaken to investigate how the nature of the anionic guest influences aggregate formation, in which the emission intensity of **4·XB** in THF was measured in the presence of 10 equivalents of a range of anions (Figure 4.14). In all cases except acetate, the addition of an anion induced a fluorescence intensity increase. In accordance with the anion basicity trend this increase followed the order of Cl^- > Br^- > I^-. Notably, despite its di-anionic nature, SO_4^{2-} elicited a diminished enhancement in emission intensity in comparison to the strong chloride response.

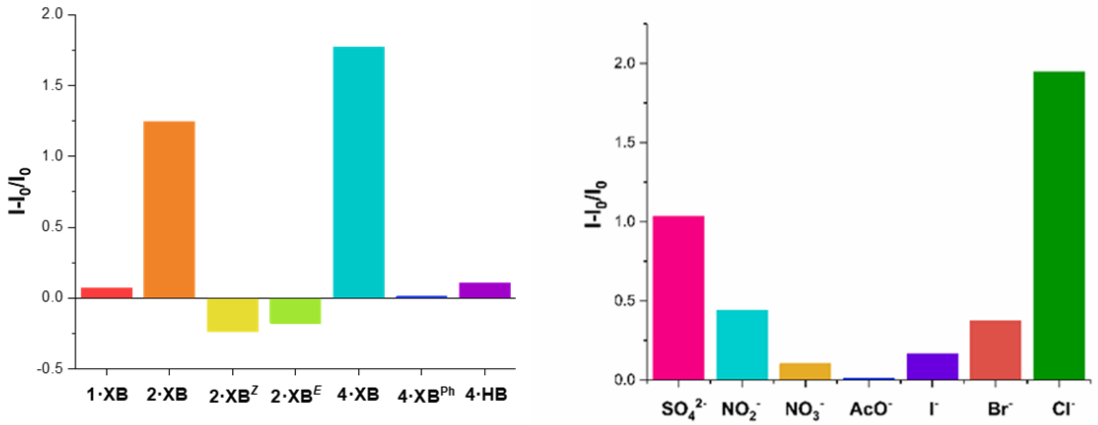


Figure 4.14 (Left) Relative fluorescence responses of the series of receptors in the presence of 10 equivalents of TBACl (THF, 10^{-5} M, λ_{ex} = 350 nm). (Right) Relative fluorescence response for **4·XB** in the presence of 10 equivalents of a range of anions (THF, 10^{-5} M, λ_{ex} =

350 nm). The considerable fluorescence response for Cl^- corresponds to a limit of detection (LOD) of 5.14 μM (183 ppb), constituting one of the most sensitive supramolecular anion sensors to-date (Figure 4.15).

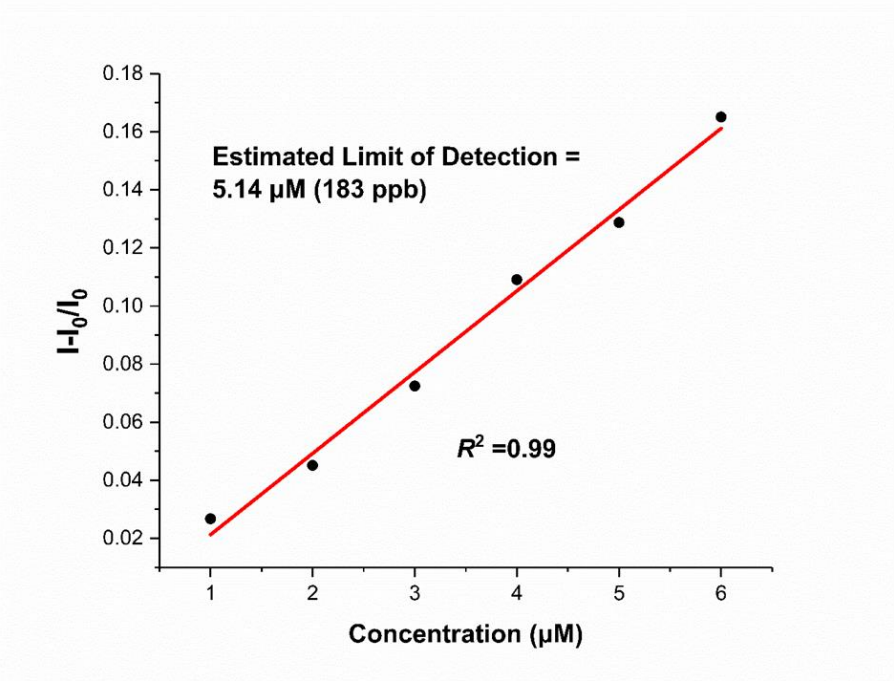


Figure 4.15 Limit of detection plot for **4·XB** with TBACl.

4.3.6 Photoswitchable Anion Receptor studies

In addition to the highly desirable luminescent properties of TPE, unsymmetrical doubly substituted TPE derivatives have the capability to function as molecular photo-switches in which photoisomerisation switches between different spatial arrangements of functional groups. Photo-switchable anion receptors in particular have attracted interest for applications including ion extraction and transport, enabling control over when and where the hosts bind or release their targets.[31] However, the utilization of TPE as a photoswitch has been hindered by practical issues in their synthesis, due to a combination of poor stereoselectivity and challenging chromatographic separation of the closely related geometric isomers. Consequently, the vast majority of reports to date using these di-functionalised TPE derivatives in material or polymer sciences have used mixtures of the isomers. Compounds **2·XB*E*** and **2·XB*Z*** are prime candidates for developing photo-switchable anion receptors due to the contrast in chloride binding affinity of the two geometric isomers ($K_{1:1}$ of 4970 and 23,200 M^{-1}, respectively) and fortuitously, could be isolated by column chromatography.

Irradiation of a solution of a pure sample of **2·XB^{E}** with 405 nm light triggered photo-isomerisation, generating an approximately equal ratio of both isomers in the photo-stationary state (52:48 **2·XB^{Z}** : **2·XB^{E}**), as determined by integration of the NMR signals of the mixture (Figure 4.16). TLC analysis of pure samples of **2·XB^{Z}** and **2·XB^{E}** compared with a post-irradiated solution of **2·XB^{E}** further confirm the unimolecular photoisomerisation process (Figure 4.16).

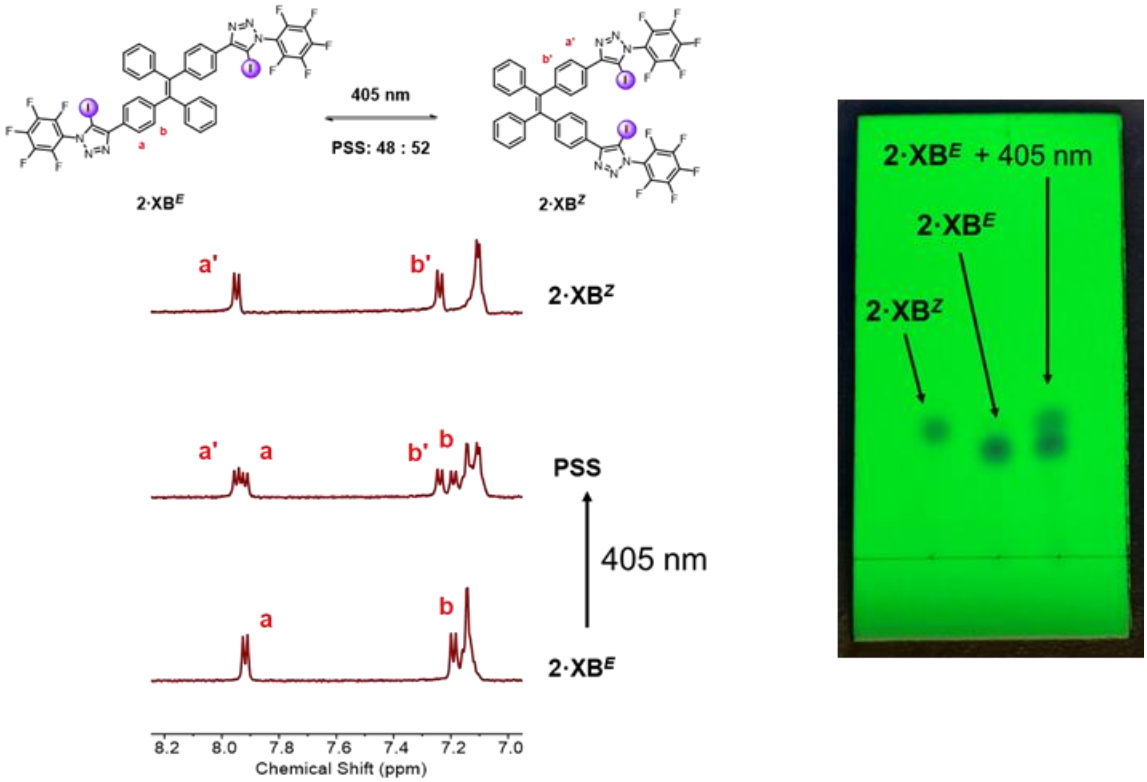


Figure 4.16 Photoisomerisation of **2·XB^{E}** (^{1}H NMR, 10^{-3} M THF-d_8, 500 MHz, 298 K) (left) and TLC analysis (eluent 20% THF:hexane 1:4 v/v) of pure **2·XB^{Z}** and **2·XB^{E}** and a post-irradiation solution of **2·XB^{E}** (right).

The effect of 405 nm irradiation on the UV vis spectrum of a solution of **2·XB^{E}** is shown in Figure 4.17a, resulting in a bathochromic shift of the absorption at low wavelength (ca. 265 nm) and a decrease in the absorption at 335 nm, with isosbestic points at 270 nm and 310 nm confirming the unimolecular nature of the isomerisation process (Figure 4.17a). The photo-stationary state was reached within 120 s, as deduced by the absence of further changes in the absorption spectrum. No thermal isomerization of **2·XB^{Z}** or **2·XB^{E}** was observed under ambient conditions in THF solution over the course of the experiment when excluded from light. Analogous irradiation experiments starting with **2·XB^{Z}** generated a similar, but reversed set of perturbations in the UV-vis profile, namely an increase in absorption at 335 nm and a hypsochromic shift in the local λ_{max} absorption at approximately 265 nm (Figure 4.17b). Importantly, the directions of the changes are those anticipated from inspection of the overlaid UV-vis spectra of **2·XB^{Z}** and **2·XB^{E}** (Figure 4.17c).

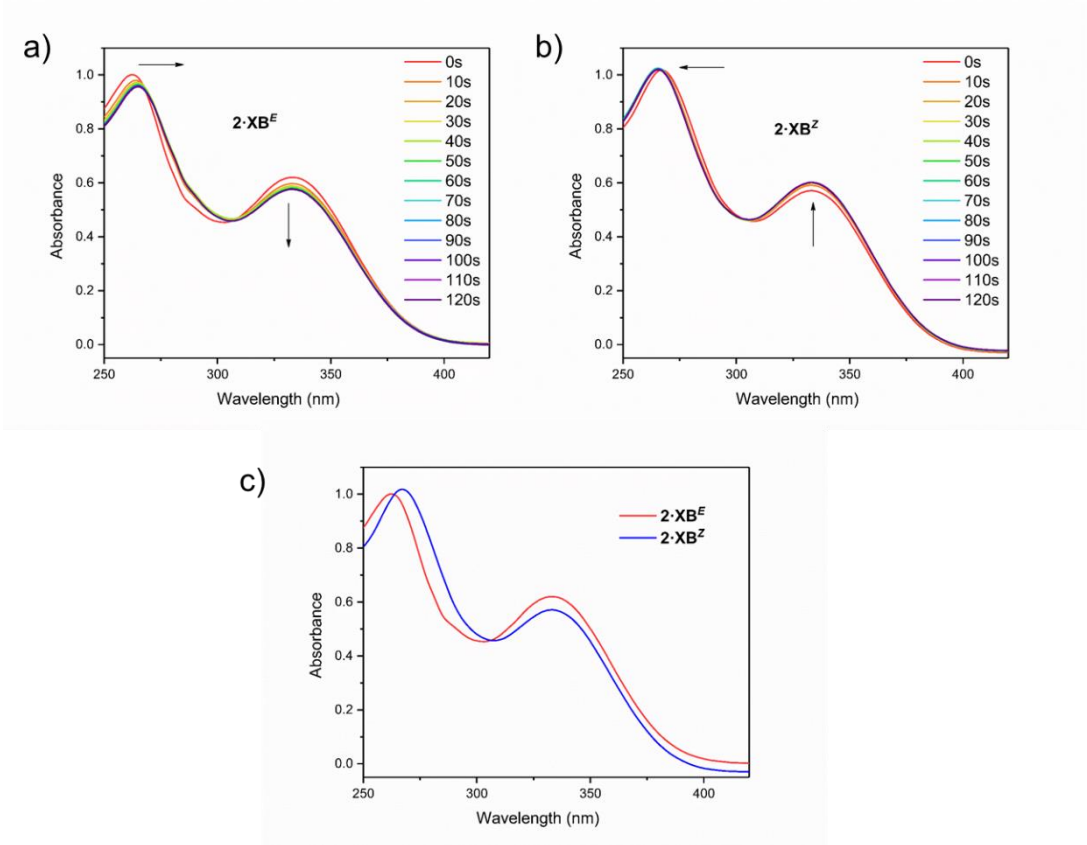


Figure 4.17 a) Photoisomerisation of **2·XB^{E}**. UV-Vis spectra of the photo-stationary state generated upon irradiation of **2·XB^{E}** with 405 nm light (THF, 10^{-5} M). b) Photoisomerisation of **2·XB^{Z}** in the presence of 10 equivalents of TBACl c) Overlaid (^{1}H NMR, THF-d_8, 500 MHz, 298 K).

Given the contrasting anion binding properties of the isomers, we anticipated that the photostationary state may be biased in favour of the Z isomer by coordination to an anion. To this end, analogous photoisomerisation experiments were conducted by irradiating the sample with 405 nm light in the presence of 10 equivalents of TBACl. In the presence of the halide, the PSS is biased in favour of the Z isomer, due to strong XB coordination to the chloride (68:32 **2·XB^{Z}**:**2·XB^{E}**) (Figure 4.18). Similar experiments were undertaken with 10 equivalents of bromide and iodide (Table 4.4), revealing that the bias of the PSS in favour of the Z isomer correlates with the anion binding affinity to **2·XB^{Z}**, namely Cl^{-}>Br^{-}>I^{-}. In contrast, in the presence of non-coordinating anion, PF_6^{-}, which demonstrated no binding to either receptor in ^{1}H NMR titration experiments, no perturbation of the position of the PSS was detected. Together, this data provides evidence for photo-switchable XB-mediated anion recognition, in which strong binding to the **2·XB^{Z}** and weaker binding to **2·XB^{E}** enables switching of binding using light, as well as modulation of the obtained ratio of isomers in the photostationary state.

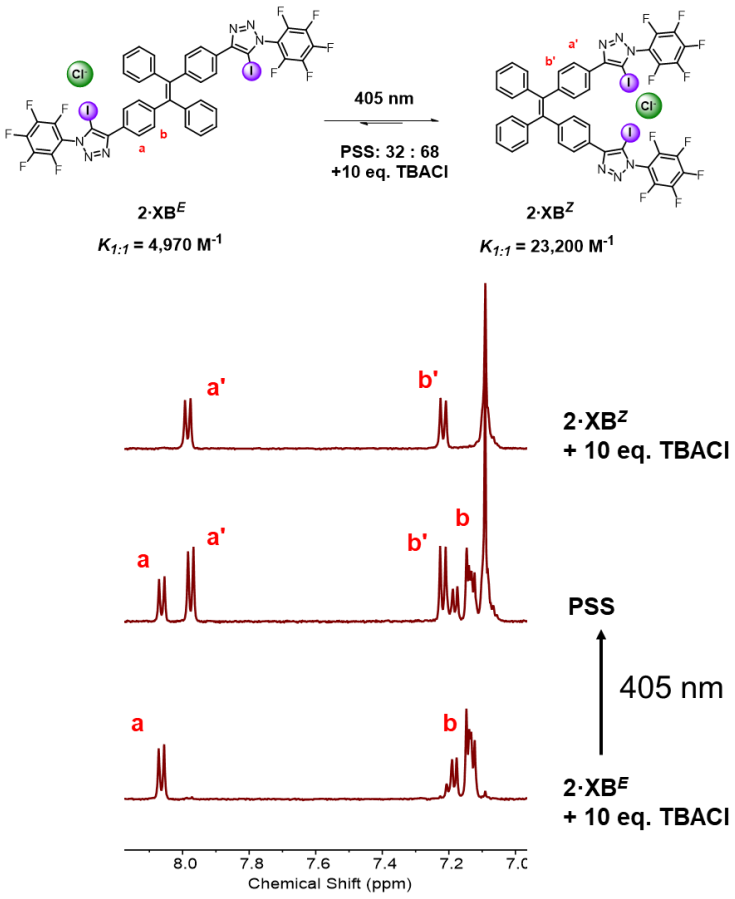


Figure 4.18 Photoisomerisation of **2·XB^{E}** in the presence of 10 equivalents of TBACl (^{1}H NMR, THF-d_8, 500 MHz, 298 K).

Table 4.4 PSS ratios determined from irradiation of 1 mM of **2·XB^{Z}**.

Anion[a]	PSS Ratio (**2·XB^{Z}** /**2·XB^{E}**)[b]
None	52:48
Cl^-	68:32
Br^-	62:38
I^-	58:42
PF_6^-	53:47

[a]10 equivalents of anion added as their tetrabutylammonium salts,10^{-3} M, THF-d_8. [b]PSS ratios determined from ^{1}H NMR integration.

4.4 Conclusions

In conclusion, a series of halogen bonding TPE-based anion receptors are described, in which the multivalency and relative orientation of the strongly potent perfluoroaryl XB donors is systematically investigated. ^{1}H NMR anion titration experiments elucidate the varied binding modes and stoichiometries of the family of halogen bonding TPE derivatives. Fluorescence anion titration experiments demonstrate that the tetra-substituted perfluorinated **4·XB** receptor, experiences a dramatic increase in emission intensity upon the addition of chloride, while the non-fluorinated **4·XB^{Ph}** or hydrogen bonding **4·HB** analogues elicit no fluorescent response. Detailed analysis of the fluorescence spectra, dynamic light scattering measurements, TEM imaging and X-ray crystal structure determination demonstrate that the origin of this switch on in emission intensity is an unprecedented XB-anion coordination induced aggregation mechanism. Furthermore, successful isolation of the difunctionalised geometric isomers **2·XB^{Z}** and **2·XB^{E}** facilitated the investigation of these TPE derivatives as photoswitchable anion receptors, in which it was demonstrated that the position of the photostationary state could be significantly biased towards **2·XB^{Z}** on the basis of enhanced halide anion affinity. These results not only provide further evidence for the advantages of XB interactions in the design of potent anion receptors, but also point to new opportunities in the development of XB anion-responsive materials, switches and sensors.

4.5 References

[1] J. Mei, Y. Hong, J. W. Y. Lam, A. Qin, Y. Tang, B. Z. Tang, *Adv. Mater.* **2014**, *26*, 5429–5479.

[2] J. Mei, N. L. C. Leung, R. T. K. Kwok, J. W. Y. Lam, B. Z. Tang, *Chem. Rev.* **2015**, *115*, 11718–11940.

[3] Y. Hong, J. W. Y. Lam, B. Z. Tang, *Chem. Soc. Rev.* **2011**, *40*, 5361–5388.

[4] J. Luo, Z. Xie, J. W. Y. Lam, L. Cheng, H. Chen, C. Qiu, H. S. Kwok, X. Zhan, Y. Liu, D. Zhu, B. Z. Tang, *Chem. Commun.* **2001**, 1740–1741.

[5] S. Suzuki, S. Sasaki, A. S. Sairi, R. Iwai, B. Z. Tang, G. Konishi, *Angew. Chem. Int. Ed.* **2020**, *59*, 9856–9867.

[6] J. Qian, B. Z. Tang, *Chem* **2017**, *3*, 56–91.

[7] Q. Lu, C.-J. Wu, Z. Liu, G. Niu, X. Yu, *Front. Chem.* **2020**, *8*, DOI 10.3389/fchem.2020.617463.

[8] M. Yu, R. Huang, J. Guo, Z. Zhao, B. Z. Tang, *PhotoniX* **2020**, *1*, 11.

[9] R. Hu, A. Qin, B. Z. Tang, *Prog. Polym. Sci.* **2020**, *100*, 101176.

[10] N.-T. Chu, R. D. Chakravarthy, N.-C. Shih, Y.-H. Lin, Y.-C. Liu, J.-H. Lin, H.-C. Lin, *RSC Adv.* **2018**, *8*, 20922–20927.

[11] H. Qu, X. Tang, X. Wang, Z. Li, Z. Huang, H. Zhang, Z. Tian, X. Cao, *Chem. Sci.* **2018**, *9*, 8814–8818.

[12] X. Yan, P. Wei, Y. Liu, M. Wang, C. Chen, J. Zhao, G. Li, M. L. Saha, Z. Zhou, Z. An, X. Li, P. J. Stang, *J. Am. Chem. Soc.* **2019**, *141*, 9673–9679.

[13] H.-T. Feng, Y.-X. Yuan, J.-B. Xiong, Y.-S. Zheng, B. Z. Tang, *Chem. Soc. Rev.* **2018**, *47*, 7452–7476.

[14] J. Feng, L. Yao, J. Zhang, Y. Mu, Z. Chi, C.-Y. Su, *Dalton Trans.* **2016**, *45*, 1668–1673.

[15] H. Fang, G. Cai, Y. Hu, J. Zhang, *Chem. Commun.* **2018**, *54*, 3045–3048.

[16] D. D. La, S. V. Bhosale, L. A. Jones, S. V. Bhosale, *ACS Appl. Mater. Interfaces* **2018**, *10*, 12189–12216.

[17] P. Sabater, F. Zapata, B. López, I. Fernández, A. Caballero, P. Molina, *Dalton Trans.* **2018**, *47*, 15941–15947.

[18] G. Jiang, X. Liu, Y. Wu, J. Wang, X. Dong, G. Zhang, Y. Li, X. Fan, *RSC Adv.* **2016**, *6*, 59400–59404.

[19] C. Wang, H. Ji, M. Li, L. Cai, Z. Wang, Q. Li, Z. Li, *Faraday Discuss.* **2017**, *196*, 427–438.

[20] J. Zhao, D. Yang, Y. Zhao, X.-J. Yang, Y.-Y. Wang, B. Wu, *Angew. Chem. Int. Ed.* **2014**, *53*, 6632–6636.

[21] M. M. Watt, J. M. Engle, K. C. Fairley, T. E. Robitshek, M. M. Haley, D. W. Johnson, *Org. Biomol. Chem.* **2015**, *13*, 4266–4270.

[22] Z. Zhang, M. I. Hashim, C.-H. Wu, J. I. Wu, O. Š. Miljanić, *Chem. Commun.* **2018**, *54*, 11578–11581.

[23] Y.-X. Yuan, J.-H. Wang, Y.-S. Zheng, *Chem. – Asian J.* **2019**, *14*, 760–764.

[24] M. H. Chua, K. W. Shah, H. Zhou, J. Xu, *Molecules* **2019**, *24*, 2711.

[25] Y. Xie, Z. Li, *Chem. – Asian J.* **2019**, *14*, 2524–2541.

[26] U. Döge, K. Eger, *Pharm. - Int. J. Pharm. Sci.* **2007**, *62*, 174–178.

[27] S. K. Talloj, M. Mohammed, H.-C. Lin, *J. Mater. Chem. B* **2020**, *8*, 7483–7493.

[28] J. Du, S. Yu, Z. Huang, L. Chen, Y. Xu, G. Zhang, Q. Chen, X. Yu, L. Pu, *RSC Adv.* **2016**, *6*, 25319–25329.

[29] Y. Liu, C. S. Diercks, Y. Ma, H. Lyu, C. Zhu, S. A. Alshmimri, S. Alshihri, O. M. Yaghi, *J. Am. Chem. Soc.* **2019**, *141*, 677–683.

[30] Z. Wang, C.-Y. Zhu, J.-T. Mo, P.-Y. Fu, Y.-W. Zhao, S.-Y. Yin, J.-J. Jiang, M. Pan, C.-Y. Su, *Angew. Chem. Int. Ed.* **2019**, *58*, 9752–9757.

[31] S. Lee, A. H. Flood, *J. Phys. Org. Chem.* **2013**, *26*, 79–86.

Chapter 5 Halogen Bonding Heteroditopic Materials for Cooperative Ion-Pair Binding and Extraction

5.1 Introduction

As discussed in Chapter 1 heteroditopic receptors, possessing binding sites for both cations and anions, frequently exhibit augmented recognition behaviour relative to their monotopic counterparts.[1–4]. The considered employment of these effects in ion-pair receptor design has been demonstrated to be a powerful strategy in augmenting not only ion-affinity, but also selectivity profiles.[5–12] Advantageously, these effects frequently translate to highly desirable functionalities leading to their successful application in fields such as sensing,[13–15] molecular logic gates[16,17] and membrane transport.[18–20] In particular, the application of heteroditopic molecular receptor systems as novel extraction agents has demonstrated enormous promise as an alternative supramolecular strategy to sequester and/or recover a range of alkali-, transition- and precious-metal salts.[5,21–24] Indeed, one of the earliest examples of the impressive extraction capabilities that can be achieved by heteroditopic receptor systems was demonstrated by Reetz et al.[25] In the 1991 report a benzo-21-crown-6 motif was endotopically functionalised with a catechol boronic ester motif (Figure 5.1a), wherein it was anticipated the array of Lewis basic polyether oxygens would be capable of K^+ complexation while the tricoordinate boron would serve as a Lewis acid for anion complexation. Multinuclear NMR spectroscopic investigations revealed that a CD_2Cl_2 solution of the receptor was capable of stoichiometric solid potassium fluoride extraction, whereas KCl and KBr were not solubilised to any extent. This selectivity for KF over KCl or KBr was attributed to the B-X (X= F, Cl, Br) bond enthalpies formed upon salt dissolution, wherein the stronger dative B-F bond formed upon ion-pair complexation compensated for the energetic cost of lattice dissolution.

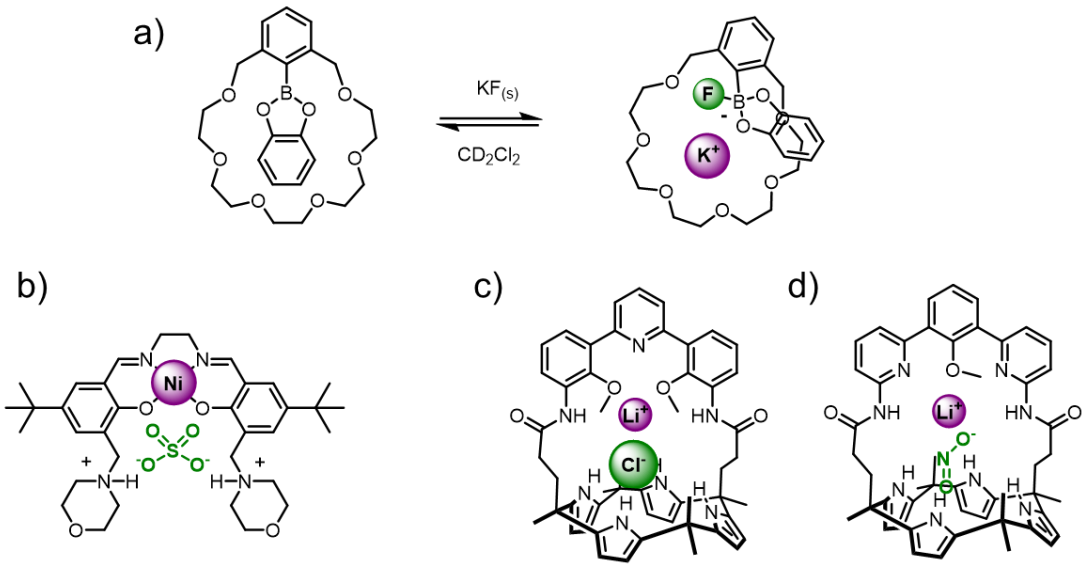


Figure 5.1 a) Reetz's KF selective receptor b) Tasker's $NiSO_4$ salen extractant**.** Sessler's c) LiCl and d) $LiNO_2$ selective receptors.

In the following years, the field witnessed an increasing diversity of ion-pair receptor types. For example Tasker's morpholine appended salen complex was capable of liquid liquid extraction of highly hydrophilic nickel sulfate from aqueous media into chloroform (Figure 5.1b),[24] wherein upon Ni^{2+} complexation a proton transfer from the constituent phenol groups of the salen unit to the pendant morpholine moieties generated a dicationic HB donor anion binding site to sequester the SO_4^{2-} counteranion. More recently, motivated by its pervasive application in energy storage materials, polymer synthesis and pharmacology, coupled with its low natural abundance, significant progress has been made in developing lithium salt selective heteroditopic extractant materials. To this end, Sessler has made considerable strides, reporting strapped calix[4]pyrrole based receptors in which subtle modulation of donor atom number or type, the cation binding cavity can be effectively modulated to elicit selectivity for the selective liquid liquid and solid liquid extraction of various lithium salts such as LiCl (Figure 5.1c) or $LiNO_2$ (Figure 5.1d).[26,27] Sessler and others have also elegantly shown that the incorporation of ion-pair receptor frameworks into polymeric or resin-based solid supports serves to not only provide a reusable extractant material, but often through subtle multivalent effects enhances extraction efficiencies relative to a discrete molecular receptor analogue.[28–31] For example, Romański and Piatek reported a receptor material, comprised of a poly(butyl methacrylate) based polymer decorated with thiourea aza-crown ether receptors, capable of extracting sodium nitrate from aqueous solution (Figure 5.2a). Whereas the discrete molecular receptor analogue (Figure 5.2b) alone could not extract $NaNO_3$ in liquid-liquid extraction studies.

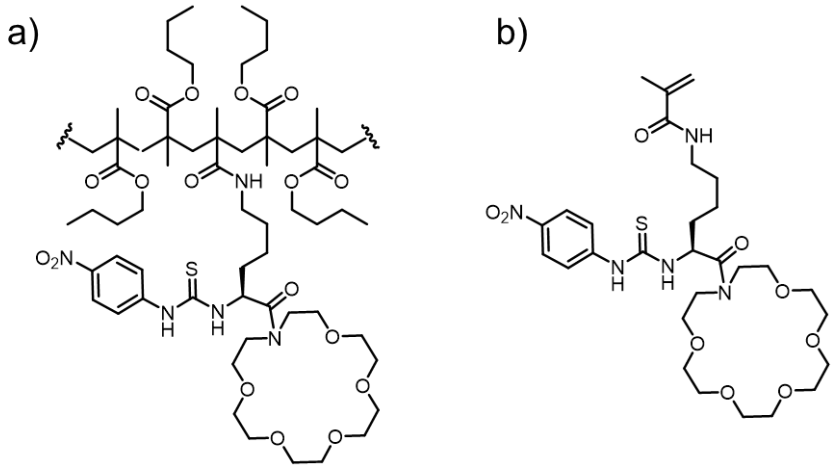


Figure 5.2 Romański's heteroditopic a) polymer extractant material b) molecular receptor analogue.

5.2 Chapter Aims

This chapter's aims are to fulfil the following goals:

- To exploit heteroditopic receptor design to develop cooperative ion-pair functional solid-immobilised XB-mediated extraction materials.

To this end, this chapter describes a series of XB and HB heteroditopic receptors covalently linked to a silica-based QuadraSil solid support material. Importantly, ICP-MS monitored extraction studies reveal the potency and unique cooperativity mechanism of XB mediated ion-pair recognition is crucial to the material's extraction performance of NaI from water.

5.3 Halogen Bonding Heteroditopic Materials for Cooperative Ion-Pair Binding and Extraction

5.3.1 Design and synthesis of XB and HB heteroditopic receptor functionalised silica materials

The synthetic strategy employed for the preparation of the target XB and HB heteroditopic receptor functionalised silica materials required the initial synthesis of mono- and bidentate iodotriazole phenyl motifs appended with B15C5 groups, wherein the functionalised ethylparaben ester moiety facilitates solid silica-based support immobilisation via amide condensation with amino-propyl groups of QuadraSil-AP™ (Figure 5.3).

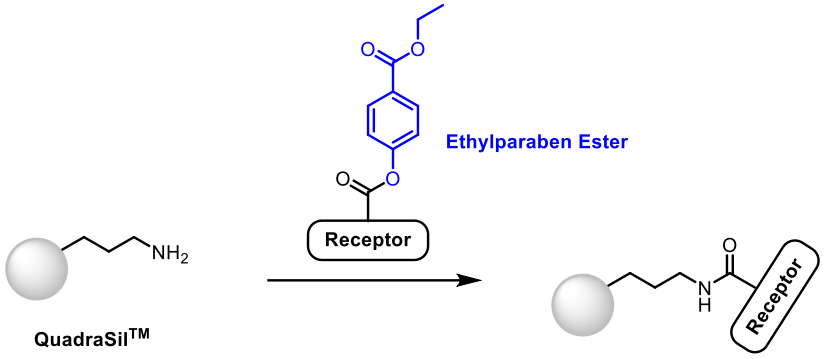
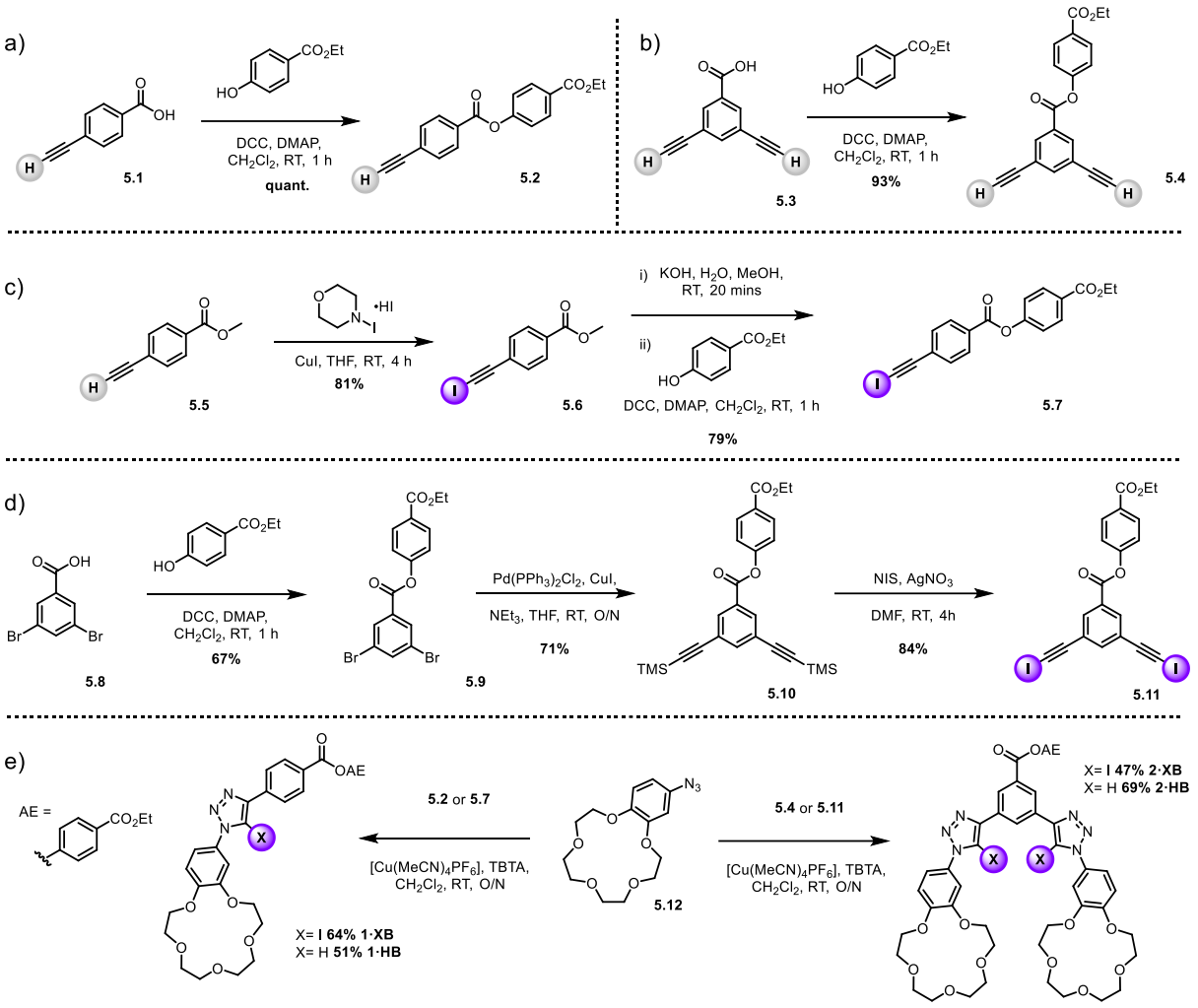


Figure 5.3 General amide condensation functionalisation strategy for QuadraSil.

The target XB and HB receptors were synthesised according to a copper(I)-catalysed azide alkyne cycloaddition (CuAAC) reaction between the appropriately functionalised alkyne precursors and azido-benzo-15-crown-5 (Scheme 5.1). The requisite mono- and bis-alkyne precursors were prepared according to Scheme 5.1a-d. For the proto-alkynes, a DCC mediated coupling reaction between the parent acids, **5.1** and **5.3**, and 4-hydroxyethylbenzoate (ethylparaben) in the presence of a catalytic amount of DMAP gave the esters **5.2** and **5.4** in excellent yields. Iodo-alkyne **5.7** was synthesized in a similar manner, in which an iodination reaction of methyl ester **5** with *N*-iodomorpholine hydroiodide/CuI, afforded **6**, in 81% yield. Subsequently the iodo-alkyne **5.6** was subjected to carefully controlled basic hydrolysis and esterified with ethylparaben under similar coupling conditions and isolated by column chromatography to afford **7** in 79% yield over three steps. The analogous bis-iodoalkyne, was synthesised via a standard Sonogashira coupling reaction with two equivalents of TMS-acetylene and ester **5.9** to afford the bis-TMS protected alkyne **5.10** in 71% yield. Simultaneous TMS-deprotection and iodination of the bis-alkyne was achieved via treatment with N-iodosuccinimide in DMF in the presence of catalytic $AgNO_3$ to afford target bis-iodoalkyne **5.11** in 84% without the need for further purification.



Scheme 5.1 a), b), c) and d) Synthesis of appropriately functionalised mono- and bis-alkyne precursors. e) CuAAC synthesis of the ethylparaben activated ester appended XB and HB heteroditopic receptors.

The isolated ester-appended mono- and bis- functionalised alkynes were subjected to CuAAC reactions, in the presence of catalytic $[Cu(MeCN)_4]PF_6$ and the rate accelerating ligand tris(benzyltriazolyl) amine (TBTA) with either 1.1 or 2.2 equivalents of azide B15C5 **12**, respectively. In all cases, after ca. 12 hours of stirring under an atmosphere of nitrogen at room temperature, TLC analysis of the crude reaction mixtures indicated complete consumption of the alkyne starting material and ESI-MS confirmed the formation of the corresponding triazole products. The reaction mixtures were subjected to an $NH_4OH/EDTA_{(aq)}$ work up procedure after which the respective crude mixture was purified by iterative trituration protocols using diethyl ether and methanol to afford the receptors **1·XB**, **1·HB**, **2·XB** and **2·HB** in yields in the range of 47-69%. All of the heteroditopic receptors were characterised by ^{1}H and ^{13}C NMR and high resolution ESI mass spectrometry. A representative example is shown in Figure 5.4.

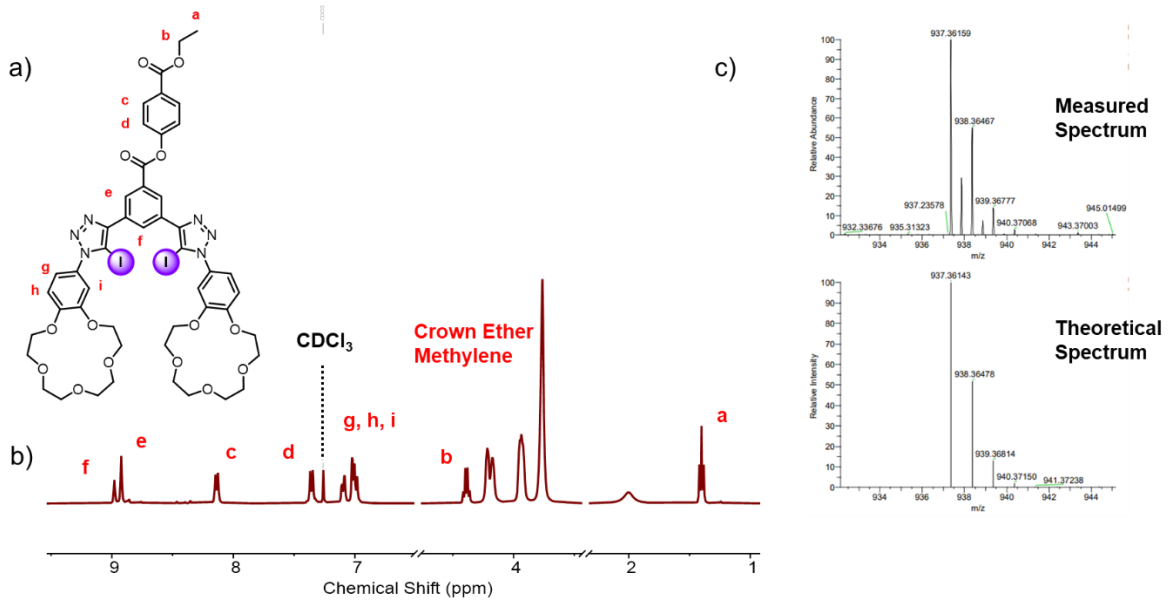
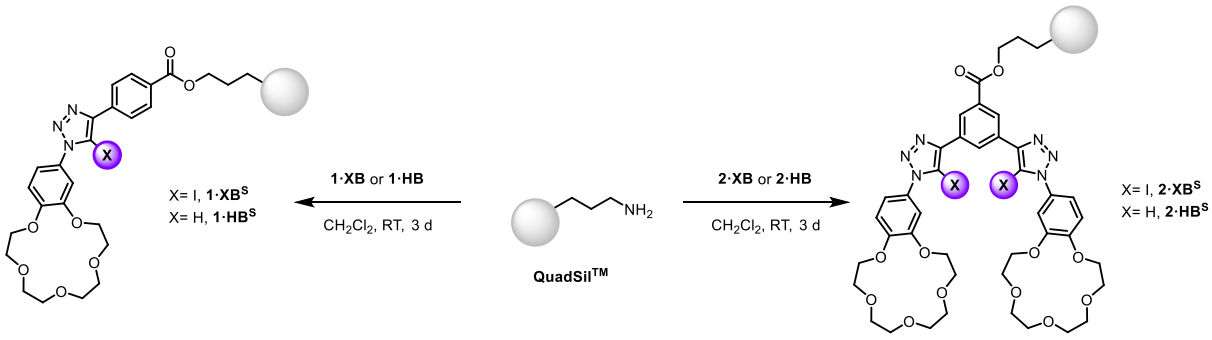


Figure 5.4 a) Chemical structure of **2·XB** b) Truncated ^{1}H NMR spectrum of **2·XB** ($CDCl_3$, 500 MHz, 298 K) c) Theoretical (bottom) and measured (top) high resolution ESI spectrum.

With the series of activated ester-appended heteroditopic receptors in hand, attention then turned to their immobilization on amino-propyl functionalised QuadraSil^{TM} (AP) solid support via an amide condensation reaction. In a general procedure, a dichloromethane solution of the receptor, containing five equivalents of the receptor relative to the average concentration of amino-propyl functional groups for a given mass of QuadraSil-AP^{TM}, was allowed to react at room temperature with a suspension of the silica-support. After three days the suspensions were decanted and under vacuum filtration, copious washing of the functionalised silica materials with CH_2Cl_2/MeOH mixtures was undertaken (Scheme 5.2), ensuring the removal of unreacted organic material and the ethylparaben aryl alcohol by-product of the amide condensation, furnishing the family of mono- and bidentate XB and HB heteroditopic silica-based materials **1·XB^{S}**, **1·HB^{S}**, **2·XB^{S}** and **2·HB^{S}**.



Scheme 5.2 Amide condensation synthesis of the functionalised silica materials.

The resultant materials were characterised by solid state ^{13}C CP/MAS-NMR (Figure 5.5a), which revealed that in addition to the diagnostic signal corresponding to the methylene groups of the amino-propyl unit (C_1-C_3), three sets of new signals are identifiable. Specifically, the broad series of resonances in the range 60 and 80 ppm, corresponding to the introduction of additional aliphatic environments of the methylene B15C5 units. A coincident series of resonances in the range 100-150 ppm were also observed, consistent with the introduction of multiple aromatic carbon environments originating from the aromatic linkers of the receptor scaffold. Additional evidence for the successful covalent attachment of the heteroditopic receptors to the silica-support material via the anticipated amide linkage was noted by the appearance of a characteristic amide carbon signal in the range 170-180ppm. In addition, FTIR analysis of the materials revealed a new absorption at approximately 1650 cm^{-1} corresponding to the carbonyl stretching frequency for an amide group (Figure 5.5b).

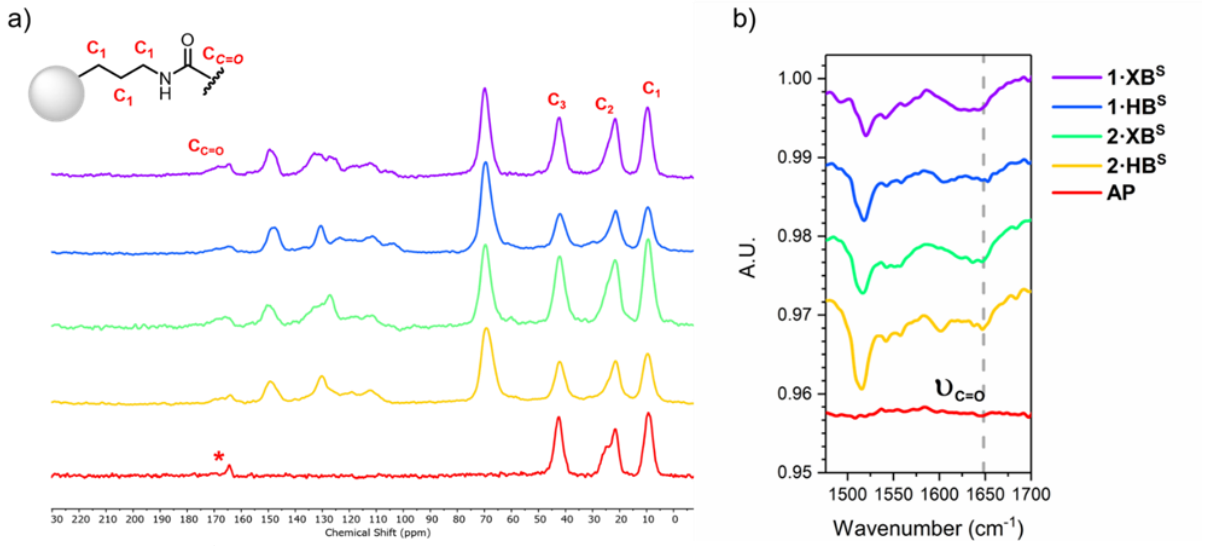


Figure 5.5 a) ^{13}C CP/MAS-NMR spectrum and b) truncated ATR-FTIR spectrum of the extractant materials **1·XB^S**, **1·HB^S**, **2·XB^S** and **2·HB^S** and the parent **AP**. Asterisk indicates the resonance arising from trace carbamate formation due to presence of atmospheric CO_2.

The extent of heteroditopic receptor incorporated to the surface of silica material was achieved by CHN combustion analysis, which determined the loadings for the four materials to be in the range of 0.23 – 0.46 mmolg^{-1} (Table 5.1).

Table 5.1 CHN analysis determined receptor loadings and amino-propyl functionalisation percentages.

Material	Loading/ mmolg^{-1} [a]	Amino-Propyl Functionalisation[c]
1·XB^{S}	0.357	30%
1·HB^{S}	0.445	24%
2·XB^{S}	0.229	15%
2·HB^{S}	0.231	16%
AP	1.49[b]	-

[a] Loading calculated on the basis CHN analysis and refers to the loading per receptor. [b] Refers to the determined loading of amino-propyl groups and is consistent with manufacturers specification of 1.5-2.0 mmolg^{-1}. [c] Refers to the calculated percentage of amino-propyl groups that have undergone an amide coupling reaction.

Inspection of Table 5.1 reveals that CHN analysis of amino-propyl group loading of the parent AP material is 1.49 mmolg^{-1} which is consistent with the manufacturer specification of 1.50 - 2.0 mmolg^{-1}. Saliently, this value facilitated the reliable determination of receptor silica material functionalisation. Table 5.1 shows the silica surface amide condensation reaction with the mono-substituted triazole-B15C5 derivatives was more efficient relative to the bidentate receptors, which may be attributable to the considerable steric demand of reactions occurring at solid surfaces.

5.3.2 Preliminary Extraction Studies

The heteroditopic materials **1·XB^{S}**, **1·HB^{S}**, **2·XB^{S}** and **2·HB^{S}** were subjected to preliminary solid-liquid extraction experiments, specifically the extraction of sodium halide ion-pairs from aqueous solution. In a typical experiment a given quantity of the silica-based extractant material was exposed to a fixed volume of a 5 mM $NaX_{(aq)}$ solution (X=Cl^{-}, Br^{-}, I^{-}). To ensure for full equilibration of the extraction process, the mixture was subjected to agitation on a roller mixer over the course of 16 hours. After which time the respective solutions were centrifuged, filtered through a 0.45 µm syringe filter and the resulting solution subjected to inductively coupled plasma mass spectrometry (ICP-MS) and ion chromatography analysis against known standards facilitating quantitative determination of anion concentration before and after exposure to the functionalised silica-based materials. In all cases a depletion of X^{-} concentration was only observed when the materials were treated with sodium iodide solutions. This selectivity towards sodium iodide is most likely a consequence of 'Hofmeister bias' which correlates with the thermodynamic parameters of the sodium salts (e.g. respective

anion hydration and lattice enthalpies). Table 5.2 summarises the calculated iodide extraction per μmol of the materials in which extraction efficiency relative to **1·HB^S** is also presented for comparison.

Table 5.2 Summarised ICP-MS determined iodide extraction capabilities.

Material	Iodide extraction/ ppm μmol^{-1} [a]	Relative Extraction efficiency[b]
1·XB^S	0.0557	1.3
1·HB^S	0.0445	1
2·XB^S	0.330	7.4
2·HB^S	0.317	4.9

[a] Calculated from the ICP-MS measured depletion of iodide concentration in the post extraction solution for a given mass of extractant material used accounting for loading of heteroditopic receptor. [b] Iodide extraction capability relative to **1·HB^S**. Errors estimated to be 10%.

For the purposes of eliminating the possibility of non-specific adsorption of charged species to the silica materials, the parent unfunctionalised AP material was also subjected to the same procedures, however in all cases no depletion of counteranion was observed. Close inspection of the extraction performances reveals that the sodium iodide extraction capabilities of the bidentate heteroditopic receptor functionalised silica materials **2·XB^S** and **2·HB^S** are considerably enhanced (at least a four-fold enhancement) relative to their monodentate material analogues **1·XB^S** and **1·HB^S** despite their reduced receptor loading values. This increase in extraction efficiency between the mono- and bidentate systems can most likely be attributed to two main factors: (i) by multivalent effects arising from increased surface concentration of B15C5 cation binding moieties and iodotriazole XB donors and (ii) a sodium cation induced polarisation of the C-I, in effect 'switching on' the XB donor anion binding potency. Notably the observed, almost, two-fold increase in iodide extraction capability of **2·XB^S** relative to **2·HB^S** serves to highlight the superiority of XB over HB for cooperative sodium iodide extraction with bidentate heteroditopic receptor functionalisation.

5.4 Conclusions

In conclusion, a series of novel XB and HB heteroditopic receptors were synthesised, comprising of B15C5 cation binding groups covalently linked to either an iodo/proto triazole XB/HB donor. The appendage of an ethylparaben active ester group enabled the facile immobilisation of mono- and bidentate heteroditopic receptor systems to an amino-propyl functionalised QuadraSil^{TM} support via amide bond formation. Characterisation of the four extractant materials by ^{13}C CP/MAS-NMR NMR and FTIR spectroscopy confirmed the successful covalent functionalization of the silica based support. Furthermore, CHN elemental analysis of the isolated materials facilitated quantification of receptor loadings. Preliminary solid-liquid ICP-MS extraction studies with a range of sodium salts (NaX, X = Cl^-, Br^-, I^- and NO_3^-) revealed exclusive extraction of NaI, where the bidentate receptor functionalised materials **2·XB^S** and **2·HB^S** displayed significantly enhanced sodium iodide extraction capabilities relative to their monodentate analogues by at least a factor of 4. Crucially, the determined NaI extraction capability of the XB-based receptor **2·XB^S**, is enhanced two-fold relative to the HB analogue **2·HB^S**, which is attributed to a combination of enhanced XB-mediated NaI affinity and the unique through-bond co-bound cation induced polarisation mechanism observed in sigma-hole based heteroditopic receptor systems. These results not only serve to illustrate the advantages conferred by exploiting the unique nature of sigma-hole recognition behaviour, but in the context of functional materials demonstrates an exciting opportunity for the real-world application of sigma-hole mediated recognition in the context of salt recovery.

5.5 References

[1] A. J. McConnell, A. Docker, P. D. Beer, *ChemPlusChem* **2020**, *85*, 1824–1841.

[2] Q. He, G. I. Vargas-Zúñiga, S. H. Kim, S. K. Kim, J. L. Sessler, *Chem. Rev.* **2019**, *119*, 9753–9835.

[3] A. J. McConnell, P. D. Beer, *Angew. Chem. Int. Ed.* **2012**, *51*, 5052–5061.

[4] S. K. Kim, J. L. Sessler, *Chem. Soc. Rev.* **2010**, *39*, 3784–3809.

[5] B. Hua, L. Shao, Z. Zhang, J. Liu, F. Huang, *J. Am. Chem. Soc.* **2019**, *141*, 15008–15012.

[6] M. Zakrzewski, N. Kwietniewska, W. Walczak, P. Piątek, *Chem. Commun.* **2018**, *54*, 7018–7021.

[7] B. Akhuli, P. Ghosh, *Chem. Commun.* **2015**, *51*, 16514–16517.

[8] R. Molina-Muriel, G. Aragay, E. C. Escudero-Adán, P. Ballester, *J. Org. Chem.* **2018**, *83*, 13507–13514.

[9] E. N. W. Howe, M. Bhadbhade, P. Thordarson, *J. Am. Chem. Soc.* **2014**, *136*, 7505–7516.

[10] X. Chi, G. M. Peters, F. Hammel, C. Brockman, J. L. Sessler, *J. Am. Chem. Soc.* **2017**, *139*, 9124–9127.

[11] S. K. Kim, V. M. Lynch, N. J. Young, B. P. Hay, C.-H. Lee, J. S. Kim, B. A. Moyer, J. L. Sessler, *J. Am. Chem. Soc.* **2012**, *134*, 20837–20843.

[12] M. P. Wintergerst, T. G. Levitskaia, B. A. Moyer, J. L. Sessler, L. H. Delmau, *J. Am. Chem. Soc.* **2008**, *130*, 4129–4139.

[13] M. Denis, L. Qin, P. Turner, K. A. Jolliffe, S. M. Goldup, *Angew. Chem. Int. Ed.* **2018**, *57*, 5315–5319.

[14] M. Alfonso, I. Fernández, A. Tárraga, P. Molina, *Org. Lett.* **2015**, *17*, 2374–2377.

[15] K. Maity, D. K. Panda, R. J. Gallup, C. K. Choudhury, S. Saha, *Org. Lett.* **2018**, *20*, 962–965.

[16] M. Alfonso, A. Espinosa, A. Tárraga, P. Molina, *Chem. Commun.* **2012**, *48*, 6848–6850.

[17] M. Alfonso, A. Espinosa Ferao, A. Tárraga, P. Molina, *Inorg. Chem.* **2015**, *54*, 7461–7473.

[18] A. V. Koulov, J. M. Mahoney, B. D. Smith, *Org. Biomol. Chem.* **2003**, *1*, 27–29.

[19] C. C. Tong, R. Quesada, J. L. Sessler, P. A. Gale, *Chem. Commun.* **2008**, 6321–6323.

[20] M. G. Fisher, P. A. Gale, J. R. Hiscock, M. B. Hursthouse, M. E. Light, F. P. Schmidtchen, C. C. Tong, *Chem. Commun.* **2009**, 3017–3019.

[21] P. D. Beer, P. K. Hopkins, J. D. McKinney, *Chem. Commun.* **1999**, 1253–1254.

[22] J. M. Mahoney, K. A. Stucker, H. Jiang, I. Carmichael, N. R. Brinkmann, A. M. Beatty, B. C. Noll, B. D. Smith, *J. Am. Chem. Soc.* **2005**, *127*, 2922–2928.

[23] Z.-H. Sun, F.-F. Pan, Triyanti, M. Albrecht, G. Raabe, *Eur. J. Org. Chem.* **2013**, *2013*, 7922–7932.

[24] D. J. White, N. Laing, H. Miller, S. Parsons, P. A. Tasker, S. Coles, *Chem. Commun.* **1999**, 2077–2078.

[25] M. T. Reetz, C. M. Niemeyer, K. Harms, *Angew. Chem. Int. Ed. Engl.* **1991**, *30*, 1472–1474.

[26] Q. He, N. J. Williams, J. H. Oh, V. M. Lynch, S. K. Kim, B. A. Moyer, J. L. Sessler, *Angew. Chem. Int. Ed.* **2018**, *57*, 11924–11928.

[27] Q. He, Z. Zhang, J. T. Brewster, V. M. Lynch, S. K. Kim, J. L. Sessler, *J. Am. Chem. Soc.* **2016**, *138*, 9779–9782.

[28] A. Aydogan, D. J. Coady, S. K. Kim, A. Akar, C. W. Bielawski, M. Marquez, J. L. Sessler, *Angew. Chem. Int. Ed.* **2008**, *47*, 9648–9652.

[29] X. Chi, G. M. Peters, C. Brockman, V. M. Lynch, J. L. Sessler, *J. Am. Chem. Soc.* **2018**, *140*, 13219–13222.

[30] K. Ziach, M. Karbarz, J. Romański, *Dalton Trans.* **2016**, *45*, 11639–11643.

[31] J. Romanski, P. Piątek, *Chem. Commun.* **2012**, *48*, 11346–11348.

Chapter 6 Conclusions

Chapter 2 details a library of structurally homologous acyclic anion receptors containing ChB and XB donors integrated into a neutral 3,5-bis-triazole pyridine scaffold appended with various phenyl and electron-withdrawing fluoroaryl substituents. In the first receptor series, it was demonstrated that sigma-hole donors, and especially ChB donors, are highly sensitive to local electronic environments where dramatic augmentation of halide anion binding potency can be achieved by replacement of triazole appended phenyl substituents with electron withdrawing perfluorinated aryl analogues, whilst HB receptor analogues demonstrate no measurable change. Importantly, the through bond inductive electronic polarization mechanism of ChB sigma-hole donor potency is further explored through extensive ^{1}H NMR anion titration experiments, in which the systematic variation of electron-withdrawing/-donating properties of triazole appended- or directly Te-bound- aryl-substituents facilitated linear free energy relationship (LFER) Hammett plot analysis. It is noteworthy this revealed a remarkable range in ChB donor atom potency can be achieved (ca. 4 orders of magnitude in K_a values). Most importantly, this electronic tunability translates into modulating halide anion selectivity behaviour, presenting an unprecedented means of engineering potency and selectivity in sigma-hole anion receptor design.

Chapter 3 reports the synthesis of two ChB heteroditopic receptors containing tellurium ChB donors functionalised with B15C5 motifs integrated into a 3,5-bis-triazole nitrobenzene scaffold and their alkali metal cation-halide anion ion-pair recognition properties have been investigated via extensive ^{1}H NMR titration studies. It is demonstrated that K^+, Rb^+ and Cs^+ are capable of forming an intramolecular co-facial bis-B15C5 sandwich complex which not only serves to allosterically preorganise the Te centres for convergent anion binding, but to also inductively activate ChB donor anion binding potency via a cation induced through bond polarisation mechanism. Determined ion-pair association constant values reveal the perfluorinated aryl substituent functionalized ChB heteroditopic receptor binds KCl with high affinity and selectivity relative to all other alkali metal chlorides. This translates to the receptor's successful application as a proficient KCl selective solid-liquid and liquid-liquid extractant material. The ion pair binding mode is confirmed through X-ray structural analysis of KX (X= Cl, Br, I), RbI and CsI complexes, which demonstrate simultaneous alkali metal cation crown ether mediated binding and bifurcated ChB-halide anion interactions. The receptor's capability to exhibit selective KCl transport in liquid membrane studies, is particularly notable in the context of developing ionophores capable dissipating ion concentration gradients in biological systems for potential biomedical applications and demonstrates the first example of KCl selectivity exhibited by a heteroditopic receptor system.

Chapter 4 introduced a series of novel XB TPE-based anion receptors and demonstrated their anion recognition and sensing behaviour is dramatically dependent on the multivalent nature and relative orientation of the XB donor arms. Detailed investigation of the

XB-TPE systems by fluorescence spectroscopy, dynamic light scattering measurements, transmission electron microscopy and X-ray structural analysis showed the receptors are capable of forming chloride-anion assembled aggregates, concomitant with a dramatic enhancement in emission intensity. This anion coordination induced aggregation, mediated by halogen bonds, represents an unprecedented sensory signal transduction mechanism. In addition, the chapter also described the first example of a photo-switchable anion receptor that employs XB interactions for anion binding. It is noteworthy the contrasting anion recognition properties of the two geometric isomers was found to have a profound influence on the position of the photo-stationary state, in which the Z isomer is capable of strong halide binding, through chelating XB cooperativity.

Chapter 5 describes the synthesis of a series of novel solid-phase extraction materials, in which molecular XB-mediated heteroditopic receptors, comprised of iodotriazole XB donors appended with benzo-15-crown-5 cation binding units, are linked via covalent amide bond formation to QuadraSil™ silica-based supports. Investigation into the material's sodium iodide extraction capabilities from aqueous solution by ICP-MS demonstrated that an XB derivative impressively outperformed its HB analogue by a factor two. Importantly, these results serve to illustrate how the unique affinity and cooperativity behaviour of XB-mediated ion-pair recognition can be judiciously exploited towards industrially relevant applications such as salt extraction. This represents the first example of a solid-liquid XB heteroditopic extractant material and serves to further highlight the unique advantages conferred by the potential use of sigma-hole based molecular recognition in real-world applications.

In summary, the results of this thesis highlight the prodigious properties of ChB and XB interactions in the context of anion and ion-pair recognition. In addition, to the well-established increased potency of ChB- and XB-anion interactions relative to more traditional non-covalent interactions such as HB, it is evidenced that the unique electronic and geometric features of these σ-hole based interactions provide ample opportunity to further engineer anion selectivity in receptor design. However, to date thermodynamic and kinetic binding data regarding the intrinsic properties of ChB, XB and other σ-hole based interactions in solution phase supramolecular host-guest chemistry in general is sparse with extant studies providing only phenomenological information on the intrinsic nature of this family of non-covalent interactions. Future efforts should be directed towards fundamental investigations to establish the characteristic molecular recognition properties of these interactions, including solvent dependency and inherent anion selectivity trends.

Chapter 7 Experimental and Synthetic Procedures

7.1 General considerations

7.1.1 Chemicals and solvents

All solvents and reagents used in this thesis were purchased from commercial suppliers. Dry solvents were obtained by purging with nitrogen and then passing through an MBraun MPSP-800 column. Deionised water was collected from a Milli-Q$_r$ Millipore machine. TBA salts, Grubbs' I catalyst, Grubbs' II catalyst, $[Cu(MeCN)_4][PF_6]$ were stored in a vacuum desiccator containing phosphorus pentoxide prior to use. TBTA was synthesised and kept in the freezer after used. Triethylamine was distilled from a commercial package and stored over potassium hydroxide. Brine refers to a saturated aqueous solution of NaCl, $NH_4OH_{(aq.)}$ refers to a 28–30% solution of NH_3 in water. Column chromatography was carried out on Merck$_r$ silica gel 60 under a positive pressure of nitrogen, preparative TLC was performed on 20×20 cm plates, with a silica layer of thickness 1 mm.

7.1.2 Instrumentations

Routine NMR spectra were recorded on either a Varian Mercury 300, a Bruker AVIII 400 or a Bruker AVIII 500 spectrometer with 1H NMR titrations recorded on a Bruker AVIII 500 spectrometer. Chemical shifts are quoted in parts per million relative to the residual solvent peak with signal splittings denoted as singlet (s), doublet (d), triplet (t), quartet (quart.), quintet (quint.), septet (sep.) and multiplet (m). Mass spectra were carried out on Waters Micromass LCT and Bruker microTOF spectrometers.

7.2 ^{1}H-NMR titration protocols

7.2.1 Anion binding in organic and aqueous-organic mixture

Spectra for ^{1}H NMR titrations were recorded at 293 K on a Varian Unity Plus 500 spectrometer with ^{1}H operating at 500 MHz. Initial sample volumes were 0.50 mL and concentrations were 1.0 mM of host in all cases. Anion solution (50 mM) as the tetrabutylammonium salts were added in aliquots, the samples thoroughly shaken and spectra recorded. Spectra were recorded at 0, 0.2, 0.4, 0.6, 0.8, 1.0, 1.2, 1.4, 1.6, 1.8, 2.0, 2.5, 3.0, 4.0, 5.0, 7.0 and 10 equivalents of anion. In all cases where association constants were calculated, bound, and unbound species were found to be in fast exchange on the NMR timescale. In all cases where association constants were calculated, bound, and unbound species were found to be in fast exchange on the NMR timescale.

7.3 Synthetic Procedures and Characterisation for Compounds in Chapter 2

General Procedure 2.1

Freshly cleaned Mg turnings (10 mmol) were added a to dry round bottom flask to which was added a few iodine crystals under an atmosphere of nitrogen. The flask was heated until to the point at which purple iodine vapour appeared at which point heating was stopped. To this mixture was added anhydrous THF (20 ml) and left to stir for 10 minutes. After which time a

few drops of the appropriate aryl bromide was added and the mixture sonicated and stirred until the colour of the I_2 was no longer visible. After which the remaining aryl bromide was added dropwise (total 10 mmol) to the reaction mixture and upon completion left to stir for 1 hour. The reaction flask was subsequently opened and Te powder (10 mmol) was added in one portion. The reaction mixture was sonicated and stirred until a green colour appeared after which time the mixture was left to stir for a further hour. After which the mixture was diluted with sat. $NH_4Cl_{(aq)}$ (ca. 10 ml) and subsequently diluted with CH_2Cl_2 (150 ml), the organic phase was collected dried over $MgSO_4$ and the solvent removed in vacuo. The crude material was purified by column chromatography eluting with CH_2Cl_2/hexane mixtures. The target ditelluride, was isolated as a red/brown solid.

General Procedure 2.2

5 mmol of bromobenzene is added to a stirring solution of NaHTe (prepared from 10 mmol of tellurium powder and 0.45g of sodium borohydride in 20 ml of DMF heating to 90 °C for 0.5 hr). The mixture is stirred for 7 hr at 90°C, after which time 20 ml of water is added. The mixture is stirred for 0.5 hr in air. The mixture is diluted with Et_2O (300 ml) and water (300 ml), the organic phase collected and the aqueous washed with Et_2O (300 ml), the collected organic phases are dried over $MgSO_4$ and concentrated in vacuo and was purified by column chromatography eluting with CH_2Cl_2/hexane mixtures. The target ditelluride, was isolated as a red/brown solid.

2.7, **2.8**, **2.9**, **2.10**, **2.12**, **2.13**, **2.15**, **2.16** and **2.17** were synthesised according to general procedure 2.1.

2.11, and **2.14** were synthesised according to general procedure 2.2.

General Procedure 2.3

$[Cu(MeCN)_4]PF_6$ (0.2 equivalents) and TBTA (0.1 equivalents) were dissolved in the minimum amount anhydrous degassed CH_2Cl_2 (ca. 5 ml) and left to stir for 15 minutes. After which time the appropriate alkyne was added to the solution as a solid, followed by the appropriate phenyl azide (2.2 equivalents). Once complete, as determined by TLC analysis, the reaction mixture was diluted with CH_2Cl_2 (ca. 150 ml) and washed with EDTA/$NH_4OH_{(aq)}$ solution (20 ml) and water (50 ml), the collected organic phase was dried over $MgSO_4$ and concentrated to dryness and purified by 'flash' silica gel column chromatography the target products as solids.

General Procedure 2.4

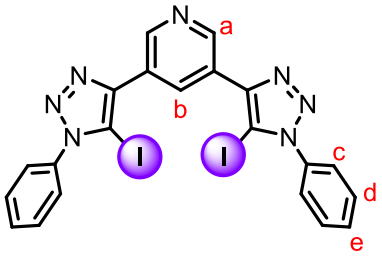
3,5-diethynyl pyridine (0.30 mmol) was dissolved in the minimum amount of MeOH (ca. 10mL) to which was added freshly ground $AgNO_3$ (2 equivalent per alkyne) followed by one drop of concentrated NH_4OH (ca. 0.1 mL) immediately inducing precipitation of the desired silver acetylide. The reaction mixture was left to stir for 30 minutes at room temperature, after which time the solvent was removed in vacuo. The silver acetylide was subsequently suspended in anhydrous THF (20 mL) under an atmosphere of nitrogen. In a separate flask the appropriate diorgano ditelluride R_2Te_2 (1 eq.) was dissolved in THF (5 ml) and cooled to 0°C, to the solution of the ditelluride 1 M of Br_2 in CH_2Cl_2 (1 eq.) was added dropwise, after which time the ditelluride solution darkened indicating the formation of RTeBr which was added immediately to the suspension of the silver acetylide dropwise. The reaction mixture was left to stir for 30 minutes at room temperature in the absence of light, after which time it was filtered through celite and the reaction mixture was concentrated to dryness in vacuo. The crude tellluromethyl/aryl alkyne was subjected to rapid column chromatography then used immediately for the following CuAAC reaction.

1·ChB^{Ph}, **1·XB^{Ph}**, **1·HB^{Ph}**, **1·ChB^{PFP}**, **1·XB^{PFP}**, **1·HB^{PFP}** were synthesised according to general procedure 2.3.

2·ChB^{mF}, **2·ChB^{2F}**, **2·ChB^{3F}** were synthesised according to general procedure 2.4.

3·ChB^{pOMe}, **3·ChB^{pMe}**, **3·ChB^{pCl}**, **3·ChB^{mF}**, **3·ChB^{mCF3}**, **3·ChB^{pCF3}**, **3·ChB^{Ph}**, **3·ChB^{pF}**, **3·ChB^{2F}**, **3·ChB^{3F}**, **3·ChB^{2CF3}** were synthesised according to general procedure 2.4 followed by 2.3.

1·XB^{Ph}



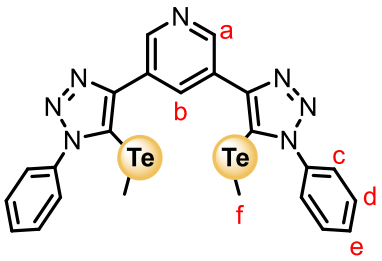
Isolated as a white solid (39%).

^{1}H NMR (400 MHz, $CDCl_3$) δ = 9.38 (s, $2H_a$), 9.09 (s, $1H_b$), 7.63 – 7.58 (m,$10H_{c,d,e}$).

^{13}C NMR (126 MHz, $CDCl_3$) δ = 148.55, 147.69, 136.92, 133.59, 130.63, 129.64, 126.64, 126.39, 78.78.

HRMS (ESI +ve) m/z: 617.9390, ($[M+H]^+$, $C_{21}H_{14}N_7I_2$ requires 617.9395).

1·ChB^{Ph}



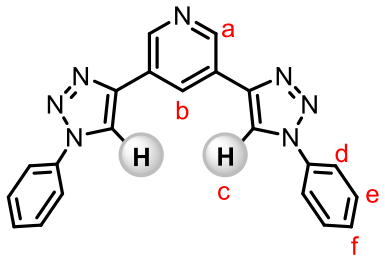
Isolated as a white solid (70%).

^{1}H NMR (400 MHz, $CDCl_3$) δ = 9.31 (d, *J* = 2.1 Hz, $2H_a$), 8.99 (t, *J* = 2.1 Hz, $1H_b$), 7.60 (s, $10H_{c,d,e}$), 1.85 (s, $6H_f$).

^{13}C NMR (126 MHz, $CDCl_3$) δ = 150.91, 148.79, 137.91, 134.86, 130.17, 129.48, 127.43, 126.40, 100.77, -12.80.

HRMS (ESI +ve) m/z: 649.9868, ($[M+H]^+$, $C_{23}H_{20}N_7Te_2$ requires 649.9870).

1·HB^{Ph}



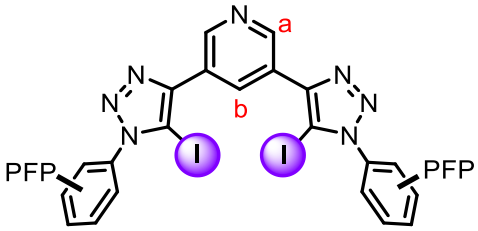
Isolated as a white solid (41%).

^{1}H NMR (400 MHz, $CDCl_3$) δ = 9.16 (d, *J* = 2.1 Hz, $2H_a$), 8.80 (t, *J* = 2.1 Hz, $1H_b$), 8.40 (s, $2H_c$), 7.84 (d, *J* = 7.5 Hz, $4H_d$), 7.60 (t, *J* = 7.6 Hz, $4H_e$), 7.51 (t, *J* = 7.3 Hz, $2H_f$).

^{13}C NMR (126 MHz, DMSO) δ = 146.07, 144.21, 136.53, 130.05, 129.01, 128.63, 126.58, 120.82, 120.15.

HRMS (ESI +ve) m/z: 366.1464, ($[M+H]^+$, $C_{21}H_{16}N_7$ requires 366.1462).

1·XB^{PFP}



Isolated as a white solid (78%).

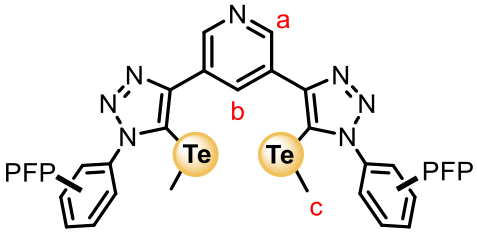
^{1}H NMR (400 MHz, $CDCl_3$) δ = 9.42 (s, $2H_a$), 9.11 (t, *J* = 2.1 Hz, $1H_b$).

^{13}C NMR (126 MHz, $CDCl_3$) δ = 148.48, 147.78, 143.77 (dm, *J* = 260 Hz), 138.20 (dm, *J*= 260 Hz), 133.12, 125.69, 112.24 (td, *J* = 14.6 Hz, *J* = 4.0 Hz,) 81.37. (Peak missing due to C-F coupling).

^{19}F NMR (376 MHz, $CDCl_3$) δ = -141.58 – -142.69 (m), -146.57 (tt, *J* = 21.4, 3.6 Hz), -158.00 – -159.39 (m).

HRMS (ESI +ve) m/z: 797.8443, ($[M+H]^+$, $C_{21}H_4N_7F_{10}I_2$ requires 797.8452).

1·ChB^{PFP}



Isolated as a white solid (81%).

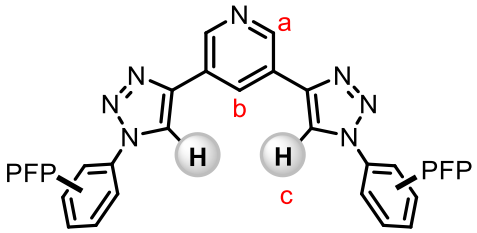
^{1}H NMR (400 MHz, $CDCl_3$) δ = 9.48 (d, *J* = 2.2 Hz, $2H_a$), 9.24 (s, $1H_b$), 2.06 (s, $6H_c$).

^{13}C NMR (126 MHz, DMSO) δ = 149.95, 148.06, 142.97 (dm, $^{1}J_{CF1or2or3}$ = 254 Hz), 137.68 (dm, $^{1}J_{CF1or2or3}$ = 256 Hz), 133.38, 126.55, 113.01 – 112.76 (m, 2C) 109.44, -11.37. (Peak missing due to C-F coupling).

^{19}F NMR (376 MHz, $CDCl_3$) δ = -143.00 – -143.18 (m), -147.83 (t, *J* = 21.3 Hz), -159.35 (tt, *J* = 21.0, 5.6 Hz).

HRMS (ESI +ve) m/z: 829.8922, ($[M+H]^+$, $C_{23}H_{10}N_7F_{10}Te_2$ requires 829.8721).

1·HB^{PFP}



Isolated as a white solid (32%).

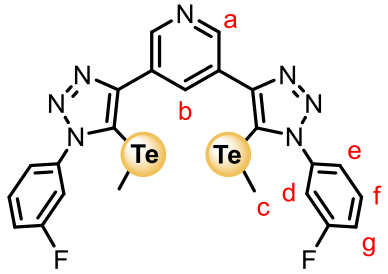
^{1}H NMR (400 MHz, $CDCl_3$) δ = 9.22 (s, $2H_a$), 8.87 (s, $1H_b$), 8.31 (s, $2H_c$).

^{13}C NMR (126 MHz, $CDCl_3$) δ = 147.23, 144.98, 142.64 (dm, *J* = 258 Hz) 138.33 (dm, *J* = 258 Hz), 130.69, 126.13, 122.89, 112.88 (td, *J* = 14.1 Hz, *J* = 4.1 Hz) (Peak missing due to C-F coupling).

^{19}F NMR (376 MHz, $CDCl_3$) δ = -145.17 – -145.32 (m), -148.89 – -149.05 (m), -158.70 – -158.91 (m).

HRMS (ESI +ve) m/z: 546.0517, ($[M+H]^+$, $C_{21}H_6N_7F_{10}$ requires 546.0520).

2·ChB^{mF}



Isolated as a white solid (72%).

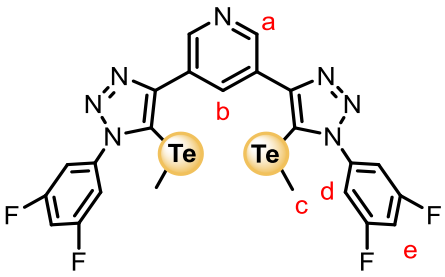
^{1}H NMR (400 MHz, DMSO) δ 9.24 (d, *J* = 2.2 Hz, 2H$_a$), 8.99 (t, *J* = 2.2 Hz, 1H$_b$), 7.81 – 7.35 (m, 8H$_{d,e,f,g}$), 1.78 (s, 6H$_c$).

^{13}C NMR (101 MHz, DMSO) δ 162.92, 160.48, 149.64,147.90, 138.98 (m), 131.05 (m), 127.28, 122.96, 116.97 (m), 114.30 (m), 105.90, -11.36

^{19}F NMR (377 MHz, DMSO) δ -106.50.

HRMS (ESI +ve) m/z: 685.9679, ([M+H]$^+$, $C_{23}H_{18}N_7F_2Te_2$ requires 685.9682).

2·ChB^{2F}



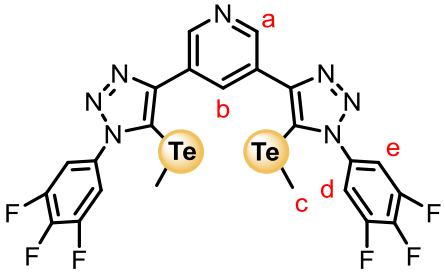
Isolated as a white solid (70%).

^{1}H NMR (400 MHz, $CDCl_3$) δ 9.26 (d, *J* = 2.2 Hz, 2H$_a$), 9.00 (t, *J* = 2.2 Hz, 1H$_b$), 7.67 – 7.57 (m, 6H$_{d,e}$), 1.80 (s, 6H$_c$).

^{19}F NMR (377 MHz, CDCl3) δ -102.65 – -103.94 (m).

HRMS (ESI +ve) m/z: 721.9489, ([M+H]$^+$, $C_{23}H_{16}N_7F_4Te_2$ requires 721.9493).

2·ChB^{3F}



Isolated as a white solid (65%).

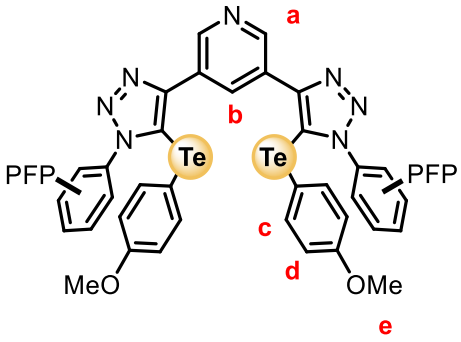
^{1}H NMR (500 MHz, DMSO) δ 9.26 (d, *J* = 2.1 Hz, 2H$_a$), 9.01 (t, *J* = 2.1 Hz, 1H$_b$), 7.94 (dd, *J* = 8.1, 6.2 Hz, 4H), 1.80 (s, 6H).

^{13}C NMR (126 MHz, DMSO) δ 149.98 (dm, *J* = 257 Hz), 149.59, 147.80, 141.03, 133.23, 127.17, 113.28 – 112.65 (m), 106.65, -11.15.

^{19}F NMR (470 MHz, DMSO) δ -133.19 (d, *J* = 22.4 Hz), -158.26 (t, *J* = 22.4 Hz).

HRMS (ESI +ve) m/z: 759.9309, ([M+H]$^+$, $C_{23}H_{14}F_6N_7Te_2$ requires 759.9316).

3·ChB^{pOMe}



Isolated as a white solid (72%).

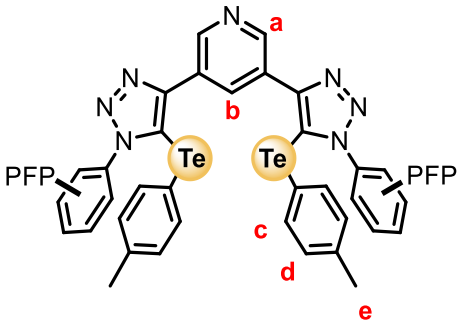
^{1}H NMR (400 MHz, $CDCl_3$) δ 9.28 (d, *J* = 2.2 Hz, 2H$_a$), 8.87 (t, *J* = 2.2 Hz, 1H$_b$), 7.42 – 7.32 (m, 4H$_c$), 6.71 – 6.55 (m, 4H$_d$), 3.75 (s, 6H$_e$).

^{13}C NMR (151 MHz, $CDCl_3$) δ 161.23, 150.68, 149.04, 144.07 (d, *J* = 12.9 Hz), 143.76 (dm, *J* = 261 Hz), 143.19 (dm, *J* = 267 Hz), 142.30 (t, *J* = 13.5 Hz), 141.01, 138.81 (d, *J* = 13.8 Hz), 137.96 (dm, *J* = 257 Hz), 137.11 (d, *J* = 13.5 Hz), 134.85, 126.61, 116.02, 113.53 (t, *J* = 13.9 Hz), 107.19, 100.34, 55.42.

^{19}F NMR (377 MHz, $CDCl_3$) δ -141.04 – -143.08 (m), -148.68 (td, *J* = 21.6, 3.1 Hz), -160.01.

HRMS (ESI +ve) m/z: 1013.9451, ([M+H]$^+$, $C_{35}H_{17}N_7F_{10}O_2Te_2$ requires 1013.9452).

3·ChB^{pMe}



Isolated as a white solid (70%).

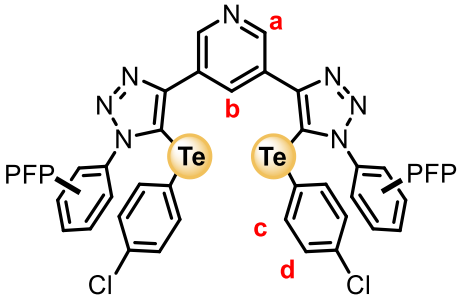
^{1}H NMR (400 MHz, $CDCl_3$) δ 9.28 (d, *J* = 2.1 Hz, $2H_a$), 8.87 (t, *J* = 2.1 Hz, $1H_b$), 7.37 – 7.27 (m, $4H_c$), 7.02 – 6.81 (m, $4H_d$), 2.30 (s, $6H_e$).

^{13}C NMR (151 MHz, $CDCl_3$) δ 150.89, 149.06, 143.72 (dm, *J* = 260 Hz), 143.18 (dm, *J* = 260 Hz), 140.40, 138.73, 137.08 (m), 134.78, 130.98, 126.57, 113.48 (t, *J* = 13.9 Hz), 107.43, 106.97, 21.29.

^{19}F-NMR (377 MHz, $CDCl_3$) δ = -142.12 – -142.29 (m), -148.38 (dd, *J* = 21.8, 3.2 Hz), -159.56 – -159.85 (m).

HRMS (ESI +ve) m/z: 983.9568, ($[M+H]^+$, $C_{35}H_{18}N_7F_{10}Te_2$ requires 983.9571).

3·ChB^{pCl}



Isolated as a white solid (51%).

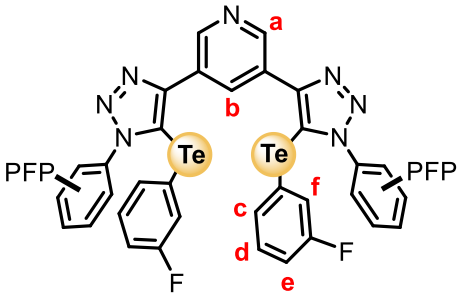
^{1}H NMR (400 MHz, $CDCl_3$) δ 9.29 (d, *J* = 2.1 Hz, $2H_a$), 8.89 (t, *J* = 2.2 Hz, $1H_b$), 7.36 – 7.28 (m, $2H_c$), 7.20 – 7.05 (m, $2H_d$).

^{13}C NMR (151 MHz, $CDCl_3$) δ 151.33, 149.11, 143.76, (dm, *J* = 254 Hz), 143.36, (dm, *J* = 261 Hz), 139.24, 138.21 (dm, *J* = 261 Hz), 136.59, 134.81, 130.52, 126.38, 109.31, 106.81.

^{19}F NMR (377 MHz, $CDCl_3$) δ -141.62 – -143.23 (m), -148.81 (td, *J* = 21.5, 3.1 Hz).

HRMS (ESI +ve) m/z: 1023.8447, ($[M+H]^+$, $C_{33}H_{12}Cl_2N_7F_{10}Te_2$ requires 1023.8473).

3·ChB^{mF}



Isolated as a white solid (80%).

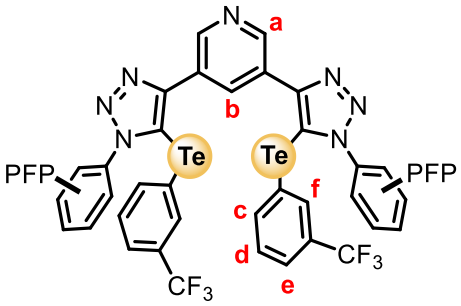
^{1}H NMR (500 MHz, $CDCl_3$) δ 9.30 (d, *J* = 2.1 Hz, $2H_a$), 8.94 (t, *J* = 2.1 Hz, $1H_b$), 7.19 – 7.05 (m, $6H_{c,d,e}$), 6.98 (ddt, *J* = 7.7, 6.6, 1.6 Hz, $2H_f$).

^{13}C NMR (126 MHz, $CDCl_3$) δ 162.74 (d, *J* = 253.8 Hz), 151.52, 149.19, 143.67 (d, *J* = 223 Hz), 136.84 (d, *J* = 25.5 Hz), 134.81, 133.25 (d, *J* = 3.3 Hz), 131.61 (d, *J* = 7.5 Hz), 126.32, 124.43 (d, *J* = 22.1 Hz), 116.95 (d, *J* = 20.8 Hz), 112.55 (d, *J* = 5.7 Hz), 106.67.

^{19}F NMR (470 MHz, $CDCl_3$) δ -109.55 (dd, *J* = 8.0, 5.3 Hz), -139.23 – -143.79 (m), -147.76 (td, *J* = 21.8, 3.4 Hz), -154.98 – -162.37 (m).

HRMS (ESI +ve) m/z: 989.9042, ($[M+H]^+$, $C_{33}H_{12}N_7F_{12}Te_2$ requires 989.9052.

3·ChB^{mCF3}



Isolated as a white solid (45%).

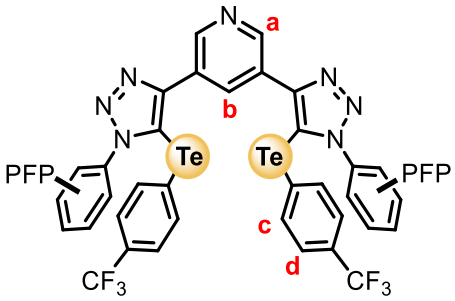
^{1}H NMR (500 MHz, $CDCl_3$) δ 9.32 (d, *J* = 2.1 Hz, $2H_a$), 8.98 (t, *J* = 2.2 Hz, $1H_b$), 7.70 –7.52 (m, $6H_{c,e,f}$), 7.29 (t, *J* = 7.7 Hz, $2H_d$).

^{13}C NMR (126 MHz, $CDCl_3$) δ 151.43, 149.18, 143.66 (d, *J* = 276 Hz), 141.23, 137.92 (d, *J* = 252 Hz), 134.79, 134.33 (q, *J* = 3.7 Hz), 132.31 (q, *J* = 32.8 Hz), 130.68, 126.53 (q, *J* = 3.6 Hz), 126.32, 124.16, 121.99, 112.29, 106.44.

^{19}F-NMR (470 MHz, $CDCl_3$) δ -63.20, -138.46 – -144.86 (m), -147.36 (d, *J* = 21.4 Hz), -155.74 – -162.59 (m).

HRMS (ESI +ve) m/z: 1089.8979, ($[M+H]^+$, $C_{35}H_{11}N_7F_{16}Te_2$ requires 1089.8989).

3·ChB^{pCF3}



Isolated as a white solid (64%).

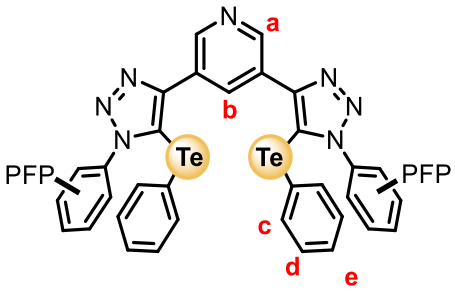
^{1}H NMR (500 MHz, CDCl3) δ 9.30 (d, *J* = 2.1 Hz, 2H$_a$), 8.93 (t, *J* = 2.1 Hz, 1H$_b$), 7.47 (d, *J* = 8.0 Hz, 2H$_c$), 7.38 (d, *J* = 8.0 Hz, 2H$_d$).

^{13}C NMR (126 MHz, $CDCl_3$) δ 151.68, 149.13, 144.74 (dm, *J* = 255 Hz), 143.36 (dm, *J* = 260 Hz), 137.99 (dm, *J* = 262 Hz), 137.09 , 134.73, 131.60 (q, *J* = 32.9 Hz), 126.80 (q, *J* = 3.6 Hz), 126.28, 124.64, 122.47, 120.31, 117.12, 113.92 – 112.86 (m), 106.49.

^{19}F NMR (470 MHz, CDCl3) δ -63.28, -142.51 (dd, *J* = 29.4, 10.4 Hz), -145.09 – -151.40 (m), -156.50 – -162.59 (m).

HRMS (ESI +ve) m/z: 1089.8981, ($[M+H]^+$, $C_{35}H_{11}N_7F_{16}Te_2$ requires 1089.8989).

3·ChB^{Ph}



Isolated as a white solid (65%).

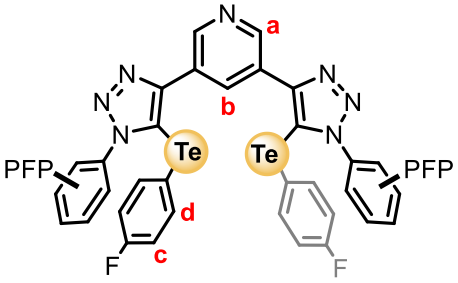
^{1}H NMR (500 MHz, $CDCl_3$) δ = 9.31 (d, *J* = 2.1 Hz, 2H$_a$), 9.03 (t, *J* = 2.1 Hz, 1H$_b$), 7.41 (dd, *J* = 8.1, 1.3 Hz, 4H$_c$), 7.34 – 7.27 (m, 2H$_e$), 7.18 – 7.10 (m, 4H$_d$).

^{13}C NMR (126 MHz, $CDCl_3$) δ = 150.61, 147.69, 143.71 (dm, *J* = 258 Hz), 143.28 (dm, *J* = 261 Hz), 138.25, 137.92 (dm, *J* = 255 Hz), 135.65, 130.26, 129.80, 127.07, 113.34 (td, *J* = 16.4 Hz, *J* = 3.8 Hz, 2C), 111.55, 107.25.

^{19}F NMR (377 MHz, $CDCl_3$) δ = -142.12 – -142.29 (m), -148.38 (dd, *J* = 21.8, 3.2 Hz), -159.56 – -159.85 (m).

HRMS (ESI +ve) m/z: 953.9233, ($[M+H]^+$, $C_{33}H_{14}N_7F_{10}Te_2$ requires 953.9241).

3·ChB^{pF}



Isolated as a white solid (63%).

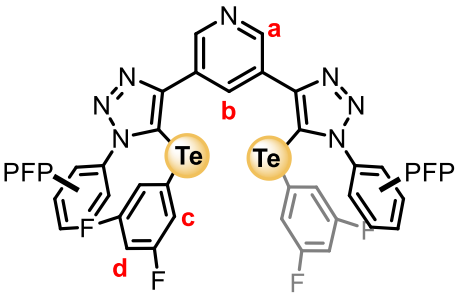
^{1}H NMR (400 MHz, $CDCl_3$) δ = 9.32 (d, *J* = 2.2 Hz, $2H_a$), 8.96 (s, $1H_b$), 7.42 (dd, *J* = 8.7, 5.4 Hz, $4H_c$), 6.86 (t, *J* = 8.6 Hz, $4H_d$).

^{13}C NMR (126 MHz, $CDCl_3$) δ = 163.87 (d, *J* = 252 Hz,), 150.79, 148.16, 143.76 (dm, *J*= 259 Hz), 143.36 (dm, *J* = 260 Hz), 140.78 (d, *J* = 8.9 Hz,), 137.99 (dm, *J* = 261 Hz), 135.45, 126.82, 117.83 (d, *J* = 21.4 Hz), 113.33 (td, *J* = 14.5 Hz, *J* = 4.0 Hz,), 107.18, 105.48 (d, *J* = 3.8 Hz).

^{19}F NMR (376 MHz, $CDCl_3$) δ = -109.17, -142.46 (dt, *J* = 21.7, 4.9 Hz), -147.75 (t, *J* = 21.6 Hz), -159.40 (dd, *J* = 21.5, 17.1 Hz).

HRMS (ESI +ve) m/z: 989.9042, ($[M+H]^+$, $C_{33}H_{12}N_7F_{12}Te_2$ requires 989.9052.

3·ChB^{2F}



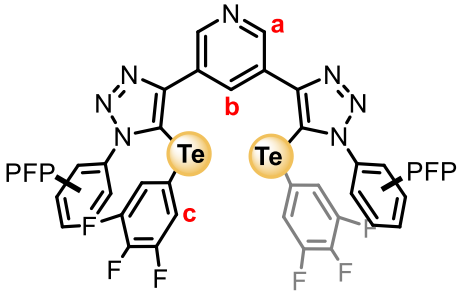
Isolated as a white solid (67%).

^{1}H NMR (400 MHz, $CDCl_3$) δ = 9.36 (d, *J* = 2.1 Hz, $2H_a$), 9.12 (s, $1H_b$), 6.88 (ddd, *J* = 5.0, 2.3, 1.1 Hz, $4H_c$), 6.73 (tt, *J* = 8.8, 2.3 Hz, $2H_d$).

^{13}C NMR (126 MHz, $CDCl_3$) δ = 163.21 (dd, *J* = 257 Hz, *J* = 11.3 Hz,), 151.38, 148.22, 143.61 (dm, *J* = 257 Hz), 143.54 (dm, *J* = 263 Hz), 138.05 (dm, *J* = 257 Hz), 135.50, 126.67, 119.79 (dd, *J* = 20.2 Hz, *J* = 6.3 Hz), 113.24 (t, *J* = 7.56 Hz,), 113.08 – 112.93 (m,), 106.70, 105.64 (t, *J* = 25.2 Hz)

HRMS (ESI +ve) m/z: 1025.8853, ($[M+H]^+$, $C_{33}H_{10}N_7F_{14}Te_2$ requires 1025.8864.

3·ChB^{3F}



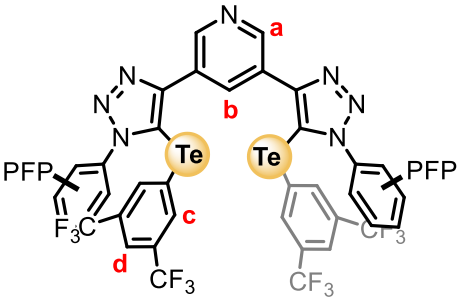
Isolated as a white solid (54%).

^{1}H NMR (400 MHz, $CDCl_3$) δ = 9.37 (d, *J* = 2.1 Hz, $2H_a$), 9.10 (t, *J* = 2.1 Hz, $1H_b$), 7.07 – 6.99 (m, $4H_c$).

^{13}C NMR (126 MHz, $CDCl_3$) δ = 151.73 (ddd, *J* = 259 Hz, *J* = 10.1 Hz, *J* = 3.78 Hz), 151.34, 148.42, 143.73 (dm, *J* = 258 Hz), 143.60 (dm, *J* = 262 Hz), 141.07 (dt, *J* = 258 Hz, *J* = 15.1 Hz), 138.11 (dm, *J* = 258 Hz), 135.41, 126.54, 121.80 (dd, *J* = 16.4 Hz, *J* = 5.04 Hz), 113.05 (td, *J* = 14.2 Hz, *J* = 3.4 Hz), 106.69, 104.26 – 104.14 (m, 2C).

HRMS (ESI +ve) m/z: 1061.8662, ($[M+H]^+$, $C_{33}H_8N_7F_{18}Te_2$ requires 1061.8676.

3·ChB^{2CF3}



Isolated as a white solid (81%).

^{1}H NMR (500 MHz, $CDCl_3$) δ = 9.38 (d, *J* = 2.1 Hz, $2H_a$), 9.17 (t, *J* = 2.1 Hz, $1H_b$), 7.83 (d, *J* = 1.6 Hz, $4H_c$), 7.79 (s, $2H_d$).

^{13}C NMR (126 MHz, $CDCl_3$) δ = 151.04, 147.97, 143.64 (dm, *J*= 262 Hz), 138.07 (dm, *J* = 255 Hz), 137.31 (d, *J* = 3.8 Hz), 135.61, 133.24 (q, *J* = 34.0 Hz), 126.74, 123.68 – 123.59 (m), 122.31 (q, *J* = 273 Hz,), 113.62, 113.01 – 112.72 (m), 106.35. (Missing signal due to coalescence).

^{19}F NMR (376 MHz, $CDCl_3$) δ = -63.39, -142.76 – -142.92 (m), -145.42 (dt, *J* = 19.1, 3.6 Hz), -146.77 (tt, *J* = 21.2, 3.4 Hz), -149.20 (tt, *J* = 21.2, 2.7 Hz), -158.76 – -159.10 (m).

HRMS (ESI +ve) m/z: 1225.8724, ($[M+H]^+$, $C_{37}H_{10}N_7F_{22}Te_2$ requires 1225.8736.

7.4 Synthetic Procedures and Characterisation for Compounds in Chapter 3

General Procedure 3.1

1,3-diethynyl-5-nitrobenzene (0.30 mmol) was dissolved in the minimum amount of MeOH (ca. 10mL) to which was added freshly ground $AgNO_3$ (1 equivalent per alkyne) followed by one drop of concentrated NH_4OH (ca. 0.1 mL) immediately inducing precipitation of the desired silver acetylide. The reaction mixture was left to stir for 30 minutes at room temperature, after which time the solvent was removed in vacuo. The silver acetylide was subsequently suspended in anhydrous THF (20 mL) under an atmosphere of nitrogen. In a separate flask the appropriate diorgano ditelluride R_2Te_2 (1 eq.) was dissolved in THF (5 ml) and cooled to 0°C, to the solution of the ditelluride 1 M of Br_2 in CH_2Cl_2 (1 eq.) was added dropwise, after which time the ditelluride solution darkened indicating the formation of RTeBr which was added immediately to the suspension of the silver acetylide dropwise. The reaction mixture was left to stir for 30 minutes at room temperature in the absence of light, after which time it was filtered through celite and the reaction mixture was concentrated to dryness in vacuo. The crude telluromethyl/aryl alkyne was subjected to rapid column chromatography then used immediately for the following CuAAC reaction.

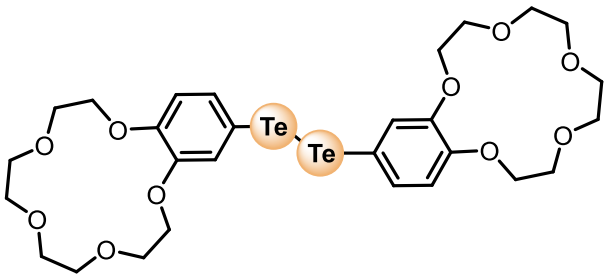
General Procedure 3.2

$[Cu(MeCN)_4]PF_6$ (0.2 equivalents) and TBTA (0.1 equivalents) were dissolved in the minimum amount anhydrous degassed CH_2Cl_2 (ca. 5 ml) and left to stir for 15 minutes. After which time the appropriate iodoalkyne was added to the solution as a solid, followed by the appropriate phenyl azide (2.2 equivalents). Once complete, as determined by TLC analysis, the reaction mixture was diluted with CH_2Cl_2 (ca. 150 ml) and washed with EDTA/$NH_4OH_{(aq)}$ solution (20 ml) and water (50 ml), the collected organic phase was dried over $MgSO_4$ and concentrated to dryness and purified by 'flash' silica gel column chromatography the target products as solids.

3.9 was synthesised according to general procedure 2.2.

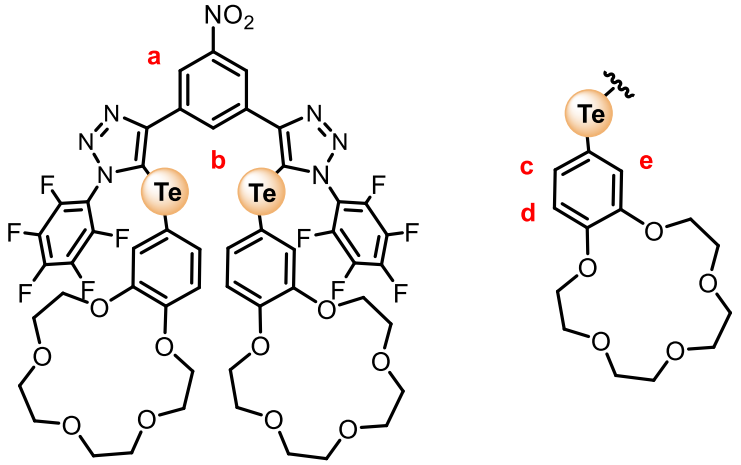
1·ChB^{PFP}and **1·ChB^{Ph}** were synthesized according to general procedure 3.1 followed by 3.2.

3.9



^{1}H NMR (400 MHz, $CDCl_3$) δ 7.30 (dd, *J* = 8.1, 1.8 Hz, 2H), 7.26 (s, 2H), 6.66 (d, *J* = 8.1 Hz, 2H), 4.15 – 4.04 (m, 8H), 3.98 – 3.84 (m, 8H), 3.75 (d, *J* = 1.8 Hz, 16H).

1·ChB^{PFP}



Isolated as a light yellow solid (72%).

^{1}H NMR (500 MHz, $CDCl_3$) δ 9.15 (t, *J* = 1.7 Hz, 1H_b), 8.98 (d, *J* = 1.7 Hz, 2H), 7.05 (dd, *J* = 8.2, 1.8 Hz, 2H_c), 7.00 (d, *J* = 1.9 Hz, 2H_e), 6.60 (d, *J* = 8.2 Hz, 2H_d), 4.05 (t, *J* = 4.3 Hz, 4H), 3.95 (t, *J* = 4.3 Hz, 4H), 3.87 (t, *J* = 4.3 Hz, 4H), 3.82 (t, *J* = 4.3 Hz, 4H), 3.71 (m, 16H).

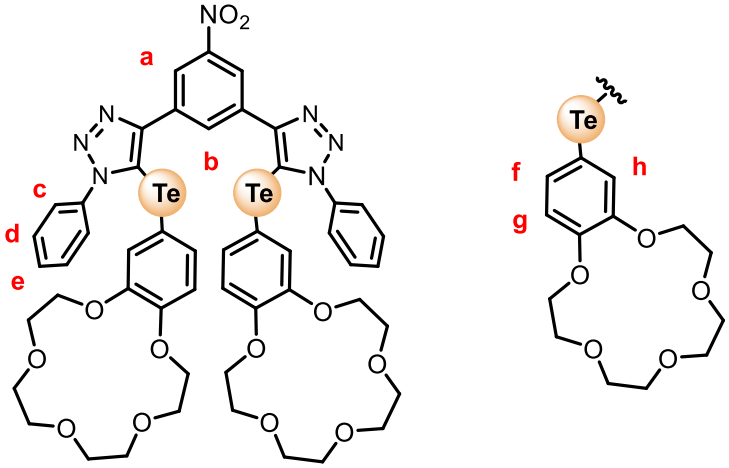
^{13}C NMR (126 MHz, $CDCl_3$) δ 151.25, 151.08, 150.09, 148.65, , 143.81 (dm, *J* = 252 Hz), 143.31 (dm, *J* = 258Hz), 138.01 (dm, *J* = 253Hz), 133.25, 133.18, 132.67, 124.48, 122.85, 114.72, 113.56 (m), 107.65, 100.39, 71.25, 70.56, 70.48, 69.42, 69.26, 68.87.

^{19}F NMR (470 MHz, $CDCl_3$) δ -141.84 – -142.89 (m), -148.06 (t, *J* = 21.5 Hz), -159.63 (dd, *J* = 21.7, 17.3 Hz).

^{125}Te NMR (126 MHz, $CDCl_3$) δ 498.60 (t, *J* = 28.7 Hz).

HRMS (ESI +ve) m/z: 1380.0784, ($[M+H]^+$, $C_{50}H_{41}F_{10}N_7O_{12}Te_2$ requires 1380.0833).

1·ChB^{Ph}



Isolated as a light yellow solid (68%).

^{1}H NMR (500 MHz, $CDCl_3$) δ 8.98 (s, 1H_b), 8.87 (s, 2H_a), 7.61 – 7.51 (m, 6$H_{c,e}$), 7.51 – 7.40 (m, 4H_a), 6.94 (d, *J* = 8.2 Hz, 2H_f), 6.87 – 6.81 (m, 2H_h), 6.53 (d, *J* = 8.2 Hz, 2H_g), 4.02 (m, 4H), 3.93 – 3.76 (m, 12H), 3.70 (m, 16H).

^{13}C NMR (126 MHz, $CDCl_3$) δ 151.57, 150.53, 149.68, 148.30, 137.90, 134.08, 133.30, 132.96, 130.16, 129.33, 126.88, 124.15, 122.91, 114.82, 105.46, 102.30, 71.19, 70.53, 70.50, 69.43, 69.11, 68.82.

^{125}Te NMR (126 MHz, $CDCl_3$) δ 492.70 (t, *J* = 29.7 Hz).

HRMS (ESI+ve) m/z: 1198.1764 ($[M+H]^+$, $C_{50}H_{52}N_7O_{12}Te$ requires 1198.1764).

Solid-Liquid Extraction (SLE) Procedure

A 2 mM solution of the receptor in $CDCl_3$ (0.7 ml) was exposed to an excess (ca. 5 equivalents) of a microcrystalline sample of the alkali-metal salt. The mixture was sonicated for 10 minutes, after which the solution was removed and passed through a syringe filter and the ^1H NMR spectrum recorded.

Liquid-Liquid Extraction (LLE) Procedure

In a typical experiment a $CDCl_3$ solution of the receptor (0.7 ml) was added to a D_2O solution of the alkali metal salt (0.7 ml), to which was added a stirrer bar and the mixture was stirred vigorously for 30 mins. After which time the biphasic mixture was allowed to settle, the organic phase removed and the ^1H NMR spectrum recorded.

Liquid Membrane Transport Studies

The chloride selective electrode (Thermo Scientific™ Orion™ ionplus® Sure-Flow® Solid State Combination ISE) was soaked in 1000 ppm chloride for extended periods (>1 hr) until readings were stable. Before each run, the electrode was calibrated by recording the potential of known chloride concentrations. The readings (mV) were converted to chloride activity using the modified Nernst equation ($y = a - \ln(x + c)$), where x is chloride activity, y is potential (mV) and a and b are parameters to be determined and c=0.

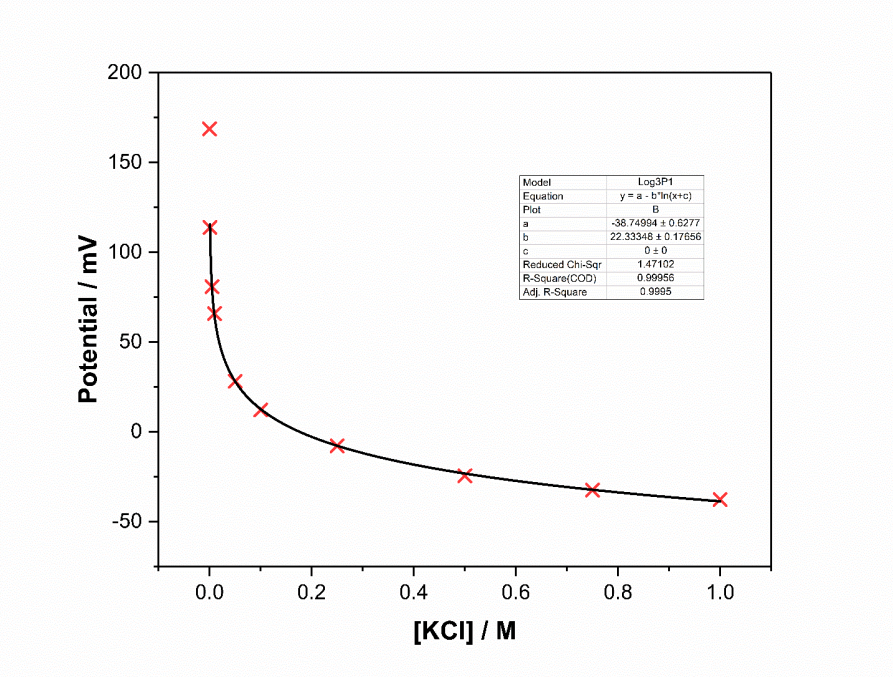


Figure 7.1 Chloride selective electrode calibration curve, experimental data indicated by red crosses and solid line indicating fitting.

In general U-tube transport experiments were conducted as follows: A stirrer bar was place in the bottom of the U-tube 30 ml of an 8 mM $CHCl_3$ receptor solution was syringed into the U-tube. On the left hand side was added 15 ml of distilled water (receivingg phase) and on the right hand side was added 15 ml 4 M $MCl_{(aq)}$ (source phase). The stirring speed was set at 600 rpm. The chloride selective electrode was immersed in the receiving phase at 0, 1, 5, 12, 18, 24 36 hours after set up and the potential recorded.

7.5 Synthetic Procedures and Characterisation for Compounds in Chapter 4

General Procedure 4.1

The appropriate benzoic acid (30 mmol) was suspended in anhydrous CH_2Cl_2 (50 ml) to which was added oxalyl chloride (25.7 ml, 300 mmol) and 3 drops of DMF, the reaction mixture was stirred under ambient conditions until homogenous. After which the mixture was concentrated to dryness, the resultant solid was dissolved in either benzene or bromobenzene (50 ml) to which was added $AlCl_3$ (4.00 g, 30 mmol), the reaction mixture was heated to 70°C for approximately 16 hours. After which time the reaction mixture was carefully quenched by the addition of H_2O (50 ml) and diluted with CH_2Cl_2 (300 ml) the organic phase was collected and washed with H_2O (3 × 50 ml). The organic phase was dried over $MgSO_4$ and the solvent removed in vacuo, the crude mixture was purified by silica gel column chromatography (CH_2Cl_2), affording a white solid.

General Procedure 4.2

To a THF solution (50 ml) of diphenylmethane (9.00 g, 53.5 mmol) at 0°C was added a 1.6 M solution of n-BuLi in hexanes (36.8 ml, 58.9 mmol) and left to stir at that temperature for 1 hour. After which a THF solution (50 ml) of the appropriate ketone (53.5 mmol) was added dropwise and left to stir at room temperature for 3 hours. After which time the reaction mixture was quenched by the addition of H_2O (1 ml) and concentrated *in vacuo* to an oily residue, which was resuspended in toluene (ca. 100 ml) and to this mixture was added $TsOH \cdot H_2O$ (ca. 1g) and $MgSO_4$ (ca. 1g). This mixture was refluxed for ca. 4 hours until determined complete by TLC (eluent CH_2Cl_2). After which time the reaction mixture was allowed to cool and diluted with CH_2Cl_2 (300 ml) washed with H_2O (2 × 100 ml) dried over $MgSO_4$ and concentrated to an oily residue *in vacuo*, the crude mixture was subjected to silica gel column chromatography (CH_2Cl_2; hexane, 1:1 v/v), affording a white solid.

Procedure 4.3

4-bromobenzophenone (2.61 g, 10.0 mmol), freshly activated Zn dust (1.31 g, 20.0 mmol) were suspended in anhydrous THF (50 ml) and cooled to 0°C. To this mixture $TiCl_4$ (1.12 ml, 10.0 mmol) was added dropwise, after which the mixture was heated to 70°C for 3 hours. Upon cooling the mixture was carefully quenched with H_2O (50 ml), diluted with CH_2Cl_2 (300 ml) and the organic phase washed with H_2O (2 × 100 ml), dried over $MgSO_4$ and concentrated to an oily residue *in vacuo*, the crude mixture was subjected to silica gel column chromatography (CH_2Cl_2; hexane, 1:1 v/v), affording a white solid consisting of approximately a 1:1 mixture of the *E* and *Z* isomers.

Procedure 4.4

Tetraphenylethylene (10 g, 30.1 mmol) was dissolved in CH_2Cl_2 (400 ml), to which was added Br_2 (10 ml, 0.389 mol) after stirred overnight under ambient conditions. The reaction was diluted with CH_2Cl_2 (400 ml) and washed with $Na_2S_2O_{3(aq)}$ solution until decolourised, after which the organic phase was copiously washed with water, dried over $MgSO_4$ and concentrated to a white solid which was subsequently recrystalised from boiling hexanes to afford the crystalline target product.

General Procedure 4.5

The appropriate bromo functionalised TPE (3.64 mmol), CuI (69 mg, 0.364 mmol) and $Pd(PPh_3)_2Cl_2$ (256 mg, 0.364 mmol) were added to a microwave vial, sealed and degassed under a constant stream of nitrogen for 15 minutes, after which the THF (8 ml) and NEt_3 (8 ml) and were subjected to stirring and sonication for 10 minutes. After which TMS acetylene (2.5 equivalents per aryl bromide) was added and the vial was heated to 120°C under microwave irradiation for 1 hour, at which time additional TMS acetylene (2.5 equivalents per aryl bromide) was added, the mixture sonicated and subjected to the same temperature for 1 hour. Once cooled, the microwave vial was opened diluted with CH_2Cl_2 (ca. 150 ml) and washed with EDTA/$NH_4OH_{(aq)}$ solution (20 ml) and water (50 ml), the collected organic phase was dried over $MgSO_4$ and concentrated to dryness and purified by 'flash' silica gel column chromatography (hexane) to afford the TMS protected alkynes as white solids.

General Procedure 4.6

The appropriate TMS protected alkyne precursor (2.00 mmol) was dissolved in the minimum amount of THF (ca. 15 ml) to which was added an equal volume of methanol to this mixture 10% $NaOH_{(aq)}$ (10 ml) was added and left to stir under ambient conditions until complete as determined by TLC (ca. 4 hours). The mixture was then diluted with CH_2Cl_2 (150 ml) and the organic phase washed with water (3 × 50 ml) and dried over $MgSO_4$, the solvent was removed *in vacuo* to afford the alkyne as a white solid.

General Procedure 4.7

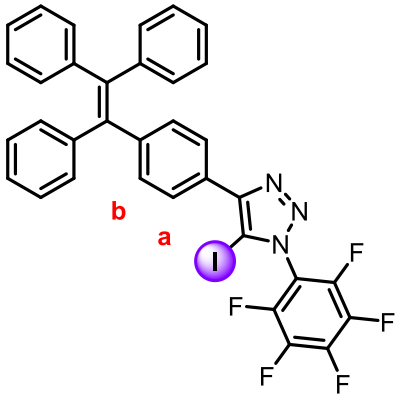
The appropriate alkyne precursor (0.40 mmol) was dissolved in anhydrous THF (20 ml) and cooled to -78°C. To this solution a 1.6 M nBuLi solution (1.5 equivalents per alkyne) was added dropwise and left to stir for 30 minutes after at this temperature. After which a THF solution (10 ml) of I_2 (2 equivalents per alkyne) was added dropwise, the temperature was maintained at -78°C for 10 minutes, the cooling bath removed and allowed to warm to room temperature over the course of 30 minutes. The reaction mixture was then diluted with CH_2Cl_2 (150 ml), washed with $Na_2S_2O_{3(aq)}$ solution until decolourised and subsequently with water (2 × 50 ml), the collected organic phase was dried over $MgSO_4$ and solvent removed *in vacuo*. The crude residue was dry loaded onto silica gel and extracted with CH_2Cl_2:hexane (1:9 v/v) to afford iodoalkyne precursor as a yellow solid which was used immediately for the subsequent CuAAC reaction.

General Procedure 4.8

$[Cu(MeCN)_4]PF_6$ (0.1 equivalents per iodo/proto-alkyne) and TBTA (0.1 equivalents per iodo/proto-alkyne) were dissolved in the minimum amount anhydrous degassed CH_2Cl_2 (ca. 5 ml) and left to stir for 15 minutes. After which time the appropriate iodoalkyne was added to the solution as a solid, followed by the appropriate phenyl azide (1.1 equivalents per iodo/proto-alkyne). Once complete, as determined by TLC analysis, the reaction mixture was diluted with CH_2Cl_2 (ca. 150 ml) and washed with EDTA/$NH_4OH_{(aq)}$ solution (20 ml) and water (50 ml), the collected organic phase was dried over $MgSO_4$ and concentrated to dryness and purified by 'flash' silica gel column chromatography the target products as yellow solids.

4.1 and **4.2** were synthesised according to general procedure 4.1.
4.3 and **4.4** were synthesised according to general procedure 4.2.
4.5 was synthesised according to procedure 4.3.
4.6 was synthesised according to procedure 4.4.
4.7, **4.8**, **4.9** and **4.10** were synthesised according to general procedure 4.5 followed by 4.6.
1·XB, **2·XB, 2·XB^{E}**, **2·XB^{Z}**, **4·XB**, **4·XB^{Ph}** were synthesised according to general procedure 4.7 followed by 4.8.
4·HB was synthesised according to general procedure 4.8.

1·XB



Isolated as yellow solid (83%).

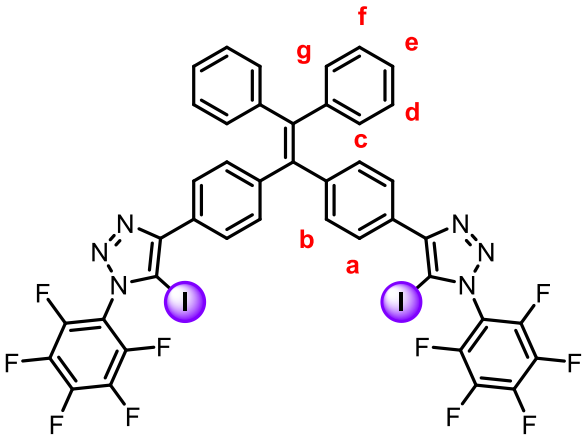
^{1}H NMR (400 MHz, $CDCl_3$) δ 7.82 (d, *J* = 7.3 Hz, $2H_a$), 7.18 (d, *J* = 7.3 Hz, $2H_b$), 7.15 – 7.01 (m, 15H).

^{19}F NMR (377 MHz, $CDCl_3$) δ -142.16 – -142.56 (m), -147.45 (tt, *J* = 21.4, 3.4 Hz), -158.80 – -159.56 (m).

^{13}C NMR (126 MHz, $CDCl_3$) δ 150.30, 145.03, 143.77 (dm, *J* = 260 Hz), 143.66, 143.57, 143.56, 141.98, 140.32, 138.10 (dm, *J* = 252 Hz), 131.88, 131.55, 131.49, 131.46, 127.99, 127.92, 127.83, 127.03, 126.87, 126.76, 126.64, 112.55 (m), 79.75.

HRMS (ESI+ve) m/z: 692.0612 ($[M+H]^+$, $C_{34}H_{20}F_5IN_3$ requires 692.0617).

2·XB



Isolated as yellow solid (67%).

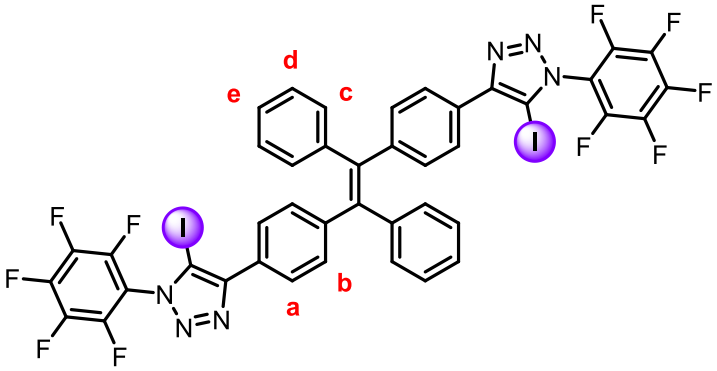
^{1}H NMR (500 MHz, $CDCl_3$) δ 7.85 (d, *J* = 8.62 Hz, $4H_a$), 7.22 (d, *J* = 8.62 Hz, $4H_a$), 7.18 – 7.07 (m, $10H_{c-g}$).

^{19}F NMR (470 MHz, $CDCl_3$) δ -141.85 – -142.66 (m), -147.40, -158.75 – -159.59 (m).

^{13}C NMR (126 MHz, $CDCl_3$) δ 150.23, 144.69, 143.80 (dm, *J* = 265 Hz), 143.54 (dm, *J* = 265 Hz), 143.38, 142.84, 139.55, 138.11 (dm, *J* = 261 Hz), 131.96, 131.48, 128.04, 127.28, 127.05, 126.76, 112.53 (m), 79.85.

HRMS (ESI+ve) m/z: 1050.9592 ($[M+H]^+$, $C_{42}H_{19}F_{10}I_2N_6$ requires 1050.9595).

2·XB*E*



Isolated as yellow solid (34%).

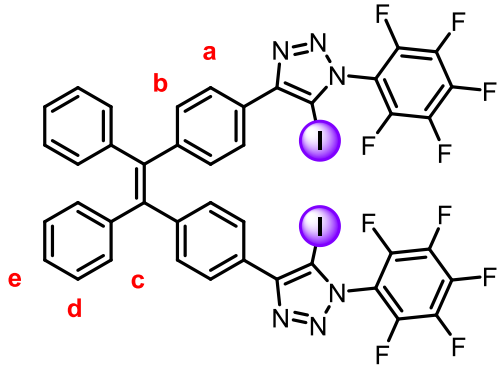
^{1}H NMR (500 MHz, $CDCl_3$) δ 7.83 (d, *J* = 8.1 Hz, $4H_a$), 7.22 (d, *J* = 8.1 Hz, $4H_b$), 7.19 – 7.05 (m, $10H_{c,d,e}$).

^{19}F NMR (470 MHz, $CDCl_3$) δ -142.34, -147.37 (t, J = 22.3 Hz), -158.78 – -159.61 (m).

^{13}C NMR (126 MHz, $CDCl_3$) δ 150.42, 144.78, 143.62 (dm, *J* = 236 Hz), 143.23, 141.27, 139.13, 138.12 (dm, *J* = 262 Hz), 137.08, 131.92, 131.54, 127.99, 127.40, 127.00, 112.53, 80.31.

HRMS (ESI+ve) m/z: 1050.9586 ($[M+H]^+$, $C_{42}H_{19}F_{10}N_6$ requires 1050.9595).

2·XB^{Z}



Isolated as yellow solid (38%).

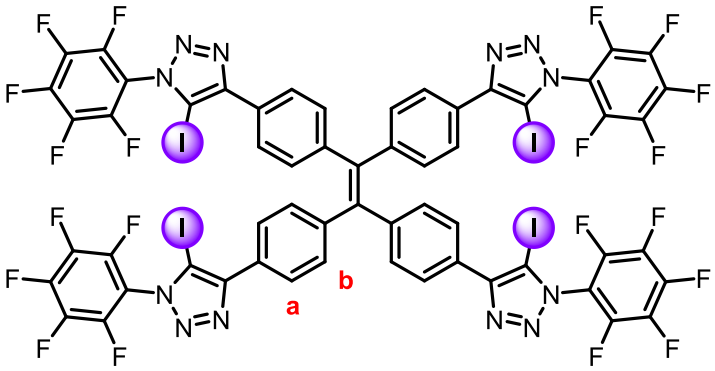
^{1}H NMR (400 MHz, $CDCl_3$) δ 7.84 (d, *J* = 8.4 Hz, $4H_a$), 7.22 – 7.05 (m, $14H_{b,c,d,e}$).

^{19}F NMR (470 MHz, $CDCl_3$) δ -141.71 – -142.64 (m), -146.79 – -147.81 (m), -158.51 – -159.52 (m).

^{13}C NMR (126 MHz, $CDCl_3$) δ 150.25, 144.80, 143.72 (dm, *J* = 281 Hz) 143.28, 141.19, 138.13 (dm, *J* = 261 Hz), 135.92, 131.88, 131.58, 128.13, 127.24, 127.09, 126.68, 125.67, 79.79.

HRMS (ESI+ve) m/z: 1050.9581 ($[M+H]^+$, $C_{42}H_{19}F_{10}N_6$ requires 1050.9595).

4·XB



Isolated as yellow solid (65%).

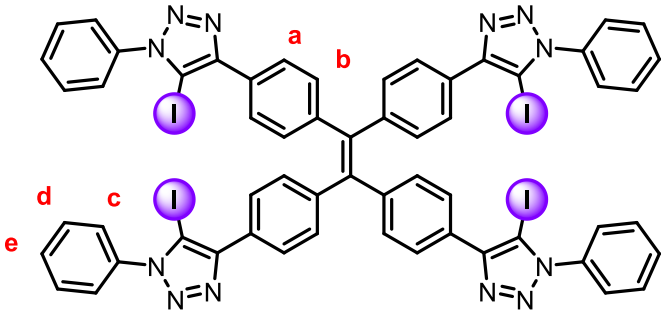
^{1}H NMR (400 MHz, $CDCl_3$) δ 7.89 (d, *J* = 8.62 Hz, $8H_a$), 7.29 (d, *J* = 8.62 Hz, $8H_b$).

^{19}F NMR (377 MHz, $CDCl_3$) δ -141.96 – -142.63 (m), -147.09 – -147.69 (m), -158.90 – -159.51 (m).

^{13}C NMR (126 MHz, $CDCl_3$) δ 150.29, 144.11, 143.81 (dm, *J* = 263 Hz), 143.56 (dm, *J* = 257 Hz) 141.37, 138.09 (dm, *J* = 259 Hz), 132.00, 127.86, 127.17, 112.51 (m), 80.42.

HRMS (ESI+ve) m/z: 1768.7538 ($[M+H]^+$, $C_{58}H_{17}F_{20}I_4N_{12}$ requires 1768.7553).

4·XB^{Ph}



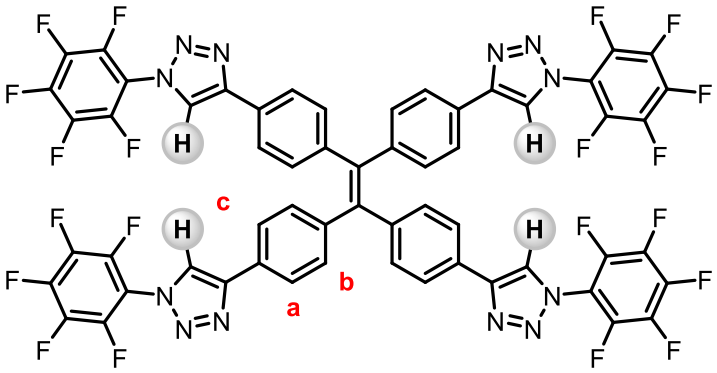
Isolated as yellow solid (56%).

^{1}H NMR (400 MHz, $CDCl_3$) δ 7.89 – 7.80 (m, $8H_a$), 7.61 – 7.48 (m, $20H_{c,d,e}$), 7.32 – 7.27 (m, $4H_b$).

^{13}C NMR (126 MHz, $CDCl_3$) δ 150.32, 143.83, 141.43, 137.18, 131.90, 130.33, 129.49, 128.73, 127.44, 126.66, 78.30.

HRMS (ESI+ve) m/z: 1408.9425 ($[M+H]^+$, $C_{58}H_{37}I_4N_{12}$ requires 1408.9437).

4·HB



Isolated as yellow solid (32%).

^{1}H NMR (500 MHz, DMSO) δ 9.08 (s, 4H_c), 7.84 – 7.78 (m, 8H_a), 7.27 – 7.17 (m, 8H_b).

^{19}F NMR (377 MHz, DMSO) δ -146.70 – -147.66 (m), -150.90 – -151.67 (m), -160.50 – -161.21 (m).

^{13}C NMR (126 MHz, DMSO) δ 146.69, 143.25, 141.93 (dm, *J* = 247 Hz), 140.63, 140.47, 137.67 (dm, *J* = 252 Hz), 131.68, 128.67, 127.81, 125.29, 124.91, 124.42, 112.47.

HRMS (ESI+ve) m/z: 1265.1687 ($[M+H]^+$, $C_{58}H_{21}F_{20}N_{12}$ requires 1265.1673).

7.6 Synthetic Procedures and Characterisation for Compounds in Chapter 5

General Procedure 5.1

The appropriate acid was suspended in anhydrous CH_2Cl_2 (ca. 20 ml per 0.5 g of acid) to which was added DCC (1.1 equivalents), ethyl 4-hydroxybenzoate (1.2 equivalents) and a catalytic amount of DMAP. The reaction mixture was left to stir at room temperature, until consumption of the acid was determined by TLC analysis (ca. 3 hours). After which time the solution was filtered and the solid carefully washed with CH_2Cl_2 (ca. 20 ml), the filtrate was collected and concentrated in vacuo. The resultant residue was subjected to silica gel column chromatography to afford the desired ester product.

General Procedure 5.2

$[Cu(MeCN)_4]PF_6$ (0.1 equivalents per alkyne) and TBTA (0.1 equivalents per alkyne) were dissolved in the minimum amount anhydrous degassed CH_2Cl_2 (ca. 5 ml) and left to stir for 15 minutes. After which time the appropriate alkyne was added to the solution as a solid, followed by azido-benzo-15-crown-5 (1.1 equivalents per alkyne). Once complete, as determined by TLC analysis, the reaction mixture was diluted with CH_2Cl_2 (ca. 150 ml) and washed with EDTA/$NH_4OH_{(aq)}$ solution (20 ml) and water (50 ml), the collected organic phase was dried over $MgSO_4$ and concentrated to dryness. The crude solid obtained was washed with Et_2O (10 × 10 ml) followed by MeOH (10 × 10 ml) followed by Et_2O (10 × 10 ml) to obtain the desired CuAAC product as an off white solid.

General Procedure 5.3

A CH_2Cl_2 solution of the appropriate receptor (5 equivalents per amino-propyl for a given mass QuadraSil-AP used) was exposed to QuadraSil-AP and stirred at room temperature for 3 days. After which the mixture was filtered, and the solid material was washed with CH_2Cl_2 (ca. 500 ml).

General extraction procedure

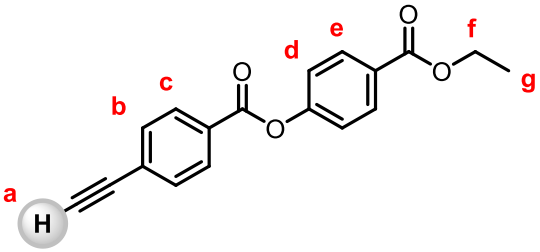
A typical extraction procedure was conducted as follows; a known amount of a given silica-based material (ca. 20 mg) is exposed to a (1 ml) centrifuge tube to which was added a 5 mM solution of a NaX (X= Cl^-, Br^-, I^- and NO_3^-) aqueous solution. The sealed centrifuge tube was placed on a roller mixer and left mixing for 12 hours to allow equilibration. After this time the tube was placed in a centrifuge and the solution pipetted off, diluted to the required concentration, and subjected to ICP-MS analysis.

5.2, **5.4** and **5.9** were synthesised according to general procedure 5.1.

1·HB, **1·XB**, **2·HB** and **2·XB** were synthesised according to general procedure 5.2.

1·HB^S, **1·XB^S**, **2·HB^S** and **2·XB^S** were synthesised according to general procedure 5.3.

5.2



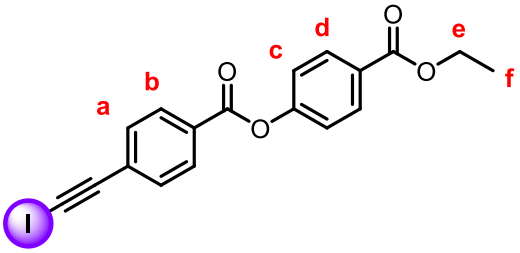
Isolated as a white solid (quant.).

^{1}H NMR (400 MHz, $CDCl_3$) δ 8.14 (m, $4H_{b,c}$), 7.69 – 7.56 (m, $2H_e$), 7.35 – 7.27 (m, $2H_d$), 4.39 (q, *J* = 7.2 Hz, $2H_f$), 3.29 (s, $1H_a$), 1.40 (t, *J* = 7.2 Hz, $3H_g$).

^{13}C NMR (101 MHz, $CDCl_3$) δ 165.94, 164.11, 154.48, 132.46, 131.34, 130.23, 129.19, 128.41, 127.90, 121.75, 82.73, 80.93, 61.26, 14.47.

HRMS (ESI+ve) m/z: 295.09644 ($[M+H]^+$, $C_{18}H_{15}O_4$ requires 295.09649).

5.7



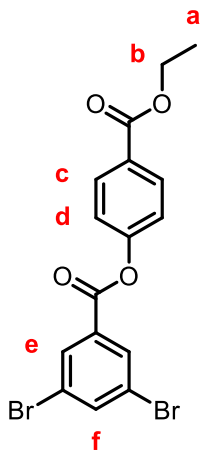
5.5 (250 mg, 1.56 mmol), N-iodomorpholine hydroiodide (798 mg, 2.34 mmol) and CuI (30 mg, 0.156 mmol) were dissolved in anhydrous THF (14 ml) and left to stir, excluded from light, for 4 hours at room temperature. After which time the mixture diluted with CH_2Cl_2 (ca. 100 ml) and filtered through an alumina plug. Silica was added to the resultant filtrate and concentrated to dryness. The silica-adsorbed compound was eluted with EtOAc:hexane (1:9, v/v) mixtures, and the collected filtrate concentrated to dryness to afford the iodo-alkyne and used immediately for the next step. Which was dissolved in MeOH (15 ml), to which was added H_2O (1.5 ml), to this solution an aqueous solution of KOH (9 mg, 0.156 mmol), dissolved in H_2O (1.5 ml), was added dropwise. The reaction mixture was left to stir at room temperature excluded from light, until determined complete by TLC analysis (ca. 1 hr). After which time the reaction mixture was diluted with 1 M $HCl_{(aq)}$ until determined to in the pH range 2-3, the resultant aqueous phase was extracted into EtOAc (3 × 50 ml). The combined organic phases were washed with H_2O (2 × 20 ml), and dried over $MgSO_4$ to afford the alkyne-acid intermediate. The solid isolated as a dark yellow solid was subsequently subjected to general procedure 5.2, excluded from light throughout, to afford **5.7** as white solid in 79% yield over three steps.

^{1}H NMR (500 MHz, $CDCl_3$) δ 8.23 – 8.07 (m, $4H_{a,b}$), 7.62 – 7.48 (m, $2H_d$), 7.35 – 7.27 (m, $2H_c$), 4.39 (q, *J* = 7.2 Hz, $2H_e$), 1.41 (t, *J* = 7.2 Hz, $3H_f$).

^{13}C NMR (126 MHz, $CDCl_3$) δ 165.96, 164.10, 154.50, 132.68, 131.36, 130.20, 129.08, 129.03, 128.42, 121.76, 93.45, 61.28, 14.48, 11.74.

HRMS (ESI+ve) m/z: 420.99292 ($[M+H]^+$, $C_{18}H_{14}O_4I$ requires 420.99313).

5.9

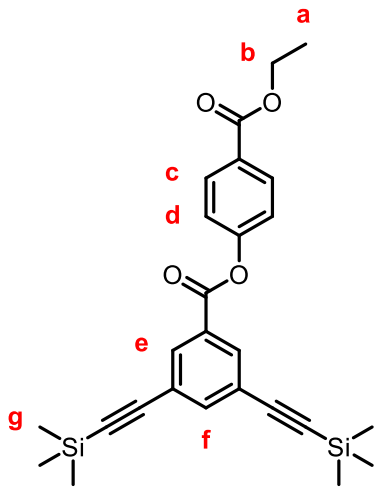


Isolated as a white solid (67%).

^{1}H NMR (500 MHz, $CDCl_3$) δ 8.26 (d, *J* = 1.8 Hz, $2H_e$), 8.14 (d, *J* = 9.2 Hz, $2H_c$), 7.94 (t, *J* = 1.8 Hz, $1H_f$), 7.29 (d, *J* = 9.2 Hz, $2H_d$), 4.40 (q, *J* = 7.1 Hz, $2H_b$), 1.41 (t, *J* = 7.1 Hz, $3H_a$).

^{13}C NMR (126 MHz, $CDCl_3$) δ 165.84, 162.32, 154.08, 139.30, 132.48, 132.03, 131.45, 128.76, 123.46, 121.60, 61.34, 14.48.

5.10



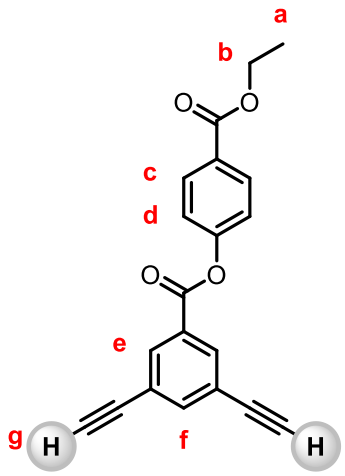
Isolated as a white solid (71%).

5.9 (1.00 g, 2.34 mmol), $Pd(PPh_3)_2Cl_2$ (164 mg, 0.234 mmol) and CuI (45 mg, 0.234 mmol) were dissolved in an anhydrous and degassed mixture of THF (20 ml) and NEt_3 (5 ml). The resultant mixture was left to stir at room temperature overnight under an atmosphere of N_2. After which time the crude mixture was filtered through a celite plug and diluted with CH_2Cl_2 (150 ml), the filtrate was washed with 0.1M EDTA/$NH_4OH_{(aq)}$ (25 ml) and H_2O (25 ml). The organic phase was dried over $MgSO_4$ concentrated to dryness and purified by silica gel column chromatography to afford **5.10** as an off white solid (768 mg, 1.66 mmol, 71%).

^{1}H NMR (400 MHz, $CDCl_3$) δ 8.19 (d, *J* = 1.6 Hz, $2H_f$), 8.13 (d, *J* = 8.8 Hz, $2H_c$), 7.81 (t, *J* = 1.6 Hz, $1H)_f$, 7.29 (d, *J* = 8.8 Hz, $1H_d$), 4.40 (q, *J* = 7.1 Hz, $2H_b$), 1.41 (t, *J* = 7.1 Hz, $3H_a$), 0.26 (s, $18H_g$).

^{13}C NMR (126 MHz, $CDCl_3$) δ 165.94, 163.45, 154.35, 140.03, 133.24, 131.40, 129.75, 128.52, 124.43, 121.72, 102.75, 96.89, 61.29, 14.49, -0.06.

5.4



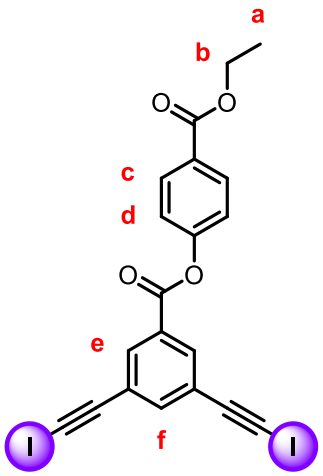
Isolated as a white solid (93%).

^{1}H NMR (400 MHz, $CDCl_3$) δ 8.27 (d, *J* = 1.6 Hz, $2H_e$), 8.14 (d, *J* = 8.6 Hz, $2H_c$), 7.85 (t, *J* = 1.6 Hz, $1H_f$), 7.30 (d, *J* = 8.6 Hz, $2H_d$), 4.39 (t, *J* = 7.1 Hz, $2H_b$), 3.18 (s, $2H_g$), 1.41 (t, *J* = 7.1 Hz, $3H_a$).

^{13}C NMR (101 MHz, $CDCl_3$) δ 165.89, 163.21, 154.26, 140.25, 133.86, 131.41, 130.07, 128.60, 123.57, 121.67, 81.46, 79.54, 61.30, 14.48.

HRMS (ESI+ve) m/z: 319.09661 ($[M+H]^+$, $C_{20}H_{15}O_4$ requires 319.09649).

5.11



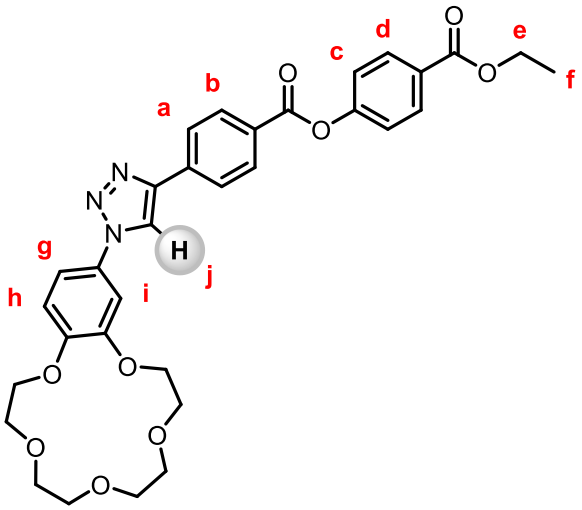
5.10 (500 mg, 1.06 mmol) was dissolved in anhydrous DMF (15 ml), to which was added $AgNO_3$ (36 mg, 0.212 mmol) and NIS (716 mg, 3.18 mmol), the mixture was left to stir for 4 hours at room temperature excluded from light. After which time the reaction mixture was diluted with H_2O (500 ml) and the resultant precipitate isolated by filtration under vacuum. The obtained solid was copiously washed with water, the solid was then dissolved in CH_2Cl_2 dried over $MgSO_4$ and solvent removed in vacuo to afford **5.11** as yellow solid (508 mg, 0.890 mmol, 84%).

^{1}H NMR (500 MHz, $CDCl_3$) δ 8.18 (d, *J* = 1.6 Hz, $2H_e$), 8.16 – 8.10 (m, $2H_c$), 7.73 (t, *J* = 1.6 Hz, $1H_f$), 7.31 – 7.27 (m, $2H_d$), 4.39 (q, *J* = 7.1 Hz, $2H_b$), 1.41 (t, *J* = 7.1 Hz, $3H_a$).

^{13}C NMR (126 MHz, $CDCl_3$) δ 165.90, 163.16, 154.24, 140.59, 134.00, 131.41, 129.90, 128.58, 124.65, 121.65, 92.03, 61.31, 14.48, 10.31.

HRMS (ESI+ve) m/z: 570.88970 ($[M+H]^+$, $C_{20}H_{13}O_4I_2$ requires 570.88977).

1·HB



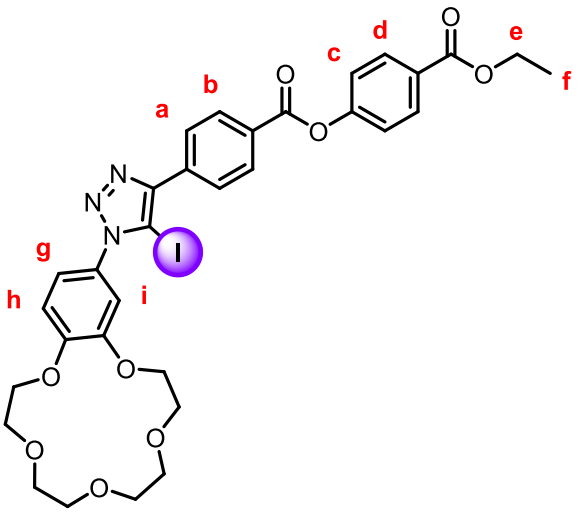
Isolated as a brown solid (51%).

^{1}H NMR (400 MHz, $CDCl_3$) δ 8.28 (s, $1H_j$), 8.25 (m, $2H_b$), 8.16 – 8.11 (m, $2H_d$), 8.08 – 8.02 (m, $2H_a$), 7.38 (m, $1H_i$), 7.36 – 7.28 (m, $2H_c$), 7.22 (dd, *J* = 8.6, 2.5 Hz, $1H_g$), 6.97 (d, *J* = 8.6 Hz, $1H_h$), 4.39 (q, *J* = 7.1 Hz, $2H_e$), 4.21 (m, 4H), 3.94 (m, 4H), 3.87 – 3.71 (m, 16H), 1.40 (t, *J* = 7.1 Hz, $3H_f$).

^{13}C NMR (101 MHz, $CDCl_3$) δ 165.97, 164.42, 154.63, 150.09, 149.88, 147.06, 135.72, 131.31, 131.07, 130.75, 128.73, 128.29, 125.90, 121.83, 119.09, 113.98, 113.09, 107.26, 71.24, 70.51 (d, *J* = 3.2 Hz), 69.51, 69.39 (d, *J* = 2.5 Hz), 69.31, 61.23, 14.46.

HRMS (ESI+ve) m/z: 604.22856 ($[M+H]^+$, $C_{32}H_{34}O_9N_3$ requires 604.22896).

1·XB



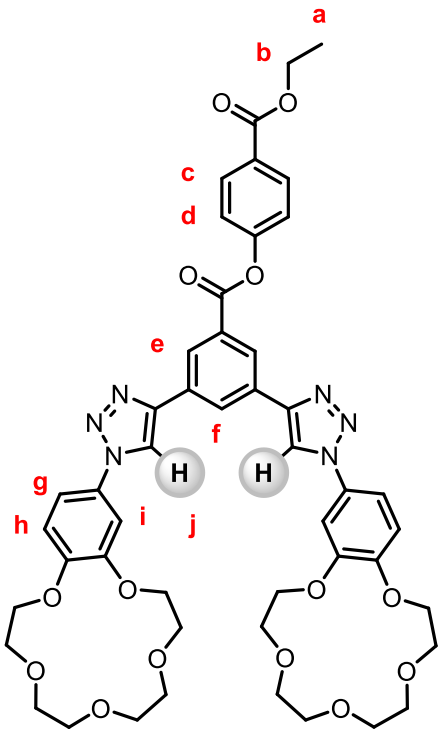
Isolated as a brown solid (64%).

^{1}H NMR (500 MHz, $CDCl_3$) δ 8.33 (d, *J* = 8.4 Hz, $2H_b$), 8.23 (d, *J* = 8.4 Hz, $2H_a$), 8.19 – 8.12 (m, $2H_d$), 7.35 (m, $2H_c$), 7.12 – 6.95 (m, $3H_{g,h,i}$), 4.40 (q, *J* = 7.1 Hz, $2H_e$), 4.21 (m, 2H), 3.95 (m, 2H), 3.78 (q, *J* = 4.1, 3.5 Hz, 8H), 1.41 (t, *J* = 7.1 Hz, $3H_f$).

^{13}C NMR (126 MHz, $CDCl_3$) δ 165.92, 164.36, 154.57, 150.77, 149.41, 148.74, 135.61, 131.28, 130.62, 129.88, 129.01, 128.27, 127.65, 121.79, 119.61, 113.10, 112.23, 71.21, 70.43, 69.40, 69.32, 69.22, 69.13, 61.20, 14.43.

HRMS (ESI+ve) m/z: 730.12561 ($[M+H]^+$, $C_{32}H_{33}O_9N_3I$ requires 730.12560).

2·HB



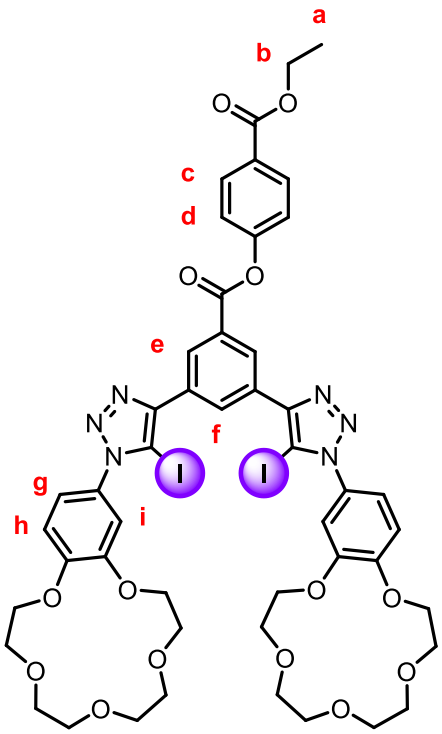
Isolated as a brown solid (69%).

^{1}H NMR (500 MHz, DMSO) δ 9.06 (s, 2H$_j$), 8.45 (d, *J* = 1.8 Hz, 1H$_f$), 8.18 (d, *J* = 1.6 Hz, 2H$_e$), 7.64 (d, *J* = 8.7 Hz, 2H$_c$), 7.15 – 7.04 (m, 6H$_{g,h,i}$), 6.71 (d, *J* = 8.7 Hz, 2H$_d$), 3.90 (q, *J* = 7.1 Hz, 2H$_b$), 3.75 (s, 4H), 3.68 (s, 4H), 3.36 (s, 8H), 3.26 – 3.14 (m, 16H), 0.90 (t, *J* = 7.1 Hz, 3H$_a$).

^{13}C NMR (126 MHz, DMSO) δ 165.07, 163.85, 154.32, 149.09, 148.75, 145.70, 132.02, 130.88, 130.37, 130.08, 127.83, 125.84, 122.55, 120.58, 113.83, 112.36, 106.02, 70.53, 69.70 (d, *J* = 2.7 Hz), 68.79, 68.71 (d, *J* = 2.9 Hz), 68.65, 60.94, 14.18.

HRMS (ESI+ve) m/z: 937.36159 ([M+H]$^+$, $C_{48}H_{53}O_{15}N_6$ requires 937.36143).

2·XB



Isolated as a brown solid (47%).

^{1}H NMR (400 MHz, $CDCl_3$) δ 8.98 (s, 1H_f), 8.92 (s, 2H_e), 8.14 (d, *J* = 8.4 Hz, 2H_c), 7.36 (d, *J* = 8.4 Hz, 2H_d), 7.16 – 6.91 (m, 6$H_{g,h,i}$), 4.39 (q, *J* = 7.1 Hz, 2H_b), 4.28 – 4.08 (m, 8H), 3.94 (m, 8H), 3.77 (m, 16H), 1.40 (t, *J* = 7.1 Hz, 3H_a).

^{13}C NMR (101 MHz, $CDCl_3$) δ 165.97, 164.13, 154.56, 150.71, 149.38, 148.76, 131.60, 131.33, 130.27, 129.98, 129.34, 128.36, 121.82, 119.61, 113.08, 112.18, 71.16, 70.42, 69.58 – 68.99 (m), 61.24, 14.46.

HRMS (ESI+ve) m/z: 937.36159 ($[M+H]^+$, $C_{48}H_{53}O_{15}N_6$ requires 937.36143).

7.7 Crystal structure determination

Single crystals suitable for X-ray analysis were each coated with Paratone-N oil, suspended on a 200 µm MiTeGen loop, and placed in a cold gaseous nitrogen stream on an Oxford Diffraction Supernova X-ray diffractometer performing φ- and ω-scans at 150(2) K. Diffraction intensities were measured using graphite monochromated Cu Kα radiation (1.54184 Å). Data collection, indexing, initial cell refinements, frame integration, final cell refinements and absorption corrections were accomplished using the program CrysAlisPro.[11] Scattering factors and anomalous dispersion corrections were taken from the International Tables for X-ray Crystallography. All structures were solved by direct methods and refined against F2 on all data by full-matrix least squares following established refinement strategies. Structures were was solved using the CRYSTALS suite or SHELXS and SHELXL. All non-hydrogen atoms were refined anisotropically. All hydrogen atoms were included into the model at geometrically calculated positions and refined using a riding model. Details of the data quality and a summary of the residual values for the refinements are listed in Table S4. Figures of the crystal structures have been created using the open-source PyMOL Molecular Graphics System (version 2.4.0a0, Schrödinger LLC).

7.7.1 Structures for Chapter 2

Deposition Number(s) 2081712 (for **1·ChB^{PFP}**) and 2081709 (for **1·XB^{PFP}**) and 2081707 (for **1·HB^{PFP}**) and 2081718 (for **3·ChB^{pCl}**) and 2081716 (for **3·ChB^{2F}**) and 2081717 (for **1·ChB^{3F}**).

7.7.2 Structures for Chapter 3

Empirical formula	C50 H41 Cs F10 I N7 O12 Te2	
Formula weight	1636.91	
Temperature	150(2) K	
Wavelength	1.54184 Å	
Crystal system	Triclinic	
Space group	P-1	
Unit cell dimensions	a = 14.4539(3) Å	a= 115.718(2)°.
	b = 18.4545(3) Å	b= 97.669(2)°.
	c = 18.4961(4) Å	g = 100.608(2)°.
Volume	4240.27(16) Å3	
Z	2	
Density (calculated)	1.282 Mg/m3	
Absorption coefficient	12.172 mm-1	
F(000)	1576	
Crystal size	0.400 x 0.400 x 0.400 mm^3	
Theta range for data collection	3.620 to 76.462°.	
Index ranges	-18<=h<=18, -20<=k<=23, -23<=l<=22	
Reflections collected	70615	
Independent reflections	17510 [R(int) = 0.0659]	
Completeness to theta = 67.684°	99.90%	
Absorption correction	Sphere	
Max. and min. transmission	0.07118 and 0.00693	
Refinement method	Full-matrix least-squares on F2	
Data / restraints / parameters	17510 / 0 / 748	
Goodness-of-fit on F2	1.021	
Final R indices [I>2sigma(I)]	R1 = 0.0886, wR2 = 0.2267	
R indices (all data)	R1 = 0.0948, wR2 = 0.2420	
Extinction coefficient	n/a	
Largest diff. peak and hole	4.493 and -0.754 e.$Å^{-3}$	

Table 7.1 Selected Crystallographic and Refinement Data for X-ray Crystal Structures of **1·ChB^{PFP}**·CsI.

Empirical formula	C54.50 H45.50 Cl14.50 F10 K N7 O12 Te2	
Formula weight	1988.8	
Temperature	150(2) K	
Wavelength	1.54184 Å	
Crystal system	Triclinic	
Space group	P-1	
Unit cell dimensions	a = 17.0958(2) Å	a= 85.3110(10)°.
	b = 20.8045(4) Å	b= 89.2730(10)°.
	c = 25.0324(4) Å	g = 68.248(2)°.
Volume	8240.2(3) Å3	
Z	4	
Density (calculated)	1.603 Mg/m3	
Absorption coefficient	11.051 mm-1	
F(000)	3908	
Crystal size	0.4 x 0.4 x 0.4 mm^3	
Theta range for data collection	3.271 to 76.350°.	
Index ranges	-20<=h<=21, -26<=k<=25, -28<=l<=31	
Reflections collected	95933	
Independent reflections	33973 [R(int) = 0.0584]	
Completeness to theta = 67.684°	99.80%	
Absorption correction	Sphere	
Max. and min. transmission	0.12587 and 0.03254	
Refinement method	Full-matrix least-squares on F2	
Data / restraints / parameters	33973 / 0 / 1819	
Goodness-of-fit on F2	1.026	
Final R indices [I>2sigma(I)]	R1 = 0.0725, wR2 = 0.1893	
R indices (all data)	R1 = 0.0827, wR2 = 0.2057	
Extinction coefficient	n/a	
Largest diff. peak and hole	2.661 and -1.077 $e.Å^{-3}$	

Table 7.2 Selected Crystallographic and Refinement Data for X-ray Crystal Structures of **1·ChB^{PFP}**·KCl.

Empirical formula	C54.50 H45.50 Br Cl13.50 F10 K N7 O12 Te2	
Formula weight	2033.26	
Temperature	150(2) K	
Wavelength	1.54184 Å	
Crystal system	Triclinic	
Space group	P-1	
Unit cell dimensions	a = 17.3075(2) Å	a= 85.3740(10)°.
	b = 20.7661(3) Å	b= 89.0520(10)°.
	c = 25.1018(3) Å	g = 68.0790(10)°.
Volume	8341.38(19) Å3	
Z	4	
Density (calculated)	1.619 Mg/m3	
Absorption coefficient	11.183 mm-1	
F(000)	3980	
Crystal size	0.400 x 0.400 x 0.400 mm3	
Theta range for data collection	3.533 to 76.656°.	
Index ranges	-21<=h<=18, -26<=k<=26, -31<=l<=31	
Reflections collected	175477	
Independent reflections	34525 [R(int) = 0.0607]	
Completeness to theta = 67.684°	99.90%	
Absorption correction	Sphere	
Max. and min. transmission	0.12562 and 0.03228	
Refinement method	Full-matrix least-squares on F2	
Data / restraints / parameters	34525 / 0 / 1819	
Goodness-of-fit on F2	1.037	
Final R indices [I>2sigma(I)]	R1 = 0.0630, wR2 = 0.1775	
R indices (all data)	R1 = 0.0693, wR2 = 0.1870	
Extinction coefficient	n/a	
Largest diff. peak and hole	2.456 and -1.469 e.Å-3	

Table 7.3 Selected Crystallographic and Refinement Data for X-ray Crystal Structures of **1·ChB^{PFP}**·KBr.

Empirical formula	C53 H44 Cl9 F10 I K N7 O12 Te2	
Formula weight	1901.2	
Temperature	150(2) K	
Wavelength	1.54178 Å	
Crystal system	Triclinic	
Space group	P-1	
Unit cell dimensions	a = 14.5034(3) Å	a= 118.166(3)°.
	b = 18.4077(5) Å	b= 99.957(2)°.
	c = 18.5490(6) Å	g = 97.552(2)°.
Volume	4168.5(2) Å3	
Z	2	
Density (calculated)	1.515 Mg/m3	
Absorption coefficient	12.181 mm-1	
F(000)	1852	
Crystal size	0.2 x 0.2 x 0.2 mm3	
Theta range for data collection	3.191 to 76.336°.	
Index ranges	-18<=h<=16, -22<=k<=23, -22<=l<=23	
Reflections collected	79897	
Independent reflections	17205 [R(int) = 0.0682]	
Completeness to theta = 67.679°	99.90%	
Absorption correction	Sphere	
Max. and min. transmission	0.09152 and 0.01392	
Refinement method	Full-matrix least-squares on F2	
Data / restraints / parameters	17205 / 0 / 856	
Goodness-of-fit on F2	1.164	
Final R indices [I>2sigma(I)]	R1 = 0.0943, wR2 = 0.2564	
R indices (all data)	R1 = 0.1009, wR2 = 0.2733	
Extinction coefficient	n/a	
Largest diff. peak and hole	3.960 and -1.446 e.Å-3	

Table 7.3 Selected Crystallographic and Refinement Data for X-ray Crystal Structures of **1·ChB^{PFP}**·KI.

Empirical formula	C52 H43 Cl6 F10 I N7 O12 Rb Te2	
Formula weight	1828.2	
Temperature	150(2) K	
Wavelength	1.54184 Å	
Crystal system	Triclinic	
Space group	P-1	
Unit cell dimensions	a = 14.4929(2) Å	a= 117.326(2)°.
	b = 18.4361(2) Å	b= 99.9420(10)°.
	c = 18.4714(3) Å	g = 97.8410(10)°.
Volume	4185.59(12) Å3	
Z	2	
Density (calculated)	1.451 Mg/m3	
Absorption coefficient	11.491 mm-1	
F(000)	1772	
Crystal size	0.4 x 0.4 x 0.4 mm3	
Theta range for data collection	3.194 to 76.226°.	
Index ranges	-17<=h<=18, -23<=k<=23, -23<=l<=21	
Reflections collected	91967	
Independent reflections	17243 [R(int) = 0.0651]	
Completeness to theta = 67.684°	100.00%	
Absorption correction	Sphere	
Max. and min. transmission	0.08917 and 0.01300	
Refinement method	Full-matrix least-squares on F2	
Data / restraints / parameters	17243 / 0 / 820	
Goodness-of-fit on F2	1.064	
Final R indices [I>2sigma(I)]	R1 = 0.0613, wR2 = 0.1602	
R indices (all data)	R1 = 0.0683, wR2 = 0.1700	
Extinction coefficient	n/a	
Largest diff. peak and hole	2.231 and -0.551 e.Å-3	

Table 7.4 Selected Crystallographic and Refinement Data for X-ray Crystal Structures of **1·ChB^{PFP}**·RbI.

7.7.3 Structures for Chapter 4

Deposition Number(s) 2083103 (for 4·XB) and 2082363 (for 4·XB·NaCl) and 2082364 (for 4·XB·NaI).